AN INVESTIGATION OF THE ROLES OF MAGNESIUM IONS IN THE CATALYTIC CYCLE OF THE PROTEIN KINASE CDK2: A MOLECULAR LINK BETWEEN ALLOSTERIC ACTIVATION AND CATALYTIC ACTIVITY.

by

Douglas M. Jacobsen

A dissertation submitted in partial fulfillment
of the requirements for the degree of
Doctor of Philosophy
(Bioinformatics)
in The University of Michigan
2012

Doctoral Committee:

Assistant Professor Matthew A. Young, Co-Chair
Professor Charles L. Brooks III, Co-Chair
Professor Philip C. Andrews
Professor Daniel M. Burns, Jr.
Associate Professor Mark A. Saper

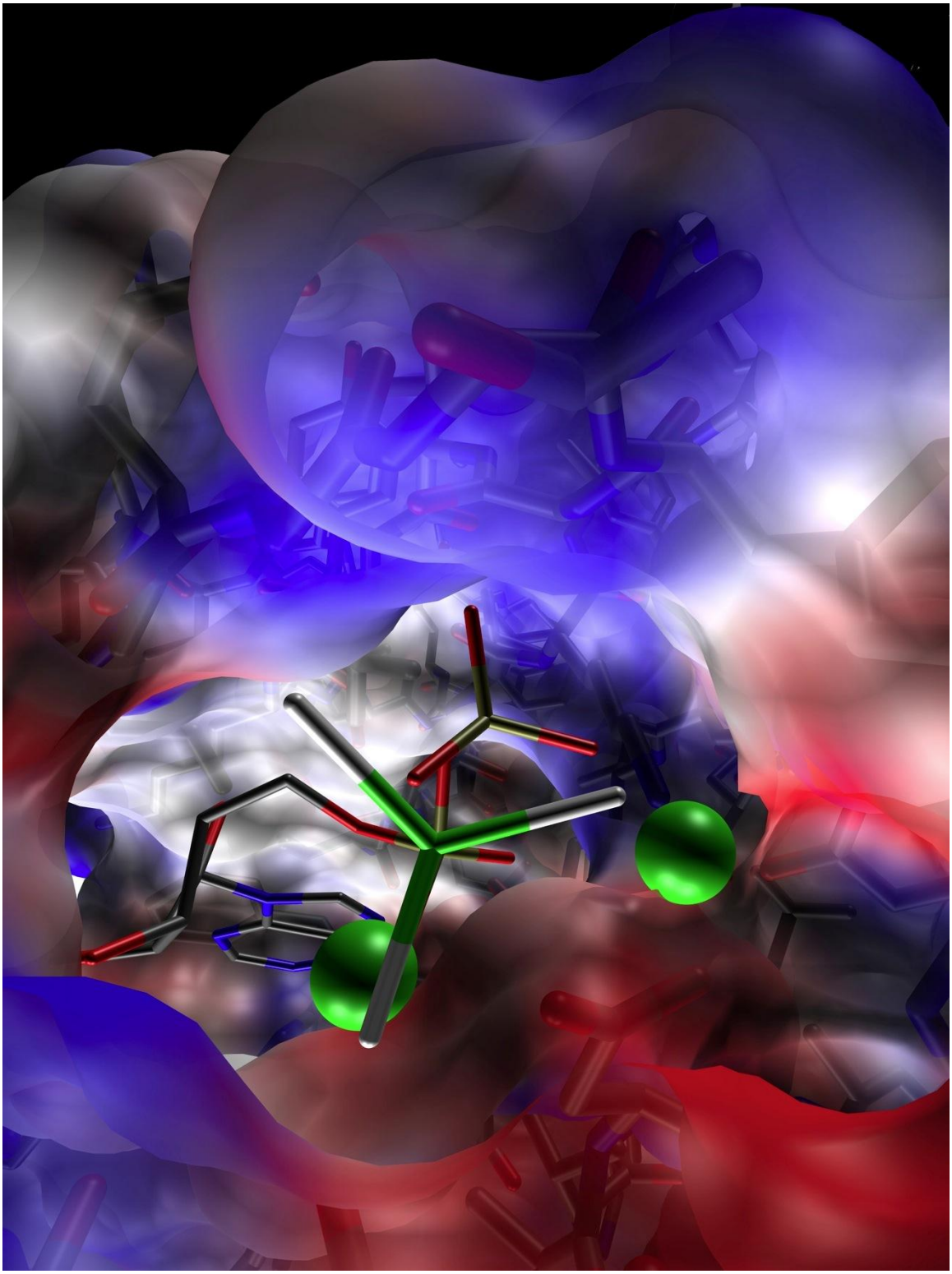

DEDICATION

This dissertation is dedicated to the memory of my father, Douglas E. Jacobsen.

ACKNOWLEDGEMENTS

I sincerely and gratefully thank my advisor, mentor, and friend, Matthew Young. Matt has been an excellent and inspiring advisor and mentor. He has always taken the time to discuss my research with me, allowed me to present my ideas, and helped me to clarify my thinking. I first met Matt in a Bioinformatics survey course where he introduced structural biology and X-ray crystallography. This introduction had a strong and lasting effect on me – in fact I changed my planned course of study because I found protein structure and crystallography absolutely fascinating. Matt took a chance on me, allowing a purely computational person to learn experimental investigation techniques in his laboratory. Matt and I together have demonstrated how experiments and calculations can be used in combination to investigate important questions in much greater depth than using either approach singly. From Matt I have learned how to be a scientist. Thank you. Matt.

Following my preliminary exams, Charles Brooks invited me to attend his group meetings, and when I needed to add a co-advisor, Charlie welcomed me to join his group. In our many discussions about my research, Charlie has always helped to me to look at my data from a different perspective. Charlie has made my research possible by providing me with the computational resources necessary to perform my calculations and by allowing me to benefit from the extensive collective experiences of both himself and

his group. I thank Charlie for his continual help and support throughout my graduate career.

The remaining members of my committee, Philip Andrews, Daniel Burns, and Mark Saper have been integral to my success. During the admission process to the Bioinformatics program, I interviewed with both Phil and Dan, and our discussions during the interview increased my enthusiasm about joining this graduate program. Furthermore, both Phil and Dan have provided an outside opinion of the research throughout – and I thank them for their help. I first met Mark in the Biophysics crystallography class, and I invited Mark to join my committee because of his incredible strengths as a teacher. Mark has always been enthusiastic about my work, and has provided great advice as my thesis research progressed.

I also thank Patrick O'Brien for his help with the enzyme kinetics experiments. He has patiently worked with me as I explored the complexities of enzymology – and specifically the complexities of this enzyme. Pat's help with the interpretation of the experiments and the significant improvements to the Chapter 3 text has been instrumental to the progression and completion of this work.

Annie Bao has always helped me with the experiments – and with her friendly words. We've been working together for over 4 years now – the entire time I've been in Matt's lab. I can attribute much of my success in the lab to the helpful guidance that Annie provided as I first started picking up a pipette and making buffers. Beyond this initial help, Annie has also tirelessly supported all the efforts of the lab and my project. She performed all the molecular biology and prepared much of the protein I used in my

experiments. Annie also worked to find the initial crystallization conditions used to obtain the crystal structures throughout the results chapters.

From the Brooks group, David Braun and Jennifer Knight both helped me a great deal in my work. David is excellent at his job and it would not be possible to perform the vast calculations required for this work without his tireless efforts to tame the herd of graduate students and post docs all vying for time on the cluster. I also thank Jennifer who helped me a great deal with the free energy perturbation calculations, specifically by providing her scripts and protocols for my reference when I was setting up my own calculations for Chapter 4.

The Department of Computational Medicine and Bioinformatics (DCMB) staff, in particular Julia Eussen and Jeff de Wet have been very helpful throughout my time in the bioinformatics program, but in particular in the last semester. Julia has actively helped me with the logistics of this final semester, but in many ways has kept my progress on track by taking care of the details I didn't even know existed, such as managing the funding sources and keeping them up-to-date. Jeff was the first instructor I met in the Bioinformatics program, and appropriately, was the last that I worked with when he allowed me to assist him with the teaching duties for BIOINF 575. I thank everybody in the DCMB for their help and support.

Sharon Kardia gave me my first opportunity at the Ann Arbor campus at the University of Michigan. Though only serving as a systems administrator for her group, by allowing me to contribute to the research efforts of her laboratory, I gained that crucial first experience in scientific investigation that I used to launch into my graduate studies.

That initial support from Sharon and her group members, Yan Sun, Reagan Kelly, Jennifer Smith, Todd Greene, and Kristin Meyers helped to set me on this path, and for that I am extremely grateful to all them.

My parents, David and Peggy, and my sisters, Elizabeth and Rebecca, have been instrumental to my success – not only with this thesis and graduate school experience, but also in all aspects of my life. They have each inspired me, nurtured my curiosity, and helped me to form a sense of purpose and identity that has enabled all of my achievements.

Finally and most importantly, I thank my wife and partner, Melinda. As I persevered through graduate school, Melinda was with me every step of the way. In many ways this has been a family effort, and little of this achievement would be possible without Melinda. Her companionship, patience, and loving support have been the foundation shaping all aspects of my life these last 13 years. As we turn to new things together, I thank Melinda for making so much of what we have already accomplished together possible.

TABLE OF CONTENTS

LIST OF FIGURES

LIST OF TABLES

LIST OF SCHEMES

ABSTRACT

Phosphorylation activity of the Cyclin Dependent Kinase (CDK) family of protein kinases regulates the progression of the cell cycle. Improper regulation of CDK activity is associated with the development of many cancers and other proliferative disorders. In this work, we have investigated the catalytic mechanism of fully activated CDK2 and have determined that under normal physiological conditions maximum activity is dependent on the binding of two Mg^{2+} ions in the kinase active site. We have shown that these two Mg^{2+} ions function to recruit ATP, stabilize the enzyme transition state to accelerate phosphoryl transfer, and then can limit and even slow the rate of ADP release. These are the first results that demonstrate that CDK2 requires two Mg^{2+} ions, resolving some ambiguities of the protein kinase mechanism. The complex, dynamic, and multiple activating and rate-limiting roles of the two Mg^{2+} ions observed for CDK2 may also exist in other kinases and explain why some kinases are observed to be activated by Mg^{2+} while others are inhibited. We have investigated the molecular details of the structure, dynamics, and activity of CDK2 at each stage of the catalytic cycle using X-ray crystallography, molecular dynamics calculations, and enzyme kinetics. We demonstrated the significance of the precise properties of Mg^{2+} binding by showing how allosteric effectors regulate the activity of CDK2 by tuning affinity of the second Mg^{2+} site. This same regulatory mechanism is conserved in other families of protein kinases.

CHAPTER 1

Introduction

The goal of my thesis research is to elucidate the molecular mechanisms of allosteric regulation of protein kinase activity. In other words, how do regulatory effectors of protein kinases actually manipulate phosphorylation activity? In particular, the focus is on how essential Mg^{2+} co-factors are related to both the catalytic mechanism and regulatory influence.

Protein kinases are known to function as molecular switches (Huse and Kuriyan, 2002). That is, kinase activity can be regulated, meaning that the cell can control a kinase's catalytic competency. Once turned on, kinase phosphorylation activity can then alter the functionality of other proteins. The fact that kinase activity can be regulated implies that regulatory effectors must be able to exert some control over the protein kinase chemical reaction mechanism. Therefore, to understand the mechanisms of protein kinase regulation, we must first understand the catalytic mechanism of the enzyme. Thus, my work has two important goals: 1) investigate CDK2 kinase activity to determine a kinetic description of the role of each component in the reaction, including the enzyme, substrates, products and cofactors, and 2) show how this kinetic mechanism relates to the regulation of kinase activity. This topic is of interest because protein kinases play crucial roles in the regulation of nearly all biological processes by functioning as cellular signaling enzymes. The need for the cell to maintain appropriate regulatory control over cellular signaling networks is paramount because the signals

transduced and integrated by protein kinases are well known to determine cell fate (Santamaria et al., 2007).

Protein kinases function as information processors of the cell, and therefore must respond to external, sometimes environmental, stimuli, then transmit a signal that the cell can make use of. The way that protein kinases achieve this is by phosphorylating other proteins – post-translationally labeling specific sites of substrate proteins by transferring the γ-phosphate of an ATP•Mg substrate to the target site. In the human "kinome" there are 518 functional protein kinases and a number of pseudokinases (catalytically incompetent kinases) (Manning et al., 2002). These 518 kinases are divided into a number of evolutionarily divergent families of protein kinases, all of which can be classified as Ser/Thr kinases, receptor Tyrosine kinases, and non-receptor tyrosine kinases. In this work, I primarily focus on the Ser/Thr kinase, Cyclin Dependent Kinase 2 (CDK2), but will begin to generalize to other kinases in the later chapters of the dissertation.

Role of protein kinases in oncogenesis

The role of protein kinases as cellular signal messengers and functional regulators places protein kinases in a critical role in the development of many cancers. The first identification of an oncogenic protein kinase was v-Src in the retroviral Rous sarcoma virus (Collett and Erikson, 1978; Levinson et al., 1978; Martin, 2004). The loss of a regulatory phosphorylation site on the c-terminal section of c-Src, caused the viral Src, v-Src, to become constitutively active (Smart et al., 1981; Thomas and Brugge, 1997). Unregulated tyrosine phosphorylation activity of v-Src was determined to be wholly responsible for the development of the cancer phenotype associated with Rous

sarcoma virus (Levinson et al., 1978). This is possible because v-Src signaling can activate a number of different cellular signaling pathways, resulting in cellular transformation. When a specific oncogene plays a causal role in the development of cancers, and the continued survival of the affected cells depends on the oncogene, inhibition of that oncogene may be therapeutic – the "oncogene addiction" hypothesis (Weinstein, 2002). The propagation of chronic myelogenous leukemia depends upon the unregulated activity of the oncogenic tyrosine kinase Bcr-Abl. The therapeutic inhibitor Imatinib for Bcr-Abl showed for the first time that inhibition of an oncogenic kinase could solely treat a cancer (Druker et al., 2001). One fascinating aspect of the interaction between Imatinib and the Abl catalytic kinase domain is that the drug functions by stabilizing a catalytically inactive conformation of the kinase, rather than directly out-competing one of the substrates to diminish kinase activity (Nagar et al., 2002). Another example of kinase involvement in cancer development is the CDK family protein kinases. The primary role of the CDKs is the regulation of the cell cycle – thus improper CDK activity can allow a cell to inappropriately enter or advance through the cell cycle. One of the hallmarks of the progression of many cancers is the loss of regulatory control of the cell cycle (Malumbres and Barbacid, 2007).

Regulation of protein kinases

Protein kinases have evolved many ways to regulate their activity. One important theme is the binding of an allosteric regulator to either activate or inactivate the protein kinase (Huse and Kuriyan, 2002; Jura et al., 2011). For example, in the family of Cyclin Dependent Kinases (CDKs), the CDKs are only active when heterodimerically bound to

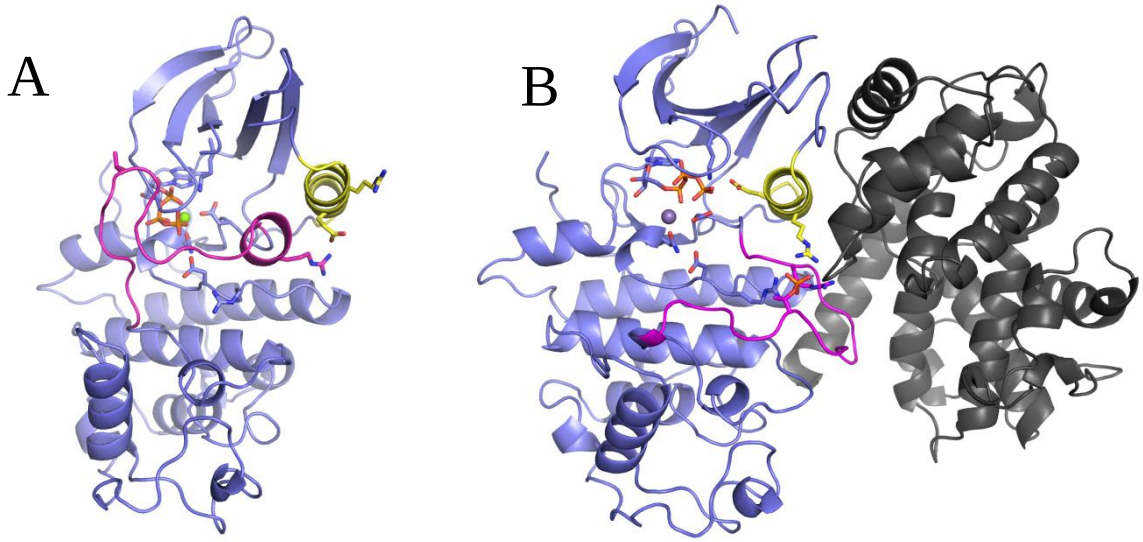

Figure 1-1. Structures of monomeric CDK2 and active pCDK2/Cyclin

A) Inactive monomeric CDK2 (PDB: 1HCK), **B)** Fully active pCDK2/Cyclin A with activation loop Thr160 phosphorylated (PDB: 1JST). **In all panels)** The c-α-helix is highlighted in yellow, and the activation loop in magenta on each structure. Residues shown in stick form include active site residues Lys33, Asp145 and Asn132, and regulatory residues Glu51 and Thr160.

an allosteric activator called Cyclin, structures shown in Figure 1-1 (Radzio-Andzelm et al., 1995; Stevenson et al., 2002). Another common activation theme is single- or multiple-phosphorylation on the kinase activation loop (Thr160 for CDK2) (Hagopian et al., 2001). Many kinases also have inactivating phosphorylation sites, particularly on the Gly-rich loop near the ATP-binding cleft, and allosteric protein inhibitors, such as p27/ink4 for the CDKs, or the SH2 domain of c-Src.

For the CDKs, the role of Cyclin is not limited to allosteric activation, and it is important to understand the larger context of the regulatory apparatus acting upon CDK activity. There are many different Cyclins which are either expressed or specifically ubiquitinated and then degraded at different stages of the eukaryotic cell cycle, and many

of the CDKs can bind different Cyclins (Santamaria et al., 2007). For example, CDK2 binds Cyclin E or Cyclin A as part of its physiological function, while CDK1 binds Cyclin A or Cyclin B (Malumbres and Barbacid, 2007). In fact, there is redundancy in the CDK catalytic domain roles, such that CDK1 can largely replace CDK2 in CDK2-knockout mice (Santamaria et al., 2007). Furthermore, viral Cyclins can activate the CDKs to escape some of the normal regulatory mechanisms (Mittnacht and Boshoff, 2000). The Cyclins provide a temporal signal to activate the CDKs, but also guide CDK substrate specificity by providing substrate recruitment binding sites distal to the target phosphorylation site that the CDK acts upon (Brown et al., 1999a). For example, under normal physiological conditions, CDK2 in combination with Cyclin E provides the phosphorylation signal to move the cell through the restriction point separating Growth Phase 1 from DNA Replication phase (Zetterberg et al., 1995; Malumbres and Barbacid, 2007). Next, CDK2 bound to Cyclin A provides a phosphorylation signal to a different set of substrates to push the cell through DNA Replication phase. Regulatory mechanisms working to optimize activity on multiple levels is a theme we will return to later in this dissertation document.

Structure of Protein Kinases

Protein kinases are well known to switch between inactive conformations and a structurally conserved active conformation as a direct result of cellular regulatory action on the kinase domain. The active conformation of many protein kinases have been characterized by X-ray crystallography. There are relatively fewer crystal structures of inactive kinase conformations. Some representative kinases for which inactive and active structures have been characterized include Src (non-receptor tyrosine kinase) (Xu et al.,

1999; Azam et al., 2008), EGFR (receptor tyrosine kinase) (Jura et al., 2011), and CDK2 (Ser/Thr kinase) (Radzio-Andzelm et al., 1995; Schulze-Gahmen et al., 1996). The active conformation of protein kinases is strongly conserved, while the structurally variable inactive conformations are representative of the many regulatory strategies that are employed in stabilizing or destabilizing the active kinase conformation (Huse and Kuriyan, 2002).

The overall fold and composition of the protein kinase catalytic domain is shown in Figure 1-2. Protein kinases have a bi-lobal tertiary structure where the N-lobe is primarily composed of β-sheets and the C-lobe is principally α-helical. The active site (ATP•Mg binding site) is sandwiched between the N- and C-lobes. There are several universally conserved amino acid residues located in the active site of an active conformation protein kinase. Using human CDK2 protein sequence numbering, Lys33 coordinates the α/β nucleotide phosphates, which is in turn coordinated by Glu51. From the C-lobe, Asn132 and Asp145 (the "DFG" motif Asp) coordinate catalytically functional Mg^{2+} ions, which in turn coordinate nucleotide phosphate positioning. Finally, Asp127 (the "HRD" motif Asp) and Lys129 help to coordinate the protein substrate during catalysis. The functional role of Asp127 as a proton-acceptor (catalytic base) has been debated and remains an open question in the kinase field.

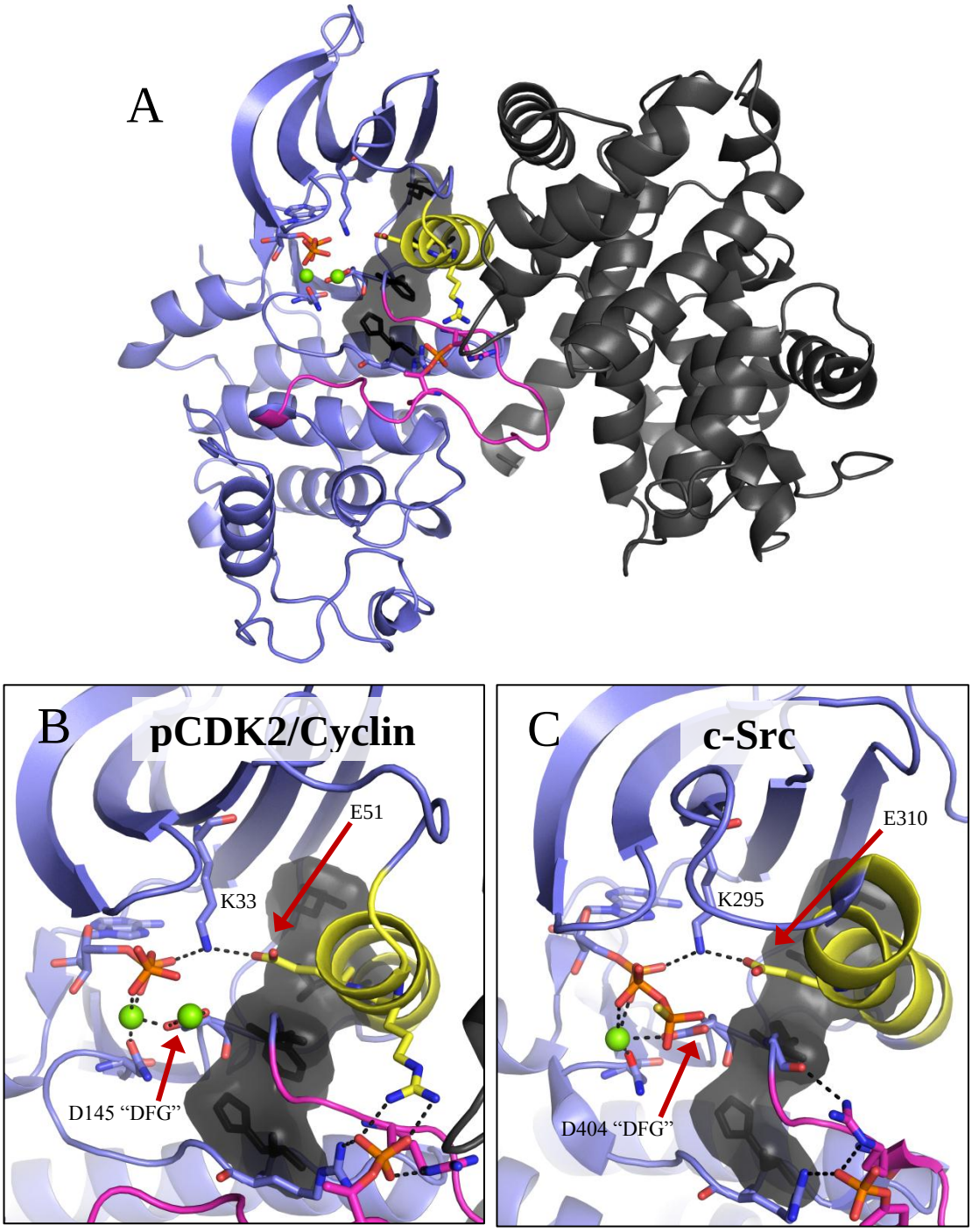

Figure 1-2. Protein kinase conserved elements.

Panel A) Active conformation pCDK2/Cyclin bound to ADP. Panel B) Active site closeup of pCDK2/Cyclin bound to ADP. Panel C) Active site closeup of active c-Src (PDB: 3DQX). C-a-helix shown in yellow. Activation loop shown in magenta. Black surface shows hydrophobic spine.

Besides the specific organization of the conserved active site residues, there are a number of important conserved structural elements, shown in Figure 1-2. The c-α-helix, which will be discussed in depth in Chapter 4, is the only N-lobe α-helix, and plays a strong role in chemistry and kinase activity regulation. The active conformation "hydrophobic spine", also called the R spine, is a series of non-consecutive hydrophobic residues that stack from the C-lobe (F-helix) through to the N-lobe (Kornev et al., 2006). The contribution of stabilizing effects of the R spine are not well established, however the His in the "HRD" catalytic motif, and the Phe in the "DFG" motif both participate in the R spine, suggesting that these interactions may stabilize the residues of these important motifs (Taylor and Kornev, 2011). The activation loop is another site of kinase regulation which helps to determine protein substrate specificity. Activation loop conformation and phosphorylation states affect substrate binding by both providing active site accessibility as well as providing specific electrostatic interactions to the protein substrate (Radzio-Andzelm et al., 1995; Schulze-Gahmen et al., 1996; Stevenson et al., 2002). Finally, the conformational variability of the Gly-rich loop on the N-lobe plays a role in catalytic cycle progression, as will be discussed in chapters 2 and 3.

As previously mentioned, the active conformation of the kinase catalytic domain is strongly conserved, especially the construction of the active site (Huse and Kuriyan, 2002). Inactive conformations are less well characterized. Some of the mechanisms of protein kinase regulation have been inferred by comparing inactive conformations to active conformations. For example, the "DFG flip", first observed in Abl kinase, re-organizes the Mg/phosphate-binding DFG motif to be incapable of coordinating phosphates (Nagar et al., 2003). Another common theme is rotation/alteration of c-α-

helix conformation to, among other changes, break the conserved active site Lys33-Glu51 salt bridge (Radzio-Andzelm et al., 1995; Williams et al., 1997; Zhang et al., 2006). Finally, the activation loop of many inactive kinases is disordered or sterically occludes the active site, preventing protein substrate from assuming a catalytically competent binding conformation (Huse and Kuriyan, 2002).

The cell can control kinase activity by using allosteric regulators to influence the relative stability of a kinase's active or inactive conformation. One scheme is the allosteric activation that Cyclin confers to CDK2, whereby monomeric CDK2 most stably assumes the inactive conformation, and the binding of Cyclin stabilizes the active conformation of CDK2 (Radzio-Andzelm et al., 1995; Stevenson et al., 2002). Other CDK regulatory proteins, such as INK4 or $p27^{Kip1}$ disrupt the active conformation or sterically block substrate binding to prevent catalytic activity (Russo et al., 1996a; Pavletich, 1999). c-Src, on the other hand, is held in its inactive conformation by the regulatory interaction of the c-Src SH2 domain with a phosphorylated Tyrosine on the C-terminal region of the c-Src catalytic domain (Williams et al., 1997). When the interaction between the catalytic and SH2 domains of c-Src is disrupted, the active conformation is relatively stabilized (Huse and Kuriyan, 2002). Thus some kinases, like CDK2, are catalytically inactive by default, while others, like Src, are active by default.

Protein kinase catalytic cycle

Once the active conformation of a protein kinase is properly assembled and stabilized, the kinase is competent to enter into its catalytic cycle. Since the function of a protein kinase is to transfer the γ-phosphate from ATP•Mg to a target protein sidechain, the kinase must bind both ATP•Mg and the protein substrate to the active site prior to the

chemistry step. Following the enzyme/substrate complex assembly, phosphoryl transfer can proceed, producing two reaction products: ADP•Mg, and phospho-protein. Finally, the release of these two products allows the apo kinase to then re-enter the catalytic cycle. This basic reaction cycle is shown in Scheme 1-1 (Adams and Taylor, 1992).

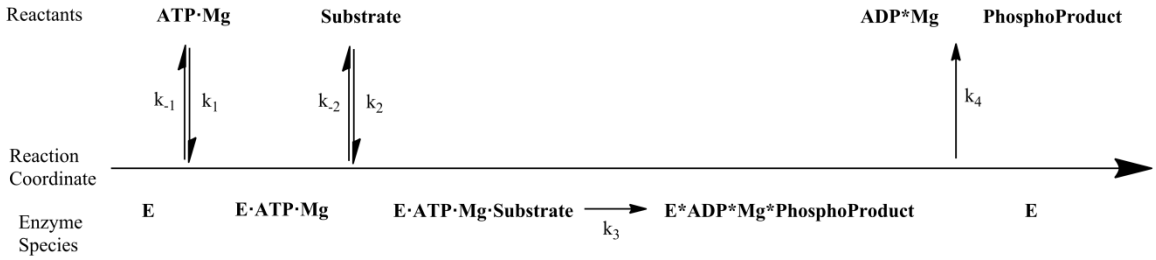

Scheme 1-1. Classic kinase reaction scheme

Nucleotide di- and tri-phosphates bind Mg^{2+} and other divalent metals extremely efficiently (Kd ADP:Mg ~ 400μM [Mg], Kd ATP:Mg ~ 28μM [Mg], (Storer and Cornish-Bowden, 1976)). Under normal physiological conditions ATP^{4-} chelates a single Mg^{2+} ion, forming the $(ATP•Mg)^{2-}$ complex. Thus, many enzymes, including small G-proteins (Zhang et al., 2000), DNA polymerases (Yang et al., 2004), helicases (Frick et al., 2007), and kinases (Adams, 2001), which make use of NTPs do so by coordinating at least one Mg^{2+} ion to coordinate the phosphates. The phosphate binding portion of the protein kinase active site is extremely electronegative, having a number of conserved negative charges including E51, D127, D145, and others depending on the kinase. Thus, to bind and coordinate the electro-negative phosphates into the similarly electro-negative active-site, the kinase utilizes Mg^{2+} ions to adapt the phosphates into the active-site environment. Crystal structures of protein kinase A (PKA) bound to ATP•Mg and

protein substrate identify two Mg^{2+} ions in the active site (Zheng et al., 1993a, 1993b) whereas nearly all other protein kinases, such as CDK2 (Radzio-Andzelm et al., 1995), bound to ATP or ATP analogues identify a single Mg^{2+} ion in the active site. Furthermore, it was found in PKA that these two Mg^{2+} sites have different stability constants – meaning that one site binds Mg^{2+} tighter than the other site (Zheng et al., 1993a). The kinetic behavior of PKA as Mg^{2+} is titrated into the reaction led to the conclusion that tighter binding Mg site is "essential" and the weaker Mg site is "inhibitory" (Adams and Taylor, 1993).

The different observations of either one or two Mg^{2+} ions in different protein kinases, combined, in my opinion, with the proclaimed inhibitory nature of the 2^{nd} Mg^{2+} ion in PKA, has led some to conclude that protein kinases require a single Mg^{2+} ion to catalyze the phosphoryl transfer reaction. At least two QM/MM simulation studies have computed potentials of mean force (PMFs) of the pCDK2/Cyclin reaction using a single metal (De Vivo et al., 2007; Smith et al., 2011).

Growing evidence in many kinases including CDK5 (Liu et al., 2010), ERK2 (Waas and Dalby, 2003), v-Fps (Saylor et al., 1998), and Csk (Grace et al., 1997) have shown that the phosphoryl transfer reaction is activated – not inhibited – by the presence of a second Mg^{2+} ion, either through effects on k_{cat} (the maximal reaction rate), or $K_{M(ATP•Mg)}$ (utilization/binding of ATP•Mg). Furthermore, QM/MM calculations of PKA have shown that the second Mg^{2+} ion stabilizes transition state formation rather than inhibiting the reaction (Cheng et al., 2005). Finally, predictions from our own longer timescale MD simulations (50-250ns) of pCDK2/Cyclin bound to the either ATP or ADP indicate that phosphate and active site positional stability over the course of the

simulation is greatly enhanced by the inclusion of a 2nd Mg^{2+} ion, or as will be seen, some other countercharge.

Therefore there are open questions about what the true role of the 2nd Mg^{2+} ion is in the protein kinase active site. Is the 2nd Mg^{2+} an inhibitor of the reaction, a non-essential activator, or an essential component of the transition state? It is surprising that there is so much confusion over this point, and that the proposed roles of the 2nd Mg^{2+} ion in the reaction are opposing – either activating or inhibiting! The reason for this is that the tight binding affinities of di- and tri- phosphates for Mg^{2+} leads to complex effects in the reaction which make it hard to separate the contributions of ATP•Mg, ADP•Mg, and free Mg^{2+} ions – and of course all three species play a role in the kinase reaction. Combined with the variance in the response of different protein kinases to magnesium concentration, the difficulty in unraveling the role of magnesium is understandable.

Overview of the Dissertation

The principal function of the protein kinase is to manipulate the phosphates to catalyze the phosphoryl transfer reaction, and therefore it is critical to have a more complete description of how the kinase achieves this. Due to the close association between ATP and Magnesium and the unclear nature of the interaction between Magnesium and protein kinases, it is therefore critical to gain better understanding of how Magnesium interacts with the kinase, the substrates, and the reaction products. The hypothesis is that a more complete description of the catalytic mechanism of CDK2, and thus a more complete description of the chemical constraints on the reaction, will help to explain the molecular mechanism of the regulatory activation by Cyclin of CDK2.

In chapter 2, a transition-state mimic structure of pCDK2/Cyclin reveals the conformation and chemical components required to stabilize the transition state of the reaction. The binding of a second Mg^{2+} ion to the active site stabilizes the conformational changes associated with formation of the transition state.

In chapter 3, the essential role of the second Mg^{2+} ion in the reaction is established. The dual nature of the second Mg^{2+} in the active site is explored, and the metal is found to activate ATP•Mg binding and phosphoryl transfer while simultaneously limiting the rate of the reaction by cooperatively enhancing binding of the ADP•Mg product to the active-site.

In chapter 4, the molecular mechanism of allosteric activation by Cyclin upon CDK2 is investigated. The electrostatic effects of rotating Glu51 into the active-site, a conformational change stabilized by Cyclin binding, enhances binding of the second Mg^{2+}, resulting in activation by making Mg^{2+} binding favorable under physiological conditions. Calculations and kinetic measurements of evolutionarily distant c-Src show that these conclusions may be generalized to the wider protein kinase family, at least those kinases that are regulated by c-α-helix rotation.

CHAPTER 2

Briefly bound to activate: transient binding of a second catalytic magnesium activates the structure and dynamics of CDK2 kinase for catalysis.

Foreword

This chapter has been previous published in the May, 2011 issue of *Structure*, and is reproduced in this dissertation with permission from Cell Press/Elsevier. The content has not been altered from the published form except that the citation form and figure names and table names have been altered to meet the standard of the formatting requirements of the dissertation document. Additionally, the online supplementary material is included herein as the Chapter 2 Appendix.

The reference for the published document:

Bao ZQ*, Jacobsen DM*, Young MA. "Briefly bound to activate: transient binding of a second catalytic magnesium activates the structure and dynamics of CDK2 kinase for catalysis.", *Structure*, 2011; 19 (5): 675-690; *Co-first authors

This work represents a collaborative portion of the dissertation research, and thus I will enumerate major individual contributions. The inclusion of this work is critical to the understanding of all subsequent discussion and presentation in the dissertation.

Bao ZQ's contributions: molecular biology (protein DNA cloning, *E. coli* transformation), protein preparation & purification, development of pCDK2/Cyclin

complex crystallization protocol, preparation of transition-state-mimic crystals, and PK/LDH enzyme coupled kinase assay experiments (shown specifically in this work).

Jacobsen DM's contributions: protein crystal data collection, contributed (with MY) in determining structure solution, determined new crystal soaking protocol to enhance TS electron density, equilibrium molecular dynamics simulation and analysis, development of analytical tools to highlight active site motion, preparation of many figures and figure captions in paper, wrote some of the methods, and assisting in editing the paper prior to submission.

Young MA's contributions: advising Bao and Jacobsen throughout project, ^{32}P labeling assay (kinase enzyme kinetics), protein crystal data collection, structure solution, and wrote/edited much of the published document.

Abstract

We have determined high-resolution crystal structures of a CDK2/Cyclin A transition state complex bound to ADP, substrate peptide, and MgF_3^-. Compared to previous structures of active CDK2, the catalytic subunit of the kinase adopts a more closed conformation around the active site and now allows observation of a second Mg^{2+} ion in the active site. Coupled with a strong [Mg^{2+}] effect on in vitro kinase activity, the structures suggest that the transient binding of the second Mg^{2+} ion is necessary to achieve maximum rate enhancement of the chemical reaction, and Mg^{2+} concentration could represent an important regulator of CDK2 activity in vivo. Molecular dynamics simulations illustrate how the simultaneous binding of substrate peptide, ATP, and two Mg^{2+} ions is able to induce a more rigid and closed organization of the active site that

functions to orient the phosphates, stabilize the buildup of negative charge, and shield the subsequently activated γ-phosphate from solvent.

Introduction

Protein kinases represent one of the fundamental components of cell-signaling pathways in all organisms. CDK2 is a mammalian Ser/Thr kinase that plays a critical role in controlling the progression from G1 to S phase of the cell cycle (Morgan, 1997). CDK2 is functionally homologous to the well-studied cdc28a *S. cerevisiae* protein. Consistent with its important role in influencing progression through the cell cycle, the activity of the enzyme is subject to many levels of regulation. Misregulation of CDK2 activity, for example through mutation, may contribute to the development of human cancers (Milde-Langosch et al., 2001; Greenman et al., 2007; Malumbres and Barbacid, 2007), and CDK2 represents a potential therapeutic target (Malumbres and Barbacid, 2009). The isolated 34 kDa catalytic subunit of CDK2 exhibits relatively negligible catalytic activity, and the cellular concentration remains constant through the cell cycle. Maximum protein kinase activity is not obtained until the catalytic subunit is bound by an allosteric Cyclin protein (Radzio-Andzelm et al., 1995) and the catalytic domain has been phosphorylated on Thr-160, located within the kinase "activation loop" motif (Stevenson et al., 2002). The binding of Cyclin and the phosphorylation of Thr-160 have both been shown to stabilize large-scale conformational changes in the catalytic domain that function both to increase affinity for substrate (reduce K_M) as well as enhance the catalytic rate of the reaction (increase k_{cat}) (Pavletich, 1999; Brown et al., 1999b). In addition to allosterically upregulating catalytic activity upon binding to the catalytic domain, the Cyclins are also able to assist in the recruitment of specific protein substrates

by binding to recruitment motifs. CDK2 is negatively regulated by the binding of a number of inhibitory proteins such as the p21Cip and p27KIP families, as well as by the phosphorylation of Tyr-15 and Thr-14 within the catalytic subunit. Multiple crystal structures are available for a number of the functional states of CDK2 (Pavletich, 1999).

Because they carry out very similar chemistries, it has been suggested that the majority of protein kinases may be subject to functional restrictions that require them to adopt very similar conformations when they are in their catalytically competent state. Hence, it could be the differences between their catalytically downregulated structures that might be responsible for much of their functional diversity (Huse and Kuriyan, 2002). Although there is growing evidence to support this hypothesis, direct structural and experimental data on active kinases caught in the act of catalysis have been difficult to obtain. Many enzymes catalyze similar reactions that liberate the γ-phosphate from a nucleotide triphosphate (NTP), but details such as the nature of the stabilizing protein side chains or the number of catalytic metals are not always conserved. Given the large number of protein kinases and the diverse signaling pathways they take part in, we cannot assume that they all operate using identical chemistries. For example, whereas many protein kinases are believed to require two divalent metal ions for optimum catalysis (Adams, 2001), it was recently established that at least one protein kinase, CASK, is only active in the complete absence of any divalent ions (Mukherjee et al., 2008). There is structural evidence that many kinases may only utilize a single divalent ion. The potential difference in the number of Mg^{2+} ions utilized by different kinases is especially important in the context of looking at the entire ensemble of over 500 protein kinases in the human genome (Manning et al., 2002) because identifying any differences in the details of how

individual enzymes catalyze the reaction could provide important insight into the origins of functional and regulatory diversity among kinases. This information could also contribute to our understanding of how activating mutations result in misregulation of specific kinases and could even be helpful in the rational design of specific protein kinase inhibitors. Kinase-specific differences in the function of the highly conserved "DFG" motif, which is essential for coordinating active site Mg^{2+} ions, are believed to be a critical determinant of the specificity profile of the clinically successful kinase inhibitor Gleevec as well as other DFG-out or "type-II" kinase inhibitors (Liu and Gray, 2006).

The most detailed model for the transition state (TS) conformation of a protein kinase is the AlF_3 TS mimic of protein kinase A (PKA) (Madhusudan et al., 2002). This 2.0 Å structure highlights a significant point of distinction between PKA and CDK2: all published structures of CDK2 bound to nucleotides identify at most a single Mg^{2+} ion in the active site, whereas the PKA TS structure clearly contains two catalytic Mg^{2+} ions that are in direct coordination with the reactive phosphates. Many NTP enzymes utilize a single metal ion, and a one Mg^{2+} (1Mg) mechanism for CDK2 is certainly reasonable. A structure of active CDK2 bound to nitrate (NO_3^-), a potential TS mimic, has been determined, showing a single Mg^{2+} ion in the active site (Cook et al., 2002), and a single Mg^{2+} mechanism for CDK2 has been proposed and shown to be energetically feasible via quantum mechanical simulations (De Vivo et al., 2007). Given the flexible nature of protein kinases, it is likely that a number of different protein conformations and ligand/activator states are sampled along the reaction cycle and that different structures may indeed represent different conformations within the same ensemble of transiently occupied states. Extensive studies of PKA support the notion that the role of Mg^{2+} ions at

different stages of the catalytic cycle is dynamic and rather complex, with one of the two Mg^{2+} ions referred to as "essential" and the second as "inhibitory" (Shaffer and Adams, 1999). Therefore, it is still uncertain whether CDK2 utilizes a single Mg^{2+} ion for the phosphoryl-transfer step and is truly different from the two Mg^{2+} (2Mg) mechanism observed in PKA or whether a 2Mg CDK2 state has just not yet been observed.

A related and also elusive question in the mechanism of protein kinases is the possible role that protein dynamics may play in both the catalytic mechanism as well as the regulation of catalytic activity. Structures of a number of protein kinases have revealed how flexible the catalytic domain can be, especially in facilitating the disassembly of the catalytically competent active site to adopt a downregulated state. It has been proposed that kinases, like other enzymes, may have evolved to channel or funnel specific protein motions in order to assist the reactants in sampling and progressing through the high-energy TS of the reaction (Henzler-Wildman et al., 2007; Kamerlin and Warshel, 2010), but this idea is difficult to prove (Li et al., 2002; Kamerlin and Warshel, 2010). Once again, the challenges associated with obtaining experimental and structural data on protein kinases at each step of the catalytic reaction have made it difficult to fully understand the functional roles of protein dynamics and its differences within the divergent protein kinases.

To better understand the detailed mechanism of the CDK2 kinase reaction, we have determined new crystal structures of an active phospho-CDK2/Cyclin A complex bound to ADP, a substrate peptide, and MgF_3^-, a mimic for the γ-phosphate of ATP in the TS. We believe this complex provides an informative model of the structure of the enzyme during the phosphoryl-transfer step, one of the key rate-limiting steps of the

reaction. We have carried out a series of molecular dynamics (MD) simulations to investigate the possible roles of protein dynamics in the catalytic mechanism of CDK2. Based on these results, we propose that the transient binding of a second activating Mg^{2+} ion to the active site of CDK2 helps facilitate the phosphoryl-transfer step by simultaneously closing down the active site by expelling water, electrostatically stabilizing the reactants, and reducing the conformational flexibility of the ATP.

Results

Overall Structure of the Complex

The architecture of the phosphorylated P-Thr160 CDK2/Cyclin A complex (pCDK2/Cyclin A) bound to ADP/MgF_3^-/peptide is shown in Figure 2-1A. We have determined two independent but very similar structures of the complex, solved at slightly different pHs (Table 1). The overall conformation of the complex in the TS structures is similar to previously published structures of P-Thr160 CDK2 bound to Cyclin A, all crystallized in different buffer conditions and different space groups. The overall Cα rmsd to an ATP-γS bound CDK2/Cyclin A complex is 1.1 Å (Russo et al., 1996b), and Cα rmsd to an AMPPNP/peptide CDK2/Cyclin A complex is 0.7 Å (Brown et al., 1999a).

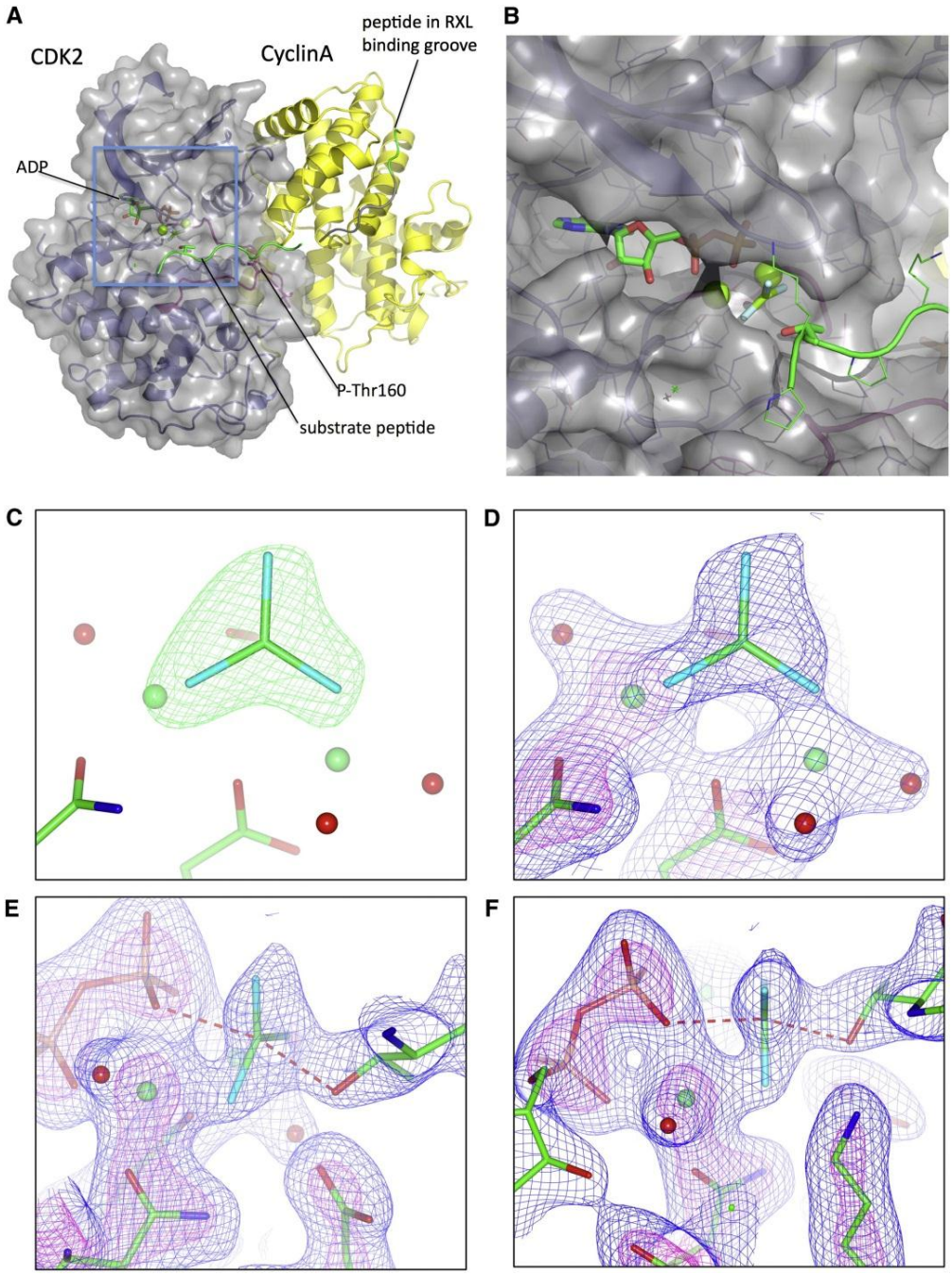

Figure 2-1. Structure of pCDK2/Cyclin A/ADP/MgF_3^-/Peptide Complex and Details of the Active Site.

(A) Overview of the complex. Catalytic subunit is gray and Cyclin A is yellow. (B) Close-up of the protein active site (region highlighted in A) showing the ADP, Mg ions, MgF_3^-, and the peptide substrate (green). The C-terminal region of a second copy of the substrate peptide (PKTPKKAKKL) was determined to have bound to the "RXL" substrate-binding groove on Cyclin A and is also shown in green. The N-terminal region of this peptide shown in gray is largely disordered and was modeled at zero occupancy. (C) fo-fc difference map (5σ) from an averaged kicked omit map where the MgF_3^- was omitted from the model. (D–F) Three views of the 2fo-fc electron density (blue, 1.25σ; magenta, 3.5σ) at the active site. Red spheres are waters and green spheres are Mg^{2+}. See also Figure 2-10.

Table 2-1. Data collection and Refinement Statistics

	pCDK2/Cyclin A/MgF_3^- /Peptide (pH 8.0)	pCDK2/Cyclin A/MgF_3^- /Peptide (pH 8.25)
Data Collection		
Space Group	$P2_1$	$P2_1$
Cell dimensions		
a, b, c (Å)	a = 70.69, b = 163.91, c = 73.28	a = 71.03, b = 163.45, c = 73.39
α, β, γ (°)	α = 90.0, β = 107.38, γ = 90.0	α = 90.0, β = 107.08, γ = 90.0
Resolution (Å)	2.17 (2.29-2.17)[a]	1.91 (2.01-1.91)[a]
R_{sym}	13.2 (112)	14.0 (114)
I/σ(I)	7.4 (1.5)	8.6 (1.5)
Completeness (%)	100 (100)	100 (100)
Redundancy	3.9 (3.8)	7.6 (7.5)
Refinement		
Resolution (Å)	37.8-2.17	39.75-1.91
Number of reflections	323,456 (83,902 unique)	935,485 (123,328 unique)
R_{work}/R_{free}	17.38%/20.71%	19.02%/21.42%
Number of atoms	10,089	10,041
Protein	9,476	9,438
Ligand/ion	33	33
Water	613	684
B factors		
Protein	54	42
Ligand/ion	66	46
Water	59	47
RMSD from ideal		
Bond lengths (Å)	0.012	0.008
Bond angles (°)	1.3	1.1

Values in parentheses are for highest-resolution shell. [a]Data were collected from a single crystal.

A close-up view of the pCDK2/Cyclin A active site is shown in Figure 2-1B. Each structure contains two copies of the CDK2/Cyclin A complex, and we can clearly visualize the ADP, the 10-residue substrate peptide, and a trigonal-planar MgF_3^- ion positioned between the ADP β-phosphate and the Thr γ-O atom of the substrate peptide in each of them. A 2Fo-Fc electron density map of the reactants is shown in Figure 2-1D–F, including distinct density for the 2Mg ions we observe. Each Mg^{2+} is in direct van der Waals contact with one of the fluorine atoms of the MgF_3^- phosphate mimic as well as five additional electronegative oxygen atoms at distances of 1.9–2.5 Å, described in more detail below.

MgF_3^- Transition State Mimic

A number of different chemical species have been employed along with an NDP to mimic the γ-phosphate TS in NTP reactions, including AlF_3, AlF_4^-, BeF_3, NO_3^-, and vanadate. Different species work best with different enzymes. Here, we use MgF_3^- as a TS mimic of the γ-phosphate of ATP. The titration of MgF_3^- into the CDK2 kinase reaction demonstrates that MgF_3^- is able to inhibit the CDK2 kinase reaction in vitro (see Figure 2-10 in chapter appendix). The TS crystals were prepared by soaking apo crystals of the pCDK2/Cyclin A complex in buffer containing ADP, Mg^{2+}, NaF, and substrate peptide. To verify presence of MgF_3^- in the crystal, Figure 2-1A shows an Fo-Fc "average kicked" omit map calculated in PHENIX(Adams et al., 2010) after removing the MgF_3^- from the model. A series of studies have suggested that MgF_3^- can function as a superior TS mimic for certain phosphoryl-transfer enzymes because the −1 charge of MgF_3^- more closely resembles the true PO_3^- intermediate compared with neutral-charge species such as AlF_3 (Graham et al., 2002; Baxter et al., 2006, 2008). This hypothesis is

supported by the observation that AlF_3 is sometimes converted to the square-planar AlF_4^- form when used as a TS mimic. The trigonal-planar MgF_3^- in the CDK2 TS structures is coordinated by a number of positively charged protein atoms as well as metal ions, suggesting that reproducing the −1 charge of the true PO_3^- metaphosphate anion intermediate (Westheimer, 1987) is important.

Glycine-Rich (Gly-rich) Loop

The conformation of the Gly-rich loop (residues 10–18) that functions somewhat like a lid on top of the ATP phosphates is quite different from what has been observed in all previously published structures of the pCDK2/Cyclin A complex. As shown in Figure 2-2, the N-lobe of the kinase is rotated clockwise in the direction of the nucleotide phosphates relative to 1JST.pdb, a structure of ATP γ-S bound pCDK2/Cyclin A with a single Mn^{2+} ion, such that the TS conformation significantly reduces the volume of the nucleotide-binding pocket that sandwiches the phosphates. Although there is considerable variation in the N-lobe position between the two conformations, Lys-33, which interacts with both an ATP α-phosphate oxygen and Glu-51 in α helix C, is nearly structurally invariant between the two conformations and appears almost to function as a fixed pivot point for the N-lobe rotation and closure.

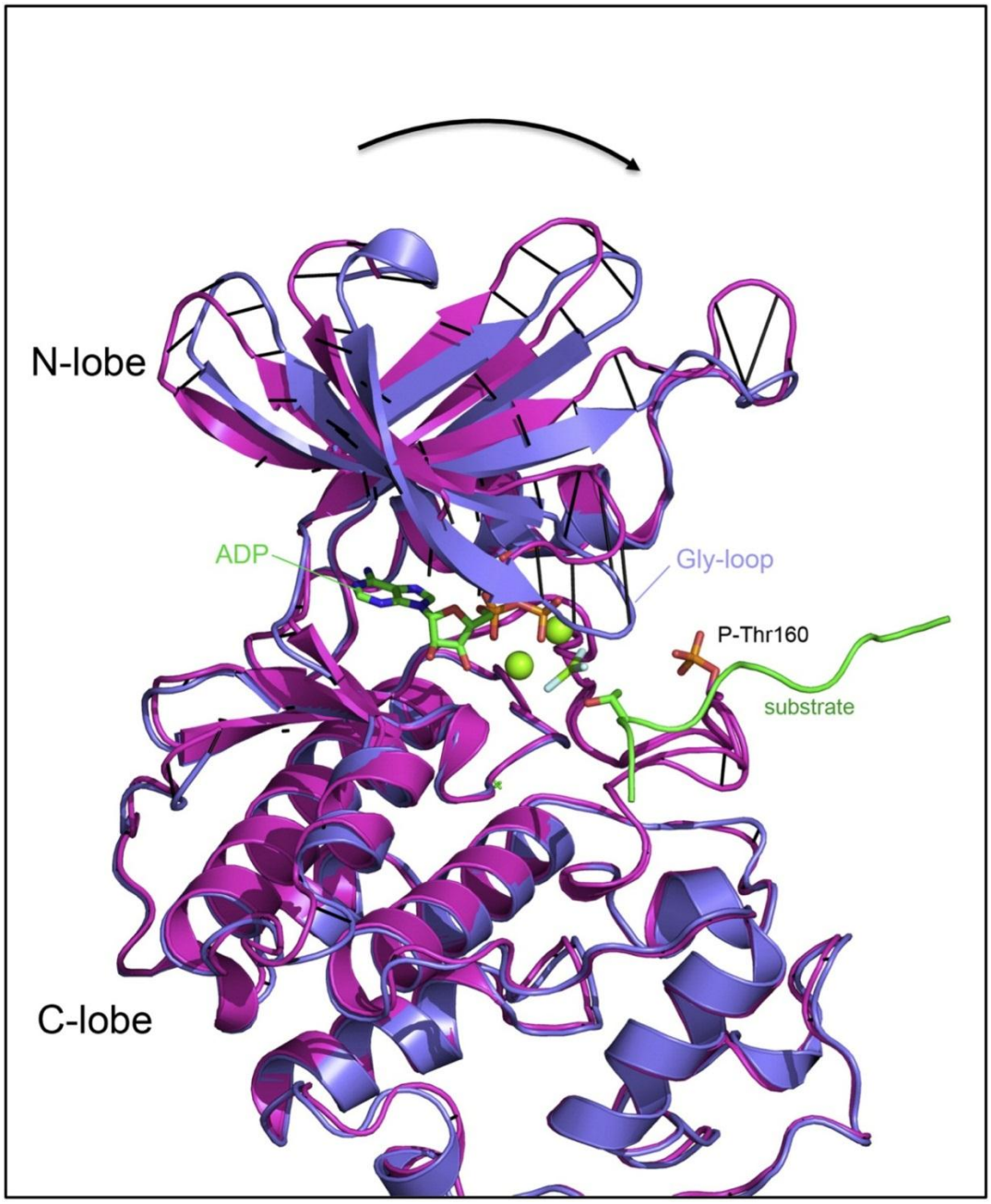

Figure 2-2. Motion of the N-Lobe Induced upon Binding of Peptide Substrate and the Second Mg^{2+} Ion.

Magenta is 1JST.pdb, the pCDK2/Cyclin A complex bound to ATP and 1 Mn^{2+} ion. Blue is the TS structure of pCDK2/Cyclin A bound to ADP/MgF_3^-/2×Mg^{2+}/peptide substrate. The structures were aligned on α -Carbons (Cα) of the whole complex using PyMOL (Schrödinger, 2010) with black lines drawn to indicate equivalent Cα atom positions.

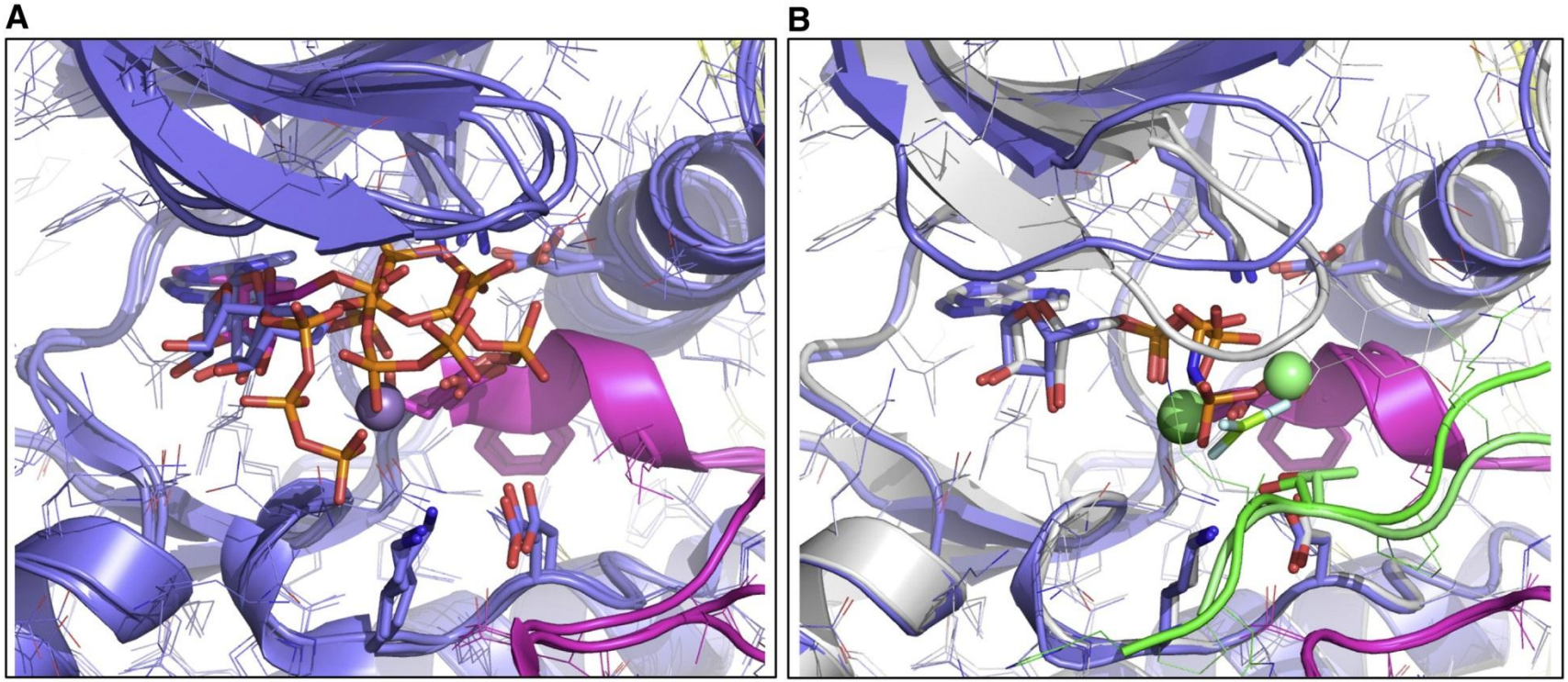

Figure 2-3. A Comparison of the Active Site Region of CDK2/Cyclin A Bound to ATP Analogs and CDK2/Cyclin A with the TS Complex.

Panel A) A superimposition of three independent crystal structures of the CDK2/Cyclin complex showing the different conformations of the nucleotide and Gly-rich loop (pdb entries: 1fin, 1jst, 2hcc). Residues in the kinase activation loop (145–168) are colored magenta. **Panel B)** Superposition of 1QMZ.pdb, pCDK2/Cyclin A bound to AMPPNP/1Mg ion/substrate peptide (blue), with the TS structure (gray).

We compare the conformation of the CDK2 Gly-rich loop TS structure with four published structures of pCDK2/Cyclin A bound to ATP analogs in Figure 2-3. The range of Gly-rich loop conformations illustrates the flexibility of this substructure. The conformations of the nucleotide phosphates in these structures, especially the β- and γ-phosphates, appear to mirror this flexibility. Despite the range of conformations observed for the ATP phosphates and the local flexibility of the Gly-rich loop, the positioning of the flexible Gly-rich loop in our TS structure (indicated in gray in Figure 2-3B) is a notable outlier. The conformation of the Gly-rich loop in the TS has closed down in such a way that the backbone amides make direct interactions with both the ADP β-phosphate and the MgF_3^- γ-phosphate mimic. The Gly-rich loop region of the protein is far from any crystallographic neighbors in the TS structure, so it is not likely to be a consequence of crystal packing.

This closed conformation of the TS Gly-rich loop is similar to the one observed for the inactive state of the CDK2 catalytic domain (1HCK.pdb) (Schulze-Gahmen et al., 1996). Although the conformation of the unphosphorylated activation loop in the inactive CDK2 monomer inhibits substrate peptide from binding via steric hindrance, we believe that the similar Gly-rich loop conformation attests to the thermodynamic stability of the closed conformation of the Gly-rich loop for CDK2.

The structure of the CDK2 TS Gly-rich loop is also strikingly similar to the structure of the TS mimic structure of PKA bound to ADP/AlF_3 and a high-affinity PKI-derived substrate peptide (1L3R.pdb, Figure 2-4). Although the TS active site conformations are very similar, CDK2 is different from PKA because it appears to undergo both structural changes and an overall ordering of the active site when

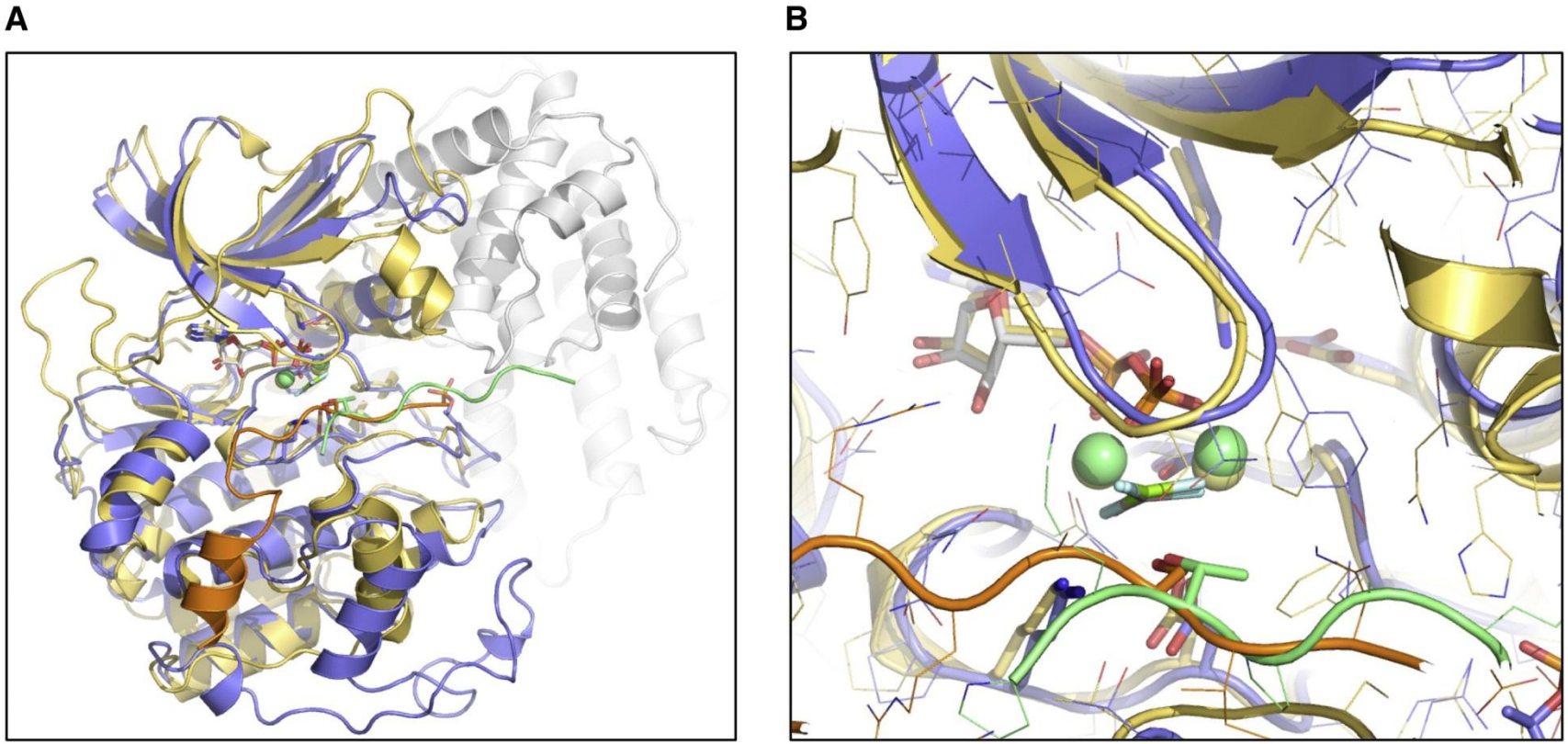

Figure 2-4. Comparison of the CDK2 TS Complex with PKA.

(Panel A) Superimposition of the TS mimic complexes of CDK2 and PKA (1l3r.pdb). CDK2 is blue/green, Cyclin A is gray, and PKA is gold/orange. (Panel B) Close-up of the active sites

transitioning from the ATP-bound state to the TS conformation, whereas PKA was described to undergo only very slight structural changes (Madhusudan et al., 2002). However, it should be noted that recent results and discussion point to the possibility that the PKA Gly-rich loop might also behave in a more dynamic way and undergo open to closed motions similar to what we see in CDK2 (Masterson et al., 2010) when not interacting with high-affinity peptide inhibitors (Zimmermann et al., 2008).

Two Magnesium Ions

To the best of our knowledge, these are the first pCDK2/Cyclin A crystal structures grown in the presence of Mg^{2+} because Mg^{2+} was observed to inhibit the growth of other CDK2/Cyclin A crystal forms (Jeffrey et al., 1995). The TS crystals were grown in the presence of 20 mM Mg^{2+} and were then transferred and soaked in a solution containing a more physiologically relevant 10 mM $MgCl_2$ prior to mounting. This might have resulted in our ability to identify 2Mg ions in the TS structure, which was not previously reported for other CDK2 structures. A series of views of the active site of the TS structure including the 2Mg ions are shown in Figure 2-5. The ions have been labeled MgI and MgII, consistent with the nomenclature used in other protein kinases (Adams, 2001). Although MgI has been described as the "essential" catalytic Mg^{2+} in PKA and MgII as "inhibitory" (Cook et al., 1982; Shaffer and Adams, 1999), MgII is the only Mg^{2+} that has been observed in previously published structures of pCDK2/Cyclin A, and the MgI site has always been unoccupied. In the CDK2 TS structure, MgII is observed to be in a classic hexa-coordinate octahedral geometry with distances between Mg^{2+} and ligands ranging between 1.8 and 2.5 Å (Figure 2-5D and Figure 2-5G). It is coordinated by a single water molecule, the ADP α- and β-phosphate oxygen, one of the MgF_3^-

fluorine atoms, Asn132 δ−O, and one oxygen from Asp145 of the conserved kinase DFG motif. The second Mg^{2+} ion we observe (Figure 2-5D and Figure 2-5F) is positioned in precisely the same position as MgI in the PKA TS. Unlike MgII, MgI is not in an ideal octahedral Mg^{2+} coordination geometry. This is largely due to the fact that it is positioned at the bisector of the two Asp145 (of the DFG motif) oxygens. The 2.1 and 2.3 Å distances to each of these oxygens result in a roughly 60° angle (Figure 2-5E), rather than the 90° angle found in the ideal octahedral coordination geometry. The other coordinating groups include two waters (2.2 and 2.5 Å), an ADP β-phosphate oxygen (1.9 Å), and one MgF_3^- fluorine (2.2 Å). Although the geometry is not a perfect octahedron, this "bidentate" Mg^{2+} coordination has been determined to be the most stable conformation for Asp or Glu:Mg interactions in certain cases (Dudev and Lim, 2004), and we believe the distances to the coordinating oxygens are too short for this to be either a water or a monovalent Na^+ ion. It is possible that the imperfect geometry could result in MgI being less thermodynamically stable compared to MgII, which could partially explain why MgI has not been observed in other pCDK2/Cyclin A structures. The 2Mg TS structure also places a slight strain on the backbone of the DFG motif residues.

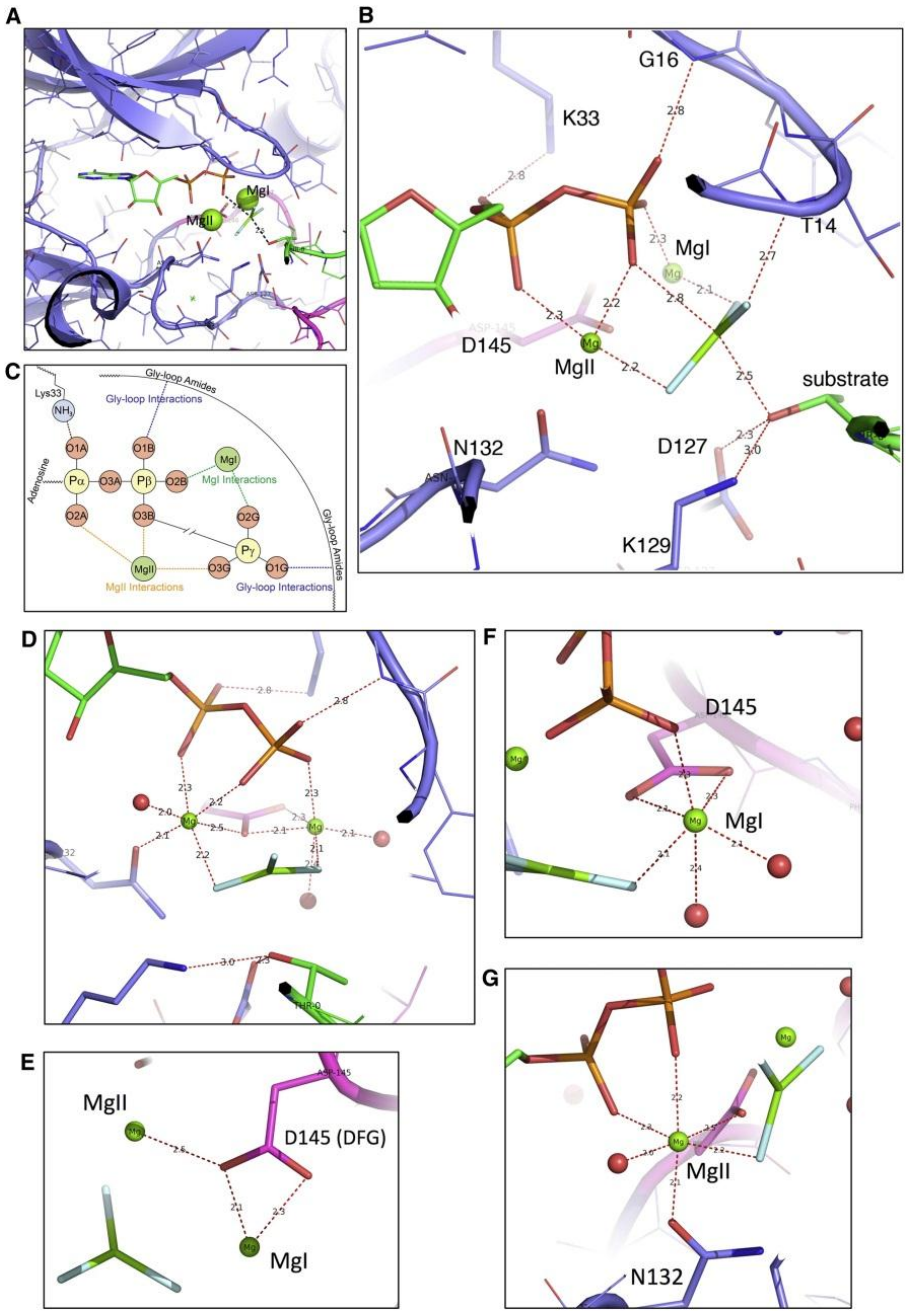

Figure 2-5. Coordination of the Reactants and Mg^{2+} Activators in the CDK2 Active Site (MgI has not been seen in previous CDK2 nucleotide structures).

(A) Overview showing MgI and MgII (green) at 50% VdW contact radius. (B) Close-up highlighting the phosphate and substrate Thr interactions: α-phosphate, Lys33,MgII; β-phosphate, Gly16-NH,MgI,MgII; γ-phosphate(MgF_3^-),MgI,MgII,Thr14-NH; and substrate Thr, Asp127,Lys129. Amides from the Gly-rich loop contact both the β- and γ-phosphates. Asp127 and Lys129 participate in hydrogen bonds with the reactive substrate Thr. (C) Schematic of ATP phosphate interactions. (D) Coordination environment of the two Mg ions. (E) Coordination of Asp145 in the DFG motif. (F) MgI is coordinated by both Asp145 (DFG) oxygens, two waters, the β-phosphate, and the γ-phosphate mimic. (G) MgII is coordinated by Asn132, the α- and β-phosphates, a water, and the γ-phosphate mimic.

Mg^{2+} Dependence of the Reaction

To evaluate the functional relevance of the 2Mg ions, we have carried out in vitro kinase assays to measure the reaction velocity as a function of Mg^{2+} concentration (Figure 2-6). The non-hyperbolic shape of the curve indicates a potentially complex behavior. Although activity is barely detectable at less than 1–2 mM $[Mg^{2+}]_{total}$, the reaction velocity begins to be slightly inhibited by $[Mg^{2+}]$ greater than about 5–7 mM. This type of curve has been observed for other kinases (Sun and Budde, 1997; Waas and Dalby, 2003; Liu et al., 2010), and a number of models have been proposed to explain the behavior. All models invoke a second essential activating Mg^{2+} to explain the sharp stimulatory $[Mg^{2+}]$ effect at 0–5 mM $[Mg^{2+}]_{total}$. Because the stability constant of the first Mg^{2+} to ATP equates to a KD in the low micromolar range (O'Sullivan and Smithers, 1979), the 800 μM ATP^{4-} in this reaction should become saturated with a single Mg^{2+} at concentrations only about 50–100 μM higher than what is needed for 1:1 stoichiometry, i.e., at less than 1 mM total Mg^{2+}. So, consistent with earlier crystal structures, ATP×1Mg is the species that would be available to bind to the protein at 1 mM Mg^{2+}. The fact that we observe almost no activity at this concentration of Mg^{2+} indicates that an additional Mg^{2+} ion is needed at some step of the reaction. Details of these models will be discussed in the next section.

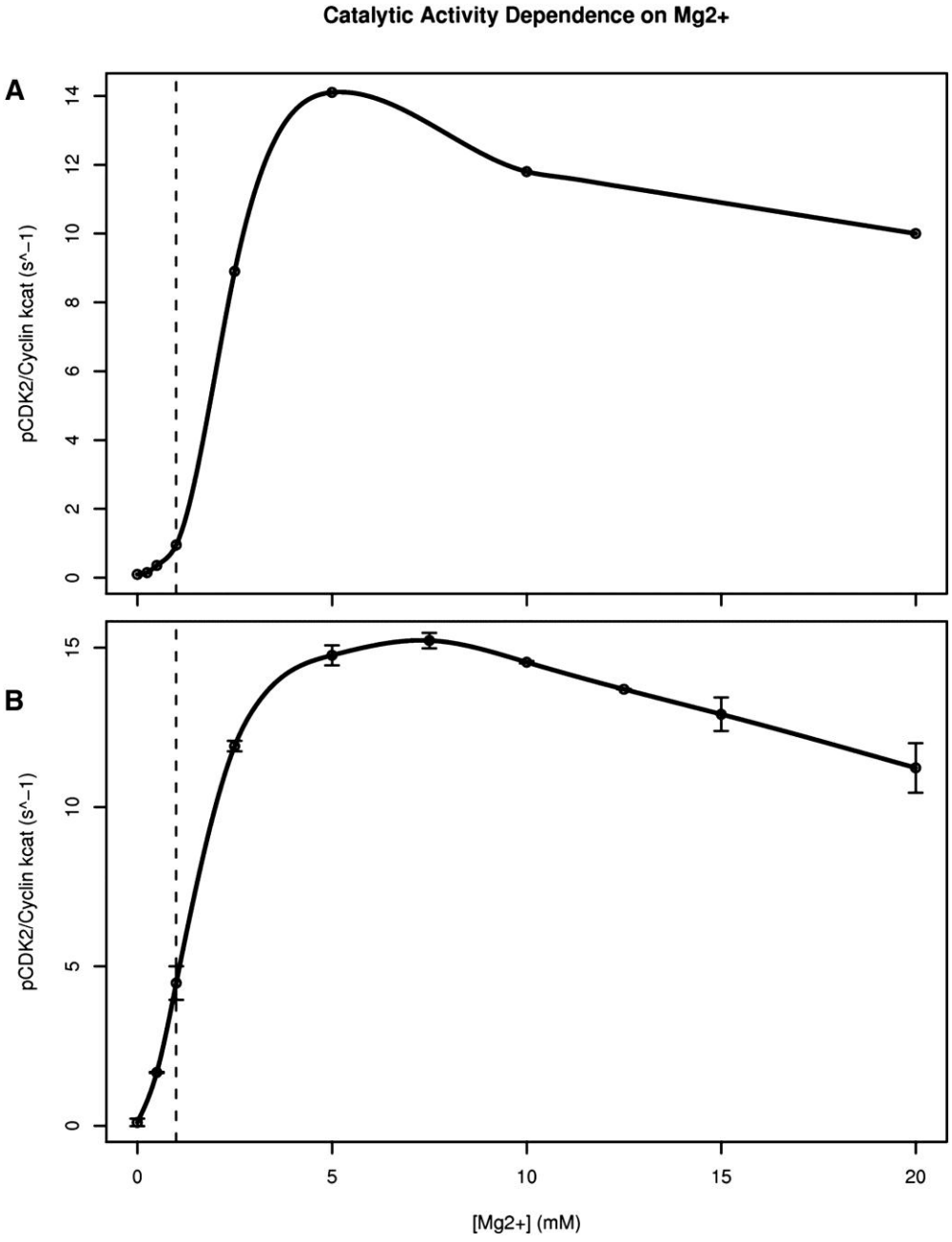

Figure 2-6. Mg^{2+} Dependence of the Reaction.

Activity of the pCDK2/Cyclin A complex as a function of Mg^{2+} concentration. The dashed line indicates 1 mM [Mg^{2+}] where the 800 μM ATP is expected to be saturated with one bound Mg^{2+}. (A) Assay using γ-P32-labeled ATP and peptide substrate. (B) Coupled kinase assay using histone H1 substrate. Both assays were performed with saturating substrate concentrations. Error bars indicate standard error over all replicates.

Positioning and Activation/Stabilization of the Nucleophile

Two different basic reaction mechanisms have been proposed for the majority of protein kinases (Adams, 2001; Cook et al., 2002; De Vivo et al., 2007). They differ primarily in the mechanism of the substrate OH group activation. In the first reaction scheme, the substrate OH (a threonine side chain in this structure) is deprotonated, most likely by a residue acting as a general base, to activate and stabilize the electronegative substrate oxygen that acts as a nucleophile to attack the closely positioned γ-phosphate. The primary difference in the second reaction scheme, sometimes referred to as "substrate catalysis," is that the phosphate transfer is initiated via a simultaneous transfer of the substrate OH proton to one of the ATP γ-phosphate oxygens rather than a protein side chain. Therefore, the key difference is in the mechanism of deprotonation. The present structure places the Thr oxygen 2.3 Å from Asp127 and 2.6 Å from the closest MgF_3^- fluorine, thus within a H-bond distance from either of these potential proton acceptors (Figure 2-5). To distinguish between the two schemes, it may be important to note that Lys129 is positioned roughly 3.2 Å from the phosphate-mimic F closest to the substrate Thr and 3.0 Å from the substrate Thr oxygen. This orientation, along with the additional cation:MgF_3^- interactions described below, would significantly decrease the likelihood that a γ-phosphate oxygen could accept a proton from the Thr-OH in its current environment. However, it would allow Lys129 to help stabilize the buildup of charge on the (unprotonated) γ-phosphate and ensure its correct alignment with the Thr-O− as it is being transferred. If this is what is occurring, Asp127 is optimally positioned to function either as a general base to enhance the substrate's reactivity as a nucleophile, or to function as a proton trap or shuttle (Valiev et al., 2003) functioning to align and

accept the proton from the substrate Thr via the first reaction scheme (Zhou and Adams, 1997).

In both schemes the destabilization of the dissociating β-γ-phosphate bond can be accelerated by the action of one or two divalent metal ions, possibly assisted and/or substituted by additional cationic groups, that stabilize the buildup of negative charge on the β- and γ-phosphates via direct interaction with the phosphate oxygens. If the γ-phosphate is subject to nucleophilic attack while it is still closely associated with the β-phosphate and proceeds through a penta-coordinated intermediate, the reaction is classified as "associative." Alternatively, if the γ-phosphate largely breaks the connection to the β-phosphate and forms a trigonal-planar anionic intermediate before nucleophilic attack, it is classified as a dissociative reaction. These are two extremes of the reaction intermediate, and most phosphoryl-transfer reactions probably exist somewhere in between (Mildvan, 1997).

The geometry of the CDK2 TS structure more closely resembles a dissociative TS, but it is not 100% dissociative. In monomer A the distances of the γ-phosphate mimic to both the ADP leaving group and Thr nucleophile are 2.75 and 2.5 Å. In the two extreme reaction mechanisms, the ideal O-P TS distance in a 100% associative reaction is 1.73 Å, whereas the fully dissociative O-P distance is 3.3 Å (Mildvan, 1997). Once formed, the final O-P phosphate covalent bond is roughly 1.6 Å. Based on the total O-P-O distances alone, the TS is roughly 57% dissociative: 100% associative = 3.46 Å < TS crystal = 5.25 Å < 100% dissociative = 6.6 Å. Although we cannot rule it out from the current structure, the generation of a purely penta-coordinated associative intermediate would require significant additional motion in the active site to simultaneously bring the

ADP and peptide Thr oxygen close enough to one another to form the associative penta-coordinated γ-phosphate bridge. What is also evident from this structure is that further protein and reactant motion is not necessarily required for the phosphoryl transfer to occur because the total $O_{leaving}$-P_{γ}-$O_{nucleophile}$ distance is already considerably less than what is observed in a purely dissociative reaction.

Protein Dynamics of CDK2

In order to clarify the role of Mg^{2+} ions in the CDK2 active site and better understand the structural consequences of having either one or two Mg^{2+} ions present, we have carried out a series of explicit-solvent MD simulations of both the TS complex and the ATP-bound complex coordinated to either one or two Mg^{2+} ions.

TS-mimic simulations were carried out with a deprotonated Thr on the substrate peptide (the proton was transferred to Asp127) because this state is more stable in the simulations and may be what is present in the crystal. A 50 ns simulation of the ADP/MgF_3^-/2Mg^{2+}/peptide complex demonstrates the stability of the crystallized conformation. The backbone atom rmsd of the simulation structures fluctuates at 1.70 ± 0.17 Å from the TS crystal structure, and the rmsd of the average atomic structure computed over the entire MD trajectory relative to the crystal structure is 0.98 Å. As shown in the top time series panel in Figure 2-7, the Gly-rich loop remains in the closed conformation, and the Gly-rich loop amides maintain one or more direct contacts with the β-phosphate and/or MgF_3^- throughout the entire 50 ns trajectory.

Figure 2-7. Structures and Analysis from Four MD Simulations of the pCDK2/Cyclin A Complex.

The simulations predict that the binding of the second Mg ion in the active site (MgI position) stabilizes the down conformation of the Gly-rich loop, expels waters from around the nucleotide phosphates, and reduces the conformational flexibility of the phosphates. (A–C) Three snapshots (orange) from a simulation of pCDK2/Cyclin A bound to ATP and 2Mg ions beginning from1QMZ.pdb (pCDK2/Cyclin A/AMPPNP/1Mg/peptide). The crystal structure of the TS is superimposed in gray. A second Mg was placed in the MgI site at the start of the simulation. The Gly-rich loop converts to the closed conformation after ~18 ns. (D) A superposition of 1 ns interval snapshots from the last 30 ns of the trajectory, after the Gly-rich loop has adopted the closed conformation. (E) One nanosecond interval snapshots from a 50 ns simulation also starting from 1QMZ.pdb but with only 1Mg bound in the active site (MgII position). The top and middle time series graphs quantify the Gly-rich loop proximity to the ATP phosphates by measuring the distance from the ATP or ADP β-phosphate to the closest amide group in the Gly-rich loop. The origins of the structures shown in (A)–(C) and (E) are indicated with circles. The top graph shows simulations of the TS mimic (gray) and the 2Mg×ATP pCDK2/Cyclin A complex. The middle graph illustrates two simulations of pCDK2/Cyclin A bound to 1Mg and ATP. The corresponding distances measured in three crystal structures are indicated by horizontal lines. The bottom graph is a measurement of the number of waters less than 4 Å away from the ATP/ADP β-phosphate during the indicated trajectories (1 ns window average with 1 standard deviation). (F and G) Snapshots from the 2Mg (F) and 1Mg (G) trajectories showing the waters less than 4 Å away from the ATP phosphates

.

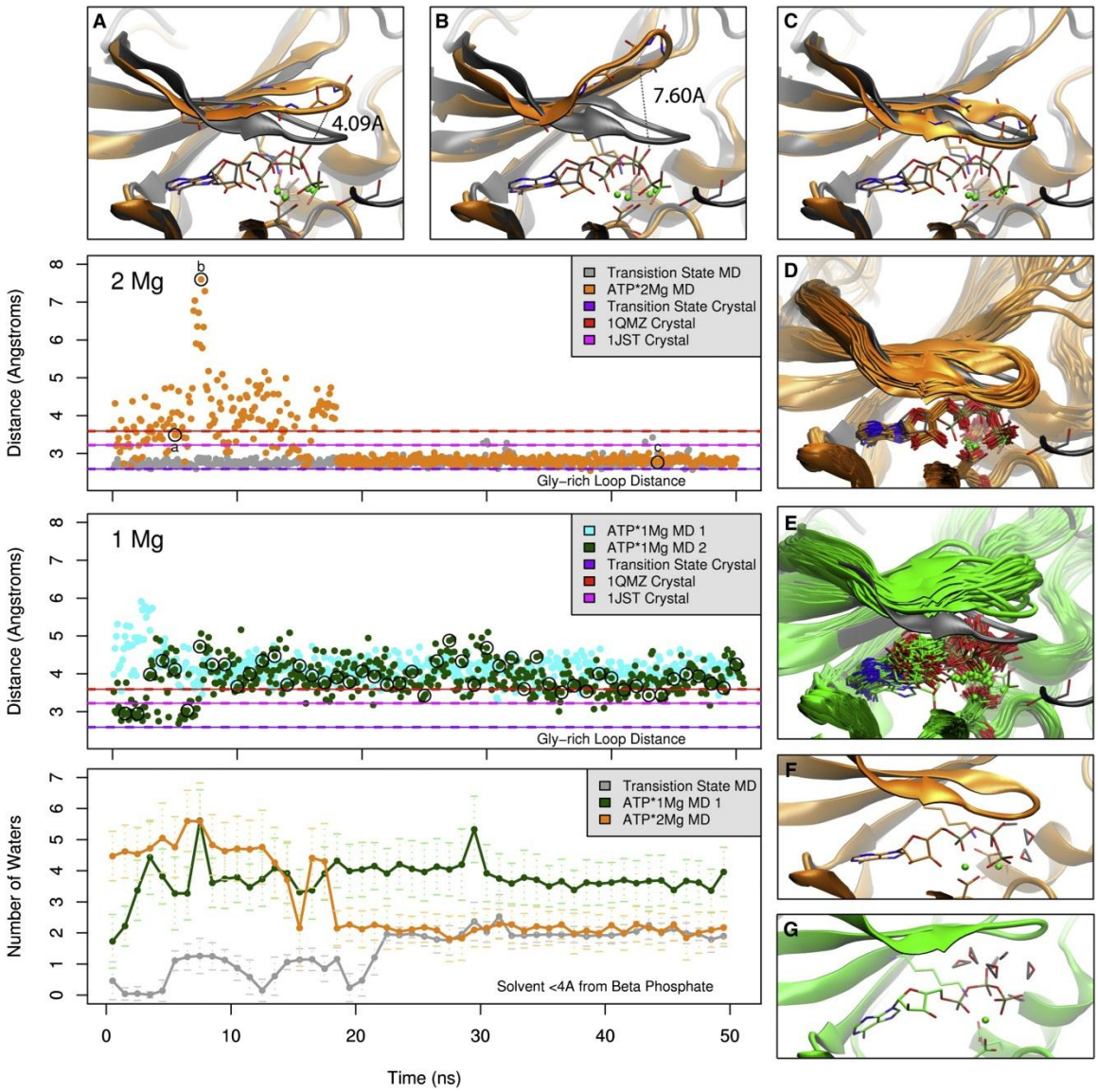

Figure 2-7. Structures and Analysis from Four MD Simulations of the pCDK2/Cyclin A Complex.

We have found that the substrate peptide can be quite flexible and somewhat weakly bound in simulations of the ATP-bound complex, and to minimize simulation-sampling limitations, here, we report results from ATP simulations carried out without a substrate peptide. The instability of the substrate peptide in the simulations is consistent with the somewhat weak apparent affinity of this peptide (K_M = 120 μM at 150 mM KCl) (Figure 2-11). Full-length protein substrates are typically much better substrates for CDK2, due to stabilizing interactions located outside of the active site, e.g., the substrate-binding groove found in the Cyclin A subunit (Brown et al., 1999a).

Gly-rich Loop Conformations

Figure 2-7D and Figure 2-7E show superimpositions of snapshots at 1ns intervals from one of the two Mg simulations and one of the 1Mg ATP simulations. These simulations were both started from the same AMPPNP×1Mg/peptide structure (1QMZ.pdb), but the second Mg^{2+} ion was modeled in the MgI site for the 2Mg simulation. Data are also shown from an additional 1Mg simulation started from a different ATP structure (1JST.pdb). Although both the 2Mg and 1Mg simulations are very stable overall (backbone rmsd = 2.0 and 1.6 Å relative to the 1QMZ.pdb starting structure, respectively), we find that the presence of the second Mg^{2+} ion results in two notable changes to the CDK2 active site: (1) a spontaneous transition to the closed conformation of the Gly-rich loop seen in the TS structure, and (2) considerably less motion of the ATP phosphates. Considerable motion is observed in the Gly-rich loop in the beginning of all three simulations, but roughly 18 ns into the 2Mg simulation, the Gly-rich loop closes down and remains in that conformation for the duration of the 50 ns trajectory. Once closed, the Gly-rich loop backbone amides make direct contacts with

both the ATP β- and γ-phosphates (Figure 2-7C). This closed conformation (shown in Figure 2-7C and Figure 2-7D) is virtually identical to the conformation observed in the TS crystal structure (superimposed in Figure 2-7).

The closed conformation of the Gly-rich loop is only sampled once a layer of water molecules located between the Gly-rich loop and the ATP phosphates has been expelled. The number of water molecules found less than 4 Å away from the β-phosphate is shown in the bottom time series plot in Figure 2-7. The closing down of the Gly-rich loop, seen at ~18 ns in the top time series plot, is concurrent with the discreet drop in the number of waters directly contacting the phosphates indicated in the bottom panel. Once the layer of phosphate-solvating waters has been expelled, the number of waters interacting with the phosphates remains exactly the same as is observed for the TS-mimic simulation. Thus, the analysis in the time series panels in Figure 2-7 indicates that direct ATP phosphate:water interactions are replaced by direct interactions with Gly-rich loop backbone amides when the Gly-rich loop adopts the closed TS-like conformation.

We have also observed that the Gly-rich loop spontaneously transitions in the opposite direction, from closed to open, when simulations are started with the closed (TS) conformation but with only a single Mg^{2+} bound to the ATP. The simulations as a whole clearly support a model where the Gly-rich loop exchanges between closed and open conformations and that the population of the open-closed equilibrium is strongly influenced by the binding of the second Mg^{2+} at the MgI site. All of these simulations have been repeated after randomizing ion positions within the solvent. In total, four out of five 2Mg simulations started from the open Gly-rich loop conformation transitioned to a closed conformation within 50 ns, and three out of five 1Mg simulations started from the

closed Gly-rich loop conformation transitioned to an open conformation during the same time period. This Gly-rich loop equilibrium is also supported by the TS crystal structures. We have been able to build one of the four CDK2 TS Gly-rich loops reported here into two 50% occupancy closed and open conformations, and the occupancy of the MgI site in this subunit is somewhat less well defined.

Reduced Motion in the Active Site

In addition to influencing the closing of the Gly-rich loop, the simulations also indicate that the binding of the second Mg^{2+} ion notably reduces the magnitude of nanosecond timescale fluctuations for the ATP phosphates, Gly-rich loop, and the active site region of the protein. This is evident both in the structural superimpositions shown in Figure 2-7D and Figure 2-7E and in the analysis shown in Figure 2-8A–C, depicting backbone protein flexibility by drawing ellipsoids describing the extents of 50% positional occupancy of the protein Cα, nucleotide, and Mg^{2+} ions over the 20–50 ns time period of each simulation. The results show that there is a hierarchy of nanosecond timescale flexibility at the protein active site that is correlated with both substrate and activator Mg^{2+} binding. The most flexible state is the ATP×1Mg complex, followed by the ATP×2Mg complex, and the least flexible is the 2Mg ADP/TS/peptide complex.

The multiple ATP phosphate conformations the CDK2 active site is able to accommodate (Figure 2-3A and Figure 2-3B) probably reflect an equilibrium of states that exists prior to the phosphoryl-transfer event. Although we do not observe interconversion between the precise crystal structure conformations within the current simulation time periods, we suggest that the differences in the nanosecond timescale

dynamics between the ATP×1Mg and ATP×2Mg states are reporting on the relative flexibilities of these two states. By replacing diffuse water interactions with explicit Gly-rich loop amide and direct Mg^{2+} interactions, the ATP phosphates become more tightly integrated into an extensive scaffold of ionic interactions within the protein active site. What follows is that the binding of the second Mg^{2+} ion not only reduces the magnitude of the nanosecond timescale fluctuations of the ATP, but the additional ionic interactions it enables may also limit the permitted conformations of the ATP phosphates.

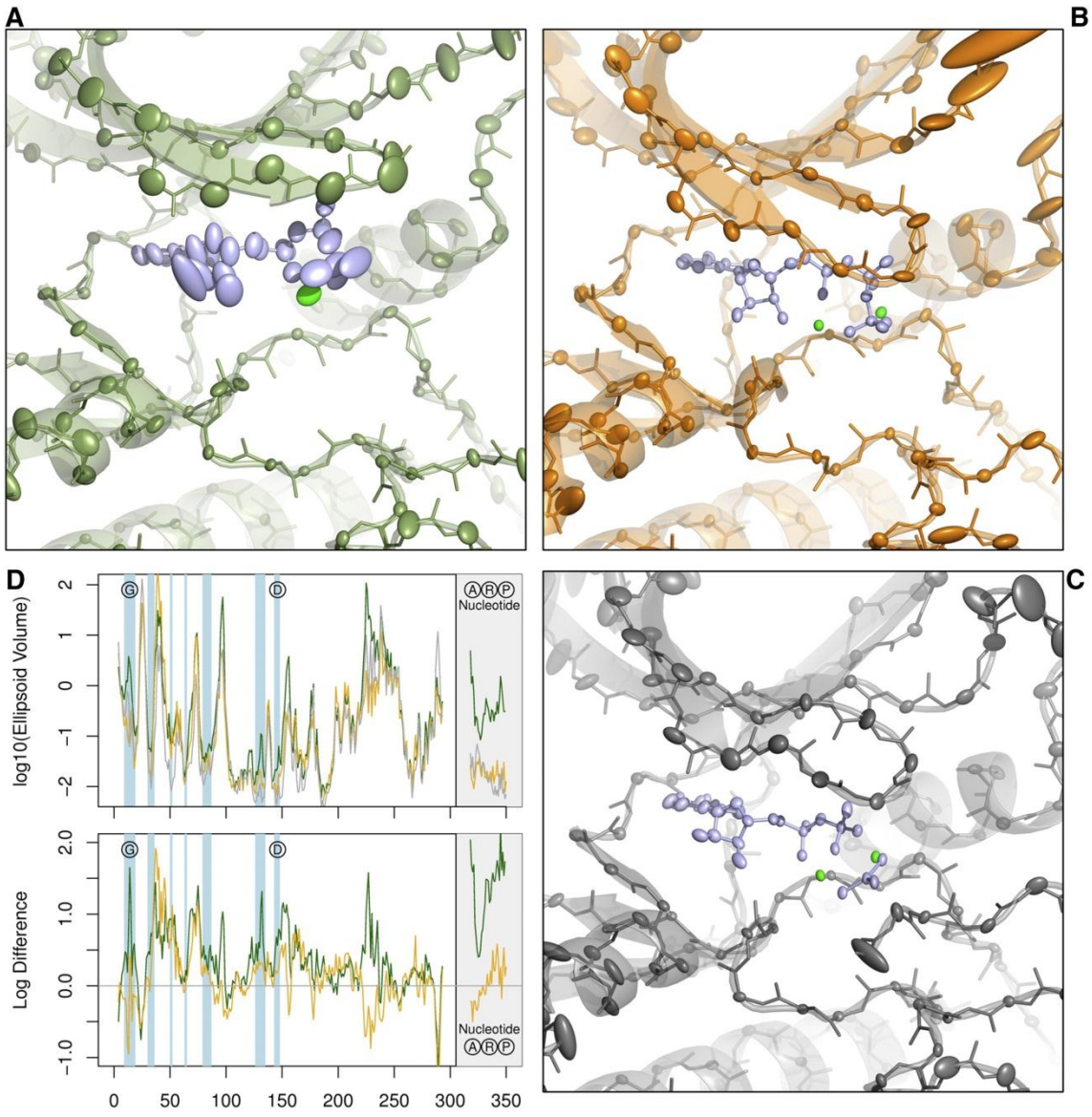

Figure 2-8. Extent of Protein Backbone Fluctuations in Three MD Trajectories.

Anisotropic thermal ellipsoids are displayed to encompass 50% atomic positional probabilities for the Cα atoms, computed relative to the average atom positions over the 20–50 ns time period of each simulation. Simulations are the same as in Figure 2-7. (A) pCDK2/Cyclin A with ATP and 1Mg. (B) pCDK2/Cyclin A with ATP and 2Mg. (C) pCDK2/Cyclin A/ADP/2Mg/MgF_3^-/substrate peptide. (D) The top graph indicates the extent of fluctuation for each residue by plotting the log10 of the 50% probability Cα ellipsoid volumes. The bottom plot shows the difference between the fluctuations (log10 ellipsoid volumes) in the TS simulation and the 1Mg (green) and 2Mg (yellow) simulations. Shaded regions indicate residues within 5.0 Å of the nucleotide. G, the Gly-rich loop; D, DFG region; A, R, P, adenosine, ribose, and phosphate atoms in the ATP.

Taken together, this model and the available structural data suggest that the binding of the second activating Mg ion must be an ordered, possibly sequential, event that results in numerous changes to the active site that contribute to phosphoryl transfer when it occurs after ATP×1Mg binding during the catalytic cycle. In addition to directly coordinating the ATP β-phosphate, the binding of the second (MgI) ion results in the ATP simultaneously becoming more ordered, more shielded from solvent, and participating in additional ionic interactions with the protein. Simulations of the ATP×1Mg state containing only a single Mg at the MgII site suggest that the MgI site would certainly be accessible to ions from outside the protein because we consistently observe transient localization of monovalent Na^{+} ions from the simulation bulk solvent into the vacant electronegative MgI site. Free Mg^{2+} ions were not present in the simulation bulk solvent. Simulations starting with a single Mg at the MgI site are less stable and, thus, consistent with the crystallographic evidence that the MgII site is the first to become populated when ATP×1Mg binds.

Catalytic Mechanism

The CDK2 TS structure illustrates how CDK2 achieves two general mechanisms that enzymes can employ to accelerate chemical reactions: (1) correctly positioning the reactants in the optimum orientation, and (2) electrostatically stabilizing the high-energy TS and/or product leaving groups. The structural and dynamic changes of the CDK TS relative to reactant complexes support a model where the enzyme only optimally performs both of these rate-enhancing mechanisms once all the necessary ligands are bound in the active site. Notably, if either the second activating Mg^{2+} ion (MgI) or the peptide substrate is missing from the active site, the Gly-rich loop is predominantly in the

up conformation, and the position of the β- and γ-phosphates is more delocalized and flexible. As all of the reactants bind, the complex network of ionic interactions is completed, the active site becomes less flexible, and the restricted flexibility may force the phosphates to converge upon the TS geometry.

Positioning the Phosphates and Holding Them Still

Further evidence that optimal phosphate alignment appears to be correlated to the binding of the second Mg^{2+} ion is the observation that each of the 1Mg crystal structures and MD simulations lacks one or more of the direct phosphate interactions that are observed in the TS structure shown in Figure 2-5B and Figure 2-5C. This is in addition to missing the direct MgI:phosphate interactions. In particular the β-phosphate is held in place by direct interactions with MgII:O3B, MgI:O2B, and Gly16(NH):O1B, and the MD simulations find that not a single one of these three interactions is maintained in the 1Mg-bound state. The γ-phosphate mimic is held in place by interactions with MgII:O3G, MgI:O2G, and Thr14(NH):O1G. The only one of these γ-phosphate interactions observed in the 1Mg state is MgII:O2G. Although the MD finds that the position of the γ-phosphate may not be as sensitive to the loss of the stabilizing interactions in the 1Mg state as the β-phosphate is, the orientation of the β-γ-phosphate linkage that is cleaved in the reaction is still non-optimal in the 1Mg state as a result of the flexible β-phosphate position.

In addition to being affected by the binding of MgI, the conformation of the β-phosphate may also be sensitive to the presence of substrate peptide. In the simulation of CDK2 bound to ATP×2Mg, but without peptide, both MgI and the Gly-rich loop amides

make stabilizing interactions with O1B and O2B of the β-phosphate, but the MgII:O3B interaction that was present in the beginning of these simulations is not preserved. O3B is the β-γ bridging oxygen that is dissociated from the γ-phosphate during the reaction. The MgII:O3B interaction is observed in 1QMZ.pdb, a structure with AMPPNP/1Mg and peptide (where the O3B is replaced with a nitrogen). Thus, although the nanosecond timescale dynamics of the phosphates are greatly reduced when both MgI and MgII are present, the notable loss of the O3B:MgII interaction in the 2Mg simulations without substrate results in a β-γ-phosphate geometry that is quite different from the TS orientation. Thus, our hypothesis is that the precise β-γ-phosphate coordination and positioning are sensitive to the presence of both the second Mg^{2+} ion (MgI) and the protein substrate. This apparent linkage between β-phosphate positioning and both substrate binding and Mg^{2+} coordination could reduce the probability of a water substituting for the Ser/Thr OH as a nucleophile that would lead to ATP hydrolysis to ADP + Pi, a nonproductive side reaction known to occur for CDK2 and many other activated protein kinases.

Discussion

Roles of the Flexible Glycine-Loop

The flexible Gly-rich loop that rests on top of the nucleotide phosphates is present in most protein kinases and is thus believed to be critical to the function of these enzymes. It is the site of numerous mutations that confer drug resistance to Abl protein kinase (Shah et al., 2002). The protein kinase Gly-rich loop is homologous to the lid-like Gly-rich loop region found in many NTPase enzymes that is often referred to as the P-loop (for phosphate-binding loop, illustrated in Figure 2-12). This and other similarities

support the likelihood that many of the mechanisms used by NTPase enzymes to accelerate the reaction will be related, regardless of the exact details of the catalytic mechanism. For example it has been shown that stabilization of the buildup of negative charge on the β-phosphate of the NDP leaving group can lead to a substantial rate increase for GTPase enzymes (Maegley et al., 1996). This is accomplished in small GTPases by at least three mechanisms, all of which can function as points of regulation: (1) a coordinating Mg^{2+} ion, (2) a cationic side chain such as an Arg "finger" from a GAP, and (3) backbone amide groups from the Gly-rich "P-loop" motif.

We believe that the similar reaction catalyzed by the well-studied small G proteins provides a useful model for understanding aspects of our current CDK2 structure. The presence of a second catalytic Mg^{2+} ion in CDK2 means that CDK2 also utilizes two cations to stabilize the β-phosphate, only replacing the Arg finger with a second Mg^{2+} (Figure 2-12). The GTPases also help us understand the implications of multiple conformations of the Gly-rich loop in CDK2. One of the most potent oncogenic mutations in small GTPases is a Gly to Val mutation in the Gly-rich P loop that renders the enzymes nearly unable to catalyze the hydrolysis of GTP to GDP, hence, locking them in a perpetual GTP-bound signaling state (Maegley et al., 1996; Chen et al., 2009). This mutation functions by sterically limiting the ability of the P loop amides to adopt the somewhat contorted conformation required to intimately interact with the GTP phosphates and stabilize the buildup of charge during the reaction. Our structure demonstrates how the Gly-rich loop in CDK2 carries out a similar role of electrostatically stabilizing the ATP phosphates during catalysis (Maegley et al., 1996). The positive

electrostatic potential presented to the phosphates generated by the down conformation of the Gly-rich loop is depicted in Figure 2-9A and Figure 2-9B.

The structural heterogeneity of the CDK2 Gly-rich loop across various structures suggests that the Gly residues fulfill several unique functions: (1) they must be flexible enough to accommodate the closed conformation of the loop; (2) additional flexibility may also be required to allow the Gly-rich loop to open, potentially facilitating nucleotide binding and release; and (3) despite the lack of functional side chains, the backbone amides of the Gly residues are flexible enough to adopt otherwise unfavorable backbone torsions required to provide optimal electrostatic stabilization of the TS. The protonated Thr14 side chain also contributes to the electrostatic stabilizing potential of the Gly-rich loop. The stabilizing capacity of this residue would be eliminated upon phosphorylation of Thr14 and/or Tyr15 by Myt1/Wee1, two inhibitory modifications of CDK2. Figure 2-9A and Figure 2-9B also highlight the strong electronegative coordination environment surrounding both Mg^{2+} sites, testament to the likelihood of localizing divalent ions at both sites.

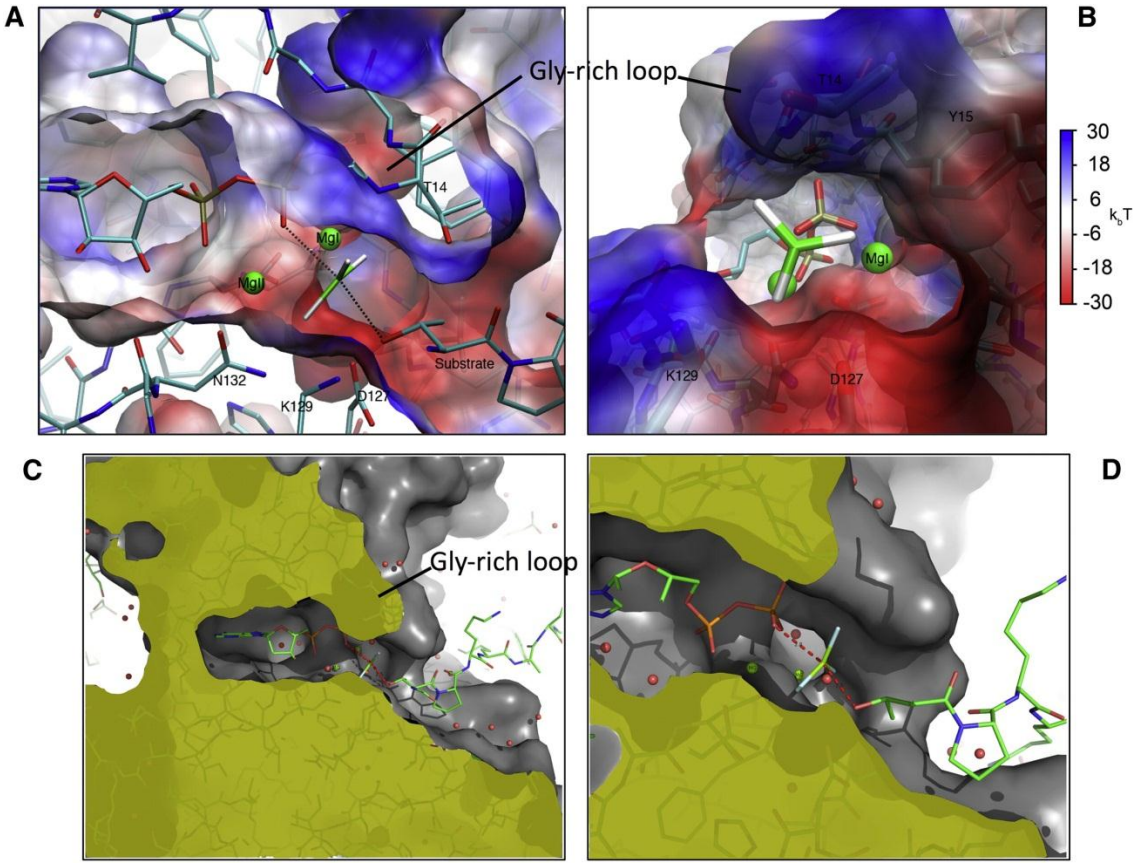

Figure 2-9. Flexible Glycine Loop.

(A and B) Two views of the electrostatic potential in the active site of CDK2 in the TS structure. The scale ranges from −30 kT (red) to 0 kT (white) to +30 kT (blue). Only the protein atoms are included in the calculation, but the ADP (stick), Mg ions (green spheres), and MgF_3^- (stick) are shown for reference. The view in (B) is rotated roughly perpendicular relative to (A) such that the viewpoint is from the perspective of the substrate Thr, along the Thr-MgF_3^--ADP reaction vector. (C and D) Closing of the Gly-rich loop expels solvent and encloses the phosphates. Two slices through a solvent-accessible surface rendering of the active site.

An additional function of the flexible Gly-rich loop in CDK2 is to exclude solvent surrounding the ATP phosphates. Two views of the tight channel formed around the ATP phosphates in the TS are shown in Figure 2-9C and Figure 2-9D. As described above, this closed conformation is stabilized by additional ionic interactions between the phosphates and backbone amides in the Gly-rich loop and only appears to occur once the second

Mg^{2+} and substrate peptide have become bound. The substrate/Mg^{2+} activator-triggered closure may function to minimize undesirable ATP hydrolysis that occurs when ATP reacts with a water molecule instead of a substrate Ser/Thr. The exclusion of solvent should also result in an amplification of the electrostatic-stabilizing effects of the Gly-rich loop amides by reducing the dielectric environment surrounding the phosphates.

DFG Motif

The presence of the short Asp-Phe-Gly "DFG" motif is nearly invariant in protein kinases. Located just before the N-terminal end of the activation loop motif (residues 145–147 in CDK2), Asp145 is observed to directly coordinate both of the Mg^{2+} ions at the active site in the TS complex (Figure 2-5D–G). The transient occupancy of the MgI ion could have some interesting implications for the functions of this residue. The side chain of Asp145 has been observed to exist in different conformations in some structures of CDK2 bound to nucleotides with 1Mg, such as 1HCK.pdb. Returning again to GTPases as a model, Kannan and Neuwald, 2005 pointed out that conformational changes of the homologous Asp residue in GTPases, sometimes induced by the binding of exchange factor proteins (GEFs), can function to destabilize a bound Mg^{2+} ion and facilitate nucleotide exchange. It will be interesting to determine if the observed Asp145 conformational changes play a role in the binding or release of MgI during the catalytic cycle. Wedged in between the two Asp145 oxygens and the ATP β- and γ-phosphates, the MgI site in CDK2 has an extremely negative electrostatic potential, even greater than the nucleotide-free potential shown in Figure 2-9C and Figure 2-9D. We have found that when monovalent ions present in our MD simulations spontaneously localize at or near the MgI site, they do not have the same structural, dynamic, or electronic effects as a

bound divalent Mg^{2+}. A PROPKA (Bas et al., 2008) calculation of the 1Mg-bound nucleotide state of CDK2 (1QMZ.pdb) suggests that the DFG Asp has a highly elevated pKa (>10.5), and it, or the nucleotide γ-phosphate, may predominantly exist in a protonated state at neutral pH. Because they could shift the equilibrium of MgI binding, both of these observations have important implications for salt and pH effects in the model where the MgI site is only transiently occupied by Mg^{2+}. The DFG-facilitated MgI equilibrium is also consistent with the results of simulations investigating the mechanism of ADP release from PKA that demonstrated that it would be extremely energetically unfavorable to remove the 2Mg-bound ADP from the active site of PKA (Khavrutskii et al., 2009). Like the ordered binding of ATP×1Mg before MgI, the release of MgI may be required to precede the release of ADP.

We believe that this ADP/MgF_3^-/peptide complex represents an informative model for the TS of the phosphoryl-transfer reaction catalyzed by the pCDK2/Cyclin A holoenzyme. This new model proposes that the formation of the catalytically competent active site conformation involves the creation of a transient network of ionic interactions among the protein, the ATP, 2Mg ions, and the substrate peptide. The active site TS conformation is highly homologous to another structure of a protein kinase TS mimic, the ADP/AlF_3/peptide complex of PKA. In order to achieve this active site conformation, the already-activated CDK2 is required to undergo two critical conformational transitions compared with structures lacking any one of the active site ligands: (1) a substantial closing down of the Gly-rich loop, partially stabilized by backbone amide interactions with the β- and γ-phosphates; and (2) a precise ordering of the ATP, particularly the β- and γ-phosphates. More globally, MD simulations suggest that the formation of the TS

complex is concurrent with a large-scale dampening of protein and reactant motions in and around the active site. This is partially achieved via the stabilizing effect of replacing nearly every single water-ATP phosphate interaction with direct ionic interactions, particularly interactions with the second catalytic Mg^{2+} and the Gly-rich loop backbone amides, to effectively wedge the N and C-lobes of the kinase together to more tightly engage the dissociating ATP.

Combination of the new crystal structure of the CDK2 kinase described here, with the collection of previous structures and the MD simulations, enables us to construct a more complete model of the dynamic conformational ensemble of CDK2. Before all substrates and two activating Mg^{2+} ions are bound, the active site of the "activated" state of CDK2 is still relatively flexible, and the Gly-rich loop is primarily in an open conformation. The simultaneous occupancy of the ATP, peptide, and 2Mg ion activators increases the ordering of the active site by forming a complex network of ionic interactions where the protein and Mg^{2+} activators engage every one of the ATP phosphate oxygens as well as the substrate side-chain nucleophile. This increased ordering increases the probability of aligning the ATP phosphates in the optimum alignment for catalysis, stabilizes the buildup of negative charge on the phosphate oxygens (destabilizing the β-γ-phosphate linkage), and is correlated with the release of waters from around the phosphates to both enhance the electrostatic field effect of the protein and potentially limit the ATP hydrolysis side reaction.

The inhibition of activity that we observe at high Mg^{2+} concentrations can be rationalized by three models: (1) a second Mg^{2+} slows the rate of ADP product release; (2) ATP bound to 2Mg in solution does not bind as well as ATP×1Mg; and (3) Mg^{2+} has

different relative effects on the affinities of ATP and ADP for the protein, resulting in product inhibition. We hope to investigate this phenomenon in more detail in future studies. One conclusion we can make from the observed data is that a single Mg^{2+} ion is not sufficient to achieve maximum reaction velocity.

We believe that the biochemical [Mg^{2+}] data, along with the 2Mg ions identified in the TS crystal structure, are consistent with a model where maximum reaction velocity is achieved when sufficient Mg^{2+} ions are available to bind to both sites, MgI and MgII, but that the occupancy of the MgI site in particular is near equilibrium. It is likely that 2Mg ions are at least transiently necessary to stabilize the phosphoryl-transfer step but that the presence of 2Mg ions may also function to kinetically inhibit other steps in the reaction such as the release of the ADP product. This model accounts for both observations that saturating ATP with 1Mg results in barely observable turnover, whereas even higher concentrations of Mg^{2+} inhibit the reaction. The fact that all previously determined crystal structures of active CDK2 contain a single divalent metal ion had led to much speculation that this kinase only utilizes a single divalent for catalysis. We believe that the current structure and in vitro data suggest that a second divalent ion is utilized at the active site, at least for the phosphoryl-transfer step of the catalytic cycle.

Although it is challenging to measure, there is evidence that intracellular Mg^{2+} ion concentrations vary as a function of the cell cycle (Walker, 1986) and that misregulation of intracellular Mg^{2+} levels may be associated with both cell transformation and increased proliferation (Wolf and Cittadini, 1999). Cell culture studies have identified a correlation between low intracellular Mg^{2+} levels and failure to progress through the G1-S phase transition (Killilea and Ames, 2008), the very checkpoint that is released by

CDK2/Cyclin activity. This effect has previously been associated with increased production of the CDK2 inhibitor proteins P21Cip and P16INK (Sgambato et al., 1999) at low [Mg^{2+}]. So, whereas changes in Mg^{2+} ion concentration would most likely have an effect on numerous cellular enzymes, it is possible that the Mg^{2+} dependence of the catalytic subunit of CDK2 enables CDK2 to function as one link between fluctuating local Mg^{2+} concentrations and progression through the cell cycle. ERK2 is anther protein kinase that has been shown to require 2Mg ions and has been proposed to potentially be regulated by physiological fluctuations in intracellular Mg^{2+} levels (Waas and Dalby, 2003).

Our results suggest that the chemistry carried out by CDK2 may indeed be much more similar to PKA than some had expected, whereas at the same time the regulatory mechanisms of these two kinases remain quite different. Data from PKA kinase suggest that the binding of substrates may be coupled to important entropic changes within that protein kinase (Li et al., 2002). It has been determined that still uncharacterized slow conformational transitions may occur at two critical steps of the reaction cycle of PKA: (1) following ATP binding and preceding catalysis, and (2) after catalysis and preceding the release of the reaction products (Shaffer and Adams, 1999). If we propose that the Gly-rich loop dynamics we observe in CDK2 also takes place in PKA and other kinases, perhaps it is the slow-ordered binding of the second catalytic Mg^{2+} ion and accompanied open to closed transition of the Gly-rich loop that represent the slow conformational change identified to occur after ATP binding to PKA, once hypothesized to represent Mg^{2+} binding (Zhou and Adams, 1997). Similarly, perhaps the subsequent release of the

second catalytic Mg represents the second slow conformational transition observed post-catalysis in PKA.

Recent studies of adenylate kinase (ADK) reported that the apo state of that enzyme transiently samples the closed substrate-bound conformation of the enzyme (Henzler-Wildman et al., 2007). It was proposed that the ADK enzyme has been structurally programmed through evolution to sample the TS conformation, and because of this it can more efficiently catalyze the chemical reaction once the substrates do become bound. We believe that CDK2, which is not nearly as efficient an enzyme as ADK (with a roughly 40-fold lower k_{cat}), may have evolved differently. As an integral signaling protein, CDK2 is under evolutionary pressure to be both catalytically efficient as well as robustly regulated. It is a molecular switch. Although it is similar to ADK in that conformational changes are observed upon substrate binding, CDK2 may be different in that it may work to minimize sampling of the TS conformation until it is completely activated. CDK2 appears to maintain relatively high conformational flexibility of the active site and substrates up until the enzyme is fully ready to react, and this precatalytic protein flexibility may function to probabilistically keep the enzyme away from sampling the TS conformation until it is the appropriate time to react. Although tolerating this flexibility may have the effect of slowing down the maximum possible rate of the reaction, it may also have evolved to minimize potentially damaging uncontrolled catalytic activity and to facilitate multiple points of regulation of the enzyme. The active site of the fully activated TS complex, including ATP, 2Mg, and peptide substrate, appears to be much more rigid than it is when only ATP and a single Mg^{2+} are bound. Keeping the reactants rigidly aligned could represent the most efficient way to increase

the probability of a successful nucleophilic attack on the activated γ-phosphate by the activated substrate oxygen, a low-probability event that requires the concerted occurrences of γ-phosphate dissociation and substrate oxygen deprotonation to activate or stabilize the nucleophile. If rigidity is a requirement for the reaction, any number of external influences such as Cyclin binding, Mg activator binding, substrate binding, CDK2 phosphorylation, and assembly of a hydrophobic spine (Kornev et al., 2006) could readily influence catalysis by altering the flexibility of the otherwise flexible and intrinsically inefficient enzyme.

As a final note, we would like to suggest that we believe that each of the growing number of crystal structures of the CDK2 enzyme, when taken together, is providing us a much more complete picture of the different conformations that can be sampled by this flexible enzyme. We are grateful that so many different structures of this single enzyme have been made available in the protein databank (Berman et al., 2002).

Experimental Procedures

Detailed methods are included in the Supplemental Experimental Procedures (see Chapter 2 Appendix).

The pCDK2/Cyclin A complex was generated by coexpression of three vectors containing CDK2, Cyclin A, and Cak1p in E. coli. Crystals were generated by growing crystals of the apo pCDK2/Cyclin A complex using vapor diffusion with 22% w/v Poly(acrylic acid sodium salt) 5, 100, and 20 mM $MgCl_2$, 100 mM HEPES, and then soaking these crystals with the active site ligands prior to cryoprotection. X-ray diffraction data were collected at LS-CAT (APS). Initial models were generated with

molecular replacement, and refinement was carried out using PHENIX. Enzyme kinetics were carried out using either a coupled kinase reaction with Histone H1 substrate or a P32-labeled ATP assay using peptide substrate. All MD simulations were carried out using the AMBER 10.0 package (Case et al., 2006) and FF99SB force field (Hornak et al., 2006).

Acknowledgements

D.M.J. was supported by Bioinformatics Training Program T32 GM070449-05 and Proteome Informatics of Cancer Training Program T32 CA140044-01. M.A.Y. was supported by Burroughs Wellcome career award at the scientific interface 1003999. We thank Bernard Rupp for advice during refinement and Peng Jiang for assistance with ATP P32 assays. We thank all of the support staff at the APS LS-CAT beamlines.

Appendix

This appendix contains supplementary material from the original publication.

Supplemental Experimental Procedures

Protein expression and purification

Protein for the crystals was grown using a co-expression of three proteins in BL21 E. coli: Full-length CDK2 in a pCDF-Duet vector containing a TEV cleavable His-tag, residues 173-432 of mouse CyclinA in a modified pET24 vector containing an N-terminal His tag-Smt3 fusion, and GST-Cak1p in pGEX- 2T (a gift of Mark Solomon, Yale University) to phosphorylate the CDK2. Cells were grown in 1L flasks of TB media containing 3 antibiotics and 5mM MgSO4 at 37 deg until OD600 ~1.4, when they were equilibrated to 18 deg C and protein expression was induced with 0.2mM IPTG. Expression continued for 20hrs.

Cells were harvested by centrifugation at 5000 x g, mixed with lysis buffer (100mM NaPO4, 500mM NaCl) and flash-frozen until needed. Cells were lysed using an Avestin homogenizer and 2U/ml Benzonase (Sigma). Purification began with a 5ml HisTrap HP Ni-chelating column (GE). Fractions were pooled, TEV and ULP1 proteases were added, and then dialyzed overnight to lower the salt and remove imidazole. Samples were passed through a second HisTrap column to remove the cleaved tags and tagged proteases, concentrated, and run on an S-200 size-exclusion column.

Crystallography

Crystals were grown in 96-well sitting-drop vapor diffusion trays at 22 deg C. 1ul of 12mg/ml pCDK2/CyclinA complex was mixed with an equal volume of 22% w/v Poly(acrylic acid sodium salt) 5,100, 20mM $MgCl_2$, 100mM HEPES pH 8.0. Large plate crystals typically appeared after 1-6 days. Crystals were harvested and transferred to a new tray containing ~10ul of ligand-soaking/cryoprotecting solution of 27% w/v glycerol, 2% PEG 3350, 3.2mM ADP, 10mM $MgCl_2$, 25mM NaF, 20mM peptide, 25mM HEPES pH 8.0 or pH 8.2. We also attempted to soak crystals with AlNH4 together with the NaF but we were not able to obtain comparable quality diffraction data and resolve the active site ligands. Data was collected at the 21-ID-F and D beamlines (LS-CAT) at the Advanced Photon Source (APS) at Argonne National Labs at 100 K and λ=0.97872 Å. Integration and processing were carried out using mosflm and SCALA, respectively.

An initial molecular replacement solution was obtained in the Phaser program (McCoy et al., 2007) using previously solved but unpublished structures of CDK2 and CyclinA as search models. To minimize potential model bias, residues 150-167 and 39-45 of CDK2, two potentially flexible regions, were not included in the search model. The search was carried out for the two proteins separately, locating two copies of the CDK2/CyclinA complex in the asymmetric unit. Refinement was mostly carried out using the Phenix program suite (Adams et al., 2010), with some steps in Refmac (Winn et al., 2003). Briefly, the refinement began with rigid body refinement, followed by simulated annealing and successive rounds of Cartesian and temperature-factor minimization with manual model building in Coot (Emsley et al., 2010). NCS restraints were built up during successive rounds of refinement to eventually restrain the following chemically equivalent regions to one another: chains A and C (CDK2), chains B and D

(CyclinA), chains J and K (substrate peptide). At the very end of the refinement, NCS restraints were also included for the ADPs. Distance and angle restraints were used for the Mg ions at some earlier stages of refinement but were removed in the final stages of refinement. TLS refinement was used for the protein chains, with groups calculated using the MD TLS server (Painter and Merritt, 2006). Connected density was identified in a region of the Cyclin protein previously identified to function as a substrate-recognition motif (Brown et al., 1999a). We built the c-terminal segment of the substrate peptide into this density, which turns out to match the "RXL" sequence recognized by the Cyclin motif. Density for the N-terminal portion of this peptide was visible but not well resolved so it was only included in the final model at 0 percent occupancy.

Enzyme kinetics

Magnesium dependence of the phosphoryl transfer reaction was carried out using two experiments. In the first, γ-P_{32} labeled ATP was used to measure the generation of P_{32} labeled peptide substrate. Experiments were carried out at 100mM Tris pH 8.0, 150mM KCl, increasing concentrations of $MgCl_2$ and aliquots were taken out and quenched at 30sec intervals. Substrate peptide (sequence: PKTPKKAKKL) was isolated by binding to P80 filter paper, washed and radioactivity quantified using a scintillation counter.

In a second experiment, a coupled enzyme assay was used with histone H1, a protein substrate. Results were similar between the two assays. In this assay, kinase activity was monitored using a continuous spectrophotometric assay as described before (Barker et al., 1995). The consumption of ATP is coupled via the pyruvate kinase/lactic

dehydrogenase (PK/LDH) enzyme pair to the oxidation of NADH which can be monitored through the decrease in absorption at 340 nm. Reactions contained 100 mM Tris pH 8.0, 150mM KCl, increasing concentrations of $MgCl_2$, 0.8 mM ATP, 1 mM phosphoenolpyruvate, 0.6 mg/mL NADH, 75 U/mL pyruvate kinase, 105 U/mL lactate dehydrogenase and 0.1 mM Histone H1 (Sigma) substrate. 75 μL reactions were started through the addition of 25 nM kinase (final concentration) and the decrease in absorbance was monitored over 20 min at 30°C in a microtiter plate spectrophotometer (SpectraMax).

The inhibition of the pCDK2/CyclinA complex by MgF_3^- was measured using the coupled assay described above performed in a 96-well format. The experiment was carried out by titrating Fluorine ions as NaF into a reaction mixture containing a constant 10mM $MgCl_2$. We must assume a weak equilibrium exists between the F^- and Mg^{2+} that will generate a small amount of the inhibitory MgF_3^- species. The calculated KI for NaF is roughly 15mM so we believe that MgF_3^- is probably at least a sub-millimolar range inhibitor of the CDK2 kinase reaction.

Substrate K_M experiments were carried out in 100mM Tris, pH 8.0, 150mM KCl, 10mM $MgCl_2$.

Molecular Dynamics Simulations

All simulations were carried out using the FF99SB all-atom potential (Hornak et al., 2006) in the AMBER 10.0 simulation package (Case et al., 2006). Crystal structures were prepared by taking the biological unit and associated ligands and ordered solvent molecules, protonating ionizable groups at expected pH 7.5 protonation states, immersing

in a periodic water box extending 12Å beyond all protein atoms, neutralizing the total charge with monovalent ions, and then adding Na+/Cl- ion pairs randomly throughout the solvent to approximate 150mM salt. The ATP + 1 Mg simulations were started from pdb entries 1JST and 1QMZ, after removing the substrate peptide from 1QMZ. AMPPNP was replaced with ATP and Mn was replaced with Mg, when needed. The two Mg simulation started from pdb entry 1QMZ, with the second Mg (MgI) placed in the position observed for this ion in the TS structure. The final simulation began from the TS structure. Parameters for the MgF_3^- were generated using the AMBER RESP protocol (Cieplak et al., 1995; Cornell et al., 1995) using *in vacuo* HF 6-31G* geometry optimization in Guassian03. We transferred the hydrogen from the substrate reactive Thr-OH onto Asp127 of CDK2. Parameters for phospho-Thr were obtained from (Homeyer et al., 2005) and ATP and ADP parameters originated from (Meagher et al., 2003). The systems were all energy minimized and gradually equilibrated to a temperature of 303K using while slowly decreasing harmonic positional restraints on the protein over a period of 160 picoseconds. Production phases of the trajectories were carried out using constant Temperature and constant Pressure without restraints for total simulation times of 50ns.

The electrostatic surface potentials were calculated using the AMBER all-atom FF99SB all-atom potential (Hornak et al., 2006) in the APBS Poisson-Boltzmann solver (Baker et al., 2001) including just the protein atoms (not the ligands) in 150mM added salt.

Supplementary Figures

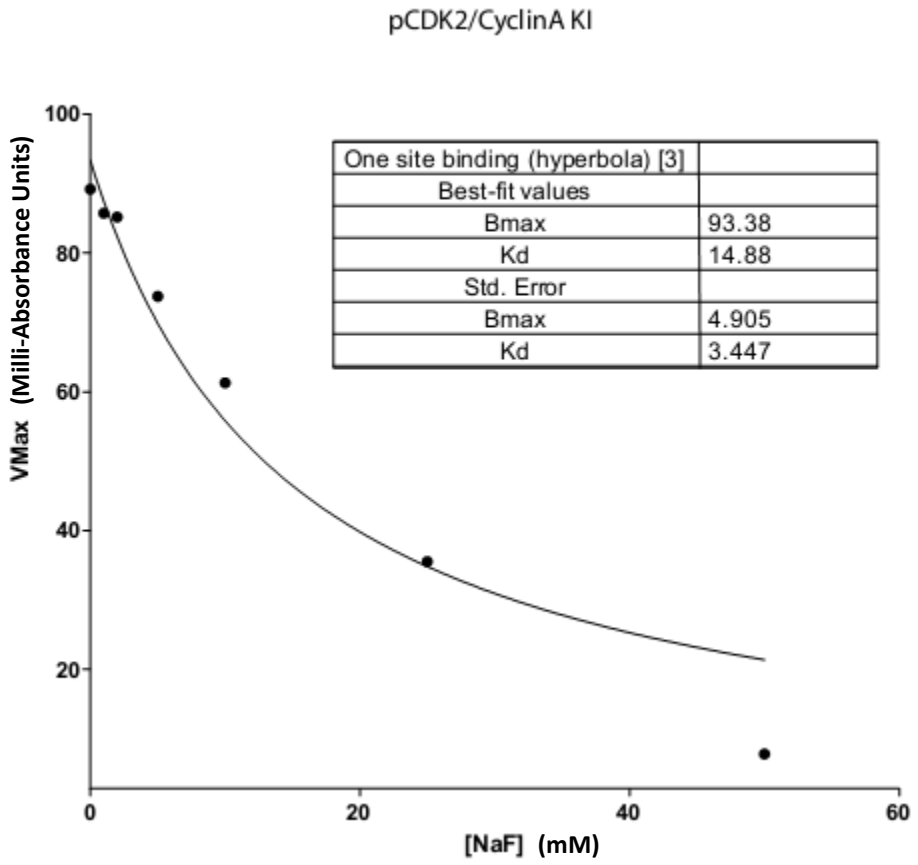

Figure 2-10. Inhibition of kinase activity by NaF (MgF_3^-)

Data was measured using a coupled kinase assay which links oxidation of NADH to the regeneration of ATP from ADP produced by the kinase. Reactions were carried out at 30˚ C using 12.5nM pCDK2/CyclinA and 100μM histone H1 as substrate. MgF_3^- is in equilibrium with Mg^{2+}/F^- in solution so MgF_3^- was generated by the addition of NaF to the reaction buffer containing 10mM $MgCl_2$. Total NaF is indicated on the x-axis. Data was fit to a standard K_M type equation.

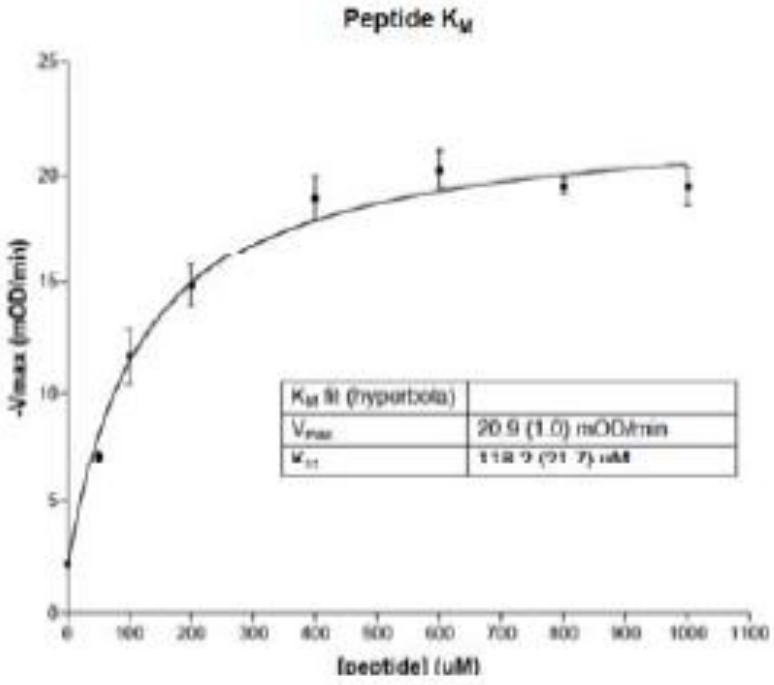

Figure 2-11. pCDK2/Cyclin A KM for peptide

Data was measured using a coupled kinase assay which links oxidation of NADH to the regeneration of ATP from ADP produced by the kinase. Reactions were carried out at 30°C using 12.5nM pCDK2/CyclinA and the same PKTPKKAKKL peptide used in the crystal structures.

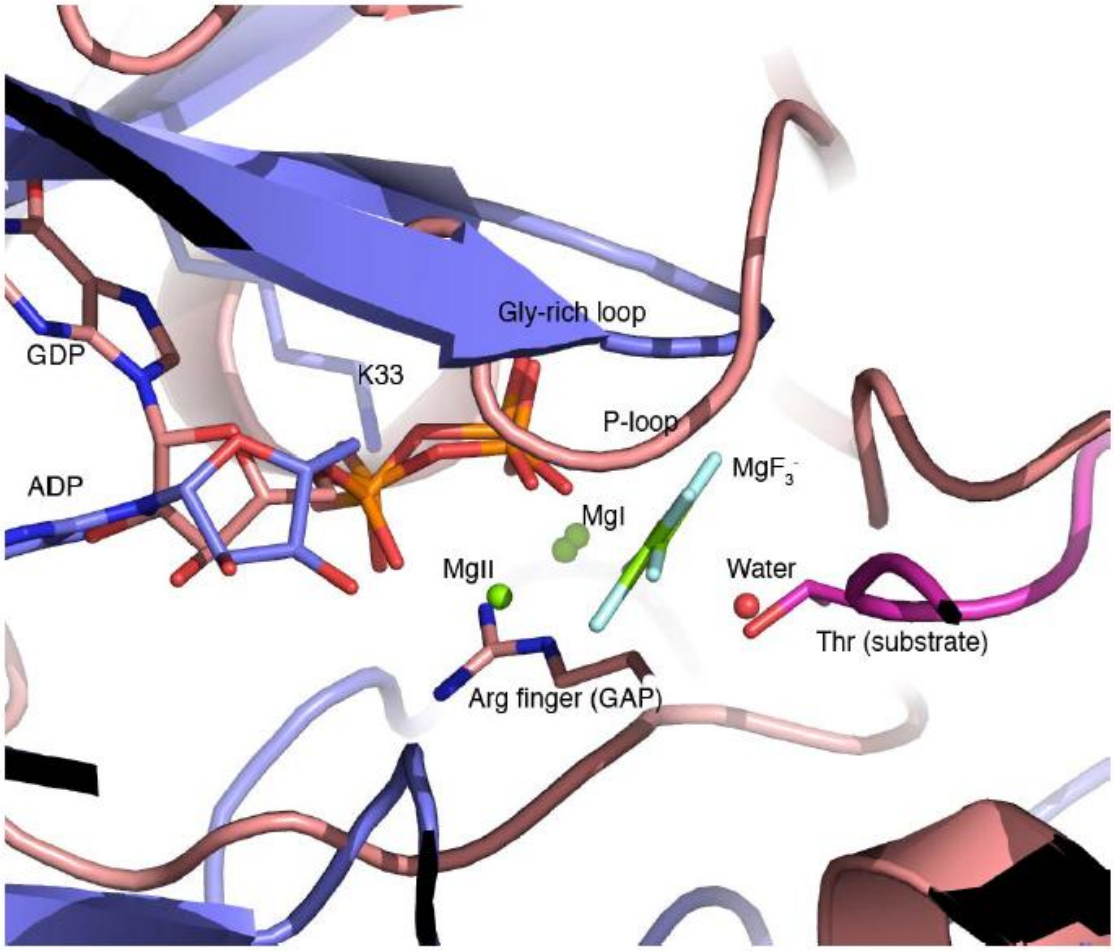

Figure 2-12. Similarity between the NTP TS geometry of CDK2 kinase and rhoA, a small G-protein.

CDK2/CyclinA is blue, rhoA/rhoGAP (3MSX.pdb) is salmon. Both have a Mg^{2+} at the MgI site. RhoGAP positions a positively-charged Arg at the MgII site of CDK2. The NDP (ADP/GDP) α and β-phosphates, γ-phosphate mimics (MgF_3^-) and substrate nucleophiles (Thr/water) are all in similar positions. The CDK2 Gly-rich loop plays a similar role to the rhoA P-loop, with backbone amides stabilizing the α and β-phosphates.

CHAPTER 3

A price to be paid for two-metal catalysis: Magnesium ions that accelerate chemistry unavoidably limit product release from CDK2 kinase.

Foreword

This chapter describes our work on establishing the essentiality of the 2^{nd} Mg^{2+} ion in the CDK2 reaction, and then determining the activating and inhibiting roles of the 2^{nd} Mg^{2+}, by isolating which steps of the reaction the Mg^{2+} affects. This chapter represents collaborative work within the Young laboratory and assisted by Prof. Patrick O'Brien. I will enumerate the specific contributions to experiments and calculations presented in this chapter:

Jacobsen DM: Prepared crystals, X-ray diffraction data collection, calculated structure solution/refinement, all enzyme kinetics experiments, and molecular dynamics calculations.

Bao ZQ: Performed cloning of CDK2, Cyclin A, and CAK, protein preparation and purification, and isothermal titration calorimetry experiments.

Patrick O'Brien: Provided guidance and assistance in the conception and then interpretation of the enzyme kinetics experiments, in particular the solvent viscosity titration experiments.

Abstract

The incorporation of divalent metal ions into an active site is a fundamental catalytic tool used by diverse enzymes. Divalent cations are used by protein kinases to both stabilize ATP binding and accelerate chemistry. Kinetic analysis establishes that Cyclin dependent kinase 2 (CDK2) requires simultaneous binding of two Mg^{2+} ions for catalysis of phosphoryl transfer. This tool comes with a price - this study contrasts the opposing rate-acceleration effects against an unavoidable rate-limiting consequence of the use of two Mg^{2+} ions by CDK2. We demonstrate that product release is rate-limiting for activated CDK2, and evaluate the effects of the two catalytically essential Mg^{2+} ions on the stability of the ADP product within the active site. We present two new crystal structures of CDK2 bound to ADP showing how the phosphate groups can be coordinated by either one or two Mg^{2+} ions, with the occupancy of one site in a weaker equilibrium. Molecular dynamics simulations suggest that ADP phosphate mobility is more restricted when ADP is coordinated by two Mg^{2+} ions compared to one. The structural similarity between the rigid ADP•2Mg product and the cooperatively assembled transition-state provides a mechanistic rational for the rate-limiting ADP release that is observed. The evolution of protein kinases must have involved the careful tuning of the affinity for the second Mg^{2+} ion in order to balance the needs to stabilize the chemical transition state and to allow timely product release. The link between Mg^{2+} site affinity and activity also presents a chemical handle that may be used by regulatory factors as well as explain some mutational effects.

Introduction

Cyclin dependent kinases (CDKs) are a well-studied family of Ser/Thr protein kinases that play a critical role in signaling progression through the eukaryotic cell cycle. CDK2/Cyclin E heterodimers provide the phosphorylation signals that move the cell through the G1 to S phase cell cycle restriction point and CDK2/Cyclin A heterodimers then push it through the S phase (Malumbres and Barbacid, 2009). To ensure proper cell cycle signaling, the specific catalytic activities of CDKs are regulated through a variety of mechanisms that either alter substrate recruitment and affinity or accelerate the rate of phosphoryl transfer. A series of studies have illustrated how monomeric CDK2 is essentially inactive, with a combination of extremely low k_{cat} values and extremely high K_M values *in vitro* (Stevenson et al., 2002). Crystal structures have shown how the allosteric activation of human CDK2 occurs by hetero-dimerization with a Cyclin protein binding partner and by phosphorylation of Thr160 on the kinase activation loop by an activating kinase (Jeffrey et al., 1995; Russo et al., 1996b; Stevenson et al., 2002). Cyclin binding and Thr160 phosphorylation stabilize large scale conformational changes that account for some, but not all, of the resulting gains in k_{cat} and substrate K_M values. Our hypothesis is that a more detailed description of the chemical mechanism of the fully activated enzyme will help illuminate how some still mechanistically elusive regulatory factors as well as potentially oncogenic mutations can either achieve or bypass normal regulation of CDK2 by alternatively deconstructing or stabilizing some of the essential features of the fully active enzyme.

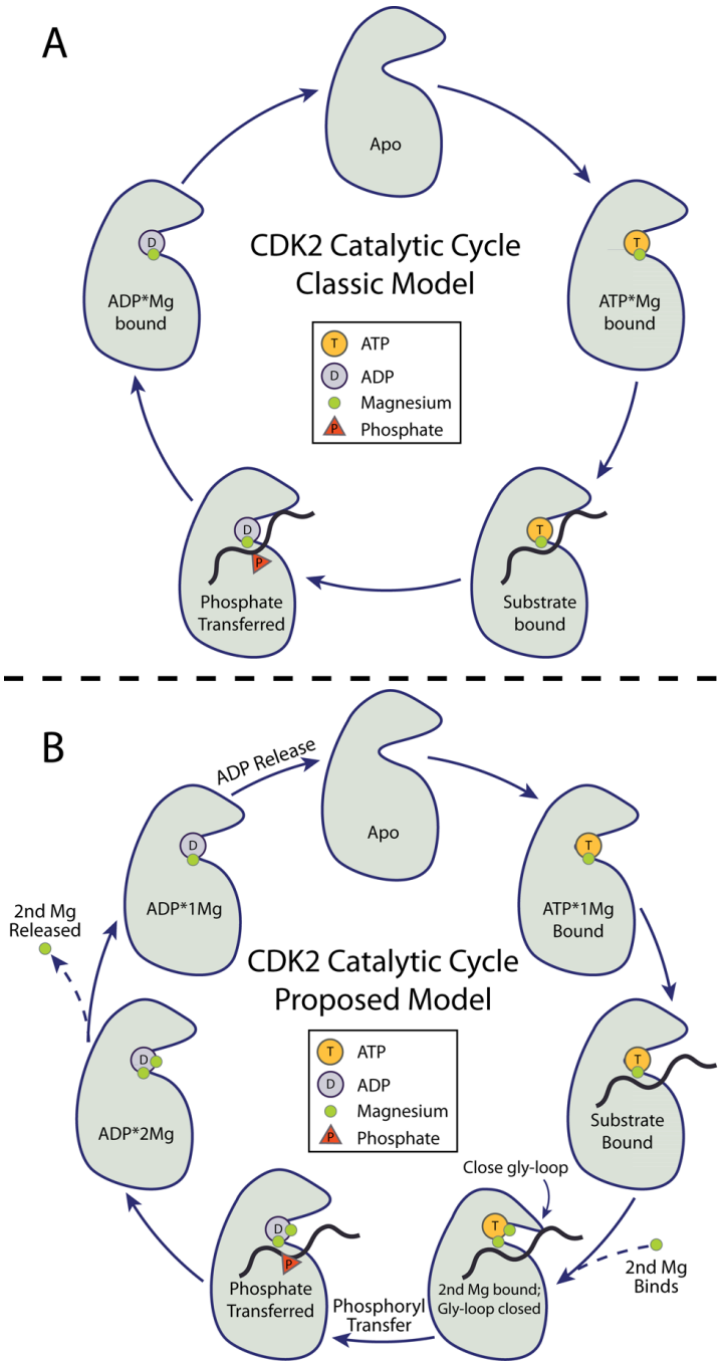

Figure 3-1 CDK2 catalytic cycle.

Panel A) The classic model of protein kinase catalysis. **Panel B)** Proposed model that binding of second Mg^{2+} ion prior to phosphoryl transfer and release of second Mg^{2+} prior to ADP release are critical to efficient progression through the catalytic cycle.

The catalytic cycle of an active protein kinase is comprised of the binding of both ATP•Mg^{2+} and protein substrate, followed by the chemical step of phosphoryl transfer, and finally product release. Progression through all steps of the catalytic cycle is required to allow subsequent rounds of catalysis, and therefore any of these steps, depicted in Figure 3-1A, could potentially be rate limiting. For a tightly regulated signaling enzyme such as CDK2, dynamic attenuation of the rate of any of these steps could provide a regulatory mechanism for kinase signaling activity. Solvent viscosity effect studies of the fully activated states of many kinases, including CDK2, have shown that product release can be slow and often rate-limiting (Hagopian et al., 2001; Harper and Adams, 2001). At the same time, the somewhat similar magnitudes of the rates of the chemistry and product release steps in many protein kinases means that both steps can contribute to the overall reaction rate and the relative contributions may vary with conditions or activation state of the enzyme. One external factor that is known to affect CDK2 and most protein kinases in an often complex way is the concentration of divalent metals (Harper and Adams, 2001; Bao et al., 2011).

The nucleotide binding and phosphoryl transfer steps of the catalytic cycle are both strongly affected by the binding of divalent cations in the active site of CDK2 (Jeffrey et al., 1995; Russo et al., 1996b; Adams, 2001; Bao et al., 2011). Of all the divalent metal ions, Mg^{2+} is by far the most abundant and available *in vivo*, and it is believed to be the species used by most protein kinases under physiological conditions (Adams, 2001). No ordered Mg^{2+} ions have been identified in CDK2 crystal structures in the absence of bound nucleotide, but under physiological conditions ATP in the cell exists as a complex with Mg2+ and the ATP•Mg2+ is the substrate of most protein

kinases (Storer and Cornish-Bowden, 1976). Although other divalent metal ions can sometimes be functional surrogates for Mg^{2+} in protein kinases *in vitro* (Zheng et al., 1993b; Grace et al., 1997), we will focus specifically on Mg^{2+} because of its physiological relevance and because alternative divalent cations can function quite differently. Mg^{2+} ions are critical to the stabilization of the nucleotide phosphates because, similar to the phosphates themselves, the active site region that surrounds the ATP phosphates is also strongly electronegative. Mg^{2+} ions neutralize this charge by forming bridging contacts between the phosphates and electronegative protein functional groups such as Asp145 in the conserved kinase "DFG" motif. There are additional Mg^{2+} effects as well, not all fully understood. Some kinases have been described as possessing both essential and inhibitory divalent binding sites (Zheng et al., 1993b), while other kinases are thought to catalyze phosphoryl transfer with a single or even zero divalent ions (Mukherjee et al., 2008). Given the strong effect that Mg^{2+} ions have on the activity of CDK2 (Bao et al., 2011), it is essential to have a detailed understanding of the roles that Mg^{2+} ions play at each step of the catalytic cycle before we can truly understand how the enzyme functions and how it can be regulated.

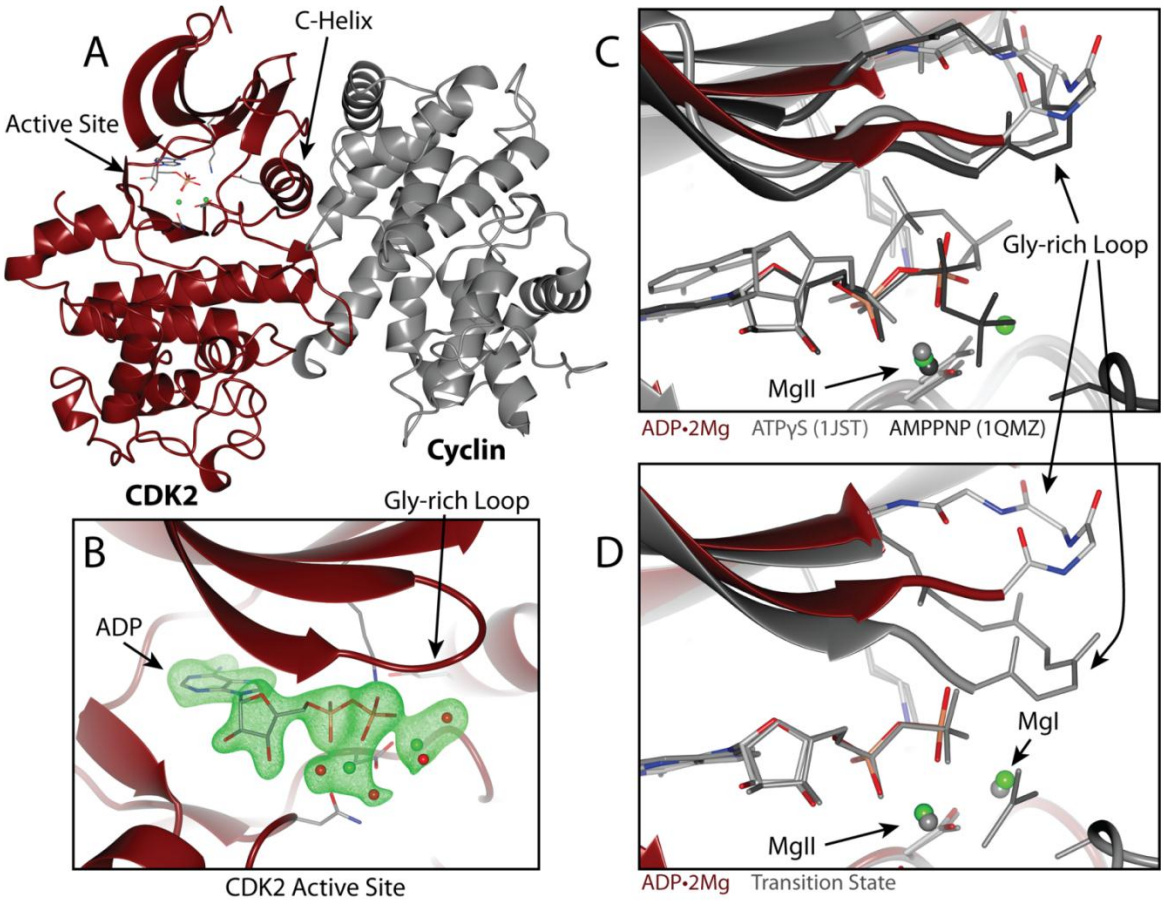

Figure 3-2 Structure of CDK2 bound to ADP, ATP, and the TS-Mimic

Panel A) Overview of pCDK2•Cyclin A complex bound to ADP with two Mg^{2+} ions. pCDK2 is shown in maroon, Cyclin A in gray. ADP, D145, K33, E51 are displayed in stick representation. Green spheres represent Mg^{2+} ions. **Panel B)** ADP•2Mg average kicked omit map. Green electron density is positive mFo-DFc map contoured to 3σ; electron density clipped to within 2Å of ADP, Mg^{2+} and coordinating water oxygen atoms. **Panel C)** Two Mg^{2+} ions identified in ADP•2Mg structure (maroon) but not ATPgS-bound pCDK2 (gray) or AMPPNP-bound pCDK2 (black). Panel D) Two Mg^{2+} ions stabilize closed Gly-loop conformation in Transition State structure, but not in ADP•2Mg structure.

Structures of CDK2 bound to ATP or ATP-analogues revealed at most a single divalent in the active site, as shown in Figure 3-2C. This metal, which is generally bound at a site that is structurally homologous to the site labeled MgII in two-metal/ATP structures of protein kinase A (PKA), coordinates the α- and β-phosphates to active site residues D145 ("DFG") and N132. The structures we recently reported of a transition state (TS) mimic of the phosphorylated CDK2•Cyclin complex (pCDK2•Cyclin),

crystalized in the presence of Mg^{2+}, were the first to observe a second divalent simultaneously bound in the pCDK2•Cyclin active site. The second Mg^{2+} ion is bound at the site labeled MgI in Figure 3-2D (Bao et al., 2011), a site that is structurally homologous to the second divalent site observed in PKA. Although this second Mg^{2+} ion may only bind transiently during the complete CDK2 catalytic cycle, it is essential that both Mg^{2+} ions be simultaneously bound to achieve optimal catalysis of the phosphoryl-transfer step.

The active site of the two Mg^{2+} bound TS of pCDK2•Cyclin is conformationally distinct from the 1Mg ATP-bound structures. The conformation of the Glycine-rich loop (Gly-loop) in the TS is closed such that it makes additional electrostatic interactions with the phosphates and excludes water from the active site. Molecular dynamics (MD) simulation of either pCDK2•Cyclin bound to ATP or the TS-mimic demonstrated that the binding of the second magnesium strongly stabilizes the closed conformation of the Gly-loop and also notably reduces the conformational flexibility of the ATP phosphates. Furthermore, it was found that pCDK2•Cyclin activity (k_{cat}^{app}) increased dramatically as total Mg^{2+} concentration is increased over the range of 0 to 7 mM (Bao et al., 2011). All these data led us to propose a model for how the second magnesium ion functions as an essential activator of the chemical step by binding to the pCDK2•Cyclin•ATP•Mg•substrate complex, closing the Glycine-rich loop and stabilizing the TS to accelerate phosphoryl transfer (Bao et al., 2011). If the presence of both Mg^{2+} ions is essential for the phosphoryl transfer step, we can assume that both Mg^{2+} ions must be present in the active site immediately following bond cleavage,

presumably coordinating the ADP^{3-} and the phosphorylated protein product in a way not unlike the geometry observed in the TS mimic structure.

In this paper we extend our examination of the role of magnesium in the CDK2 catalytic cycle by focusing on the effects of the Mg^{2+} ions just after phosphoryl transfer when the reaction products are still bound within the active site. We use crystallography, molecular dynamics simulations, and enzyme kinetics to characterize the structural and energetic effects of the equilibrium binding of the two Mg^{2+} ions to the active CDK2•CyclinA enzyme. Taken together, our results suggest that cooperative binding of the second catalytically essential Mg^{2+} ion stabilizes nucleotide binding to the extent that product release becomes rate-limiting in the fully activated state of the enzyme. Our structural and molecular dynamics data suggest that one of the two Mg^{2+} ions reversibly binds and that its release is coupled to conformational changes that facilitate release of the ADP•Mg^{2+} product. This more complex model for the multiple roles of the Mg^{2+} ions provides an explanation for why some kinases have been observed to be stimulated by Mg^{2+} (Waas and Dalby, 2003; Liu et al., 2010) while others are seen to be inhibited (Adams and Taylor, 1993).

We conclude that making use of a two Mg^{2+} mechanism of catalysis thus leaves this enzyme in an apparent conundrum; although the two Mg^{2+} stabilization of the reaction TS may be an efficient chemical mechanism to achieve acceleration of the phosphoryl transfer step of the reaction, relying on two divalent metals for catalysis may also unavoidably limit and also cause Mg^{2+} to inhibit the rate of ADP•2Mg release from the active site. For CDK2, the binding of a second active-site Mg^{2+} to the solitary MgI binding site illustrates how Mg^{2+} can alternatively function as both an activator and an

inhibitor at different steps of the catalytic cycle: functioning in the former role when the second Mg^{2+} activates phosphoryl-transfer from ATP and in the latter when it suppresses the rate of ADP release. The activating and inhibitory Mg^{2+} binding sites in CDK2 are thus exactly the same site, with the two roles differentiated only by whether the nucleotide is in the ATP or ADP state.

Experimental Methods

Crystallography

Thr160 mono-phosphorylated human CDK2 (pCDK2) and mouse Cyclin A were expressed and purified as described previously[7]. Purified pCDK2•Cyclin A complex was concentrated to 13.7 mg/mL using centrifugal filtration tubes. 0.65 μL of purified protein solution was mixed with 1.11 μL (final 4 mg/mL protein), 0.99 μL (final 4.5 mg/mL protein) or 0.89 μL (final 5 mg/mL protein) of the crystal condition. The crystallization condition is 22% w/v polyacrylic acid sodium salt 5100, 20 mM $MgCl_2$, and 100 mM HEPES pH 7.5. Apo crystals were grown in 96-well sitting-drop vapor diffusion trays at 20C. Large plate-like crystals appeared after 3-6 days and were allowed to grow for three weeks. Crystals were harvested with a nylon loop and transferred to a new drop containing 4 μL of ligand soaking/cryoprotection solution. The crystals were soaked for 1 hour in 30% v/v glycerol, 3.2 mM ADP, 10 mM $MgCL_2$, 25 mM or 50 mM HEPES pH 7.5 and 2% w/v PEG-3350 before mounting on nylon loops or mesh mounts and flash freezing in liquid nitrogen. Diffraction data were collected at the 21-ID-G and 21-ID-D LS-CAT beamlines at the Advanced Photon Source (APS), Argonne National Labs. 180° of data were collected at 100K with λ=0.97872 Å, with a 0.5° oscillation range per frame.

Data integration and scaling were performed with Mosflm (Leslie, 1992) and CCP4 Scala (Evans, 2006) using the default options.

Initial phases were determined by molecular replacement using Phaser (McCoy et al., 2007), using a previously solved structure of CDK2•Cyclin A. We removed the Gly-rich loop (residues 10-18), a loop N-terminal to the C-helix (residues 37-42), and the activation loop (residues 153-166) from the CDK2 search model in an effort to minimize model bias from the initial phases, because of the potential flexibility of these regions of CDK2. The CDK2 and Cyclin A models were searched separately, rather than as a complex. Using the obtained Phaser solution (two dimers of CDK2•Cyclin A), we performed Cartesian simulated annealing using PHENIX (Adams et al., 2010). The final refined model was obtained by iterating between manual real-space refinement in COOT (Emsley et al., 2010) and automated refinement in PHENIX. Early stages of refinement were dominated by manual re-building of the missing loops (residues 10-18, 37-42, and 153-166) using minimal refinement options, including reciprocal space atomic positions and individual atom isotropic B-factors with default NCS restraints. NCS was applied between the two CDK2 chains, A and C, and the two cyclin chains, B and D. After the protein chains were well described by the refinement model, NCS B-factor restraint weights were reduced and TLS refinement was introduced. TLS groups were identified using the TLSMD server (Painter and Merritt, 2006a, 2006b). After protein modeling was completed, the ADP ligands were built into the electron density. The phosphates were positioned by placing the phosphorous atom at the center of the strong point of density in each identified phosphate region of the electron density. Following one round of refinement after ADP placement, the magnesium ions and coordinating waters were

positioned in a similar manner. We used phenix.metal_coordination to maintain the proper coordination of the identified magnesium ions and coordinating groups. The additional restraints were necessary to prevent PHENIX from moving the coordinating groups out of the electron density, most likely due to repulsive non-bonded terms in the minimization function utilized by PHENIX. Finally, remaining ordered water molecules were identified by PHENIX (default water search options) and included in the final stages of structure refinement.

A kicked omit map was generated by removing the ADP, Mg^{2+}, and coordinating water atoms from the final ADP•2Mg model, and then computing a kicked mFo-DFc difference map (Praznikar et al., 2009). To generate a kicked map a large ensemble of slightly perturbed models are generated by moving atoms randomly to varying degrees, and then averaging maps using phases computed from those perturbed models. The resulting map should be less biased than the refined model map.

Enzyme Kinetics and Solvent Viscosity Effect Studies

Kinase activity was measured using a coupled assay in which ADP production is linked to NADH oxidation using Pyruvate kinase and Lactate dehydrogenase (PK/LDH). In all experiments presented here, the protein substrate for CDK2•Cyclin was histone H1. Since this work is focused on the nucleotide/Mg^{2+} interactions, and since $K_{M(H1)}$ doesn't change significantly as a function of $[Mg^{2+}]_{free}$ (appendix Figure 3-24 and Figure 3-25), H1 is kept at a saturating level in all conditions (200 μM ~ 10x $K_{M(H1)}$. H1 concentration was determined spectroscopically using ε_{230}=1.85 cm^2/mg (Camerini-Otero et al., 1976), and ATP concentration was determined with ε_{259}=15400 $cm^{-1}M^{-1}$. Kinase reaction progress was monitored by absorbance at 340 nm with a spectromax plus 384

spectrophotometer. Reaction buffers included 100 mM Tris pH 7.5, 1 mM phosphoenolpyruvate, 280 μM NADH, and at least 60 and 90 units of PK and LDH respectively (10x dilution of Sigma PK/LDH aqueous solution). $MgCl_2$ and KCl were included in varying amounts to achieve the desired $[Mg^{2+}]_{free}$, with a final ionic strength of 162 mM. Calculation of $[Mg^{2+}]_{free}$ assumes a K_d of ATP for the first Mg^{2+} [to form $(ATP•Mg)^{2-}$] of 28.6 μM (Storer and Cornish-Bowden, 1976), Binding of Mg^{2+} to other sources (K, Tris, other ATP species) were not considered in the $[Mg^{2+}]_{free}$ calculations for this work because the iterative Storer method indicates contributions from those sources were much weaker than the ATP•Mg interaction, and result in a linear reduction of $[Mg^{2+}]_{free}$ over the total ATP and Mg concentration ranges considered herein.

The effect of solvent viscosity on CDK2 reactions was determined for sucrose solutions of 0 g/L, 150 g/L, 240 g/L and 296 g/L. The relative viscosity was determined using $\eta_{rel} = t° * d°$, where $t°=t_{Sucrose}/t_{NoSucrose}$, t is the mean flow time of the buffer in an Ostwalt viscometer measured 10 times, and d° is the relative density of the buffers. Reactions were performed with 25 nM or 50 nM kinase at 30° C using pre-heated plates. All components of the reaction were mixed and pre-heated to 30° C and then the reaction was initiated by adding the kinase. Reaction rates were determined using the linear portion of the 340 nm absorbance trace. Rates of the lowest and highest $[Mg^{2+}]_{free}$ conditions at the lowest and highest sucrose conditions were linearly dependent on [CDK2•Cyclin]. PK/LDH, H1, and ATP•2Na were obtained from Sigma-Aldrich. The solvent viscosity effect reported in Figure 3-9A and Figure 3-9B were calculated as the slope m of the line $\eta_{rel} = m(v°/v) + \text{intercept}$; where v° is the velocity with 0 sucrose (graphically a plot of v°/v vs η_{rel}). These data are included in the supplementary material.

Isothermal Calorimetry to Measure Binding of ADP

Purified pCDK2•Cyclin was obtained as described in the Crystallography section. The calorimeter cell contained 25 μM protein buffered in 150 mM KCl, 5-10 mM $MgCl_2$, 5% Glycerol v/v, 25 mM HEPES pH 7.5. The syringe contained 5 mM ADP in the same buffer as in the cell. This experiment was performed at 20 C with magnesium concentrations of 5 mM, 7.5 mM and 10 mM $[Mg^{2+}]_{total}$ in both the protein and ADP solutions. 2.5 mM $[Mg^{2+}]_{total}$ was attempted but the signal was too low for accurate fitting. ITC data analysis was performed in the Origin software provided by MicroCal. The baseline correction was performed using the signal asymptote at high ADP:protein molar ratio. Curve fits were performed assuming a single-site binding model with ADP binding stoichiometry fixed to 1:1. Data can be viewed in supplementary Figure 3-10, Figure 3-11, and Figure 3-12.

Kinetic Model

We derived and fit a model of kinase activity to predict activity as either ATP•Mg or Mg are varied. This model assumes that the protein substrate is saturating and binds in rapid equilibrium (i.e. assume that protein substrate is always bound). The data used for fitting was the KM(ATP•Mg), Mg^{2+}_{free} Titration, and ATP titration experiments – all with 0 g/L sucrose (relative viscosity = 1). The model was fit in R 2.14.1 (R Development Core Team, 2010) using the minpack.lm package for Levenberg-Marquardt nonlinear least squares fitting (nls.lm). The model is:

$$K_{D\_ATPMg} = K_{D\_ATP2Mg} + \frac{K_{D\_ATP1Mg}}{1 + \frac{[MgFree]}{K_{MgActivation}}}$$

$$k_{3App} = \frac{k_3}{1 + \frac{K_{MgActivation}}{[MgFree]}}$$

$$k_{4App} = k_{4\_1} + \frac{k_{4\_2}}{1 + \frac{[MgFree]}{K_{MgInhibition}}}$$

$$k_{cat} = \frac{k_{3App} * k_{4App}}{k_{3App} + k_{4App}}$$

$$v = \frac{k_{cat} * \frac{[ATP \cdot Mg]}{K_{D\_ATPMg}}}{1 + \frac{[ATP \cdot Mg]}{K_{D\_ATPMg}}}$$

The fit parameters of the model are K_{D_ATP2Mg}, K_{D_ATP1Mg}, $K_{MgActivation}$, $K_{MgInhibition}$, k_3, k_{4_1}, k_{4_2}. The rate parameter k_3 represents the maximal rate of phosphoryl transfer. The rate parameters k_{4_1} and k_{4_2} represent the slow and fast rates of ADP release respectively, which we propose are the rates of ADP•2Mg and ADP•1Mg release respectively. K_{D_ATP2Mg} and K_{D_ATP1Mg} represent the limiting binding affinities of ATP when two or one Mg^{2+} ions are present respectively. $K_{MgActivation}$ and $K_{MgInhibition}$ are the thermodynamic equilibrium constants governing the activation vs. inhibition properties of the 2nd Mg binding site (the MgI site). The two activating effects observed are on $K_{M(ATP•Mg)}$ and reaction rate, which we interpret as increasing ATP•Mg stability and phosphoryl transfer rate respectively. Thus, $K_{MgActivation}$ controls the shape of the increasing hyperbola of k_{3App} rate and the decreasing hyperbola of KD_ATPMg. The inhibiting effect of the second Mg noticeable in the binding affinity of ADP, thus we suggest that the effect rate of ADP release decreases as MgI is stabilized in the product-bound state. Thus $K_{MgInhibition}$ controls the shape of the decrease hyperbola of the k_{4App} rate. Intuitively, $K_{MgActivation}$ is the binding of MgI to the E•ATP•Mg complex and

$K_{MgInhibition}$ is the binding of MgI to the E•ADP•Mg complex. The model parameters are shown in Table 3-1.

Table 3-1. Kinetic model fit parameters

Parameter	**Fit Value**	**Std. Error**	**p-value (from T-test)**
K_{D_ATP2Mg}	33.75 μM [ATP•Mg]	11.21 μM [ATP•Mg]	2.8e-3
K_{D_ATP1Mg}	3931.55 μM [ATP•Mg]	465.87 μM [ATP•Mg]	1.3e-15
$K_{MgActivation}$	367.42 μM $[Mg^{2+}]_{free}$	63.18 μM $[Mg^{2+}]_{free}$	1.5e-8
$K_{MgInhibition}$	9121.99 μM $[Mg^{2+}]_{free}$	1785.04 μM $[Mg^{2+}]_{free}$	5.7e-7
k_3	186.74 s^{-1}	19.38 s^{-1}	< 2e-16
k_{4_1}	4.785 s^{-1}	0.54 s^{-1}	< 2e-16
k_{4_2}	7.557 s^{-1}	0.48 s^{-1}	< 2e-16

Isothermal Titration Calorimetry – ADP Binding

Purified pCDK2•Cyclin was obtained as described in the Crystallography section. The calorimeter cell contained 25 μM protein buffered in 150 mM KCl, 5-10 mM $MgCl_2$, 5% Glycerol v/v, 25 mM HEPES pH 7.5. The syringe contained 5 mM ADP in the same buffer as in the cell. This experiment was performed at 20C with magnesium concentrations of 5 mM, 7.5 mM and 10 mM $[Mg^{2+}]_{total}$ in both the protein and ADP solutions. 2.5 mM $[Mg^{2+}]_{total}$ was attempted but the signal was too low for accurate fitting. ITC data analysis was performed in the Origin software provided by MicroCal. The baseline correction was performed using the signal asymptote at high ADP:protein molar ratio. Curve fits were performed assuming a single-site binding model with ADP binding stoichiometry fixed to 1:1. Data can be viewed in chapter appendix Figure 3-10, Figure 3-11, and Figure 3-12.

Molecular Dynamics

All molecular dynamics (MD) simulations were performed using the Amber99SB (Hornak et al., 2006) force field using Amber10 for MD integration (Case et al., 2005). In addition to the base Amber99SB parameters, we used ADP parameters from (Meagher et al., 2003) and phospho-threonine parameters from (Homeyer et al., 2005). Parameters for protonated ADP were generated using the AMBER RESP protocol (Cieplak et al., 1995; Cornell et al., 1995) based on a charge distribution generated *in vacuo* from HF 6-31G* geometry optimized methyl-diphosphate in Gaussian03 (Frisch et al.). The starting model for each simulation was prepared by selecting a single pCDK2•Cyclin A dimer from the crystallographic asymmetric unit (chains A and B). Next, the model was protonated and solvated in TIP3P explicit water (Jorgensen et al., 1983) arranged in a truncated octahedral box with 150 mM explicit NaCl, plus additional ions for counter-charge, using the Amber tleap software package. The simulation system was then minimized using successive rounds of conjugate gradient and then steepest descent minimization with successively reduced harmonic restraints on the protein. Next, the restrained system was slowly heated from 0K to 303K over 30 ps of constant volume simulation. Switching to a constant pressure/constant temperature (NPT) ensemble, the system was then allowed to equilibrate with continually diminishing restraints over an additional 120 ps of system equilibration. Constant temperature and pressure were regulated by a Berendsen thermostat (Berendsen et al., 1984) and pressure by isotropic volume scaling, both with very weak coupling to the dynamics. All hydrogen atom bond lengths were constrained using SHAKE. 50 ns of production dynamics were calculated for each trajectory using PMEMD (part of the Amber software package). Each starting

conformation was equilibrated and simulated in five separate trajectories. For each trajectory, the initial bulk solvent ion positions were randomly exchanged with solvent molecule positions far (at least 5 Å) from the protein solute to de-correlate the separate trajectories. The time-series and other MD analysis plots were prepared in the R statistical software package (R Development Core Team, 2010).

Results

Two Mg^{2+} Ions Are Required for Optimal CDK2 Kinase Activity

We previously reported the crystal structure of fully activated CDK2 (pCDK2•cyclin) bound to a transition state mimic (ADP•MgF_3•peptide). In this structure there was clear evidence for two catalytic Mg^{2+} ions in the kinase active site. Under conditions of constant ATP concentration a multi-phasic dependence on Mg^{2+} concentration was observed that was most simply consistent with two essential Mg^{2+} ions (Bao et al., 2011). To further investigate the requirement for multiple catalytic Mg^{2+} ions we have carried out a more complete steady state kinetic analysis of the kinase reaction using histone H1 as a substrate.

As the biological substrate of kinases is ATP•Mg^{2+}, it can be difficult to separate out the contribution from this essential Mg^{2+} that is bound along with the substrate, and the contribution of a second Mg^{2+} ion. However, the requirement for a second essential Mg^{2+} ion can be inferred from experiments in which the concentration of ATP substrate is varied at a constant total concentration of Mg^{2+} ions (London and Steck, 1969; Waas and Dalby, 2003). Under conditions in which the concentration of ATP is far above the K_d for dissociation of the ATP•Mg^{2+} complex (28.6 μM (Storer and Cornish-Bowden, 1976)), the added ATP will chelate one equivalent of Mg^{2+} thereby depleting the

concentration of free Mg^{2+} that is available. Consistent with our previous results, the effect of increasing ATP concentration is biphasic with a clear saturation of the velocity followed by a decrease in velocity as the concentration of free Mg^{2+} is depleted. At a higher concentration of total Mg^{2+} the inhibitory phase is shifted to higher concentration of ATP (Figure 3-3A). These data could be explained by a model in which ATP without Mg^{2+} is a potent inhibitor of CDK2 or by the model in which two Mg^{2+} are required for optimal activity. Below we present additional data in support of the model that CDK2 requires two Mg^{2+} ions for catalysis.

Figure 3-3 Cooperativity between nucleotide and Mg^{2+} binding to CDK2.

Panel A) Dependence of the multiple turnover kinase reaction on the concentration of ATP. Histone substrate was saturating and in excess and ADP release was measured using a coupled assay (see Methods for details). Concentration of total Mg^{2+} was fixed at either 5 or 8 mM. **Panel B)** Multiple turnover kinetics in which the concentration of ATP•Mg^{2+} was varied at a fixed concentration of either 1 mM (black) or 10 mM (red) free Mg^{2+}. The velocity was fit by the Michaelis-Menten equation (lines). The resulting steady state constants from these experiments and from data collected at additional concentrations of free Mg^{2+} (see chapter 3 appendix) are plotted in panels C-E. **Panel C)** The value of $k_{cat}/K_M^{ATP•Mg}$ is was fit to a hyperbolic binding equation, indicating a very weak affinity of ~10 mM for Mg^{2+} binding to free enzyme in the absence of nucleotide. **Panel D)** The value of k_{cat} shows a complex dependence on the concentration of free Mg^{2+}, with a highly cooperative stimulation at very low Mg^{2+} and a modest decrease in k_{cat} between 1 and 20 mM Mg^{2+}. **Panel E)** The value of K_M for ATP•Mg^{2+} is dramatically decreased by the binding of a second Mg^{2+} ion. **Panel F)** The dissociation constant for ADP was determined by isothermal calorimetry as a function of total Mg^{2+} (see chapter appendix for details).

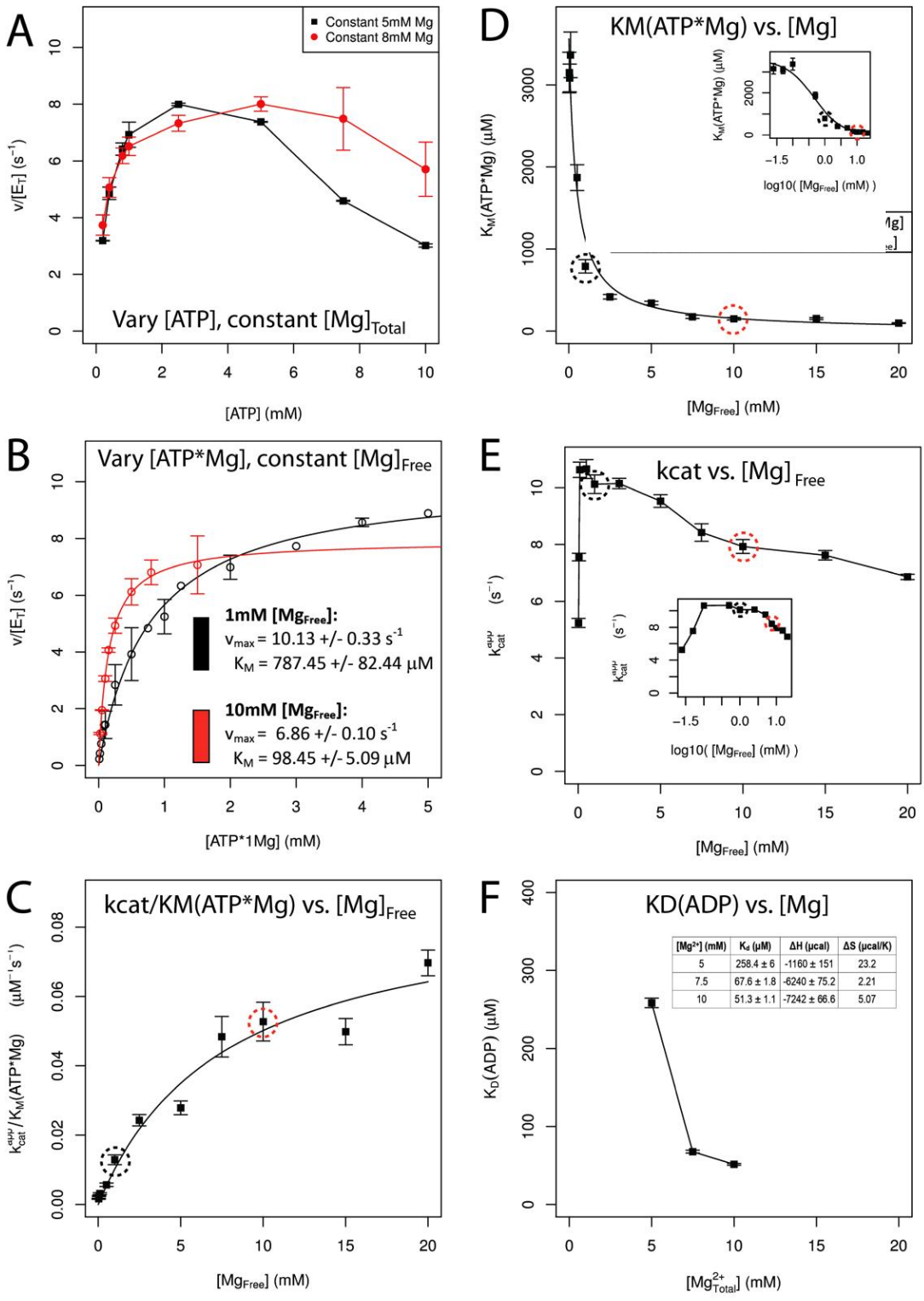

Figure 3-3 Cooperativity between nucleotide and Mg^{2+} binding to CDK2.

In order to more carefully examine the ATP utilization of CDK2 and the cooperativity between ATP•Mg^{2+} binding and the binding of the second catalytic Mg^{2+} ion, we analyzed the steady state kinetics of CDK2 at varying concentrations of ATP•Mg^{2+} with fixed concentrations of free Mg^{2+}. Under these conditions the substrate concentration dependencies followed simple Michaelis-Menten behavior (Figure 3-3B). When the concentration of ATP•Mg^{2+} was subsaturating (k_{cat}/K_M conditions), the affinity of the second essential Mg^{2+} ion for the free enzyme could be determined (Scheme 3-1). The resulting k_{cat}/K_M value gives a roughly hyperbolic or possibly linear dependence upon the concentration of free Mg^{2+}, indicating very weak binding of the second Mg^{2+} in the absence of ATP•Mg^{2+} (Figure 3-3C). This provides strong additional support that the active form of CDK2 contains two Mg^{2+} ion cofactors (Scheme 1) and this behavior is not explained by the alternative model that ATP is an inhibitor of CDK2. The analogous plot of k_{cat} as a function of free Mg^{2+} shows a more complex behavior (Figure 3-3D), with an optimal rate obtained at 1 mM free Mg^{2+} and a gradually decreasing rate constant at concentrations above 1 mM. The cooperativity between binding of the ATP•Mg^{2+} and the second Mg^{2+} is apparent by the dramatic decrease in the value of K_M ATP•Mg^{2+} (Figure 3-3E). Taken together these steady state kinetic data strongly support the proposed model that CDK2 requires two catalytic Mg^{2+} ions, and furthermore the binding of the second Mg^{2+} ion is highly cooperative with the binding of the nucleotide and its accompanying Mg^{2+} ion.

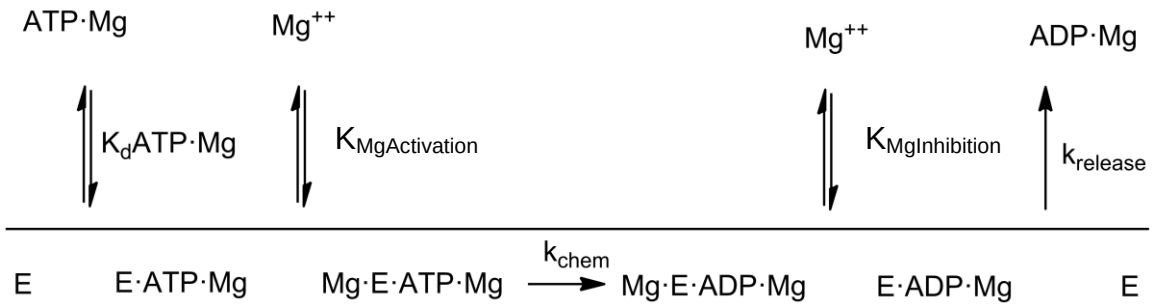

Scheme 3-1. Proposed kinetic scheme at saturating protein substrate conditions.

Crystal structures of pCDK2•Cyclin A in complex with ADP demonstrate binding of either 1 or 2 Mg.

We have structurally characterized the interaction between ADP and the kinase by determining and analyzing several new crystal structures of the pCDK2•Cyclin complex bound to ADP. We have selected two representative structures to describe here. Each of these structures has a different conformation and divalent metal coordination for ADP. One structure has two Mg^{2+} ions coordinating the ADP phosphates (ADP•2Mg), and the other has only a single Mg^{2+} ion coordinating the phosphates (ADP•1Mg).

The overall structure of the pCDK2•Cyclin complexes crystalized is shown in Figure 3-2A. The protein conformation of the two new ADP-bound structures are similar, the ADP•2Mg structure and ADP•1Mg structure have a backbone RMSD of 0.20 Å. Both are also quite similar to other published CDK2•Cyclin structures. The backbone RMSD from ADP•2Mg structure to: 1JST (a complex with ATPγS•Mn^{2+})=1.24 Å, 1QMZ (AMPPNP•Mg^{2+}/peptide)=0.65 Å, 3QHR (ADP•2Mg/MgF_3^-/peptide TS)=0.57 Å. The crystals formed in the P 1 2_1 1 space group with an asymmetric unit containing two copies each of CDK2 and Cyclin A (see table 1 for crystallography statistics). Unlike other crystal forms of pCDK2•Cyclin, this crystal form grows in the presence of Mg, and

has only been observed for pCDK2•Cyclin in our recently published transition state mimic structures (3QHR, 3QHW). The primary contact between pCDK2 and Cyclin A is along the canonical dimerization interface, which has an interface area of ~1800 $Å^2$ (buried surface area of ~3300 $Å^2$). Remaining crystal contacts have significantly smaller contact surfaces, all of which comprise of less than 420 $Å^2$ each. Importantly, none of the crystal contacts occlude the active site or restrict the motion of the Gly-loop in any obvious way. The lack of crystal contacts in the vicinity of the active site combined with the high solvent content (>60%) quite possibly makes this crystal form extremely amenable to soaking ligands into the apo crystal.

Table 3-2. pCDK2/Cyclin/ADP Crystal Structure Statistics

	ADP•2Mg (PDB XXXX)	ADP•1Mg (PDB XXXX)
Data Collection		
Wavelength (Å)	0.97856	0.97856
Resolution range (Å)	43.12 - 2.05 (2.16 - 2.05)	29.56 - 2.15 (2.27 - 2.15)
Space group	P 1 21 1	P 1 21 1
Unit cell parameters a, b, c (Å)	70.77, 164.13, 73.28	71.14, 164.14, 73.45
Unit cell parameters α, β, γ (º)	90, 107.07, 90	90, 107.04, 90
Total observations	353627 (48178)	299094 (38261)
Unique reflections	98449 (14154)	83146 (11033)
Completeness (%)	98.6 (97.3)	95.5 (87.3)
Mean I/σ(I)	7.5 (1.6)	6.4 (1.5)
Rmerge	0.119 (0.857)	0.133 (0.964)
Wilson B-factor (Å2)	25.3	31.1
Refinement		
R_{cryst}	0.197	0.199
R_{free}	0.227	0.227
Number of protein molecules per asymmetric unit	2 CDK2 + 2 Cyclin	2 CDK2 + 2 Cyclin
Number of nonhydrogen atoms		
Protein	8902	8906
Ligand	114	104
Water	521	517
Average B-factor (Å2)	39.6	45.2
Ligand Average B-factor (Å2)	53.3	62.7
RMSD from ideal		
Bond length (Å)	0.0076	0.0103
Bond angle (º)	0.8868	1.1769
Ramachandran plot (%)		
Most favored	99.09	99.18
Additionally allowed	0.91	0.64

We soaked ADP into apo crystals of pCDK2•Cyclin A at a variety of magnesium concentrations for a range of soaking times. The two crystals presented here were prepared and soaked under very similar conditions. The ADP•2Mg and ADP•1Mg crystals were soaked with 3.2 mM ADP with 10 mM $MgCl_2$ and either 25 mM or 50 mM HEPES pH 7.5 respectively for one hour each. Because the crystallization condition contains 20 mM $MgCl_2$ and the soak has 10 mM $MgCl_2$, effectively titrating Mg^{2+} from the crystal, it is difficult to know what the precise final Mg^{2+} concentration is within each crystal. Because we observe different numbers of active-site Mg^{2+} ions in different crystals prepared in such similar conditions, we believe that the effective Mg^{2+} concentration in the crystals must be close to the equilibrium binding constant for one of the magnesium ions, such that small differences in ionic strength of the soak or crystal handling are sufficient to shift the phosphate-Mg^{2+} equilibrium between 2 or 1 Mg bound per ADP.

We have high confidence in the positioning and occupancy of the ADP ligand because electron density in the active site allows for the clear identification of all ADP atoms and coordinating groups. The kicked omit mFo-DFc difference map in Figure 3-2B shows the ADP electron density in the active site for the ADP•2Mg structure. In many ways, the coordination and geometry of the ADP in these structures is similar to the nucleotide coordination observed in other CDK2•Cyclin A crystal structures, most notably the geometry of the ADP in the TS mimic complex. At the same time, we also suggest that subtle differences between the phosphate coordination in the ATP, TS, and these two new ADP structures reveal additional details of the mechanism for phosphate binding, phosphoryl transfer, and product release.

Similar to most other structures of CDK2•Cyclin bound to nucleotide, the adenine rings of both the 1Mg and 2Mg bound ADP are stabilized by a combination of specific electrostatic interactions with the protein backbone and hydrophobic interactions on either face of the nucleotide rings. The ribose 2' and 3' hydroxyls make specific electrostatic interactions with D88 and the carbonyl of N131. One α-phosphate oxygen atom is coordinated by the amine group of K33, which in turn is interacting with the carboxylate of E51 (see Figure 3-4). The alpha and beta phosphates are coordinated by the Mg^{2+} ion in the MgII site, and, in the ADP•2Mg structure the beta phosphate is additionally coordinated by the Mg^{2+} ion in the MgI site. The Mg^{2+} ions are in turn are coordinated by the CDK2 sidechains of N132 and D145.

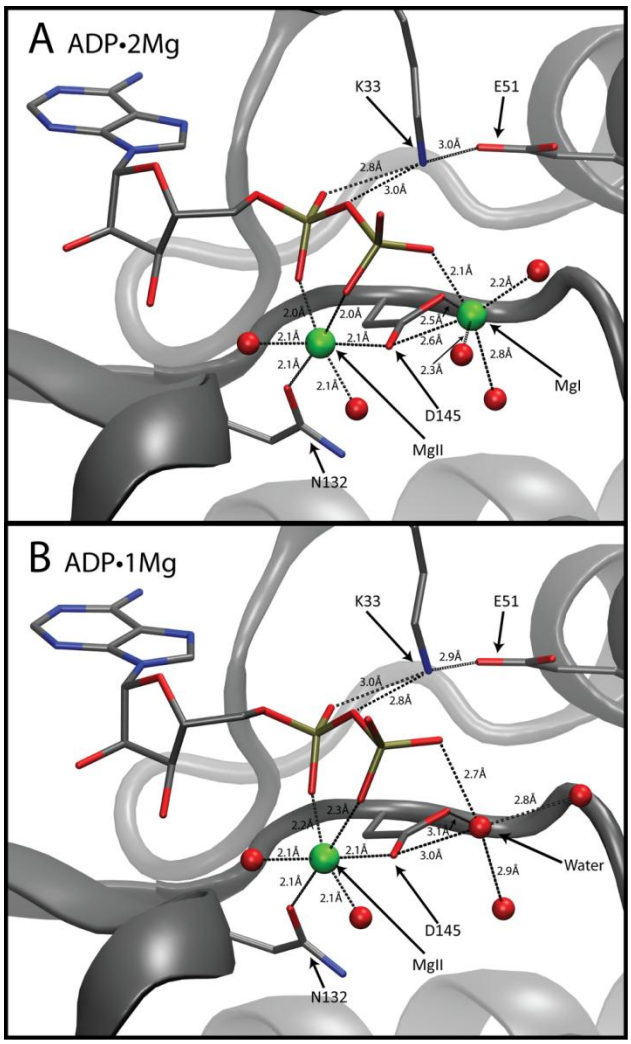

Figure 3-4 ADP Phosphates and magnesium coordination.

ADP, K33, E51, N132 and D145 drawn in stick representation. Green spheres represent Mg^{2+} ions. Red spheres represent water molecule oxygens. **Panel A)** ADP coordinated by two Mg^{2+} ions from the ADP•2Mg structure. **Panel B)** ADP coordinated by single Mg^{2+} ion from the ADP•1Mg structure. Water occupies MgI site in ADP•1Mg structure.

Compared to the CDK2 TS-mimic structure (Figure 3-2D), which features ADP, MgF_3^-, two Mg^{2+} ions, as well as substrate peptide bound in the active site, we observe significant differences in the coordination of the ADP phosphates, resulting from a shift in the conformation of the Gly-loop (CDK2 residues 12-18). The TS structure features a closed conformation of the Gly-loop that is partially stabilized by catalytically important

backbone amide interactions with both the nucleotide β and γ-phosphates. In both of the ADP-only structures, the Gly-loops have returned to the open conformation, also observed in some ATP-analog structures, where the Gly-loop residues are not participating in any direct interactions with the β-phosphate, or the no-longer-present γ-phosphate. The Gly-loop is positioned such that some ordered water molecules are identified mediating interactions between the ADP phosphates and the Gly-loop, replacing the direct Gly-loop amide interactions with the β-phosphate oxygens present in the TS.

ADP•2Mg Crystal Structure

Figure 3-4A shows the coordination of the ADP phosphates in the ADP•2Mg structure. We have labeled the two Mg^{2+} ions coordinating the ADP MgI and MgII, consistent with the cAMP dependent kinase (PKA) established nomenclature (Adams and Taylor, 1993; Zheng et al., 1993a). We established the chemical identity of the magnesium ions using two criteria: 1) interatomic distances between the Mg^{2+} and its coordinating groups, and 2) the octahedral coordination geometry (Harding, 2001). The electron density of the coordination environments of both MgI and MgII can be seen in Figure 3-5A and Figure 3-5B. The MgI site had not been occupied in structures of CDK2 until the recent TS structure (3QHR, 3QHW). It is possible that MgI had not been previously identified in CDK2 structures because many of the structures were prepared with lower magnesium concentrations (1-5mM [Mg^{2+}]) than was used in this work (Jeffrey et al., 1995; Russo et al., 1996b; Cook et al., 2002), or because they used non-hydrolyzable ATP analogues or alternative divalents, with slightly different chemical properties.

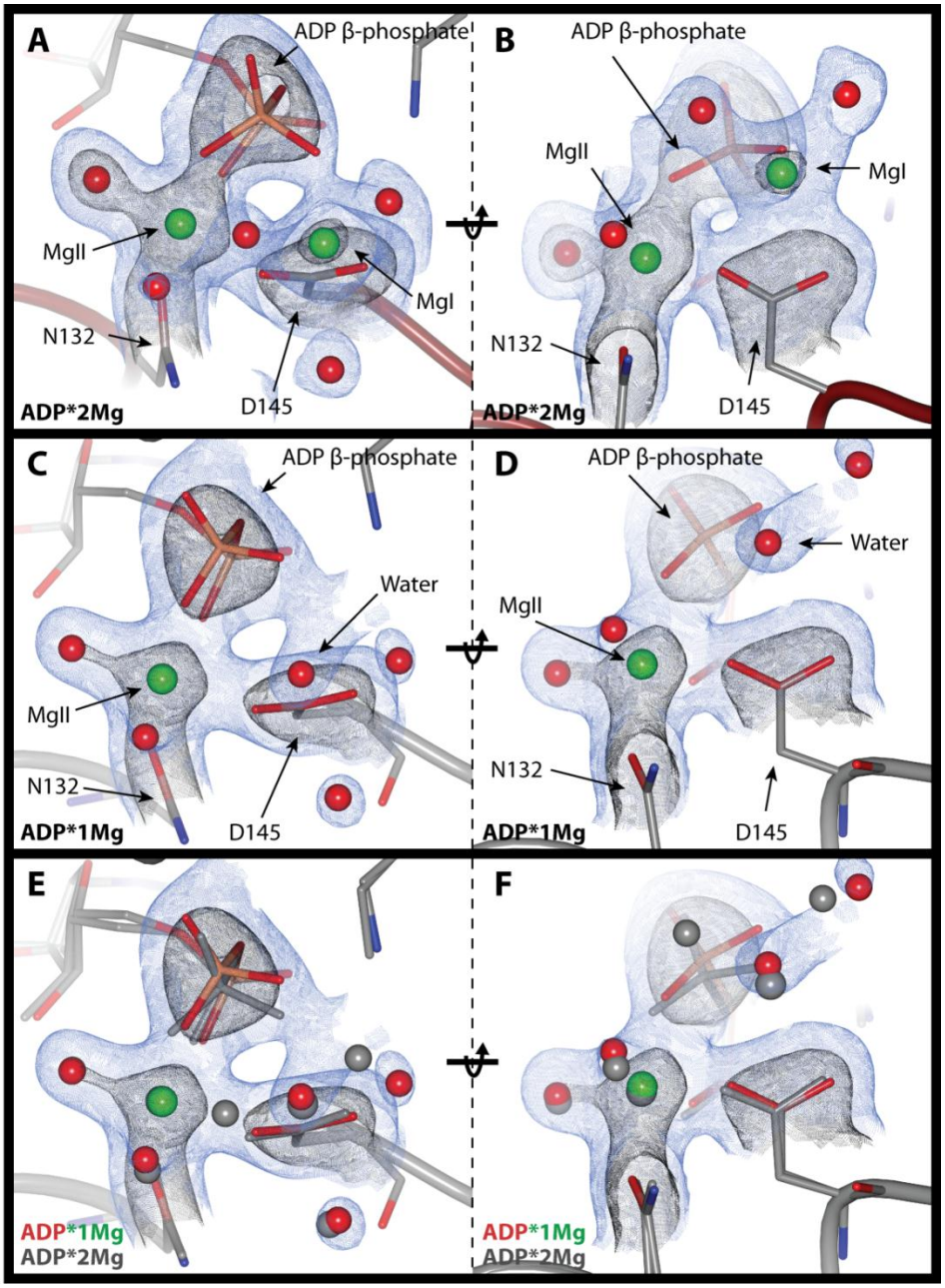

Figure 3-5. ADP Phosphates and magnesium electron density.

2mFo-DFc electron density maps; blue contoured to 1σ, black to 2.5σ. Electron density clipped to within 2 Å of ADP β-phosphate, Mg^{2+} ions and coordinating atoms, or ordered waters occupying MgI site in the ADP•1Mg structure. Left side panels show ADP β-phosphate coordination with Mg^{2+} ions. Right side panels show D145 coordination of Mg^{2+} ions (rotated 90° relative to left-side panels). **Panels A & B)** ADP•2Mg structure. **Panels C & D)** ADP•1Mg structure. **Panels E & F)** Comparison of ADP•1Mg and ADP•2Mg structures. ADP•1Mg electron density is shown, ADP•1Mg atoms in color and ADP•2Mg atoms in gray. The ADP β-phosphate is rotated away from D145 in the ADP•1Mg structure relative to the ADP•2Mg structure.

MgI is located in nearly the identical position as it is in the TS structure. MgI is coordinating the β-phosphate of ADP, participates in a bidentate interaction with both oxygens of D145, and its six-fold coordination is rounded out with three bound water molecules. As in the TS structure, the coordination geometry of MgI deviates from an ideal regular octahedron because the simultaneous coordination of the two D145 carboxylate oxygens results in a 51° angle rather that the ideal 90° O-Mg-O angle. In this ADP-bound structure, the position occupied by one of the fluorine atoms of the γ-phosphate-mimic from the TS structure is replaced by a water molecule positioned 2.2Å from MgI.

The coordination of MgII is also very similar to the TS structure. MgII interacts with the α- and β-phosphates of ADP (one oxygen each). Additionally, MgII is coordinated by one oxygen each of CDK2 residues D145 and N132. Finally, there are two ordered water molecules interacting with MgII to complete the regular six-fold octahedral coordination for magnesium. Similar to MgI, one of these ordered water molecules replaces a γ-phosphate mimic fluorine found in the TS structure. This means that following transfer of the γ-phosphate two new water molecules bind to the active site to substitute for positions occupied by γ-phosphate oxygens; one new water each coordinated to both MgI and MgII.

ADP•1Mg Crystal Structure

The phosphate and magnesium ion coordination for the ADP•1Mg structure is shown in Figure 3-4B. In this structure MgI is no longer bound to the pCDK2•Cyclin•ADP complex while MgII remains clearly defined. We conclude that MgI is not bound to the ADP•1Mg crystal in any significant population because electron

density of the ADP•1Mg structure in the vicinity of MgI (Figure 3-5C and Figure 3-5D) is quite different than that of the ADP•2Mg structure (Figure 3-5A and Figure 3-5B). There is some electron density in the bisector of the D145 carboxylate, but the distance from the center of this density to each carboxylate oxygen atom is greater than that of the ADP•2Mg structure – the distances increased from 2.5 Å to 3.0 Å. The distance to the nearest β-phosphate oxygen is also too long for proper magnesium coordination, 2.7 Å (compared to 2.1 Å in the ADP•2Mg structure). Finally, density for one of the water molecules coordinating MgI in the ADP•2Mg structure is not present. The electron density in this structure is thus strongly inconsistent with the presence of a divalent Mg^{2+} ion occupying the MgI site and is much more consistent with the presence of either an ordered water molecule or perhaps a monovalent sodium ion.

A comparison of the ADP•2Mg and ADP•1Mg structures can be seen in Figure 3-5E and Figure 3-5F. Figure 3-5E highlights how the β-phosphate coordination differs between the two structures. The β-phosphate is rotated closer to MgI in the ADP•2Mg structure than in the ADP•1Mg structure. Furthermore, the ADP•2Mg structure has clear density for two water molecules coordinating MgI, whereas the ADP•1Mg structure does not share these features.

Molecular Dynamics Simulations: ADP•2Mg is More Rigid Than ADP•1Mg

In our earlier structures and MD simulations of the phosphoryl transfer step (Bao et al., 2011), we found that the binding of the second magnesium (MgI) to the ATP•1Mg-bound active site alters the coordination of the phosphates (see Figure 3-2C and Figure 3-2D) as well as restricts their flexibility to resemble the TS conformation. Comparing the ADP•2Mg structure to the ADP•1Mg structure, differences in the electrostatic

coordination of the β-phosphate suggest that coordination by two Mg^{2+} ions may similarly restrict the flexibility of the ADP-phosphates more than coordination by a single Mg^{2+} ion. To examine how the Mg^{2+} coordination affects the conformational variability of the phosphates and the dynamics of the ADP interactions with CDK2, we have performed a series of MD simulations of the ADP•2Mg and ADP•1Mg structures, summarized in table 2. Because we cannot establish protonation states or confidently distinguish a water molecule from a Sodium ion at our present resolution, we have also simulated a number of alternative protonation states and Na/H_2O assignments that could be the best representations of our current crystal structures.

Table 3-3. Molecular Dynamics Simulations

	Starting Structure & Alterations	**Time**	**Mean Backbone RMSD (Å)**
ADP•2Mg	ADP•2Mg crystal	5x 50 ns	1.86 ± 0.22
ADP•1Mg	ADP•1Mg crystal	5x 50 ns	1.88 ± 0.29
ADP•1Mg + Na	ADP•1Mg crystal with Na+ positioned in MgI site	5x 50 ns	1.84 ± 0.20
ADP•1Mg + ProtD145	ADP•1Mg with D145 Protonated	5x 50 ns	1.77 ± 0.21
ProtADP•1Mg	ADP•1Mg with β-phosphate protonated	5x 50 ns	1.75 ± 0.20
Gly-down ADP•2Mg	TS (3QHR) without MgF3 or peptide	5x 50 ns	2.16 ± 0.29
Gly-down ADP•1Mg + Na	TS (3QHR) without MgF3, peptide or MgI. Model Na+ in MgI site	5x 50 ns	2.28 ± 0.36
Gly-down ADP•1Mg + Protonated D145	TS (3QHR) without MgF3, peptide or MgI. Protonate D145.	5x 50 ns	2.17 ± 0.26
Gly-down protADP•1Mg	TS (3QHR) without MgF3, peptide or MgI. Protonate β-phosphate.	5x 50 ns	2.32 ± 0.53

We measure the flexibility of the phosphates by considering the RMS fluctuations of just the phosphates and MgII about their mean conformation in the last 30ns of each trajectory. By superimposing trajectory structures on only the phosphorous and MgII atoms, this measure reports on the motion of phosphates in the active site without alignment-dependent contributions from motion of the kinase domain. As in Figure 3-6A, the ADP•2Mg trajectories sample conformations similar to their mean conformation more frequently than any of the ADP•1Mg-type simulations. This is indicated by the reduced spread of the ADP•2Mg distribution of RMS fluctuations, while the ADP•1Mg-type simulations have long tails extending into higher RMS fluctuations. This means that the ADP•1Mg-type simulations sample a broader range of conformations than the ADP•2Mg simulations, and thus the phosphates are more flexible when coordinated by a single Mg^{2+} ion.

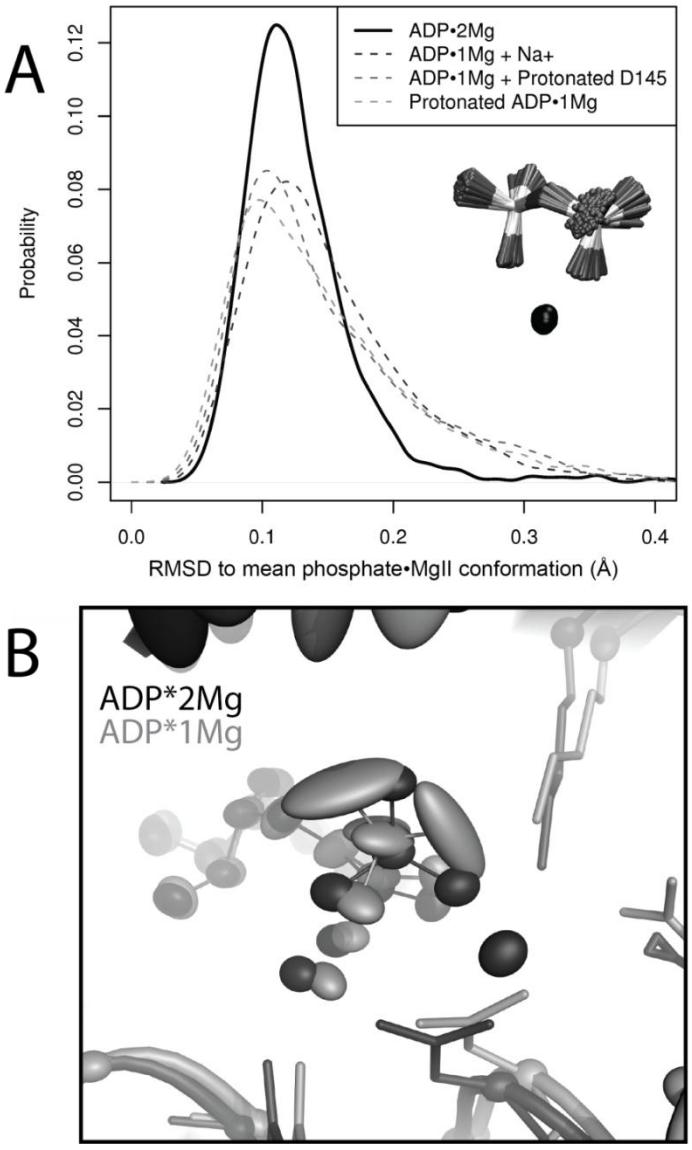

Figure 3-6 Second Mg^{2+} decreases ADP motion.

Panel A) RMS fluctuations of ADP phosphates and MgII in ADP•2Mg and ADP•1Mg-type MD simulations. Phosphorous atoms and MgII were aligned in each trajectory; fluctuations about mean conformation describes motion of just phosphate•MgII atoms. ADP•2Mg simulations show less phosphate flexibility than ADP•1Mg-type simulations. **Panel B)** Comparison of two representative simulations: ADP•2Mg (black) and ADP•1Mg +Protonated D145 (gray). Ellipsoids represent 50% probability position of atom position relative to CDK2 domain mean position. Phosphate oxygens in ADP•1Mg-type simulations are more mobile than phosphate oxygens in ADP•2Mg simulations.

Figure 3-6B shows how the increased flexibility of the ADP•1Mg phosphates corresponds to greater positional variance in the active site relative the more restrained ADP•2Mg phosphates when the trajectories are aligned on the kinase domain. The decreased mobility of the ADP•2Mg phosphates relative to the increased flexibility of the phosphates in any of the ADP•1Mg models is consistent with the 2Mg coordination positionally stabilizing the ADP product of the kinase reaction by increasing the electrostatic favorability of the phosphate-protein interactions.

Cooperativity Between Magnesium and ADP Binding

The combination of the partial occupancy of Mg binding at the MgI site with the rate dependence of CDK2 kinase activity on magnesium concentration (Figure 3-3) prompted us to examine the effect of Mg^{2+} concentration on the energetics of ADP binding. We measured the affinity of pCDK2•CyclinA for ADP as a function of magnesium concentration using Isothermal Titration Calorimetry (ITC). The dissociation constants of ADP at 5 mM, 7.5 mM, and 10 mM $[Mg^{2+}]_{total}$ are shown in Figure 3-3F. As the concentration of magnesium increases, the dissociation constant of ADP binding to CDK2 decreases, thus ADP binding to CDK2 is tighter at higher $[Mg^{2+}]_{total}$. We did not obtain a measurable ITC signal at 2.5mM $[Mg^{2+}]_{total}$, which we interpret as even weaker or no binding of ADP at lower $[Mg^{2+}]_{total}$. Consistent with the predicted electrostatic stabilizing effect of Mg binding, the favorable enthalpy of ADP binding becomes larger at higher $[Mg^{2+}]_{total}$.

Since the crystal structures suggest that the occupancy of Mg^{2+} at the MgI site of the CDK2•Cyclin•ADP•MgII complex is in equilibrium at the 10 mM $[Mg^{2+}]_{total}$ present in the crystals, it is predicted that higher magnesium concentrations will increase the

Mg^{2+} occupancy at the MgI site. The positive cooperativity between ADP and Mg binding to the enzyme (increased affinity of ADP at higher [Mg^{2+}]) can thus likely be explained by increased Mg^{2+} binding to the MgI site. It is important to note that these equilibrium ADP binding experiments differ significantly from physiological conditions. First, in many cell types of the available ("free") intracellular Mg^{2+} concentration is close to 1mM, while total [Mg^{2+}] is often greater than 20 times that amount (Grubbs, 2002). Furthermore, intracellular [ADP] is extremely low due to the activity of enzymes like pyruvate kinase and adenylate kinase, and so under these conditions the only AnP nucleotide binding species will be ATP•Mg. Thus, since both Mg^{2+} ions are essential for the chemical step, and since ADP will not be available at sufficient concentration to bind to the kinase from solution, any bound ADP must originate from the phosphoryl transfer reaction and will thus **initially** be bound to the active site with both of the two catalytically essential Mg ions. For these reasons, the question then becomes, how does Mg^{2+} interact with CDK2•Cyclin•ADP under conditions which more closely match physiological conditions, and how does this binding affect the overall activity of the enzyme?

The Glycine-rich Loop

To continue our investigation of the progression of the catalytic cycle, we next examine how the kinase transitions from the TS-mimic conformation with a closed Gly-loop to the ADP-bound state that exhibits an open Gly-loop. In our previous work, MD simulations of pCDK2•Cyclin with ATP and two Mg^{2+} ions ("ATP•2Mg"), and ATP with one Mg^{2+} ion ("ATP•1Mg") reproducibly showed that the Gly- loop spontaneously closes to a conformation similar to the TS state when ATP is coordinated by two Mg^{2+} ions, but

not when ATP is coordinated by a single Mg^{2+}. In simulations of the two-Mg TS, the Gly-loop remains closed and does not open. From this, we concluded that binding of the second Mg^{2+} ion to an ATP•Mg^{2+} bound CDK2 complex stabilizes the closed Gly-loop conformation ("Gly-down"), thus contributing to the stabilization of the TS that accelerates phosphoryl-transfer.

Unlike with ATP, simulations of ADP•2Mg or ADP•1Mg bound CDK find that the presence of two Mg^{2+} ions does not result in spontaneous closing of the Gly-loop when ADP is bound. This confirms the stability of open Gly-loop conformations observed in the crystal structures of ADP•2Mg and ADP•1Mg and suggests the presence of the γ-phosphate, in addition to the two Mg^{2+} ions, is required to stabilize the closed conformation of the Gly-loop. To see how the Gly-loop transitions from closed to open following phosphoryl transfer, and if there is a significant barrier to this transition, we carried out a series of MD simulations starting with the Gly-down conformation of the kinase, and either ADP•2Mg or ADP•1Mg in the active site. In the closed Gly-loop conformation, Gly-loop amides are within hydrogen-bonding distance of the β-phosphate, but the open Gly-loop is free to sample many different conformations. When open, a layer of water forms between the β-phosphate and the Gly-loop, breaking the direct interactions between the Gly-loop amides and the β-phosphate and increasing the distance between the β-phosphate and the Gly-loop. We classify the position of the Gly-loop by measuring the minimum distance between the β-phosphate oxygens and the Gly-loop amides, and by counting the number of waters within 4Å of the β-phosphate. We define a closed Gly-loop as being within H-bond distance (3Å) of the β-phosphate

oxygens, and having no more than 4 waters near the β-phosphate. Greater distances and numbers of waters indicate an open Gly-loop.

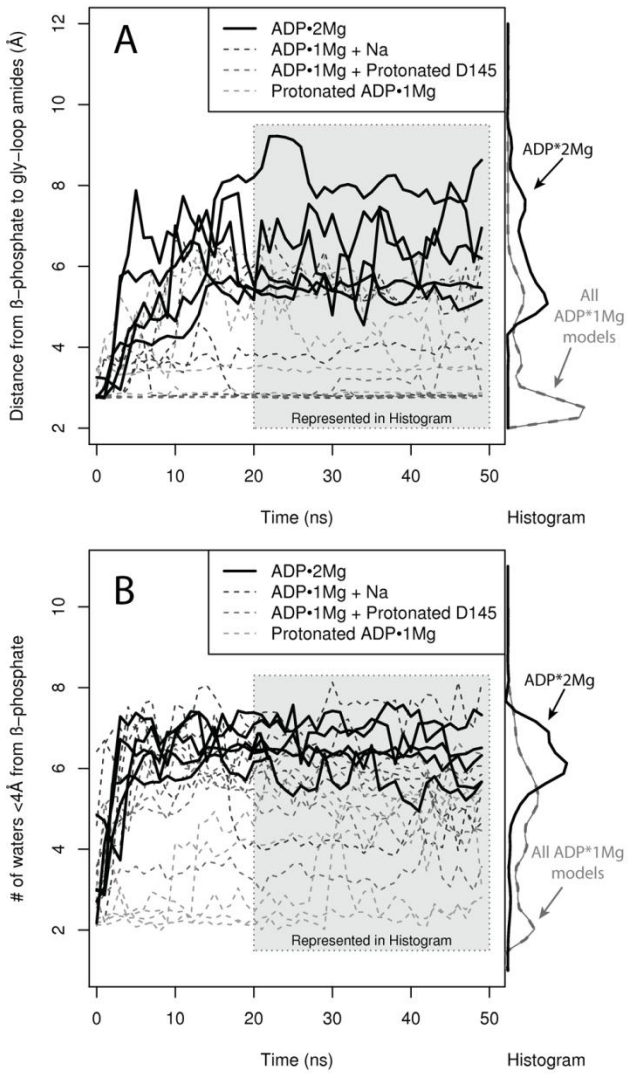

Figure 3-7 Probability of Gly-loop opening in MD simulations increased with two Mg^{2+} ions.

MD started from closed Gly-loop conformation with either ADP•2Mg coordination (solid black lines) or ADP•1Mg-type coordination (dashed gray lines). Each ADP coordination model simulated five times. Each curve in time series plot represents a single trajectory. Histograms integrate the last 30ns from all ADP•2Mg or ADP•1Mg-type trajectories into a single curve. **Panel A)** Distance between Gly-loop amides and ADP β-phosphate. ADP•2Mg simulations consistently open Gly-loop within simulation timescale, ADP•1Mg-type simulations do not. **Panel B)** Open Gly-loop conformation increases solvent accessibility of phosphates. Number of waters around β-phosphate in ADP•2Mg simulations increases rapidly and then maintains a steady population of 6-7 waters around β-phosphate. ADP•1Mg-type simulations sample closed, intermediate, and open conformations which allow 2 to 7 waters to interact within 4Å of β-phosphate.

As shown in Figure 3-7, ADP•2Mg-Gly-down simulations the Gly-loop opens within the first 4ns of each simulation and remains open for the duration of the 50 ns trajectories. The ADP•1Mg-type Gly-down simulations are not as easily interpretable, because in some the Gly-loop opens and in others it remains closed. In the ADP•1Mg-type Gly-down trajectories in which the Gly-loop does open, it opens more slowly (takes up to 10 ns to open) than in the ADP•2Mg Gly-down trajectories. This implies that the presence of two Mg^{2+} ions contributes to the opening of the Gly-loop after the γ-phosphate is transferred. The opening of the Gly-loop may make a significant contribution to the efficient release of ADP because the opening of the Gly-loop increases the solvent accessibility of the phosphates.

Electrostatic Deficit in the ADP•1Mg Structure.

The phosphate-binding portion of the active site has a strongly electronegative potential generated by the proximity of D145 and other residues in the active site, as shown in the APBS calculation (Baker et al., 2001) in Figure 3-8A. The electrostatic potential shown was calculated for an "apo" structure in which the ADP•Mg and all solvent molecules were removed from the model. This means that the surface potential shown is what is "felt" by a ligand bound (or binding) to the surface shown. The charged residues in the active site, K33, E51 and D145, have a net charge of -1e. Assuming that the binding ADP species is trianionic, addition of ADP^{3-} and two Mg^{2+} neutralizes the charge in the active site in the ADP•2Mg structure, while the ADP•1Mg structure has a -2e net charge in the active site. In this scenario, the strong electronegative potential near the MgI site shows that MgI binding is electrostatically favorable, neutralizing the overall charge in the active site.

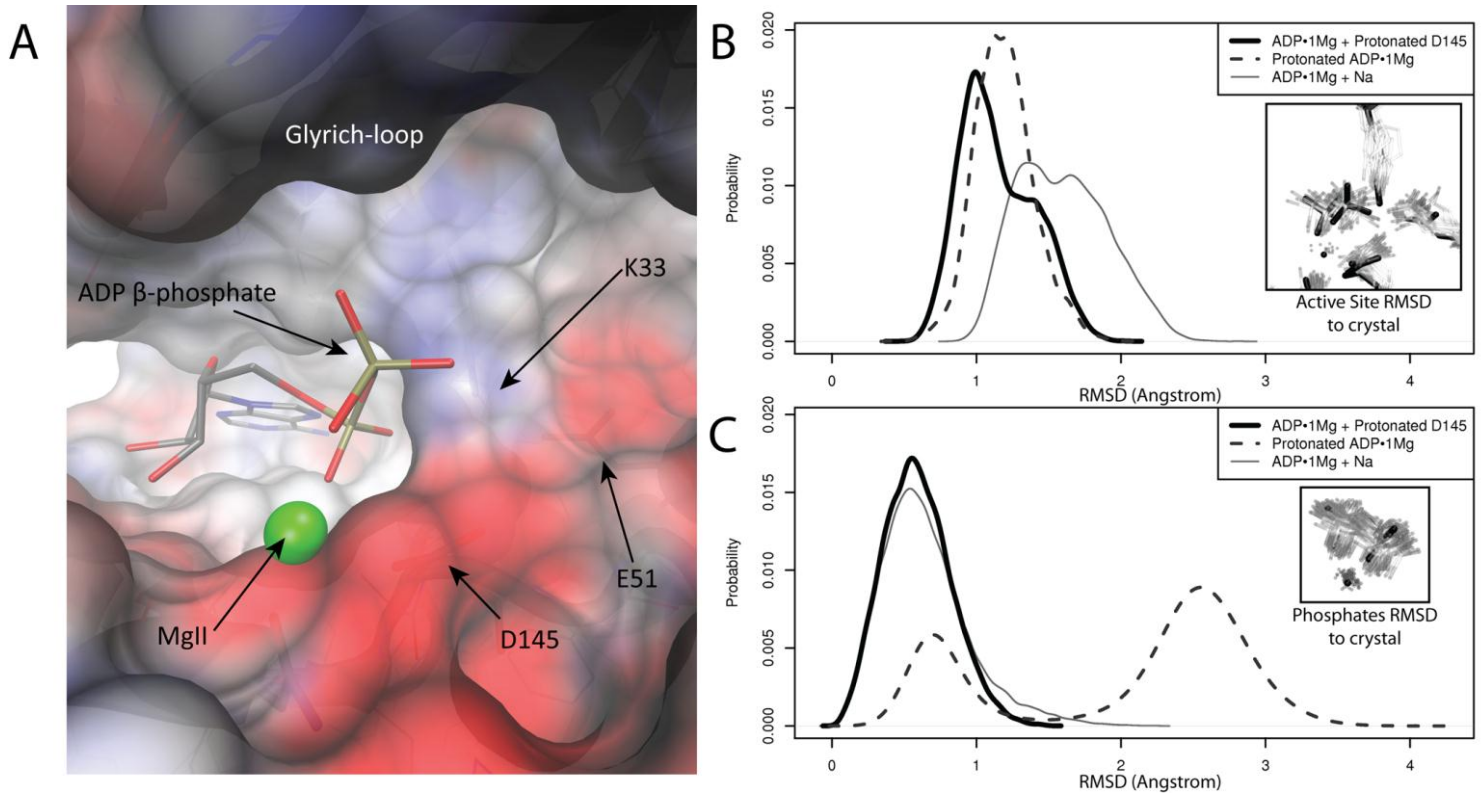

Figure 3-8 Electrostatic deficit in ADP•1Mg structure.

Panel A) Electrostatic potential of pCDK2•Cyclin A active site shows strong electronegative potential around phosphate binding region. Electrostatic potential calculated on apo structure (ADP, Mg^{2+}, and ordered solvent molecules removed from ADP•1Mg structure). Surface colored from -8 k_bT/e^- (red) to 8 k_bT/e^- (blue). ADP and magnesium shown for reference. β-phosphate interaction in active site less favorable with MgI site unoccupied. **Panel B)** MD simulation: distribution of RMS deviations of phosphates, MgII and active site residues K33 and E51 from ADP•1Mg crystal structure for each of the ADP•1Mg-type simulations. Protonation of D145 or the β-phosphate sample lower RMSD to the crystal than Na^+ binding. **Panel C)** MD simulation: distribution of RMS deviations of just phosphates and MgII from ADP•1Mg crystal structure for each of the ADP•1Mg-type simulations. Protonation of D145 reproduces phosphate coordination in ADP•1Mg structure better than β-phosphate protonation or Na^+ binding. Mode of β-phosphate protonation RMS distribution at 2.7Å corresponds to alternate phosphate positioning and is consistent with some weak electron density from ADP•1Mg crystal.

In the ADP•1Mg crystal structure, the electron density in the electrostatic deficit region was difficult to model, possibly due to heterogeneity of bound species within the crystal. We opted to model three tightly packed water molecules in this region of the ADP•1Mg structure, as this model makes the fewest assumptions about a difficult-to-build region, though the mFo-DFc difference map still indicates other models may also be consistent with the observed density.

To test alternative models of the ADP•1Mg structure, we have carried out a series of molecular dynamics (MD) simulations of different configurations in the active site of pCDK2•Cyclin, summarized in table 2. Simulations of the ADP•1Mg structure reproducibly observe the spontaneous binding of a sodium ion from the bulk solvent into the active site near the MgI site. Once the sodium ion binds it is not observed to leave the active site in the timescale of these simulations (50 ns). The binding of this monovalent ion is thus a non-equilibrium event in these simulations that functions to partially alleviate the electrostatic deficit and bring the system to a more stable state. Despite remaining in the active site, the bound monovalent is mobile within the active site, and occupies many different positions in the electrostatic deficit region.

Another model for alleviating the electrostatic deficit in the ADP•1Mg structure is protonation of either the ADP β-phosphate or D145. Therefore, we tested three different models of the ADP•1Mg active site: 1) Na^+ positioned near the MgI site from the beginning of the simulation ("ADP•1Mg+Na"), 2) D145 protonated ("ADP•1Mg+ProtD145"), and 3) the β-phosphate protonated ("ProtADP•1Mg"). Each of these models leaves the active site with a net -1e charge, but because the nature of the charge distribution in the active site is disperse and not concentrated onto the phosphates

or any particular residue in the active site (see Figure 3-8A), and because the region is somewhat solvent accessible, the remaining electronegative charge may be permissible.

The advantage of using MD simulations to test these models is that the ADP•1Mg crystal structure does not directly report on any features that allow definitive discrimination between these three models. We cannot identify a monovalent in the ADP•1Mg crystal structure, suggesting that if a monovalent does bind it is delocalized and therefore cannot be confidently modeled into the active site, consistent with the results from the MD. If either the ADP phosphates or D145 is protonated, the electron density cannot help in discriminating between these models because protons do not contribute strongly to the electron density at 2.0 Å resolution.

ADP•1Mg Model: Protonation or Cation Binding?

We performed equilibrium MD simulations of each of the ADP•1Mg models to investigate the plausibility of each of the ADP•1Mg models. The metric we have selected to assess the validity of each model is the ability of the simulation to reproduce the coordination of the ADP phosphates observed in the ADP•1Mg crystal structure. The distribution of RMS deviations of the phosphates and coordinating active site residues K33 and E51 is shown in Figure 3-8B. The protonated D145 and protonated β-phosphate models both maintain active site coordination better (i.e. lower RMS deviations) than the sodium-bound model. In Figure 3-8C, only the phosphates are included in the RMS deviation calculation – thus only reporting on the position of the phosphate atoms relative to the crystal structure. The protonated D145 model best reproduces the crystal structure, however the protonated β-phosphate model samples two different conformations of the phosphates, with the lesser occupied peak corresponding to the crystal structure. The

second peak, ~2.7 Å RMSD from the crystal conformation corresponds to an alternate conformation of the phosphates, in which the protonated phosphates break away from K33 and instead interact with the carbonyl of E13. The protonated β-phosphate position in this alternate conformation may account for some delocalized electron difference density in the ADP•1Mg crystal structure that is too weak to directly build the phosphates into. This alternate conformation may represent a minor population in the ADP•1Mg crystal.

While the protonated-D145 simulations clearly reproduce the crystal structure better than the other models simulated, protonation of D145 is also the least chemically feasible model because the pK_a of an aspartic acid in solution is 4, whereas the pK_a of an ADP phosphate is 6.8 – meaning that phosphate protonation is more likely at physiological pH. It is possible that the environment of the CDK2 active site shifts the pK_a of D145 in the ADP•1Mg bound state (i.e., when the phosphates are present, but with no occupancy of the MgI site) because of the electrostatic deficit generated by the close proximity of the β-phosphate, D145 and E51. PROPKA2 (Bas et al., 2008) predicts that the pKa of D145 is shifted to 9.5 in the ADP•1Mg structure. What is clear from these simulations of the ADP•1Mg structure is that some type of counter-charge needs to be introduced into the CDK2 active site to maintain the phosphate coordination of the ADP•MgII complex. It is possible that many different species are present in the ADP•1Mg crystal, and it is likely that the ADP•1Mg bound state is transient and only quasi-stable on the pathway to ADP release. These results also suggest that changes in pH (especially to lower pH values) could likely alter the charge-balance and electrostatic

deficit within the active site and might even alter the stability of the Mg^{2+} ions within the active site.

The Rate of ADP Release is Rate-limiting and Becomes Slower at High Concentration of Mg^{2+}

The decreased kinase activity that is observed at high $[Mg^{2+}]_{free}$ (Figure 3-3D), together with the cooperative binding of ADP•Mg^{2+} to CDK2•cyclin A (Figure 3-3F), suggests that the rate of ADP•Mg^{2+} release is rate-limiting under these conditions. To investigate this possibility, we measured the solvent viscosity effect as a function of free Mg^{2+} concentration. Solvent viscosity effects have previously been determined for pCDK2•Cyclin (only at a single Mg^{2+} concentration) as well as other kinases to determine the relative contribution of product release to the overall reaction turnover (Adams and Taylor, 1992; Saylor et al., 1998; Adams, 2001; Hagopian et al., 2001). Increased solvent viscosity will selectively slow the diffusive steps of the reaction while not affecting the non-diffusive steps. This experiment reports on the relative contribution of the rate of product release in determining the overall reaction rate for CDK2 (Adams, 2001). The relative viscosity effect at a given condition is expressed as a single number between 0 and 1, which indicates the contribution of product release to the overall rate. A value of 1 indicates the reaction is fully limited by product release and a value of 0 indicates that product release is not rate-limiting (some other step is much slower than product release).

The solvent viscosity effect on the observed steady-state velocity for both the basal ATPase activity (water as the phosphate acceptor) and the kinase activity

(saturating histone H1 as the acceptor) was measured with 1.2 mM ATP at concentrations of free Mg^{2+} that varied between 0.4 and 20 mM (Appendix Figure 3-29 and Figure 3-30) and the results are summarized in Figure 3-9A. The lack of a solvent viscosity effect for the ATPase reaction confirms the previous finding that ATP cleavage is rate-limiting in the absence of a protein acceptor and that sucrose does not inhibit or alter the structure of CDK2 (Adams and Taylor, 1992; Hagopian et al., 2001).

At high $[Mg^{2+}]_{free}$ (H1 acceptor) the solvent viscosity effect is close to 1.0, indicating that product release is almost fully rate-limiting. However, as $[Mg^{2+}]_{free}$ is reduced below 10 mM the solvent viscosity effect steadily decreases. This indicates that the identity of the rate-limiting step changes as a function of Mg^{2+} concentration. The reason for this change is that 1.2 mM ATP•Mg is not fully saturating when free $[Mg^{2+}]$ drops below 10mM, resulting in sub-optimum phosphoryl transfer throughput. Although ATP•Mg saturates with a K_M value of ~0.1 mM when $[Mg^{2+}]_{free}$ is 20 mM, the binding of the second essential Mg^{2+} ion is highly cooperative with ATP•Mg^{2+} binding (e.g., K_M for ATP is 3.4 mM when $[Mg^{2+}]_{free}$ is 0.1 mM). This positive cooperativity between ATP•Mg^{2+} and Mg^{2+} ion binding to the MgI site can be observed by titrating free Mg^{2+} at a fixed concentration of ATP•Mg as shown in Figure 3-9C. The 10-20% decrease in the kinase velocity (most apparent high [ATP] and $[Mg^{2+}]_{free}$) is not due to an effect on the enzymatic coupled assay (data not shown). To determine if this inhibitory effect can be isolated to the product release step, we measured the solvent viscosity effect with saturating ATP at a range of free Mg^{2+} concentrations.

Figure 3-9 Second Mg^{2+} activates ATP p-Transfer, limits ADP release.

Panel A) Second Mg^{2+} activates ATP p-Transfer, inhibits ADP release. **Panel A)** Solvent viscosity effect at 1.2 mM constant ATP. Specific kinase activity (200μM [H1], Squares) show increasing dependence on product release as $[Mg^{2+}]_{free}$ varied (0.4-20mM). No solvent viscosity effect on non-specific kinase activity (water as substrate, 0mM [H1], Triangles) indicates that viscogen does not alter transition state formation, or specifically inhibit activity. See supplementary figure 12. **Panel B)** Solvent viscosity effect at saturating [ATP•Mg] and [H1] (see appendix Figure 3-26, Figure 3-27, and Figure 3-28), as $[Mg^{2+}]_{free}$ varied (0.1-20mM). Dashed line is a least-squares fit linear model to the solvent viscosity effect vs. $[Mg^{2+}]_{free}$ data points. **Panel C)** pCDK2•Cyclin rate at 10 mM ATP (red), 4mM ATP (green), and 1.2 mM ATP (blue) and k_{cat} (black), $[Mg^{2+}]_{free}$ varied from 0.5-20 mM. **Panel D)** Rates of product formation and product release at 1.2 mM ATP. **Green squares** shows that the net rate of substrate binding and chemistry is activated by $[Mg^{2+}]_{free}$. **Red triangles** show the rate of product release is slowed by $[Mg^{2+}]_{free}$. **Blue circles** are the total enzyme velocity at 1.2 mM ATP (same data in Blue curve of Panel C). Rate of product release is equivalent to the black kcat curve from panel C (data from figure 3D) since the viscosity effect at saturating substrates in panel B is close to 1. Rate of product formation includes all steps of reaction required to form the products in the active-site, including ATP•Mg binding, protein substrate binding, second Mg2+ binding, and phosphoryl transfer. Green square data points calculated as $k_{productFormation} = (k_{productRelease} * v_{ATP1.2}) / (k_{productRelease} - v_{ATP1.2})$. Green curve is a hyperbolic fit to the green square data points. This curve should just be viewed as an estimate. The calculated standard error on the green squares would be very large because the modest error on the measured rates compounds such that it is a significant portion of the denominator at high Magnesium. We suggest that the trend in that data is correct because viscosity effect from panel A ([ATP] = 1.2 mM) demonstrates that the rate of product formation is much faster than the rate of product release at high Magnesium.

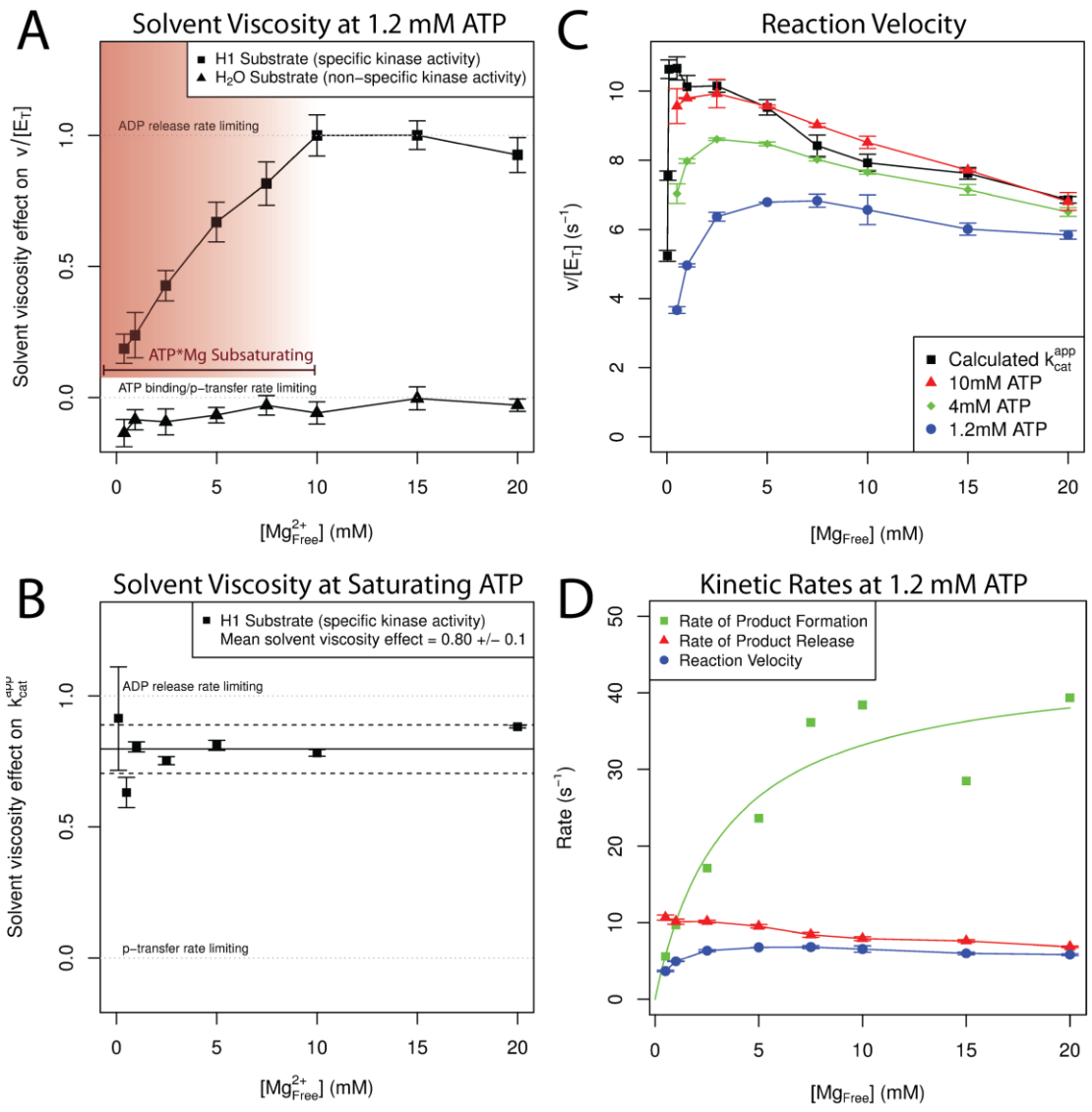

Figure 3-9 Second Mg^{2+} activates ATP p-Transfer, limits ADP release.

Figure 3-9B shows that under saturating ATP•Mg and histone H1 (the protein substrate) conditions, the viscosity effect is both close to one and invariant as a function of $[Mg^{2+}]_{free}$ at all tested conditions. This demonstrates that the rate of product release always dominates the overall reaction rate under conditions of saturating ATP•Mg and protein substrates. Because the product release rate defines the overall reaction rate, we can conclude that the origin of the inhibitory Mg effect, i.e. decrease in the overall reaction rate at higher $[Mg^{2+}]_{free}$, can be isolated to an Mg-dependent reduction in the rate of product release. We suggest that increased $[Mg^{2+}]_{free}$ specifically slows the rate of ADP•Mg release (rather than phospho-protein), given the cooperativity between ADP•Mg and second Mg^{2+} binding and because the rate of ADP release is much slower than the rate of phosphorylated-protein product release in other protein kinases (Lew et al., 1997).

Discussion

While the recruitment of Mg^{2+} ions into the active site of CDK2 kinase is absolutely essential for the catalytic mechanism of the enzyme, the use of Mg^{2+} by CDK2 has multiple effects and their combined consequences are quite complex. The integration of the structures of CDK2 bound to ADP and either one or two Mg^{2+} ions, along with the associated $[Mg^{2+}]$ dependence of ADP binding, and the dominant role that product release can play in determining enzyme turnover, enables the extension of our model for the roles that equilibrium magnesium binding plays in the CDK2 active site beyond its effects during the phosphoryl transfer step. An understanding of the unavoidable link between the activating, inhibitory, and limiting effects of the Mg ions allows us to more

completely explain the complex effects of $[Mg^{2+}]_{free}$ on the overall rate of enzyme turnover.

The TS-mimic structure of the phosphoryl transfer step demonstrates how the binding of the second Mg^{2+} ion to the kinase•ATP•Mg^{2+}•substrate active site promotes phosphoryl transfer by closing the Gly-loop, electrostatically/electronically stabilizing the TS relative to the reactants and optimizing the reactant geometry for catalysis. This new work illustrates that although the second Mg^{2+} ion is essential for the most efficient acceleration of the phosphoryl transfer step, the increased stability of the ADP product resulting from two Mg^{2+} ions in the active site also functions to limit and slow the rate of ADP release. The release of ADP•1Mg is kinetically faster than the release of ADP•2Mg. The structural similarities between the TS-mimic and the ADP•2Mg structures, along with the relatively reduced active site fluctuations of both the 2Mg-bound TS and ADP MD simulations relative to the 1Mg ATP or ADP simulations, suggest a nearly symmetric active-site assembly-disassembly process. The slow ADP off-rate can therefore be thought of as the slow reversal of the cooperative assembly of the active site that facilitated the stabilization of the transition state. Conditions that favor faster cooperative assembly of the TS (i.e. saturating substrates and high $[Mg^{2+}]_{free}$) conversely result in a slower disassembly of the highly similar ADP•2Mg product state. This is important because the solvent viscosity experiments at saturating ATP•Mg and protein substrates demonstrate that even at physiological concentrations of $Mg^{2+}{}_{free}$, the release of ADP•Mg from the active site will dominate the overall rate of the reaction.

The TS-mimic structure has a closed Gly-loop while both the ADP•1Mg and ADP•2Mg structures of pCDK2•Cyclin are both observed to have an open Gly-loop.

This suggests that the open form of the Gly-loop is energetically preferred for the ADP-bound kinase following phosphoryl transfer in the absence of the phosphorylated product. Our MD simulations starting from the "Gly-down" conformation of the CDK2•Cyclin complex confirm this, indicating that even when the ADP is coordinated by two Mg^{2+} ions, the Glycine-rich loop readily opens well within the 50 ns simulation timeframe. We conclude from these simulations and our previous TS structure and simulations[7] that although the binding of the second Mg^{2+} (to the MgI site) of CDK2•Cyclin•ATP•Mg results in Glycine-rich loop closure, once the ATP γ-phosphate is transferred and the phospho-product released, the open conformation of the Gly-loop becomes the most stable conformation, even with the continued coordination of ADP by two Mg^{2+}. This differential stability is readily explained by the loss of stabilizing interactions between the γ-phosphate and the Gly-loop amides in the ADP-bound state. Furthermore, the open conformation of the Gly-loop observed in both the ADP•2Mg and ADP•1Mg structures may be an important intermediate along the pathway of ADP release because there is sufficient space for a layer of water to occupy the space between the phosphates and the Gly-loop. Solvent accessibility of the phosphates is likely to promote release of the phosphates from the active site because of the loss of tight electrostatic coordination of the phosphate oxygens.

Although the stabilization or acceleration of Gly-loop opening by two bound Mg ions may help enable ADP-release, high concentrations of Mg will still slow the rate of ADP release due to the stabilizing electrostatic effect of the two bound divalent ions. This inhibitory effect can be somewhat minimized at physiological $[Mg^{2+}]_{free}$ by the conclusion, based on the ADP•1Mg and ADP•2Mg crystal structures, that the occupancy

of the MgI site is less than 100% even at concentrations of free Mg^{2+} as high as the 10mM concentration present in our ADP•1Mg structure. Less favorable occupancy of the MgI site is also consistent with the observation that the electron density for MgI is slightly weaker than MgII in the ADP•2Mg structure. It is also possible that the ADP•1Mg crystal had some small population of protein molecules in which both Mg's are bound – but it is not the dominant population because there is no clear electron density for MgI or its coordinating groups. Our interpretation is that Mg binding to the MgI site is less thermodynamically stable than the MgII site. Based on the ADP titration experiments (Figure 3-3F), we estimate the K_D of the MgI site in the ADP•1Mg -bound kinase is close to 5-7 mM. Given that ADP is bound to a single Mg^{2+} in solution (ADP^{3-} :Mg^{2+} $K_D \sim 400$ μM) and that our structures and simulations suggest that the occupancy of the MgII site is preferred to the MgI site, we conclude that the MgII site will remain occupied in the kinase active site as long as the ADP is bound. The relative stability of the MgII site over the MgI site in the ADP•1Mg state is also consistent with the observation that the MgI site has never been occupied in structures of CDK2 bound to ATP or ATP analogues.

Examining the electrostatic characteristics of the pCDK2•Cyclin active site, and the MD simulations of four different interpretations of the ADP•1Mg structure, we find that the electrostatic deficit generated by the close proximity of the ADP phosphates to the similarly electronegative active site residues requires the introduction of some positive countercharge to reproduce and maintain the conformation and coordination of the ADP phosphates observed in the ADP•1Mg crystal structure. This is not necessary for the ADP•2Mg state because occupancy of the MgI site satisfies the -2e active-site

electrostatic deficit by completely neutralizing the active-site charge. We suggest that the various mechanisms of introducing a +1e charge into the ADP•1Mg active site, including protonation of the ADP β-phosphate or D145 or the localization of a monovalent cation, can also stabilize ADP phosphate binding and the population in solution (and the ADP•1Mg crystal) likely includes some equilibrium between these states. But, because the +1e states only partially alleviate the total electrostatic deficit, they cannot stabilize ADP binding to the same extent as MgI and thus may represent an ensemble intermediate step prior to the release of the ADP•Mg. It should be noted that changes in pH or salt concentration are likely to alter the population of +1e states and potentially result in environmental (salt/pH) dependent changes in ADP stability as well as MgI affinity to the ATP•1Mg complex.

Since K_M(ATP•Mg) varies as a function of $[Mg^{2+}]_{free}$ (Figure 3-3E), cellular conditions are unlikely to always be saturating for ATP•Mg consumption by pCDK2•Cyclin. The results of the solvent viscosity experiment vs. $[Mg^{2+}]_{free}$ at 1.2 mM ATP (Figure 3-9A) clearly illustrate the origins of the opposing activating and inhibiting effects of [Mg], both of which, we propose, can be specifically linked to Mg^{2+} binding to the MgI site. At this concentration of ATP, the relative viscosity effect (influence of ADP release) is close to zero at low $[Mg^{2+}]_{free}$ and then increases as a function of $[Mg^{2+}]_{free}$. This indicates that the release of product only begins to dominate the overall reaction rate as $[Mg^{2+}]_{free}$ becomes significantly higher than the physiological value of 1 mM. We propose that the origin of this phenomenon is the strong cooperativity between the ATP•Mg substrate K_M and the second Mg activator. The productive assembly, activation, and bond-cleavage of the ATP•2Mg substrate dominates the overall reaction rate at lower

concentrations of either ATP•Mg or Mg^{2+}_{free} because progression through phosphoryl-transfer under these conditions is slower than the rate of ADP release. As [ATP•Mg] and $[Mg^{2+}]_{free}$ are increased to saturating concentrations (values that are co-dependent due to their cooperativity), however, the rate of productive ATP•2Mg activation and phosphoryl transfer increases and the overall reaction rate transitions to become limited by the rate of ADP release. The opposing K_M(ATP•Mg) activating and ADP release inhibitory effects of $[Mg^{2+}]_{free}$ are further illustrated in Figure 3-9D where we have calculated the apparent rates of product formation (everything up to and including p-transfer) and product release as a function of $[Mg^{2+}]_{free}$. The structures predict that the Mg activator effect arises from the second Mg binding to the MgI site along with ATP•1Mg, and the Mg inhibitor effect arises from product stabilization resulting from Mg occupancy of the MgI site of the ADP•2Mg bound enzyme.

Because the affinity of the second Mg site when ADP•Mg is bound is weaker than the physiological 1mM $[Mg^{2+}]_{free}$ and product release dominates the reaction rate when there are saturating substrates, the notable decrease in the overall rate of enzyme turnover at high Mg^{2+} concentrations is readily explained by increased population of the high-affinity ADP•2Mg state. The viscosity effect experiments at subsaturating ATP•Mg (but still saturating protein substrate) (Figure 3-9A) highlight the important limit that the ADP release-rate imposes on the maximum possible turnover rate of the enzyme. Tuning the affinity of the second Mg^{2+} site higher through evolution might be predicted to increase the rate of product formation under conditions of lower [ATP•Mg] substrate, but this strategy would also be predicted to result in even slower ADP release and lower overall enzyme activity, in the absence of additional changes that counteract this effect. In the

case of CDK2, optimum enzyme activity has not been the only selective pressure; it must also be a highly regulated signaling switch, so perhaps further tuning under different selective pressure could evolve a more active CDK2. This process may describe some oncogenic CDK2 mutants.

Conclusions

Given that the binding of a second Mg^{2+} ion increases CDK2 binding affinity for ADP, but only 1Mg is required for ADP to remain bound, our hypothesis is that the energetically preferred reaction pathway for ADP release is for MgI to be released prior to the release of the ADP•MgII complex. Two Mg ions are essential for chemistry, so ADP•2Mg is the state following phosphoryl transfer, and ADP•1Mg is the kinetically preferred intermediate along the pathway to ADP release. This is consistent with a similar result from a computational study of Protein kinase A (PKA) which concluded that release of ADP from that kinase with two Mg^{2+} ions bound is so strongly unfavorable as to be nearly impossible (Khavrutskii et al., 2009). As shown in Figure 3-1B, the sequence of events in our proposed model of CDK2 catalysis at the roughly physiological condition we tested (pH 7.5, 162 μM ionic strength, 1 mM Mg^{2+}_{free}, 3-5 mM ATP) are that ATP•Mg and protein substrates bind, then MgI binds, closing the Glycine-rich loop and promoting phosphoryl transfer (TS), next the phosphorylated protein is released and the Glycine-rich loop opens, resulting in the ADP•2Mg state, MgI is released, followed by ADP•MgII release. Finally, after ADP•Mg release the apo kinase can then bind ATP•Mg and protein substrate to start the catalytic cycle again.

Many different protein kinases are proposed to utilize two Mg ions to catalyze the phosphoryl transfer reaction (Zheng et al., 1993b; Lowe et al., 1997; Sun and Budde,

1997; Saylor et al., 1998; Xie et al., 1998; Shaffer and Adams, 1999; Waas and Dalby, 2003; Liu et al., 2010). This is supported by the strong conservation of the protein kinase active site residues coordinating the nucleotide phosphates (e.g., K33, DFG, and the catalytic HRD motif). Where the 2Mg protein kinase reaction mechanism is conserved, this model of the role of equilibrium Mg^{2+} binding in the catalytic cycle and ADP release may be relevant to many different protein kinases. Most kinases which utilize two Mg^{2+} ions to promote phosphoryl transfer by stabilizing the TS might be expected to demonstrate a similar inhibition of ADP release when both Mg^{2+} sites approach saturation at higher $[Mg^{2+}]_{free}$. Despite this prediction, some kinases, like ERK2 (Waas and Dalby, 2003), are not reported to show CDK2-like inhibition of catalytic activity at higher $[Mg^{2+}]_{free}$, while still other kinases, like PKA (Shaffer and Adams, 1999), are inhibited at relatively lower concentrations of Mg^{2+} compared to CDK2. Because the affinity of the second Mg^{2+} is a function of both structural and electrostatic effects, explanations for these differences could come from sequence variation of less conserved residues, even distant from the active site, as well as other structural differences that could alter the relative affinity for Mg^{2+} binding to the MgI site. In this scenario, kinases for which ADP release is fast would be predicted to have a relatively weak affinity for the second Mg^{2+} when nucleotide is bound, while kinases for which ADP release is slow may have relatively strong affinity for the second Mg^{2+} when nucleotide is bound. Because ATP and ADP are so similar, it is difficult to alter the Mg binding affinity to the ATP substrate MgI site without introducing similar effects to the ADP product MgI site. For fully activated CDK2, evolution appears to have succeeded at optimizing the balance between the favorable ATP activation and phosphoryl-transfer benefits of utilizing two

Mg^{2+} ions in the active site against the perhaps unavoidable efficiency limits introduced by 2Mg stabilization of the ADP product in the kinase active site. The affinity of a protein kinase for the binding of the second Mg^{2+} at the MgI site may be largely determined by the strength of the electrostatic deficit in the active site generated by the close proximity of the phosphates and other charged active site residues. The strong effects that MgI recruitment clearly has on enzyme turnover may mean that dynamically altering the MgI affinity represents a tunable mechanism used for the regulation of kinase catalytic activity. Recruitment of Mg to the MgI site could be looked at as the protein kinase regulatory equivalent of the insertion of an Arg-finger by a G-protein activator protein (GAP) (Bao et al., 2011) while destabilization of the ADP-bound MgI site may parallel the regulatory effect of a G-protein exchange factor (GEF), a key difference being that an activated protein kinase independently represents an optimal balance between the rates of these two potentially rate-determining steps.

Appendix

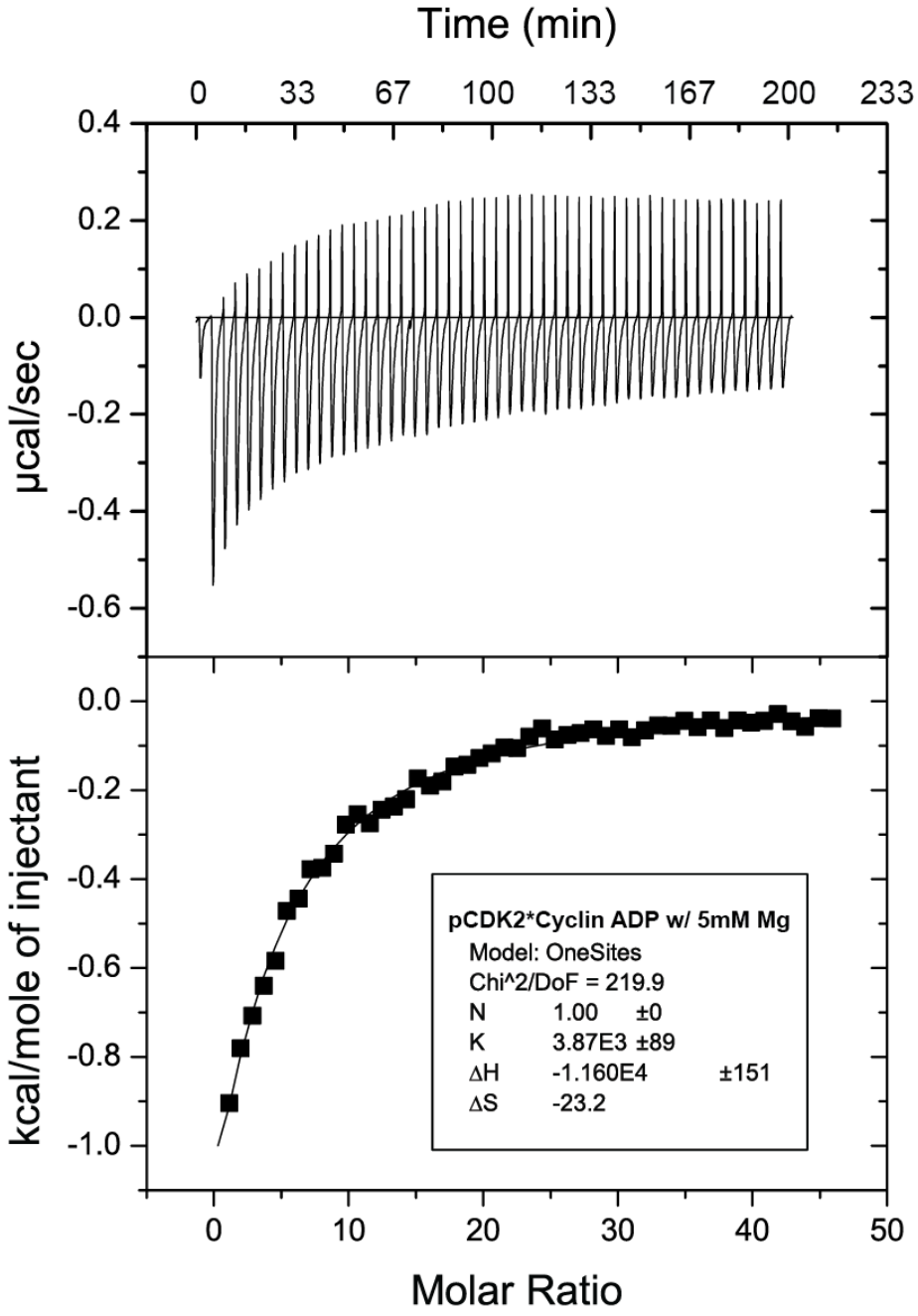

Figure 3-10 ITC of pCDK2•CyclinA binding ADP with 5 mM $[Mg^{2+}]_{total}$.

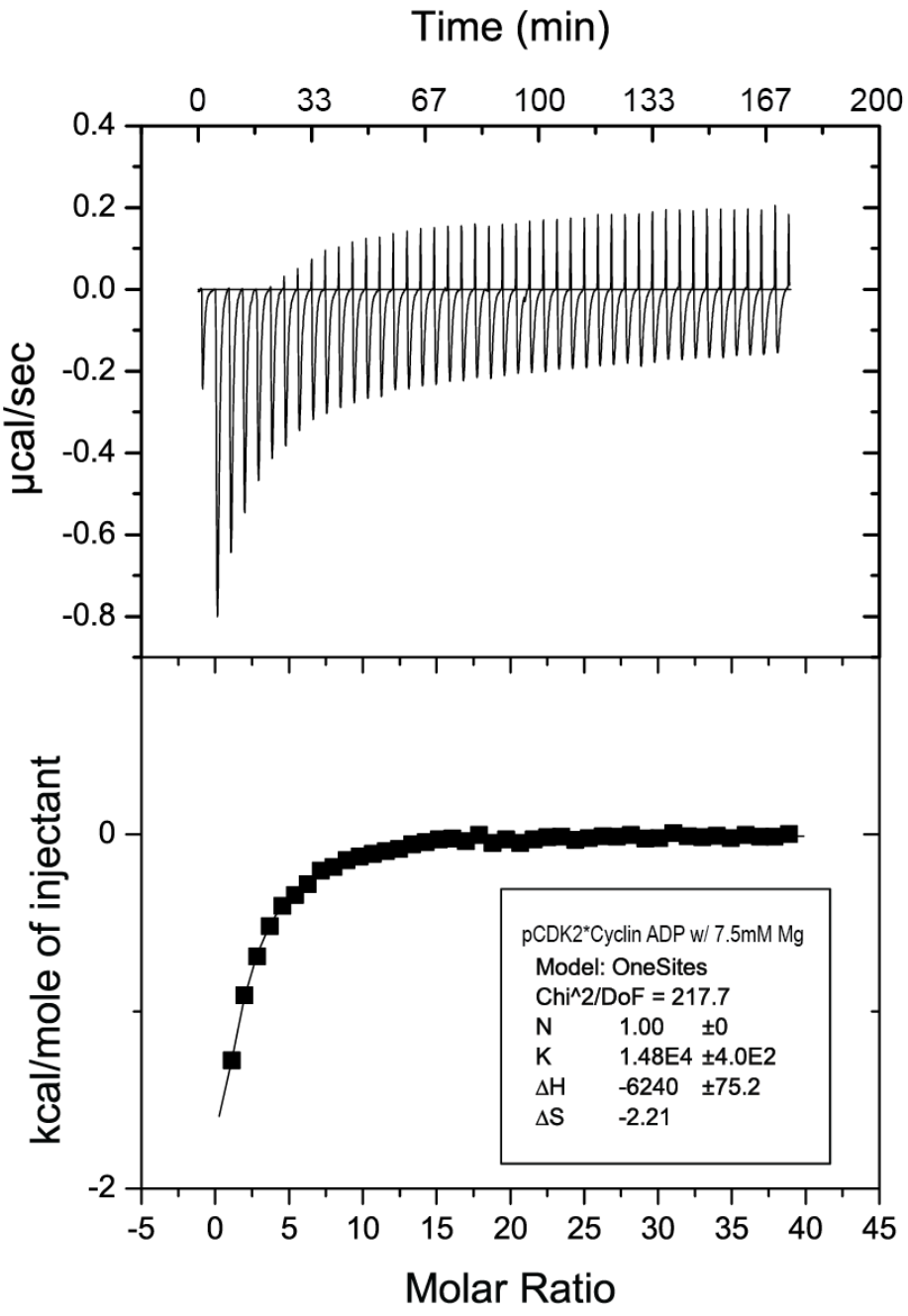

Figure 3-11 ITC of pCDK2•CyclinA binding ADP with 7.5 mM $[Mg^{2+}]_{total}$.

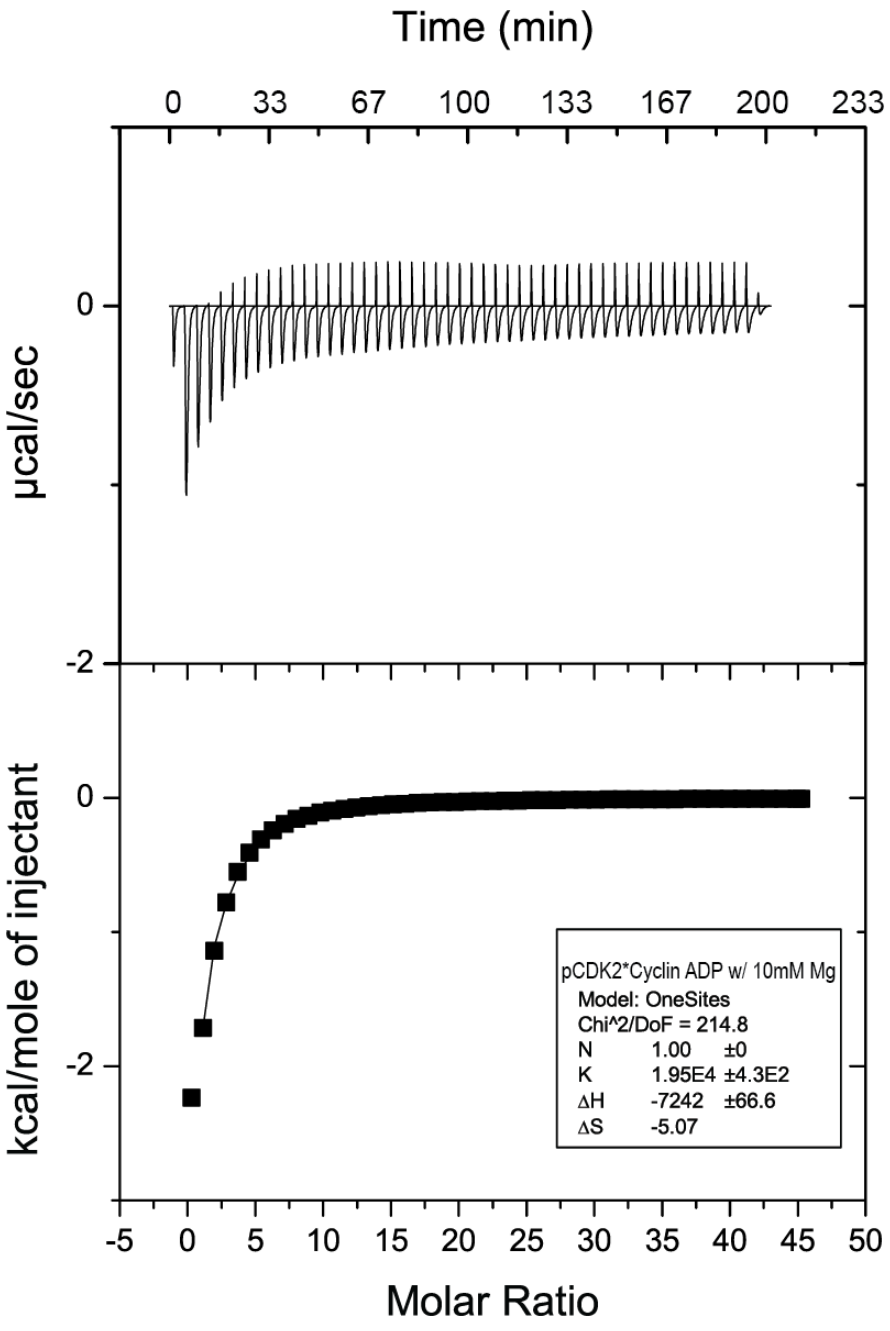

Figure 3-12 ITC of pCDK2•CyclinA binding ADP with 10 mM $[Mg^{2+}]_{total}$.

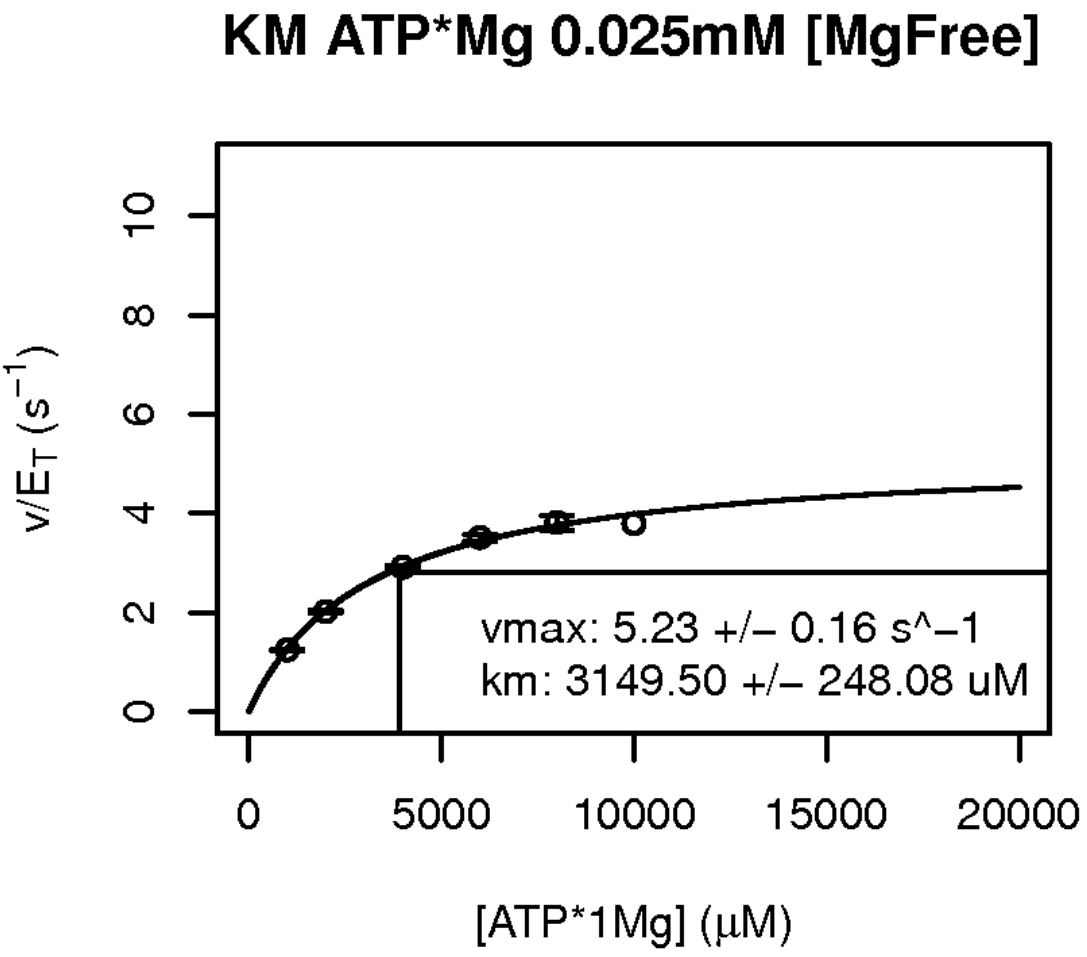

Figure 3-13 K_M for ATP•Mg substrate at 200 μM [H1], 0.025 mM $[Mg^{2+}]_{free}$.

Error bars represent standard error for data point among multiple observations. KM curve fit using nonlinear least squares method to equation v/Et = (vmax*[ATP•1Mg])/(km + [ATP•1Mg]). Total amounts of ATP/$MgCl_2$ calculated using K_D(ATP•1Mg)=28.6 μM.

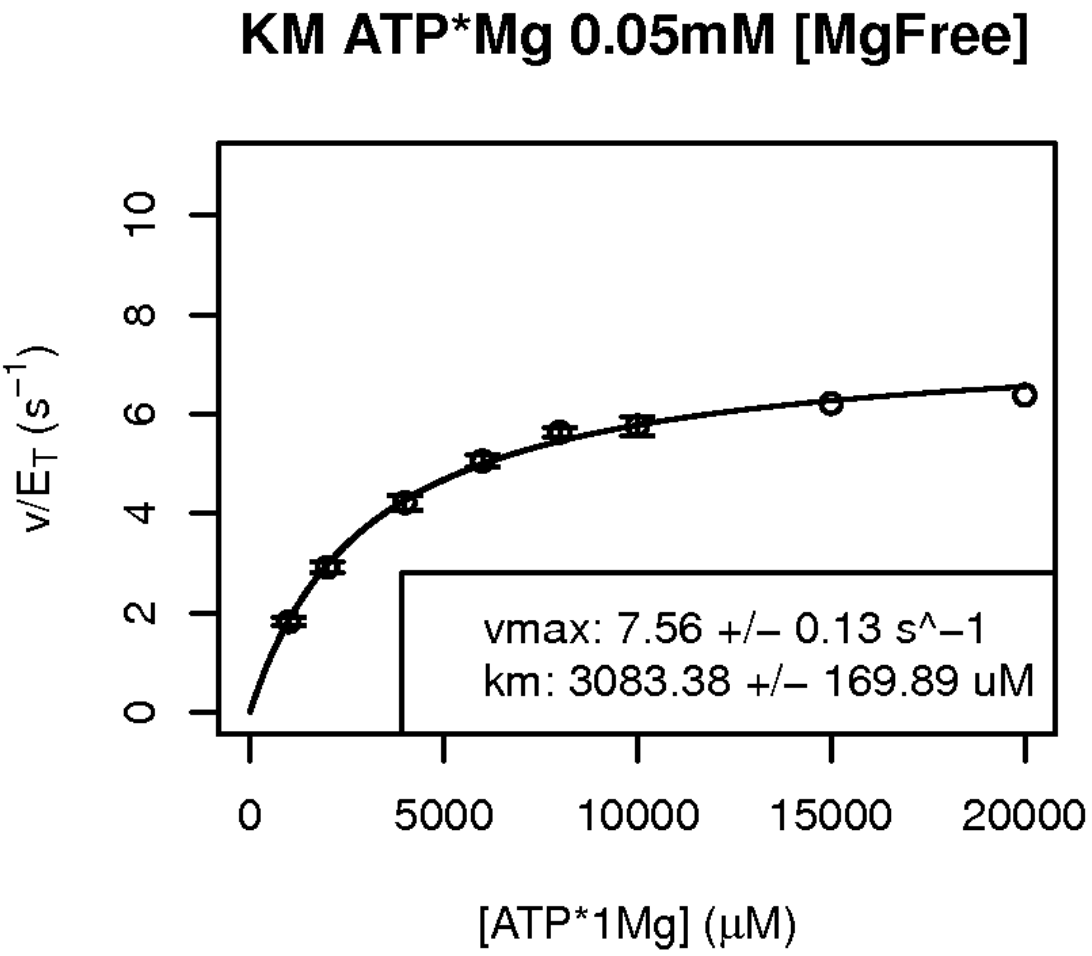

Figure 3-14 KM for ATP•Mg substrate at 200 μM [H1], 0.05 mM $[Mg^{2+}]_{free}$.

Error bars represent standard error for data point among multiple observations. KM curve fit using nonlinear least squares method to equation v/Et = (vmax*[ATP•1Mg])/(km + [ATP•1Mg]). Total amounts of ATP/$MgCl_2$ calculated using KD(ATP•1Mg)=28.6 μM.

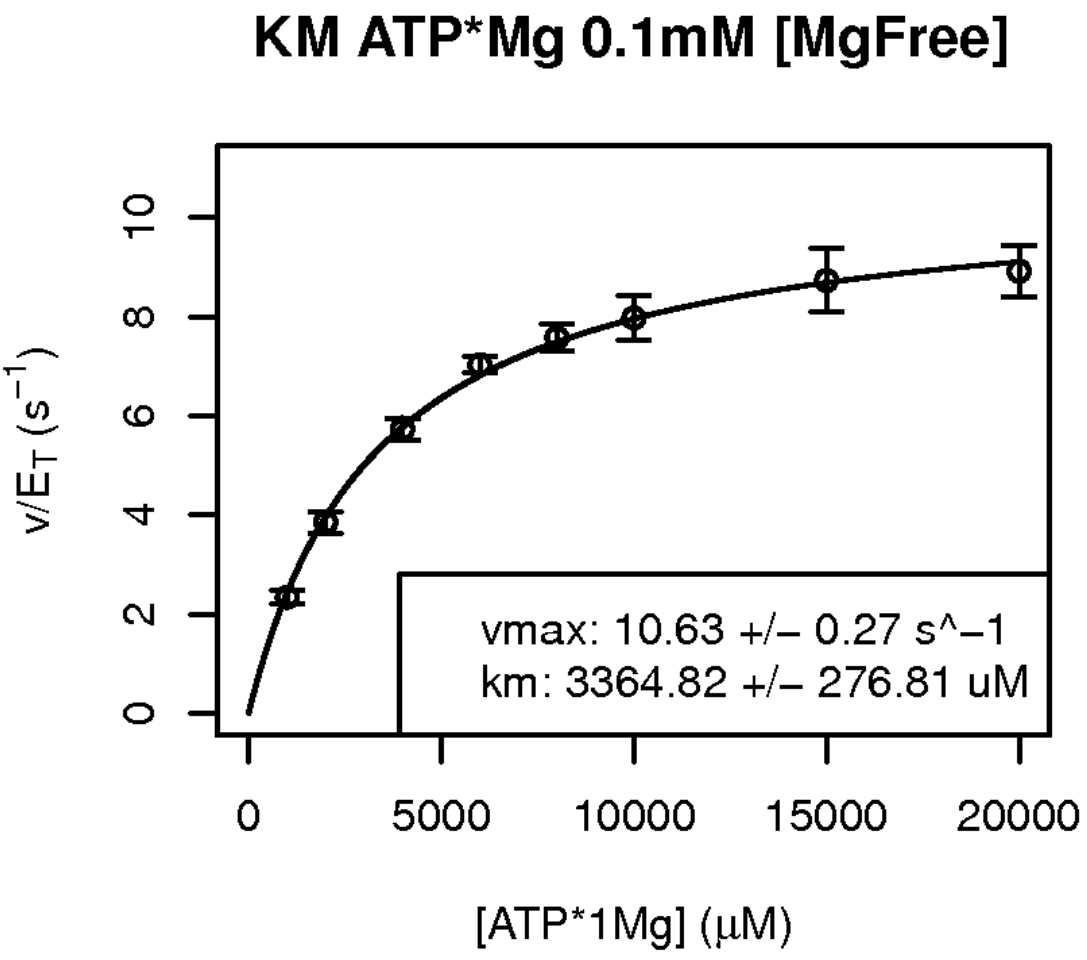

Figure 3-15 KM for ATP•Mg substrate at 200 μM [H1], 0.1 mM $[Mg^{2+}]_{free}$.

Error bars represent standard error for data point among multiple observations. KM curve fit using nonlinear least squares method to equation v/Et = (vmax*[ATP•1Mg])/(km + [ATP•1Mg]). Total amounts of ATP/$MgCl_2$ calculated using KD(ATP•1Mg)=28.6 μM.

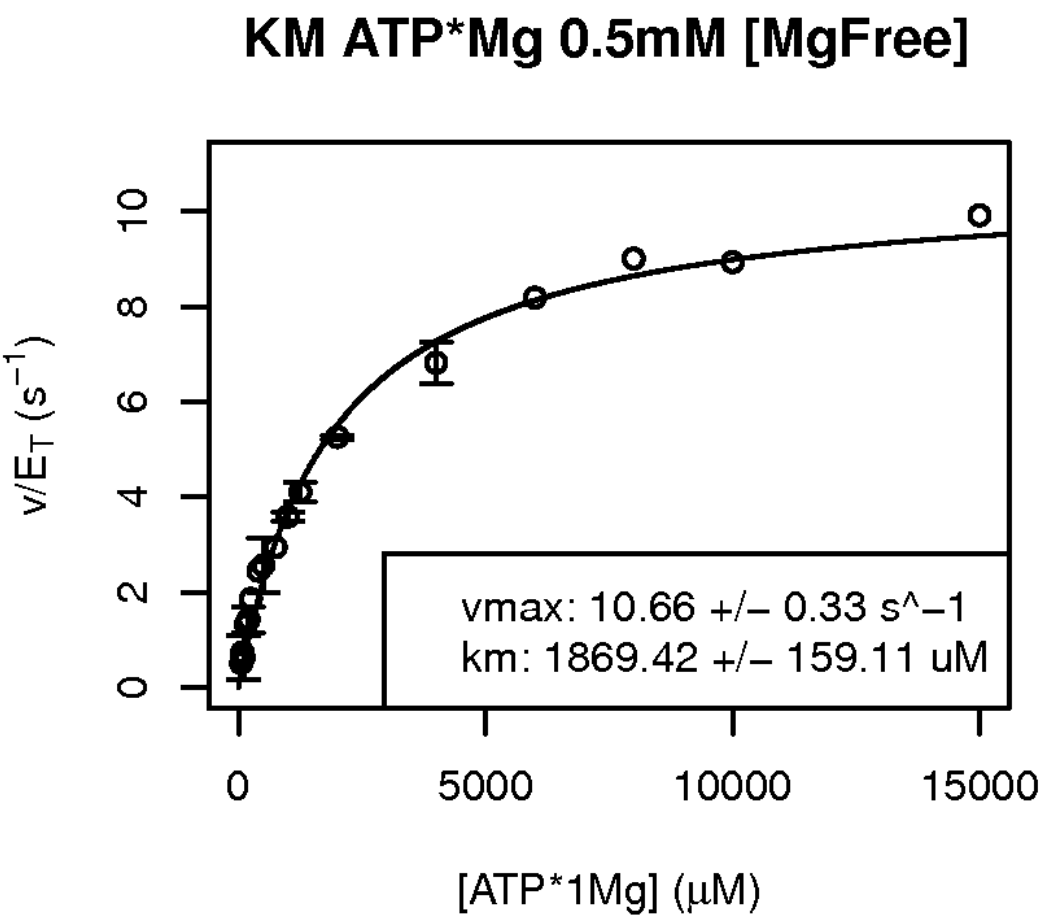

Figure 3-16 KM for ATP•Mg substrate at 200 μM [H1], 0.5 mM $[Mg^{2+}]_{free}$.

Error bars represent standard error for data point among multiple observations. KM curve fit using nonlinear least squares method to equation v/Et = (vmax*[ATP•1Mg])/(km + [ATP•1Mg]). Total amounts of ATP/$MgCl_2$ calculated using KD(ATP•1Mg)=28.6 μM.

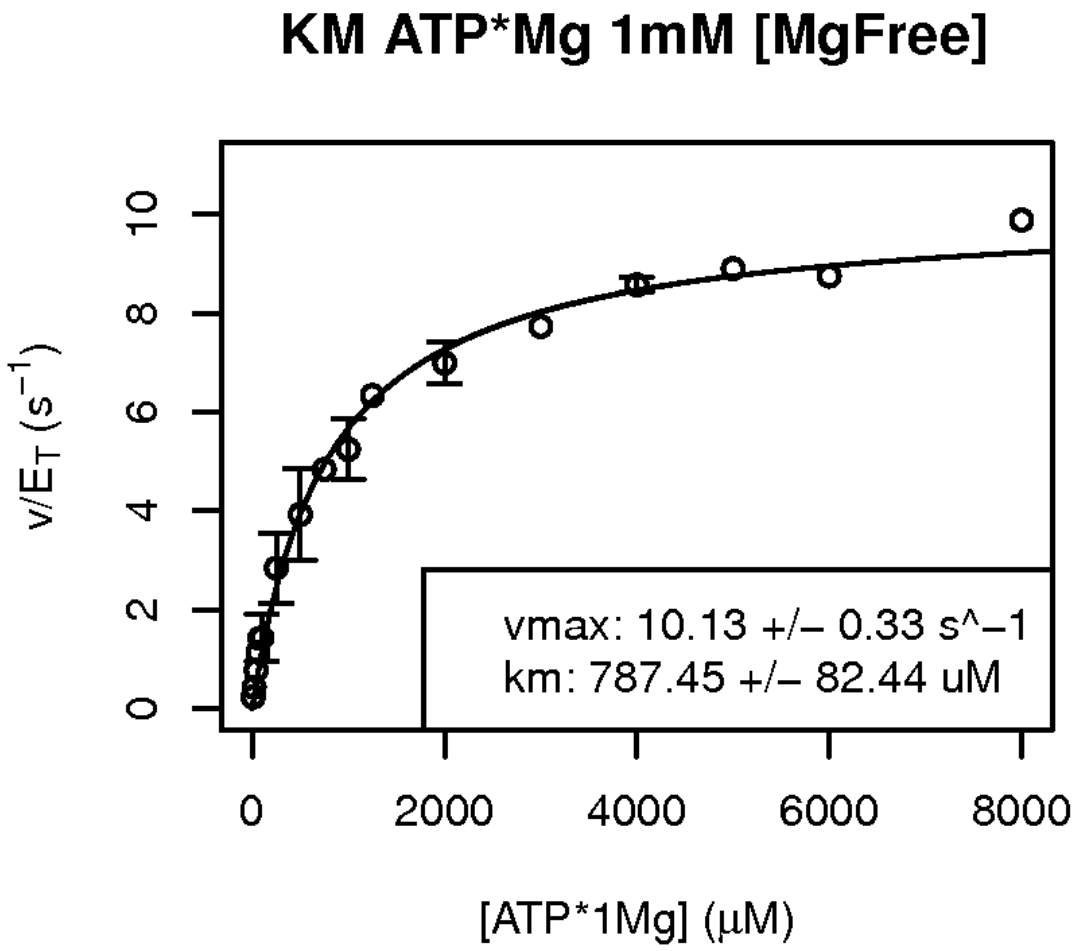

Figure 3-17 KM for ATP•Mg substrate at 200 μM [H1], 1 mM $[Mg^{2+}]_{free}$.

Error bars represent standard error for data point among multiple observations. KM curve fit using nonlinear least squares method to equation v/Et = (vmax*[ATP•1Mg])/(km + [ATP•1Mg]). Total amounts of ATP/$MgCl_2$ calculated using KD(ATP•1Mg)=28.6 μM.

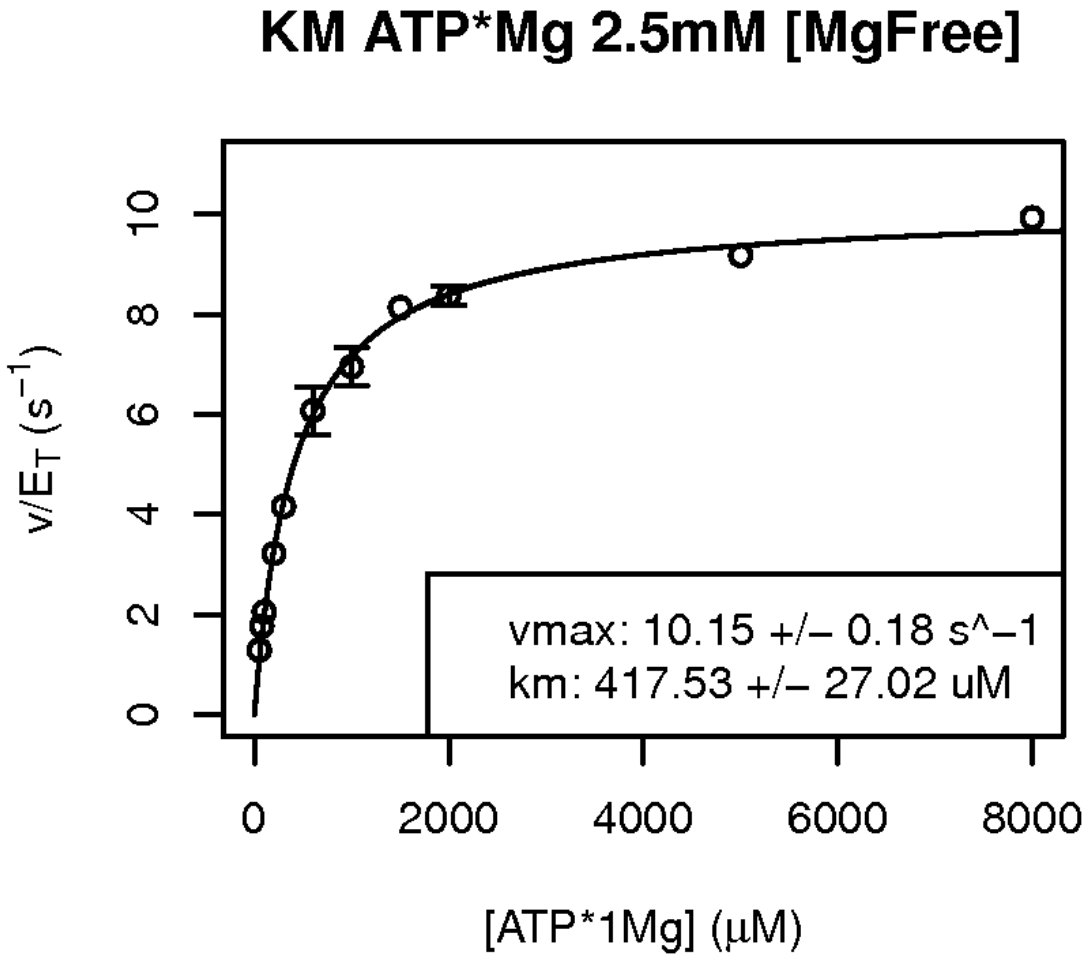

Figure 3-18 KM for ATP•Mg substrate at 200 μM [H1], 2.5 mM $[Mg^{2+}]_{free}$.

Error bars represent standard error for data point among multiple observations. KM curve fit using nonlinear least squares method to equation v/Et = (vmax*[ATP•1Mg])/(km + [ATP•1Mg]). Total amounts of ATP/$MgCl_2$ calculated using KD(ATP•1Mg)=28.6 μM.

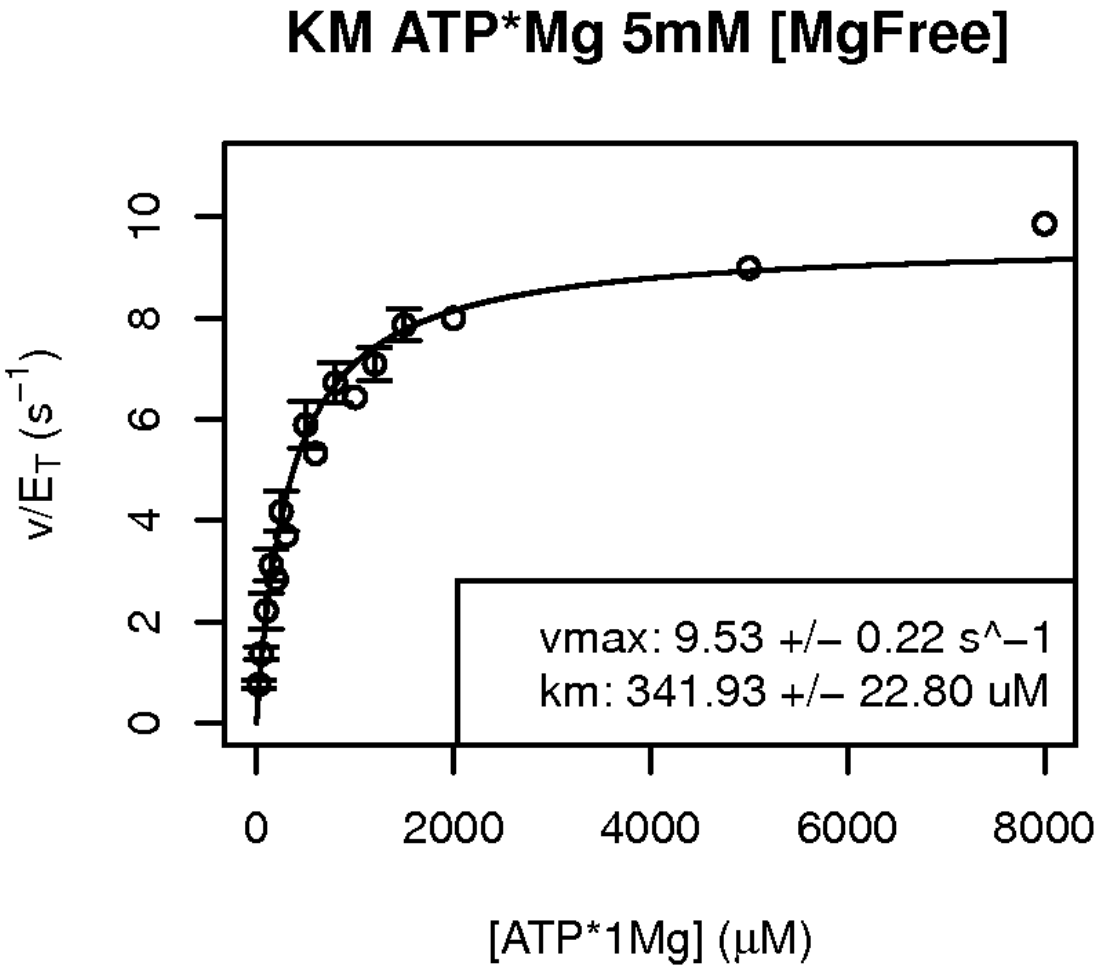

Figure 3-19 KM for ATP•Mg substrate at 200 μM [H1], 5 mM $[Mg^{2+}]_{free}$.

Error bars represent standard error for data point among multiple observations. KM curve fit using nonlinear least squares method to equation v/Et = (vmax*[ATP•1Mg])/(km + [ATP•1Mg]). Total amounts of ATP/$MgCl_2$ calculated using KD(ATP•1Mg)=28.6 μM.

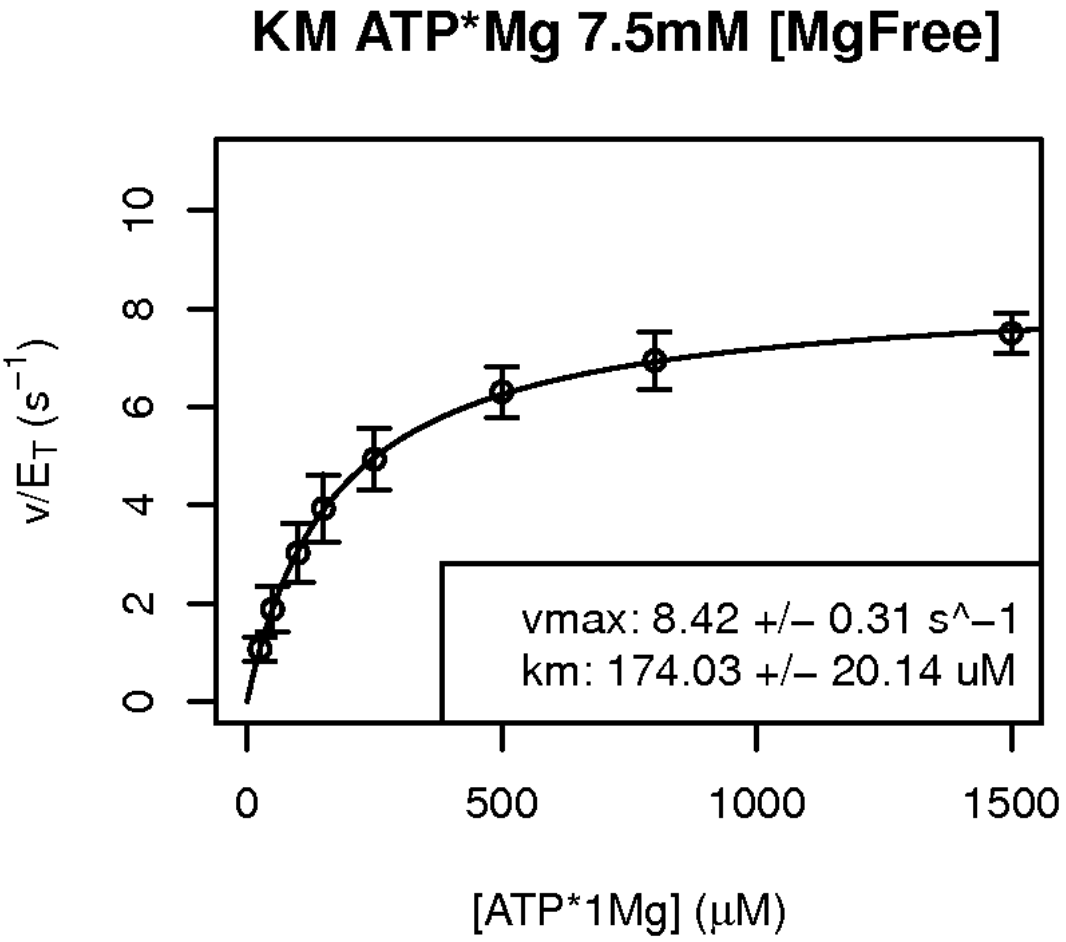

Figure 3-20 KM for ATP•Mg substrate at 200 μM [H1], 7.5 mM $[Mg^{2+}]_{free}$.

Error bars represent standard error for data point among multiple observations. KM curve fit using nonlinear least squares method to equation v/Et = (vmax*[ATP•1Mg])/(km + [ATP•1Mg]). Total amounts of ATP/$MgCl_2$ calculated using KD(ATP•1Mg)=28.6 μM.

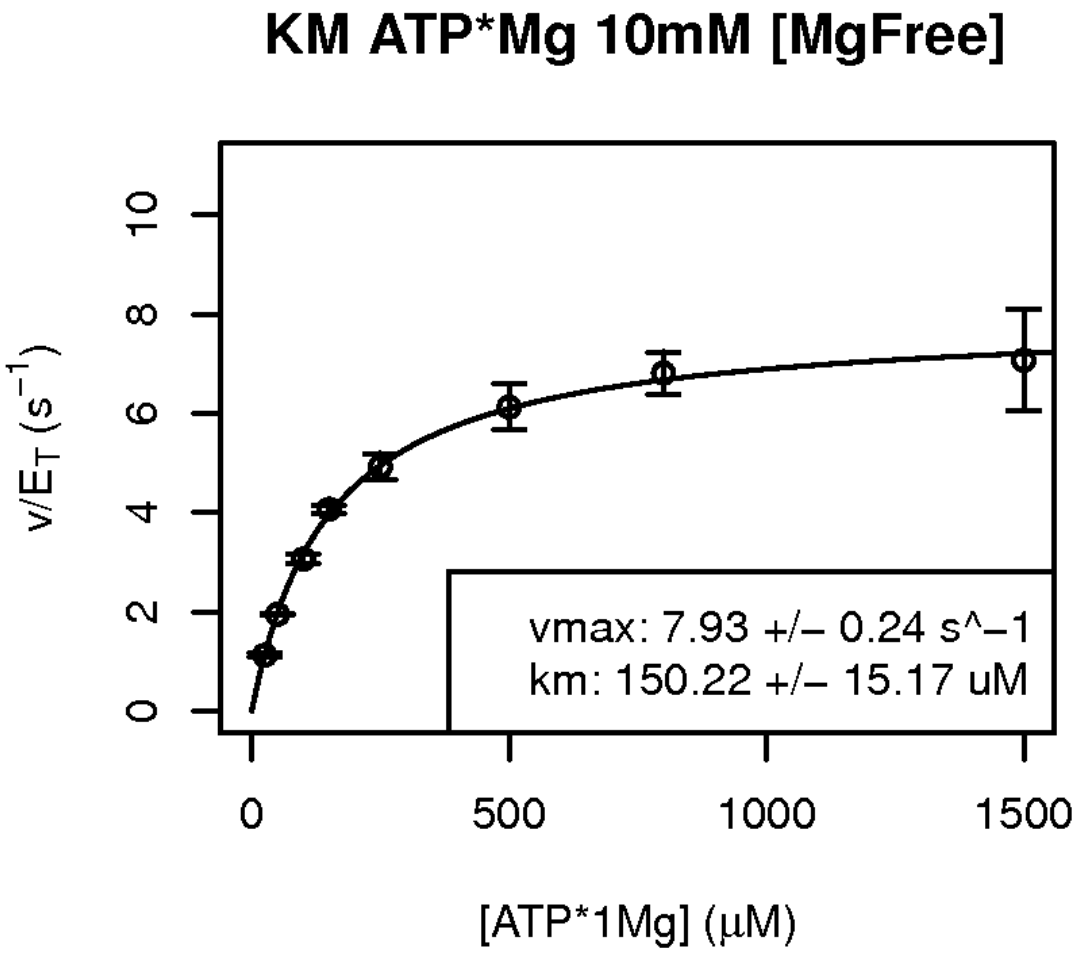

Figure 3-21 KM for ATP•Mg substrate at 200 μM [H1], 10 mM $[Mg^{2+}]_{free}$.

Error bars represent standard error for data point among multiple observations. KM curve fit using nonlinear least squares method to equation v/Et = (vmax*[ATP•1Mg])/(km + [ATP•1Mg]). Total amounts of ATP/$MgCl_2$ calculated using KD(ATP•1Mg)=28.6 μM.

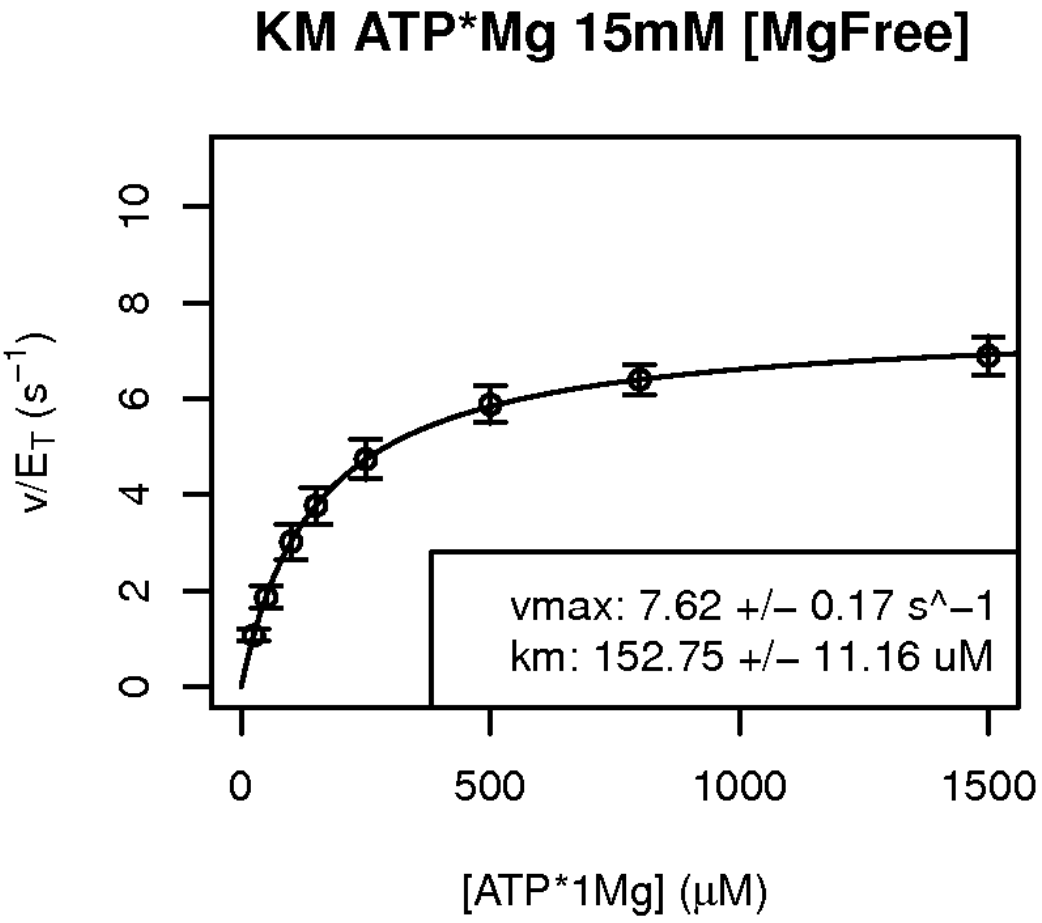

Figure 3-22 KM for ATP•Mg substrate at 200 μM [H1], 15 mM $[Mg^{2+}]_{free}$

Error bars represent standard error for data point among multiple observations. KM curve fit using nonlinear least squares method to equation v/Et = (vmax*[ATP•1Mg])/(km + [ATP•1Mg]). Total amounts of ATP/$MgCl_2$ calculated using KD(ATP•1Mg)=28.6 μM.

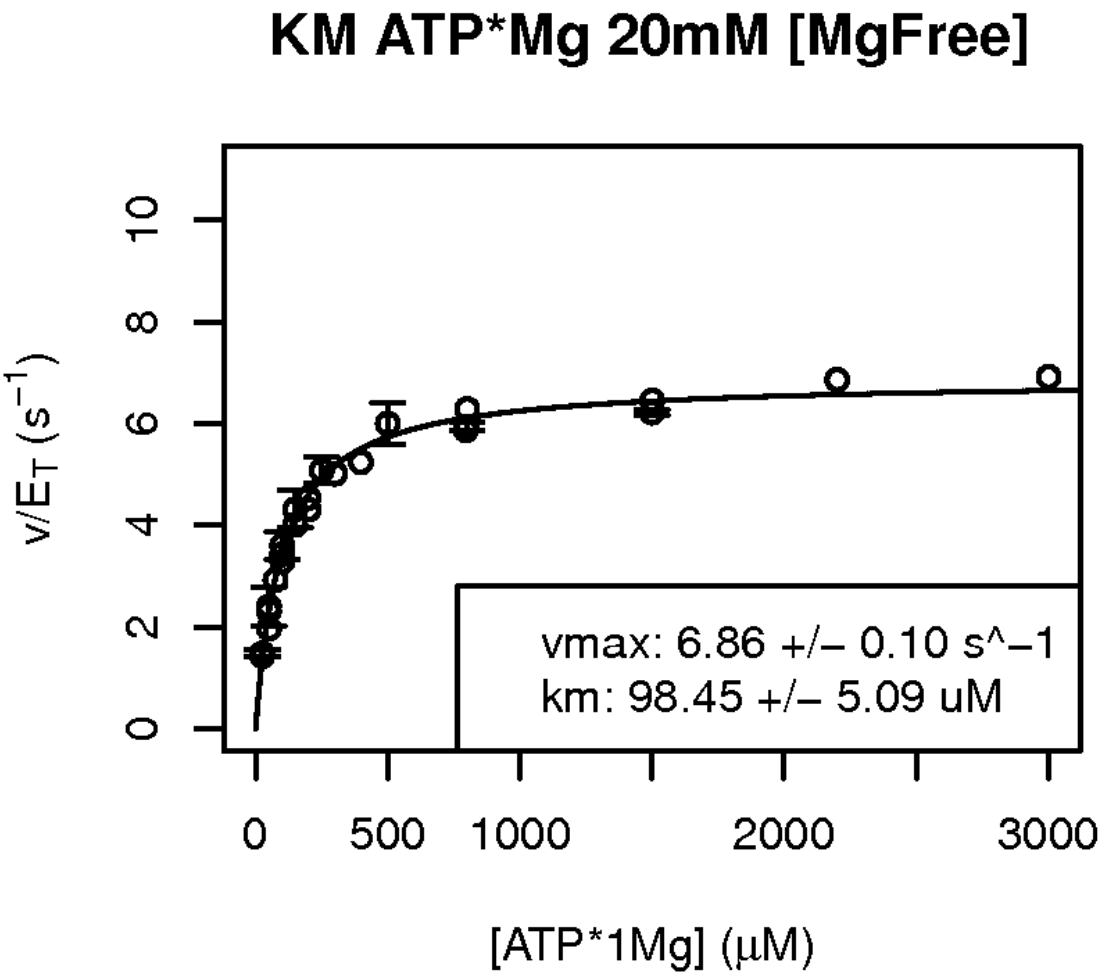

Figure 3-23 KM for ATP•Mg substrate at 200 μM [H1], 20 mM $[Mg^{2+}]_{free}$.

Error bars represent standard error for data point among multiple observations. KM curve fit using nonlinear least squares method to equation v/Et = (vmax*[ATP•1Mg])/(km + [ATP•1Mg]). Total amounts of ATP/$MgCl_2$ calculated using KD(ATP•1Mg)=28.6 μM.

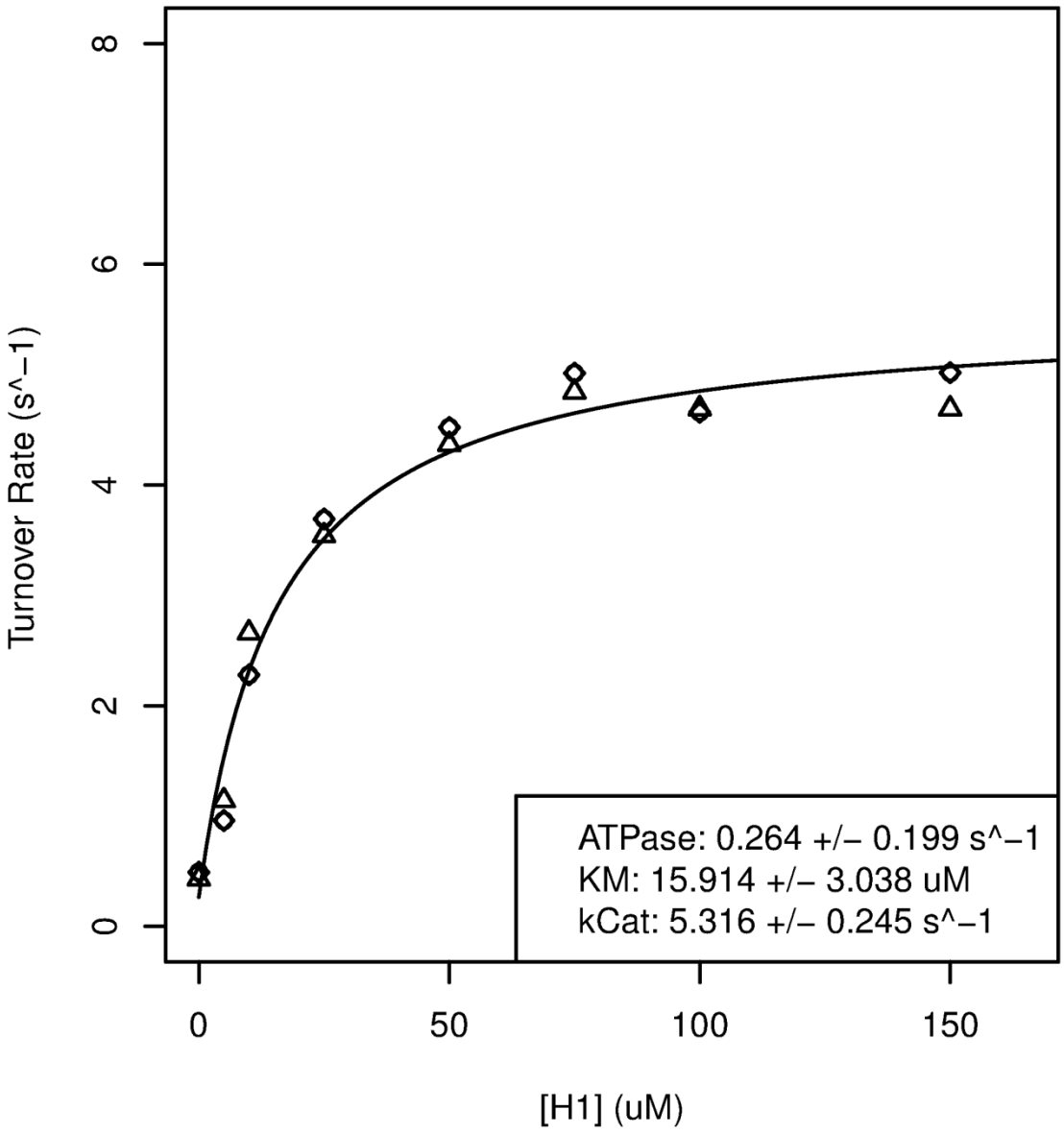

Figure 3-24 KM for protein substrate at 800 μM [ATP], 1 mM $[Mg^{2+}]_{free}$.

KM curve fit using nonlinear least squares method to equation v/Et = ATPase + (kCat*[H1])/(KM + [H1]). Total amounts of ATP/$MgCl_2$ calculated using KD(ATP•1Mg)=28.6 μM.

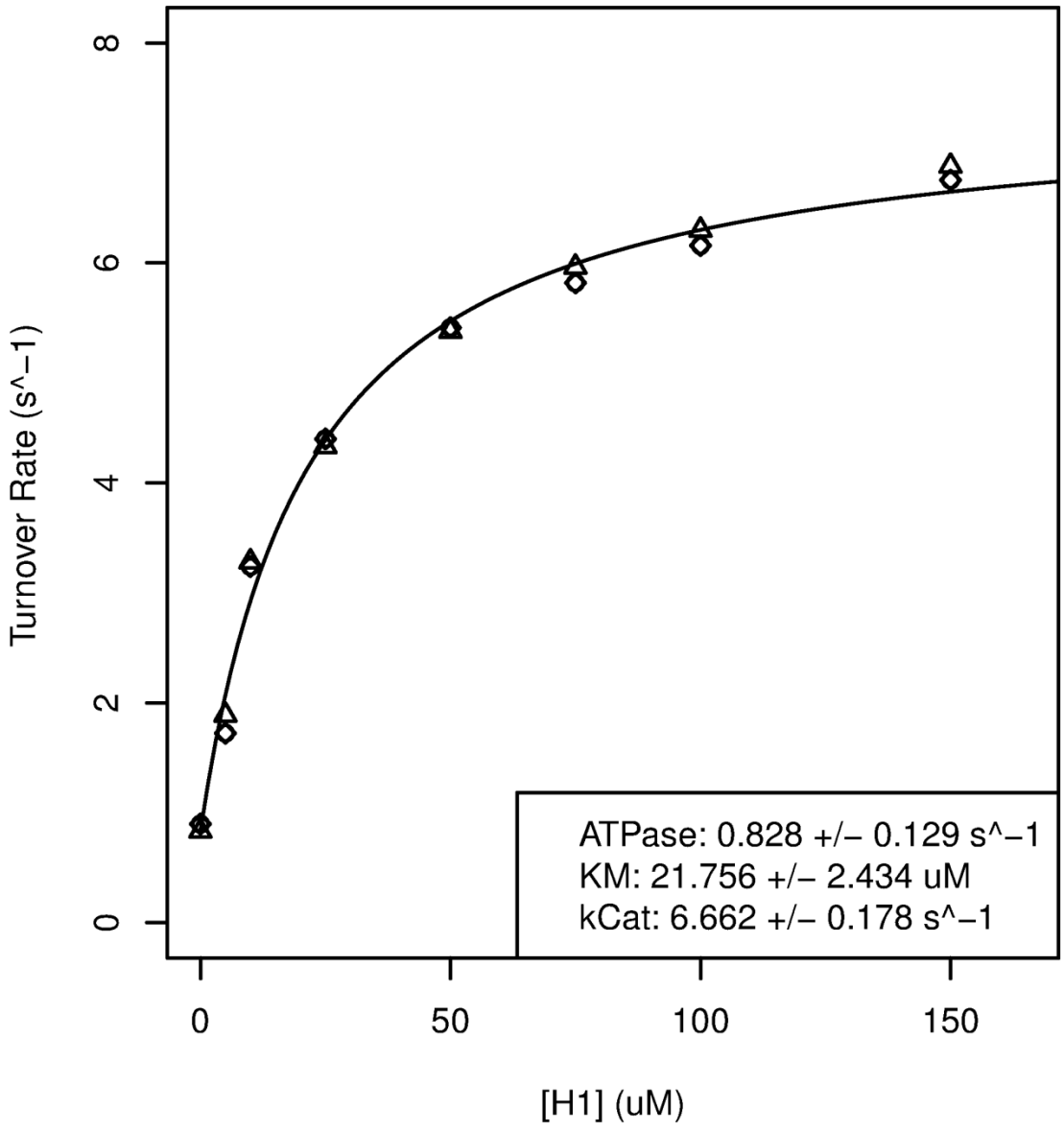

Figure 3-25 KM for protein substrate at 800 μM [ATP], 20 mM $[Mg^{2+}]_{free}$.

KM curve fit using nonlinear least squares method to equation v/Et = ATPase + (kCat*[H1])/(KM + [H1]). Total amounts of ATP/$MgCl_2$ calculated using KD(ATP•1Mg)=28.6 μM.

Solvent Viscosity Effect Experiments

Varying the solvent viscosity can help to discriminate the proportional contribution of specific steps of the catalytic cycle in the overall rate of catalysis. This is because the solvent viscosity alters the rate of diffusive steps (e.g. bi-molecular events such as substrate binding or product release) a great deal more than the rate of non-diffusive steps (e.g. the transfer of the γ-phosphate to the protein substrate – no solvent exists between the γ-phosphate and the target Ser/Thr).

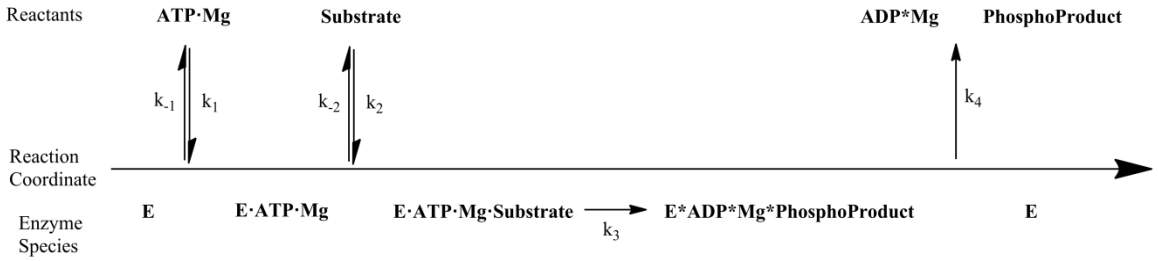

Scheme 3-2: Microscopic rates of the classic protein kinase reaction

Microscopic rate constants are: k_1 (ATP•Mg binding), k_{-1} (ATP•Mg release), k_2 (Protein substrate binding), k_{-2} (Protein substrate release), k_3 (Phosphoryl transfer), and k_4 (Product release). Previous studies of CDK2 and other kinases suggest that the binding order of the ATP•Mg substrate and the protein substrate are randomly ordered. There is less information on when the 2nd Mg binds, but the structures predict it must be concomitant with ATP•Mg binding or after ATP•Mg binding. The apparent effect on K_M(ATP•Mg) of the 2nd Mg binding further supports the cooperative binding of the ATP•Mg and Mg substrates, so we assume that k_1 and k_{-1} are the effective on and off net

rate constants of the combined ATP•Mg and second Mg substrate at each [ATP•Mg] and $[Mg^{2+}]_{free}$ condition.

If the ATP•Mg and protein substrates are saturating in the experimental conditions, then the rate of catalysis can be reduced to two sequential steps: phosphoryl transfer (k_3) and then product release (k_4), where only the rate of product release is affected by the solvent viscosity, such that the total flux through the catalytic cycle is given by (Adams, 2001):

$$k_{cat}^{App} = \frac{k_3^{App} * k_4^{App}}{k_3^{App} + k_4^{App}}$$

The "App" superscript is used in this case because k_{cat}, k_3 and k_4 are considered separately for each $[Mg^{2+}]_{free}$, and the binding of the 2nd Mg^{2+} ion may not be saturating at any of the tested $[Mg^{2+}]_{free}$. The effect of the solvent viscosity, m, on k_{cat}^{App} is determined by measuring k_{cat} at several different solvent viscosities and then fitting a line to the equation:

$$\eta - 1 = m\left(\frac{k_{cat}^{\circ,App}}{k_{cat}^{App}} - 1\right); where\ \eta = Relative\ Solvent\ Viscosity = \frac{k_4^{\circ,App}}{k_4^{App}}$$

where η is the relative viscosity of the solvent, m is the viscosity effect, k_{cat} is the measured rate of the reaction at each [sucrose], and $k_{cat}^{\circ,App}$ is the reference viscosity ([sucrose] = 0), and m is the slope of the line, which is the viscosity effect on k_{cat}^{App}. Substituting η with $k_4^{\circ,App}/k_4^{App}$, $k_{cat}^{\circ,App}$ with $k_3^{App}*k_4^{\circ,App}/(k_3^{App}+k_4^{\circ,App})$, and k_{cat}^{App} with $k_3^{App}*k_4^{App}/(k_3^{App}+k_4^{App})$, and then following algebraic manipulation of the above equation and solving for m gives:

$$m = \frac{k_3^{App}}{k_3^{App} + k_4^{\circ,App}} \quad \therefore \quad k_4^{\circ,App} = \frac{k_{cat}^{\circ,App}}{m} \;\; and \;\; k_3^{App} = \frac{k_{cat}^{\circ,App}}{1-m}$$

where the ° superscript denotes that the rate constant is the [sucrose]=0 condition.

At partially saturating ATP•Mg (with saturating protein substrate), the rate per CDK2 can be expressed as (Adams and Taylor, 1993):

$$\frac{v}{[E_T]} = \frac{k_3^{App} * k_4^{App} * \frac{[ATPMg]}{K_{ATPMg}}}{\frac{[ATPMg] * (k_3^{App} + k_4^{App})}{K_{ATPMg}} + k_4^{App}} \text{ where } K_{ATPMg} = \frac{k_{-1}^{App}}{k_1^{App}}$$

Since the solvent viscosity effects on k_{-1}^{App} and k_1^{App} should be equivalent, i.e. $= \frac{k_4^{\circ}}{k_4} = \frac{k_{-1}^{\circ}}{k_{-1}} = \frac{k_1^{\circ}}{k_1}$, thus $K_{ATPMg}° = K_{ATPMg}$. Therefore, solvent viscosity effects at partially saturating [ATP•Mg] shows the effects of product release, and not viscosity effects on ATP•Mg or protein substrate binding/release.

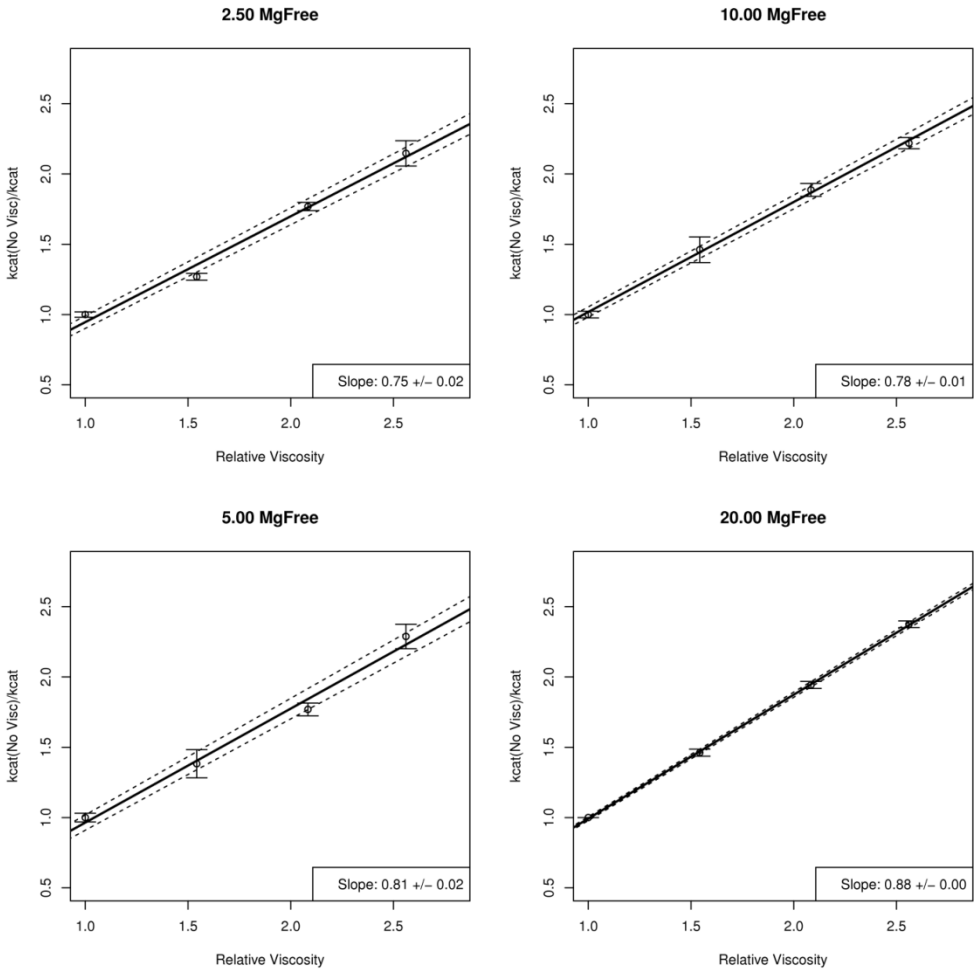

Figure 3-26 Solvent viscosity affect at constant 9.3 mM [ATP] at various $[Mg^{2+}]_{free}$.

This represents > 20x K_M(ATP•Mg) at from 2.5 mM to 20 mM $[Mg^{2+}]_{free}$. Total amounts of ATP/$MgCl_2$ calculated using K_D(ATP•1Mg)=28.6 μM. Data points plotted at mean position for observations. Error bars represent standard error for multiple observations of data point. Solid black line is the fit linear model to the equation: relVisc = m(v°/v) + intercept, where the slope of the line m is the viscosity effect reported in figure 8A. Dotted lines show the potential variation of the linear fit based on the standard error of the fit intercept and slope m.

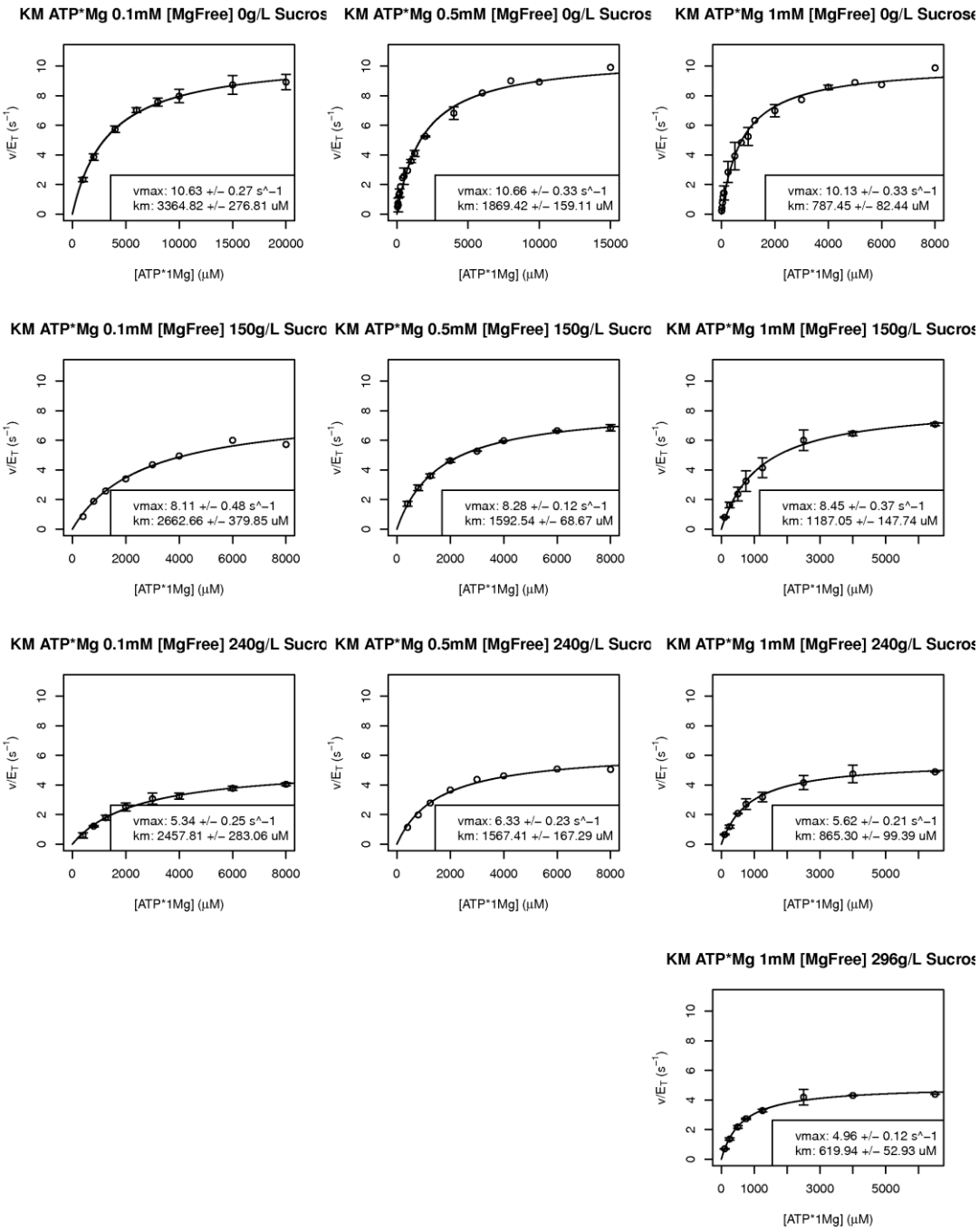

Figure 3-27 K_M for ATP•Mg substrate at 200 μM [H1] at 0.1, 0.5 and 1 mM $[Mg^{2+}]_{free}$, and 0, 150, 240, 296 g/L Sucrose.

Error bars represent standard error for data point among multiple observations. KM curve fit using nonlinear least squares method to equation v/Et = (vmax*[ATP•1Mg])/(km + [ATP•1Mg]). Total amounts of ATP/$MgCl_2$ calculated using K_D(ATP•1Mg)=28.6 μM.

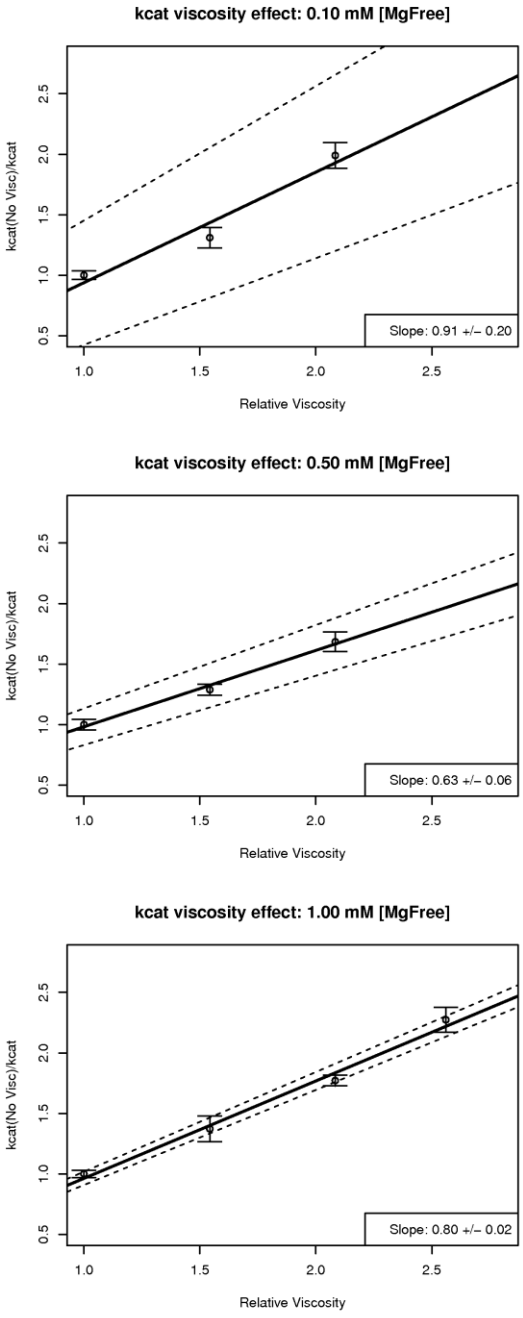

Figure 3-28 Solvent viscosity affect at calculated k_{cat} at 0.1 mM, 0.5 mM, and 1 mM $[Mg^{2+}]_{free}$

Underlying data from Figure 3-27. Error bars represent standard error for nonlinear fit of k_{cat}. Solid black line is the fit linear model to the equation: relVisc = m(v°/v) + intercept, where the slope of the line m is the viscosity effect reported in figure 8A. Dotted lines show the potential variation of the linear fit based on the standard error of the fit intercept and slope m.

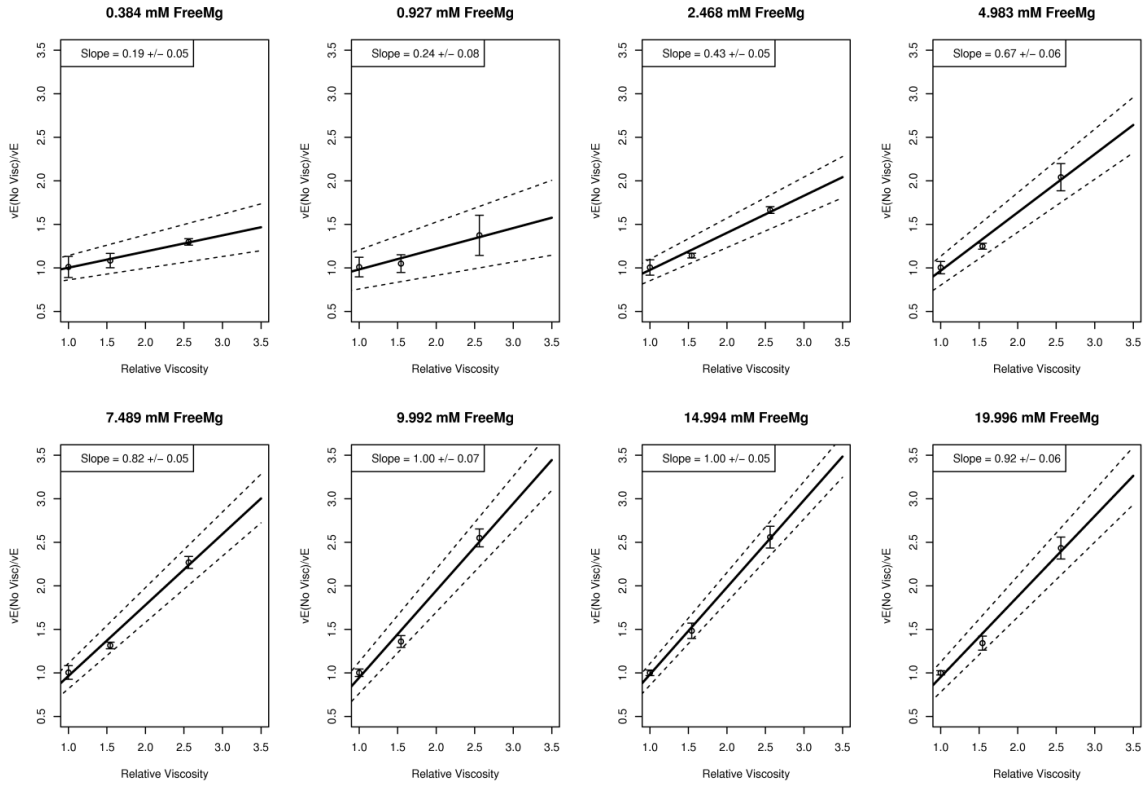

Figure 3-29 Solvent viscosity affect at constant 1.2 mM [ATP] at various $[Mg^{2+}]_{free}$ with saturating (200 μM) protein substrate histone H1.

At lower $[Mg^{2+}]_{free}$, 1.2 mM [ATP] is subsaturating, but at high $[Mg^{2+}]_{free}$, this condition does saturate. Total amounts of ATP/$MgCl_2$ calculated using K_D(ATP•1Mg)=28.6 μM. Data points plotted at mean position for observations. Error bars represent standard error for multiple observations of data point. Solid black line is the fit linear model to the equation: relVisc = m(v°/v) + intercept, where the slope of the line m is the viscosity effect reported in figure 8B. Dotted lines show the potential variation of the linear fit based on the standard error of the fit intercept and slope m.

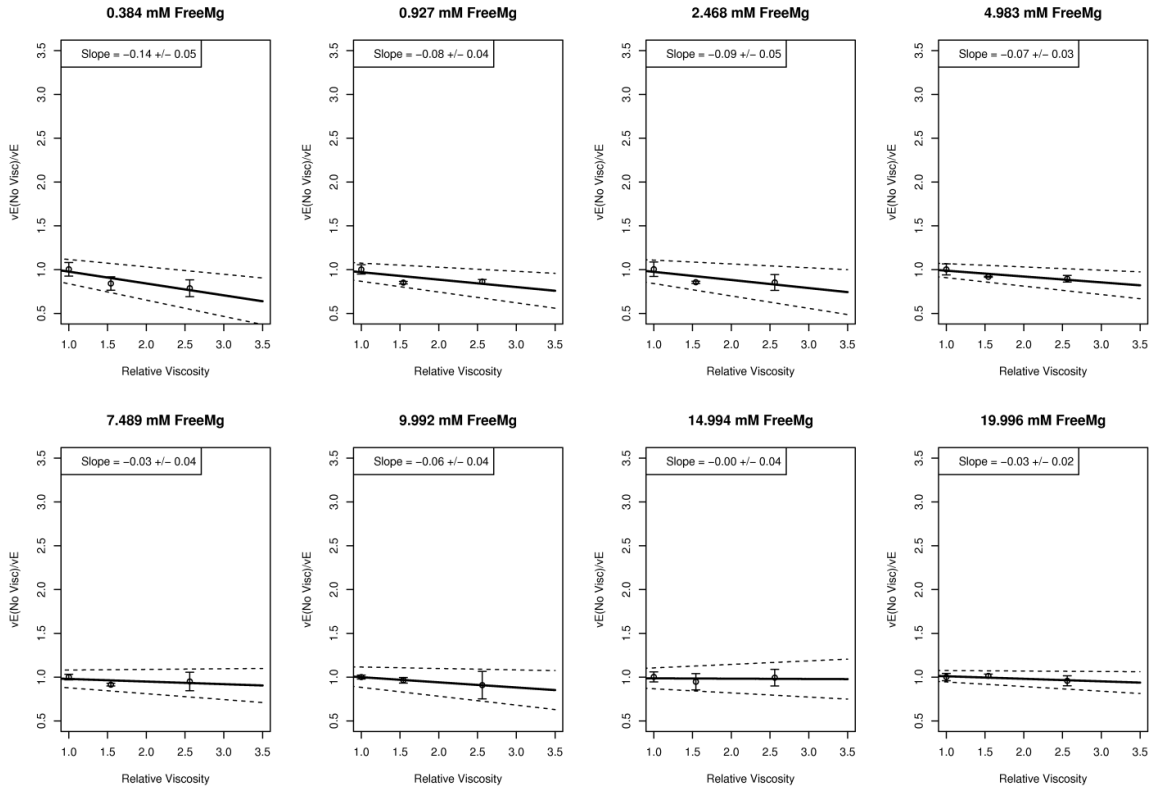

Figure 3-30 Solvent viscosity affect at constant 1.2 mM [ATP] at various $[Mg^{2+}]_{free}$ with **no protein subsrate** (water as substrate).

Total amounts of ATP/$MgCl_2$ calculated using K_D(ATP•1Mg)=28.6 μM. Data points plotted at mean position for observations. Error bars represent standard error for multiple observations of data point. Solid black line is the fit linear model to the equation: relVisc = m(v°/v) + intercept, where the slope of the line m is the viscosity effect reported in figure 8B. Dotted lines show the potential variation of the linear fit based on the standard error of the fit intercept and slope m.

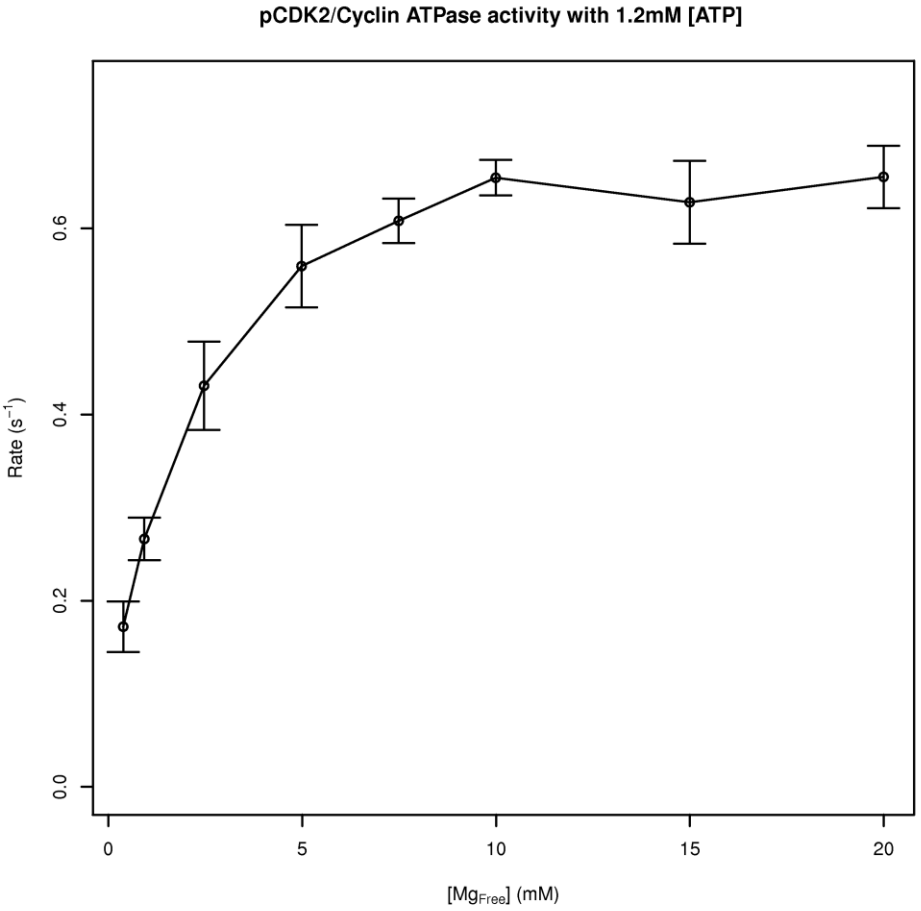

Figure 3-31 Rate of pCDK2/Cyclin ATPase reaction vs. $[Mg^{2+}]_{free}$ with 1.2 mM [ATP] and 0 protein substrate H1.

Total amounts of ATP/$MgCl_2$ calculated using K_D(ATP•1Mg)=28.6 μM. Data points plotted at mean position for observations. Error bars represent standard error for multiple observations of data point.

CHAPTER 4

Essential activation: A molecular link between allosteric activation and catalytic function of protein kinases.

Foreword

This chapter describes our work on isolating the molecular basis for the activation of protein kinase activity based on the action of a conserved regulatory mechanism – the rotation of the c-α-helix of the kinase domain. As with all my work presented thus far, this chapter represents collaborative work with my colleagues in the Brooks and Young laboratories. I will enumerate the specific contributions to experiments and calculations presented in this chapter:

Jacobsen DM: Prepared crystals (crystallization according to earlier protocols), X-ray diffraction data collection, calculated structure solution/refinement, all enzyme kinetics experiments, and molecular dynamics calculations (equilibrium and free energy perturbation calculations).

Bao ZQ: Performed cloning and mutagenesis of CDK2 and Src protein kinases, protein preparation and purification, and isothermal titration calorimetry experiments.

Knight JE: Provided protocol and training with Free Energy Perturbation calculations using the Multistate Bennet Acceptance Ratio to calculate free energies of ADP•Mg and MgI site binding to CDK2 and Src.

Abstract

Regulation of protein kinase activity is a critical feature of cellular signaling. While there is a large diversity of known regulatory mechanisms manipulating kinase activity, there are some recurring regulatory themes within the protein kinase superfamily. The conformational re-arrangement of the c-α-helix upon activation is observed in at least three different protein kinase families, but the molecular basis for catalytic activation by this conformational change is not well understood. In this chapter, I describe our work dissecting how the electrostatic properties of the active site are altered by kinase activation, and through crystal structures, ITC, enzyme kinetics experiments and extensive simulation, I show how the electrostatic alteration of the active site by c-α-helix rotation optimizes the active site for catalysis. The electrostatic consequences of rotation of the c-α-helix has two important effects: 1) increases binding affinity of Mg^{2+} to the MgI site, and 2) decreases the active site binding affinity for phosphates – which may assist in product release.

Introduction

Proper regulation of protein kinase activity is critical to the regulation of many biological processes. This is because the post-translational modification of proteins by phosphorylation is in turn used to transduce signals and regulate biological processes. For example, protein kinase activity can alter levels of gene transcription, can activate or inactivate metabolic enzymes, and manipulate the careful balance of cell division and apoptosis (Malumbres and Barbacid, 2009). The development of many cancers is thought to be dependent on aberrant activity of de-regulated kinases, such as the role of Bcr-Abl in chronic myeloid leukemia (Druker et al., 2001). Under normal physiological

conditions, the activity of CDK2, and the other CDKs, is responsible for advancing the cell cycle once the appropriate conditions are met. It has been shown that loss of regulatory control of the CDKs is associated with the progression of many cancers (Malumbres and Barbacid, 2009).

There are a variety of factors that can inactivate CDK2 (INK4 or $p27^{Kip}$ binding, phosphorylation of the Gly-loop), but two events are required for CDK2 activation: heterodimerization with Cyclin, and activation loop phosphorylation (Malumbres and Barbacid, 2007). Monomeric CDK2 is considered to be inactive, having very little kinase activity relative to the activated form (Hagopian et al., 2001). When CDK2 forms a hetero-dimer with a Cyclin binding partner, and the activation loop is phosphorylated by a CDK-activating-kinase (CAK), the holo-enzyme pCDK2/Cyclin complex is then capable of phosphorylating protein targets with maximum efficiency (Hagopian et al., 2001; Stevenson et al., 2002). Much has been reported, both here and in the primary literature, about the behavior of fully active kinases, and some of the effects of cyclin binding and activation loop phosphorylation are understood, but the molecular link between cyclin-binding and kinase activity has been elusive.

Crystal structures of inactive monomeric CDK2, partially active CDK2/Cyclin, and fully activated pCDK2/Cyclin have been reported (Jeffrey et al., 1995; Radzio-Andzelm et al., 1995; Schulze-Gahmen et al., 1996). As shown in Figure 4-1, comparing panels A and B relative to B and C, cyclin binding stabilizes a large conformational change in the CDK2 catalytic domain, while T160 phosphorylation appears to result in very little structural change. The crystal structure of the CDK2/Cyclin complex shows a large re-arrangement of the activation loop and the c-α-helix relative to the monomeric

CDK2 structure. The principal structural result of T160 phosphorylation is the formation of salt bridges between pThr160 and Arg50, Arg122, and Arg150 in the pCDK2 catalytic domain, and stabilizing interactions with a lysine in the protein substrate motif. In effect, cyclin stabilizes the active conformation of the CDK2 subunit, while pT160 electrostatically reinforces the active conformation, and helps to coordinate the protein substrate lysine. The major catalytic effect of phosphorylation of the CDK2/Cyclin complex is decreasing protein substrate K_m, rather than ATP K_m (Stevenson et al., 2002), consistent with the structural observation that pT160 helps to stabilize the position of the activation loop and electrostatically coordinate the substrate, and does not alter the active site. This however, does not explain the role of the larger conformational changes associated with cyclin binding.

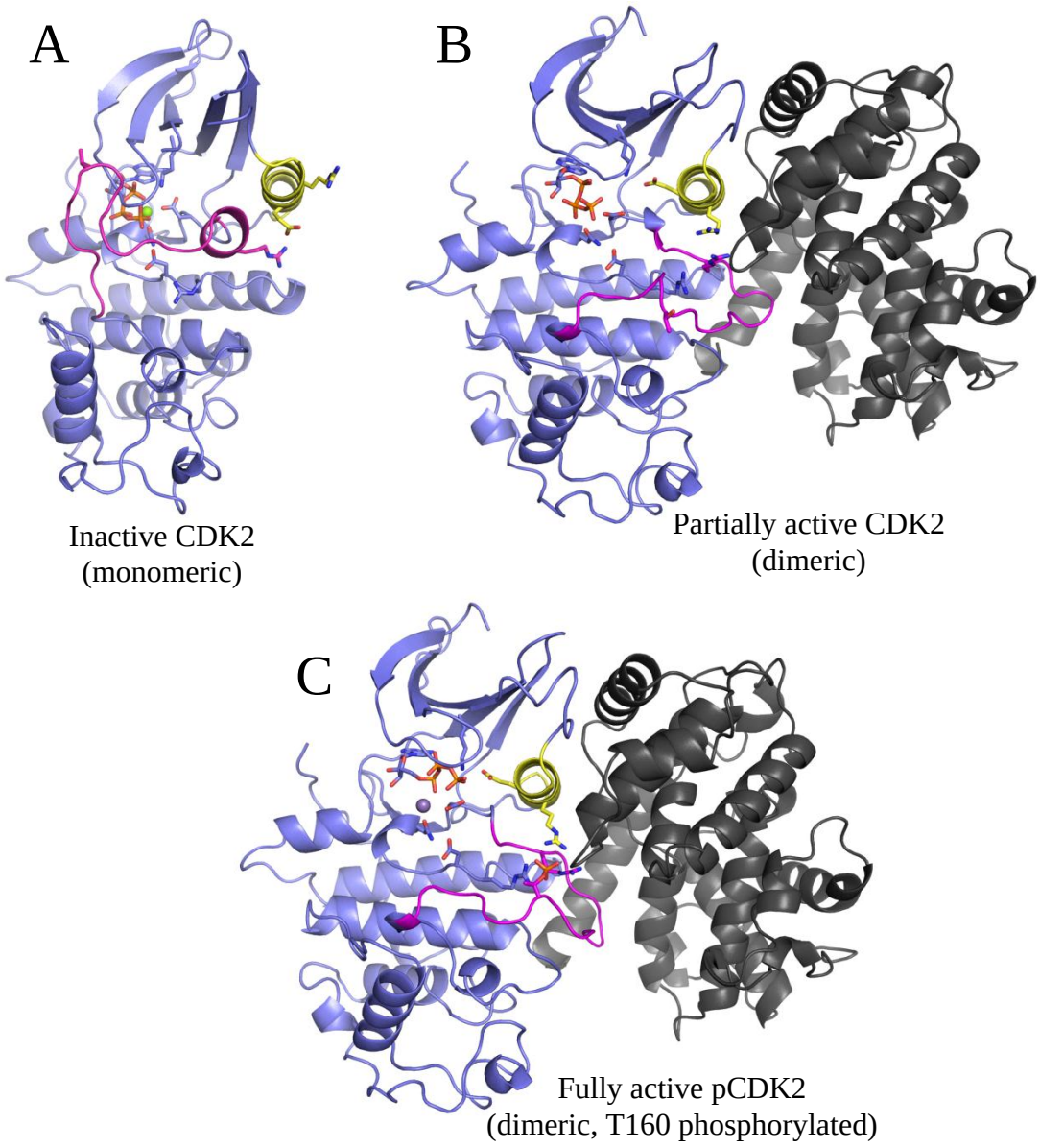

Figure 4-1. Comparison of different regulatory states of CDK2

A) Inactive monomeric CDK2 (PDB 1HCK), **B)** Partially active CDK2/Cyclin A (PDB 1FIN), **C)** Fully active pCDK2/Cyclin A with activation loop Thr160 phosphorylated (1JST). The c-α-helix is highlighted in yellow, and the activation loop in magenta on each structure. **In all panels)** Residues shown in stick form include active site residues Lys33, Asp145 and Asn132, and regulatory residues Glu51 and Thr160

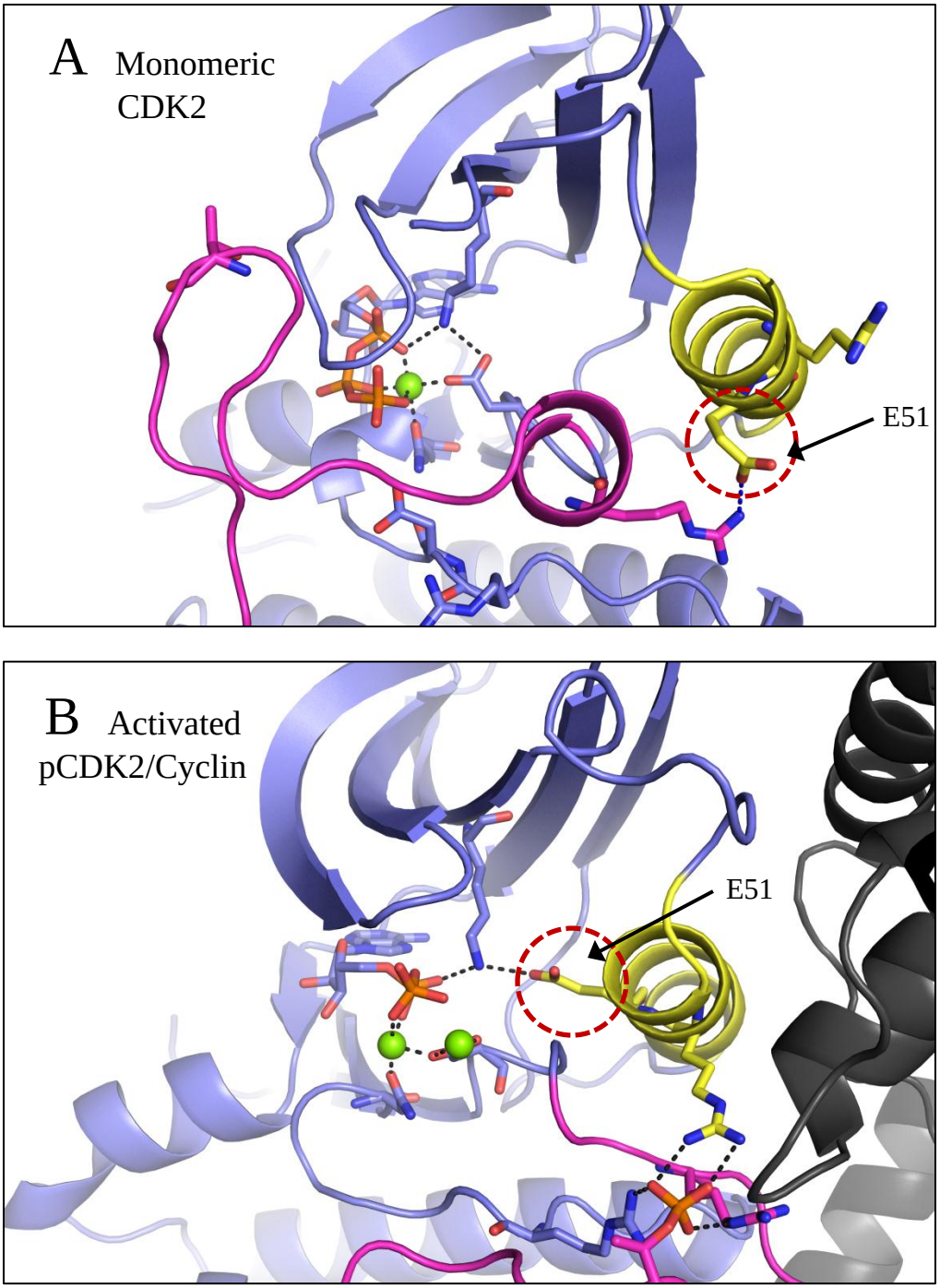

Figure 4-2. Inactive and active CDK2 active sites

A) Monomeric, inactive CDK2 bound to ATP•Mg. B) Dimeric, activated pCDK2/Cyclin bound to ADP•2Mg. Comparing panel (A) to (B) shows large conformational change between inactive and active conformations. c-α-helix rotation results in the only direct conformational change to active site (Glu51 insertion into active site). E51 highlighted in both panels with red dashed ellipse.

As shown in Figure 4-2, one of the principal conformational changes stabilized by cyclin binding is the ~120° rotation of the c-α-helix relative to the inactive monomeric form of CDK2. A consequence of the rotation of the c-α-helix is that a strongly conserved glutamate (Glu51) is inserted into the active site of the kinase domain. This conserved Glu forms a salt bridge with K33, which in turns coordinates the α-phosphate of the nucleotide, as seen in Figure 4-2B. It is known that this interaction is required for proper levels of kinase activity, as evidenced by the fact that E51A mutation to the homologous site in yeast is lethal (Endicott et al., 1994). However, the nature of the role that the Glu51-Lys33 plays in activating the catalytic cycle is not well understood. It has been speculated that this interaction allows proper coordination of the phosphates in order to achieve catalysis (Huse and Kuriyan, 2002), but the literature is silent on details of this arrangement. Figure 4-2 shows that both monomeric and cyclin-bound CDK2 can bind ATP, and that the positioning of Lys33 is similar in both the inactive and active conformation CDK2 structures.

Activation by c-α-helix rotation is not only observed in the CDK family of protein kinases. The c-α-helix is known to change conformation in this way for the CDKs, Src family kinases, and EGFR based on crystal structures of active and inactive forms of each kinase (Jura et al., 2011). These three evolutionarily divergent families of protein kinases; CDK2 – a Ser/Thr kinase, c-Src – a non-receptor tyrosine kinase, and EGFR – a receptor tyrosine kinase all exhibit this same regulatory strategy. Since there are relatively fewer crystal structures of inactive protein kinases rather than active conformations, it is not known how pervasive this regulatory mechanism is. However it has been suggested that a conserved hydrophobic patch on the c-α-helix, in

approximately the region where cyclin binds, may allow regulation in other kinases to similar effect as cyclin on the CDKs, which may function to similarly rotate or stabilize c-α-helices in many more diverse kinases (Jura et al., 2011). It is not simply the mechanical rotation and translation of the c-α-helix that is conserved, but the observation that a conserved Glutamate is inserted into the kinase site, which is the only direct change to the active site observed when the kinase becomes activated.

In chapter 3, I presented ADP-bound structures of pCDK2/Cyclin and a number of equilibrium simulations from which we concluded that there is a strong electrostatic stabilization of the nucleotide phosphates upon MgI binding. Furthermore, we found that in the absence of MgI, an additional positive charge was required to maintain the stability of the ADP phosphates, which we achieved in simulations by protonating D145, the ADP β-phosphate, or by explicitly modeling a sodium ion into the active site. This additional charge was required to satisfy an electrostatic deficit in the kinase active site when nucleotide phosphates are present. We concluded that this electrostatic deficit is responsible for the favorable binding of MgI, or in the absence of MgI, destabilizing the ADP phosphates. Another way to alleviate this electrostatic deficit is to remove a negative charge from the active site – which is in effect what c-α-helix rotation does when the kinase goes from the active conformation to the inactive conformation when the conserved Glu51 is removed from the active site. Thus, we hypothesize that an important aspect of the mechanism of regulation by c-α-helix rotation is achieved by manipulating the active site electrostatics to alter phosphate and Mg binding stability.

In this chapter, I will describe our efforts to isolate the electrostatic component of Glu51 insertion to determine the molecular basis this aspect of activation of kinase activity. To determine the electrostatic role of E51 in the active kinase, we mutated E51 to Glutamine (Gln, Q) to neutralize the net charge at that site in both CDK2 and the homologous site (E310) of the catalytic domain of c-Src. This mutation is intended to model only the active site electrostatics of the inactive kinase, that is, when the Glu is rotated out of the active site, while still maintaining all the other features of the active kinase. We hypothesize that this mutation, by alleviating the active site electrostatic deficit will simultaneously improve phosphate stability (tighter ADP binding), and destabilize MgI binding. Thus, we predict that allosteric regulation of protein kinases by c-α-helix rotation manipulates the binding of the essential activator MgI and by extension nucleotide phosphate stability.

Methods

Protein Preparation and Purification

The pCDK2/Cyclin E51Q mutation was performed using the StrataGene QuikChange II site directed mutagenesis kit using the same human CDK2 construct and protein preparation and purification methodology as was used in chapters 2 and 3. The mutation in the plasmid was confirmed via DNA sequencing at the University of Michigan sequencing core facility.

The c-Src construct was the mouse c-Src catalytic domain, residues 381-663 (mouse residue numbering), which excluded the regulatory SH2/SH3 domains. The construct was ligated into the EcoR1/Xho1 site of the ppSumo vector, which adds a

Sumo tag with Nickel affinity purification tag and a cleavable recognition sequence to remove the tag during purification. c-Src was co-expressed with the Tyrosine phosphatase YopH on the pCDF Duet plasmid to reduce toxicity in the E. coli (BL21DE3) expression system. Vectors were sequenced for DNA sequence verification at the University of Michigan sequencing core facility. The vectors were co-transformed into BL21DE3 cells. Using kanamycin (resistance provided by c-Src vector) and streptomycin (resistance provided by YopH vector), cells were transformed and grown on 2XYT media. A single colony was selected, grown in TB medium with antibiotics overnight at 37 C until OD600 > 1. Induced protein expression with 0.2 mM IPTG, allowed expression at 18 C for 24 hours. Cells were lysed in lysis buffer, with added benzonase nuclease, and then the lysate was spun down. c-Src was then purified from the supernatant using a Nickel affinity column in an FPLC. Fractions from the column elution were pooled and dialyzed overnight into 150 mM NaCl, 20 mM Tris pH 8, >5% glycerol at 4 C. ULP1 was added to cut the Sumo tag from c-Src during the dialysis. A second Nickel column was used to separate the uncut (and remaining tag) protein; the purified c-Src was collected in the column flowthrough. A final stage of purification of c-Src was performed using a gel filtration S75 (size exclusion) column into 150 mM KCl, 25 mM Tris pH 7.77 buffer. Resulting purified c-Src was concentrated to >10 mg/mL and stored at -80 C. Concentration of the purified protein was determined by Nanodrop 280 nm absorbance using ε=1.610 g/L/cm, calculated by the ExPASy ProtParam tool.

The E310Q mutation was prepared and purified identically, with the mutation introduced via the Stratagene QuikChange II site-directed mutagenesis kit and the

mutation verified by DNA sequencing at the University of Michigan sequencing core facility.

Protein Crystallization, data collection and structure refinement

Apo pCDK2^{E51Q}/CyclinA crystallized in exactly the same conditions as pCDK2^{WT}/CyclinA used in chapters 2 and 3. For the mutant, ligand soaking conditions were altered to included higher [$MgCl_2$] (up to 40 mM vs 10 mM $MgCl_2$ for WT crystals) attempting to stabilize binding of MgI. Diffraction data collection and structure refinement were performed exactly the same as for pCDK2^{WT}/Cyclin A in chapter 3. Molecular replacement search models were missing E51, D145, K33, the Gly-rich loop, and the activation loop to minimize initial model bias.

Isothermal Titration Calorimetry

Isothermal titration calorimetry experimentation was performed exactly the same as in chapter 3, except that we were able to obtain high quality at more $MgCl_2$ conditions, including 2.5 mM, 5 mM, 7.5 mM, 10 mM and 15 mM [$MgCl_2$], see the ITC data in the chapter 4 appendix, Figure 4-16 through Figure 4-20.

Kinase Enzyme Kinetics

For this work the kinase activity was measured using the PK/LDH coupled assay system as described in chapter 3. Kinase concentrations used for each series of experiments are shown in Table 4-1. The kinase concentration for each experiment was selected to balance material usage against signal-to-noise ratio in the kinase assay. The extremely low activity of the Src^{E310Q} kinase required a very long time course of data

collection to detect sufficient signal (up to 3 hours per experiment), possibly due to delays in auto-phosphorylation. To prevent artifacts in the Src^{E310Q} data collection due to evaporation of the well solution over the long time course, the experimental wells were sealed with clear tape. For the c-SrcWT and c-SrcE310Q experiments 500 μM substrate peptide (Abltide sequence EAIYAAPFAKKK) was used in all reactions. The $c\text{-}Src^{WT}$ KM(Peptide) of 2.3 mM is shown in chapter 4 appendix, Figure 4-15 at fixed 1.2 mM ATP and 10 mM $MgCl_2$. Thus use of 500 μM substrate peptide predicts that c-Src will be at approximately 18% active (v/vmax = [Peptide] / (KM + [Peptide])), however the use of higher substrate concentration would have proved to be cost prohibitive and may have resulted in undesirable solvent effects on the kinase activity.

Table 4-1. E-to-Q mutation kinetics kinase concentrations.

Kinase	Experiment	Kinase Concentration
$pCDK2^{E51Q}$/Cyclin A	ATP Titration	100 nM
	Mg^{2+}_{free} Titration	50 nM
	KM(ATP•Mg)	150 nM
	Viscosity Titration	125 nM
Src^{WT}	ATP Titration	80 nM
	Mg^{2+}_{free} Titration	80 nM
Src^{E310Q}	ATP Titration	500 nM
	Mg^{2+}_{free} Titration	500 nM

Free Energy Perturbation calculations

The relative free energies of binding MgI to the mutant relative to the wild-type kinase•ATP•Mg complex, or ADP•Mg to the kinase were calculated using CHARMM (Brooks et al., 2009) c36b1 using the AMBER 99SB force field (Hornak et al., 2006). The composition of the starting structure for each calculation are shown in Table 4-2. The equilibration of each structure *in vacuo* included 100 steps of steepest descent

minimization, followed by 1000 steps of ABNR minimization with harmonic restraints to maintain the heavy atom positions, followed by a second round with only the protein backbone restrained. Next, the structure was positioned in a rhombohedral dodecahedron of TIP3P water using the MMTSB to form a cube of water, and a custom CHARMM script to remove the excess water molecules (essentially cut the dodecahedron from a cube). The size of the dodecahedron was determined by adding 10 A of water extending beyond the maximal extents of the protein structures on each side of the protein (total 20 A along each principal x, y, and z axis). The native, solvated system was then equilibrated using Langevin temperature and pressure control for >1.25 ns where the first 250 ps were dominated by heating the system to 303 K using constant volume, and then equilibration of the box volume at a constant pressure of 1 Atm. The equilibration dynamics were calculated with restraints on the heavy protein atoms, followed by diminishing positional harmonic restraints while the protein structure and solvent box were equilibrated to each other and the force field. The final 1 ns+ of dynamics had no positional harmonic restraints on the protein structure.

Table 4-2. Kinase free energy perturbation calculation starting structures.

Simulation Set	**Starting Structure**	**Preparation Notes**
pCDK2/Cyclin ATP•2Mg	Transition state PDB:3QHR	Rename ADP to ATP, make MGF_3^- the γ-phosphate. Did not restrain γ-phosphate in initial preparation to "pull" it back into the ATP conformation. Removed substrate peptide for final-run calculations (some preliminary calculations included the substrate).
pCDK2/Cyclin ATP•1Mg	Transition state PDB:3QHR	Use pCDK2/Cyclin/ADP•2Mg solvated model (not equilibrated), replaced MgI with water.
Src ATP•2Mg	PDB:3DQW	Mutate I338 back to T338 (structure is T338I mutant). Optimize h-bond, Gln, His conformations with reduce. Model ATP•2Mg from pCDK2/Cyclin ATP•2Mg conformation. Added distance restraints on F278 and L407 to close the Gly-loop to similar conformation as pCDK2/Cyclin.
Src ATP•1Mg	PDB:3DQW	Use Src ATP•2Mg solvated model pre-equilibration), replaced MgI with water.
pCDK2/Cyclin ADP•1Mg	$pCDK2^{E51Q}$/Cyclin ADP•1Mg	Used the mutant structure because this represents the best 1Mg structure I've solved – all others likely have some MgI density, just weak.
pCDK2/Cyclin Apo	$pCDK2^{E51Q}$/Cyclin ADP•1Mg	Removed ADP•1Mg before structure preparation.
Src ADP•1Mg	PDB:3DQW	Mutate I338 back to T338 (structure is T338I mutant). Optimize h-bond, Gln, His conformations with reduce. Model ADP•1Mg from pCDK2/Cyclin ADP•1Mg conformation.
Src Apo	PDB:3DQW	Mutate I338 back to T338 (structure is T338I mutant). Remove nucleotide. Optimize h-bond, Gln, His conformations with reduce.

The free energy perturbation calculations were performed by alchemically modifying the target glutamate to glutamine. This was achieved by scaling the electrostatic interactions and Van der Waal interactions simultaneously using the BLOCK/PSSP method in CHARMM (Brooks et al., 2009). To convert the Glu to Gln, 23 separate trajectories were calculated using a different lambda value for each trajectory. A lambda value of 0 corresponds to the Gln having full-weight interactions with the rest

of the system, 0.5 where the Gln and Glu have equal interactions with the rest of the system, and 1.0 where only the Glu has interactions with rest of the system. The Gln and Glu atoms can never "see" each other (BLOCK/PSSP interaction=0). 23 windows were sampled for each system with lambda values of 0, 0.01, 0.025, 0.05, 0.075, 0.1, 0.15, 0.2, 0.25, 0.30, 0.40, 0.50, 0.60, 0.7, 0.75, 0.8, 0.85, 0.9, 0.925, 0.95, 0.975, 0.99, and 1.0. A hybrid residue to represent both the Glu and Gln atoms simultaneously within the simulation trajectories was generated using the default Amber parameterization. Distances between the analogous heavy atoms in the Glu and Gln of the back-bone and the side-chain except for OE1, OE2, and NE2, were restrained to 0 A using a 5 kcal/mol force constant to allow more efficient sampling and to decrease the likelihood of non-physical interactions between the hybrid residue and the surrounding environment. To start each window, the system was minimized for 100 SD steps, heated to 303 K over 500 steps, and then equilibrated for 30 ps (15000 steps). Dynamics were collected at constant temperature and volume for 500 ps using SHAKE, timestep=2 fs, and a Langevin thermostat maintaining 303 K. Each set of simulations were repeated three times.

Analysis of the trajectories and determination of the relative free energy estimate was calculated using the Multistate Bennett Acceptance Ratio (MBAR) approach, using the pymbar software package (Shirts and Chodera, 2008). Briefly, the total potential energy of each trajectory frame (collected every 0.05 ps) was assessed at its original lambda value, and then again at each of the neighboring lambda values. For example, a trajectory calculated with lambda=0.5 would be analyzed with lambda=0.5, lambda=0.4, and lambda=0.6. Next partial potential energy differences are calculated as $U_{ij} = U_{i,i} - U_{i,j}$ and $U_{ji} = U_{j,j} - U_{j,i}$ where i is the reference window, and j is the next greater

numbered window (e.g. i=0.0, j=0.01). $U_{i,i}$ is the potential energy of trajectory i evaluated at lambda=i, $U_{i,j}$ is the potential energy of trajectory i evaluated at lambda=j. Finally, MBAR analysis samples the U_{ij} and U_{ji} distributions and evaluates the free energy difference ΔF_{ij} contribution of the i,j window pair. The total ΔF is equal to the sum of all ΔF_{ij}. The reported ΔF is estimated by calculating the sum of the mean ΔF_{ij} generated from all three sets of trajectories, and the reported error is the standard deviation of the ΔF distribution. The $\Delta\Delta F$ is calculated according to the appropriate thermodynamic cycle shown in Figure 4-13. The results of the individual calculations are shown in chapter 4 appendix, Figure 4-21 to Figure 4-31.

Results

Crystal structures of $pCDK2^{WT}$/Cyclin and $pCDK2^{E51Q}$/Cyclin

In our earlier work we characterized the structure and dynamics of CDK2 in a variety of substrate- and product-bound states. Additionally, we have also characterized the enzyme kinetics of pCDK2/Cyclin with respect to its relationship with Magnesium in great detail. We will therefore compare $pCDK2^{WT}$/Cyclin to the $pCDK2^{E51Q}$/Cyclin mutant as the focus of this study, and then use Src^{WT} and Src^{E310Q} as a point of comparison.

If the E51Q mutation is to serve as a limited model of kinase inactivation, it is critical that only the electrostatics of the active site are altered, and not the conformation of the protein, or ideally even the thermodynamic stability of the active conformation of the kinase. To this end, use of CDK2 as a model is advantageous, because the Cyclin binding partner is known to stabilize the active conformation of the kinase with high

affinity (Jeffrey et al., 1995; Morris et al., 2002). Furthermore, because the site of mutation does not participate in the CDK2/Cyclin interface it is unlikely that introducing this mutation will alter the relative stability of the CDK2/Cyclin complex to a large degree. We determined that the degree of structural modification to the $CDK2^{E51Q}$/Cyclin complex relative to wild type is minimal by obtaining and solving the crystal structures of the near-TS-mimic, and ADP-bound $pCDK2^{E51Q}$/Cyclin complexes.

$pCDK2^{E51Q}$/Cyclin crystals formed in the same conditions as $pCDK2^{WT}$/Cyclin, and had approximately the same unit cell dimensions and space group (Bao et al., 2011). As a general trend we obtained more high quality crystals with the mutant protein than we did with any of the various $pCDK2^{WT}$/Cyclin protein preparations. Furthermore, the diffraction of the mutant crystals tended to extend to higher resolution ranges than wild-type crystals. As will be seen, the Gly-loop is fully resolved in all of the E51Q structures, whereas Gly-loop electron density was significantly less well resolved in WT crystal structures. One possible interpretation of this is that there is less dynamic motion of the mutant kinase domain relative to wild type, since protein motion decreases the resolution limit of a protein crystal. See Table 4-3 for the E51Q mutant structure statistics.

Table 4-3. X-Ray crystallography statistics.

	pCDK2^{E51Q}:TS Mimic	pCDK2^{E51Q}:ADP•Mg
Data Collection		
Space Group	P 1 2_1 1	P 1 2_1 1
Cell dimensions		
a, b, c (Å)	a=71.00, b=162.84, c=73.38	a=70.83, b=164.46, c=73.39
α, β, γ (°)	α=90.0, β=107.04, γ=90.0	α=90.0, β=107.18, γ=90.0
Resolution (Å)	2.13 (2.25 – 2.13)	1.88 (1.98 – 1.88)
R_{sym}	0.151 (0.956)	0.138 (1.264)
I/σ(I)	6.5 (1.5)	6.5 (1.5)
Completeness (%)	100% (100%)	99.93% (100%)
Redundancy	3.7 (3.7)	3.8 (3.8)
Refinement		
Resolution (Å)	37.96 – 2.13 Å	39.84– 1.88 Å
Number of reflections	88731	129,679
R_{work}/R_{free}	18.54 / 23.20	17.97 / 20.97
Number of atoms	9858	9822
Protein	9188	8933
Ligand/ion	84	74
Water	594	815
B factors		
Protein	36.6	37.0
Ligand/ion	34.2	31.6
Water	44.1	44.6
RMSD from ideal		
Bond lengths (Å)	0.0128	0.0115
Bond angles (°)	1.3705	1.2813

The structural similarity of all the pCDK2^{E51Q}/Cyclin crystals to active pCDK2^{WT}/Cyclin is very strong, as shown in Figure 4-3. The collected datasets included two dimers of pCDK2/Cyclin in the asymmetric unit in similar arrangement and conformation as the wild type crystals. The protein backbone atom position RMSD between mutant and WT crystals are shown in Table 4-4. In each of the mutant crystal structures, the electron density of Q51 is clearly visible, as in Figure 4-3B, with one of

the heavy atoms forming a salt-bridge with K33 in a similar conformation as the WT E51:K33 salt bridge. Because of this salt bridge, we were able to discriminate between the $O^{-\delta}$ and $NH_2^{+\delta}$ partially charged groups on the Q51 side chain.

Table 4-4. Structural comparison of pCDK2^{WT}/Cyclin and pCDK2^{E51Q}/Cyclin crystal structures.

Protein Backbone RMSD	pCDK2^{WT}/Cyclin TS-mimic	pCDK2^{WT}/Cyclin ADP•2Mg
pCDK2^{E51Q}/Cyclin TS-mimic	0.54 Å	0.25 Å
pCDK2^{E51Q}/Cyclin ADP•1Mg	0.50 Å	0.38 Å

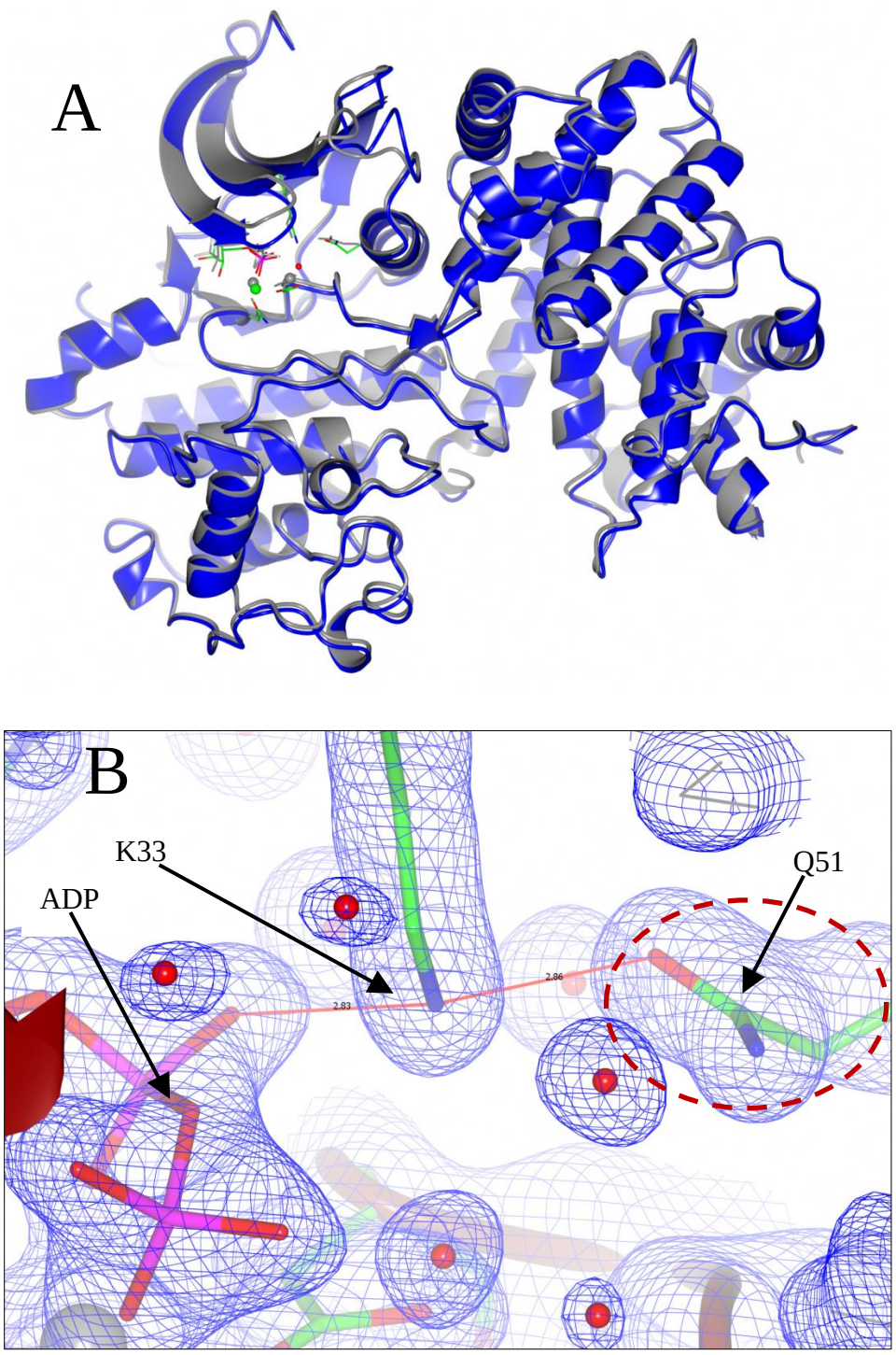

Figure 4-3 Overview of pCDK2^{E51Q}/Cyclin structures

A) Alignment of WT (Gray) and E51Q (Blue) structures bound to ADP. B) 2Fo-Fc Electron density of Q51/K33 interaction in the pCDK2^{E51Q}/Cyclin ADP•Mg structure contoured to 1.5 sigma. Site of E51Q mutation highlighted with red dashed ellipse.

Transition State Mimic

We obtained crystals soaked with similar conditions and substrate concentrations as the WT TS mimic, and again with much higher $MgCl_2$ (40 mM). As shown in Figure 4-4, the active site conformation of the mutant has some similarities to the WT TS-mimic. There is strong electron density for the substrate peptide, the ADP•Mg product, and MgF_3^- dissociated γ-phosphate mimic. There are, however, two major deviations from the WT TS-mimic: 1) the Gly-loop is in the "up" position, and 2) there is very little electron density for an Mg^{2+} ion in the MgI site. There is a small "blip" of electron density in the Fo-Fc map at the MgI site, however, attempts to build Mg^{2+}, even at reduced occupancy, into the MgI site have failed. Furthermore, there isn't sufficient evidence for octahedral coordinating groups (such as the two MgI-coordinating waters observed in the WT TS) to confidently position an Mg^{2+} ion in the MgI site.

Subsequently, we also attempted to include much higher [$MgCl_2$] (40 mM vs. 10 mM) in the TS-mimic soaking conditions, but the resulting structures were not significantly different from those presented here, and thus did not exhibit significant occupancy of the MgI site.

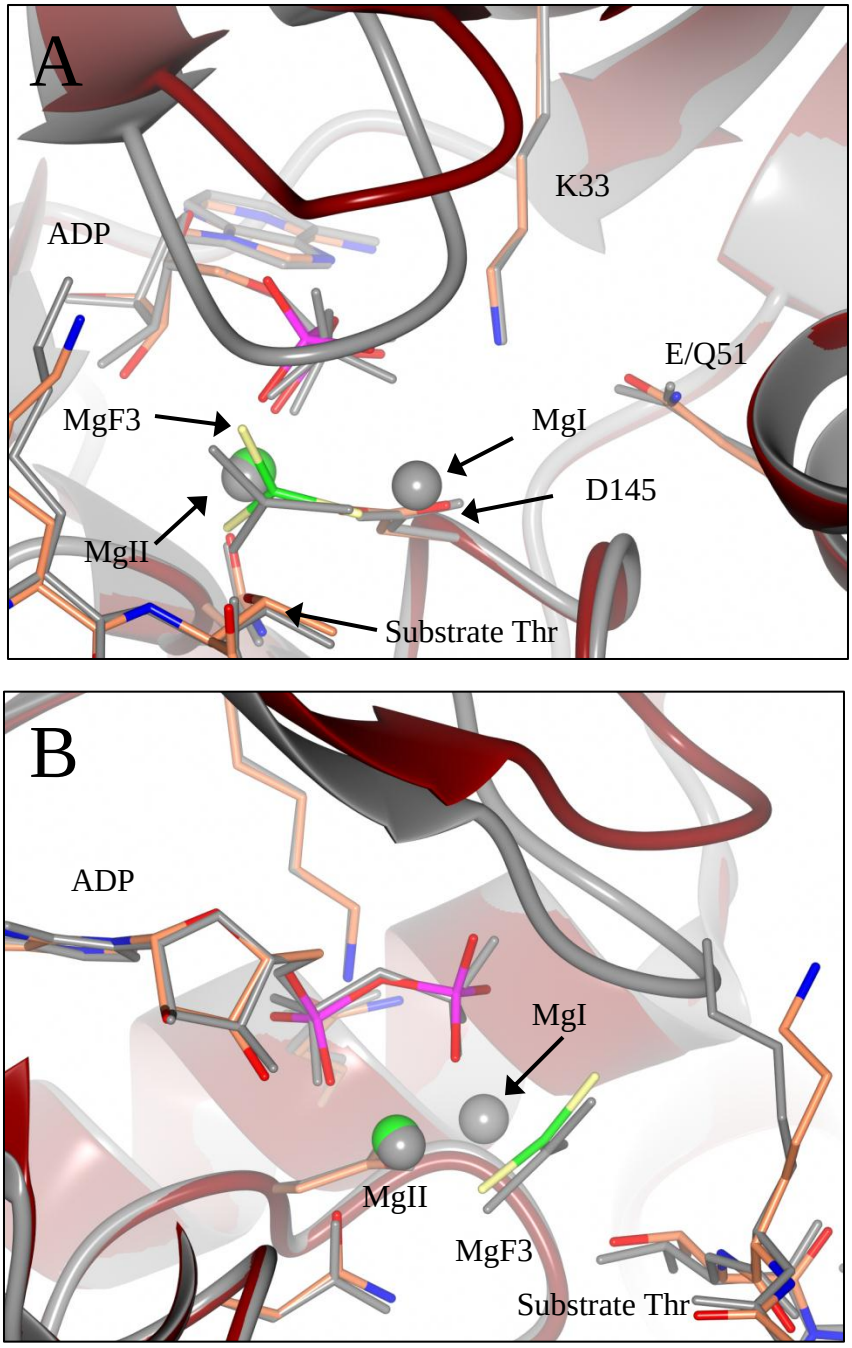

Figure 4-4. Comparison of TS-mimic pCDK2^{E51Q}/Cyclin and pCDK2^{WT}/Cyclin structures

Color structure is pCDK2^{E51Q}/Cyclin/ADP•Mg/MgF_3^-/Peptide, Gray structure is pCDK2^{WT}/Cyclin/ADP•2Mg/MgF_3^-/Peptide. Panel B rotated ~90 degrees relative to panel A to show side view. Little/No electron density was observed for MgI site in the E51Q structure.

ADP-bound

Figure 4-5 shows how the coordination of ADP•Mg differs between pCDK2^{E51Q}/Cyclin and pCDK2^{WT}/Cyclin. As discussed in Chapter 3, pCDK2^{WT}/Cyclin can coordinate ADP with either one or two Mg^{2+} ions, and we have solved crystal structures in each coordination state. Mutant pCDK2^{E51Q}/Cyclin, on the other hand, seems to only coordinate ADP with a single Mg^{2+} ion. In fact, the soaking conditions of the mutant crystals had additional [$MgCl_2$] (15 mM > 10 mM) relative to the soaking conditions of the WT crystal structures from chapter 3. As can be seen in Figure 4-5B and Figure 4-5C, the electron density for the ADP and single Mg^{2+} is unambiguous and the clarity allows precise positioning of each phosphate oxygen. The structure of the ordered water molecules in the active site has been somewhat altered by introducing the E51Q mutation into the structure. Comparing E51Q:ADP•Mg to the WT:ADP•2Mg structures reveals that the β-phosphate has a somewhat different rotation in each structure, such that a phosphate oxygen is closer to the MgI site in WT:ADP•Mg structures than in the E51Q:ADP•1Mg structure. It is reasonable to surmise that the WT:ADP•1Mg structure thus has some small population with the MgI site occupied, but not highly enough to allow modeling into the structure. In that case, the E51Q:ADP•1Mg structure may represent the limiting case where the MgI site is entirely unoccupied.

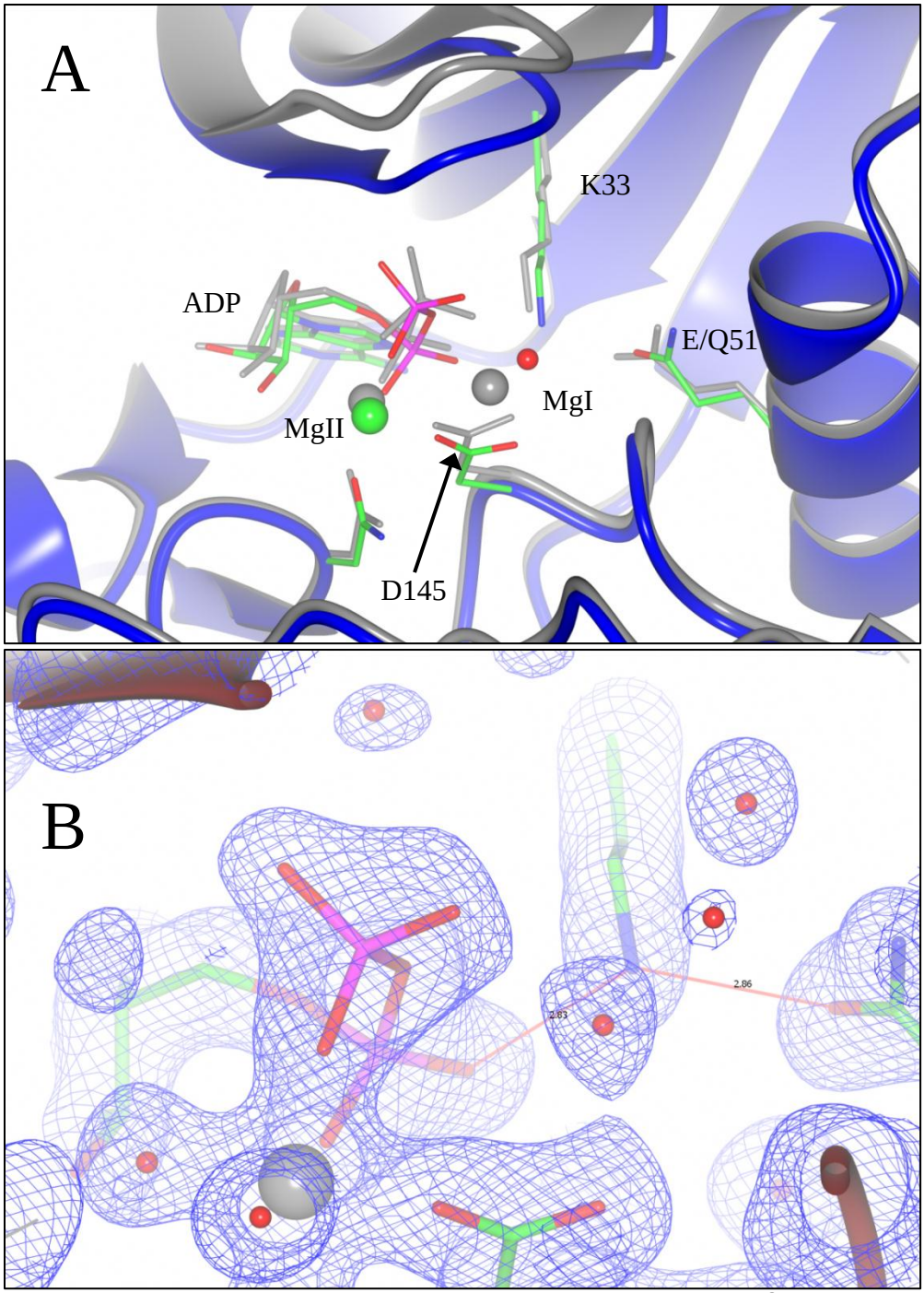

Figure 4-5. Comparison of ADP•Mg coordination by pCDK2^{E51Q}/Cyclin and pCDK2^{WT}/Cyclin

Panel A) Blue/color structure is pCDK2^{E51Q}/Cyclin/ADP•Mg, gray is pCDK2^{WT}/Cyclin/ADP•2Mg; MgI site unoccupied in mutant, water in alternate position. Panel B) 2Fo-Fc density around phosphate/Mg binding sites of pCDK2E51Q/Cyclin/ADP•Mg structure. Contoured to 1.5 sigma.

Summary of pCDK2^{E51Q}/Cyclin Structures

The structures of pCDK2^{E51Q}/Cyclin reveal several significant insights into the electrostatic role of E51 insertion by c-α-helix rotation. First, all of the structures are in the active conformation and still maintain the salt bridge between Q51 and K33 in a very similar conformation as is observed between E51 and K33 in the active site of pCDK2^{WT}/Cyclin. Second, the structures show that the mutant kinase is competent to bind nucleotides. Third, the occupancy of the mutant MgI site is sharply diminished in the mutant TS-mimic and ADP structures, relative to the pCDK2^{WT}/Cyclin structures. And finally, the Gly-loop position is not observed to close in any of the structures, and in fact, the clarity of the electron density and relatively lower B-factors of the Gly-loop suggest that there is considerably less variation in the position of the Gly-loop in the pCDK2^{E51Q}/Cyclin structures than wild type.

Isothermal Titration Calorimetry of pCDK2^{E51Q}/Cyclin binding ADP

In Figure 4-6, the dissociation constant (Kd) of wild type and mutant pCDK2/Cyclin is shown. As discussed in chapter 3, the binding affinity of pCDK^{WT}/Cyclin to ADP•Mg is dependent on the occupancy of the MgI site, and thus tighter binding of ADP•Mg is achieved at higher [Mg^{2+}]. The binding affinity of ADP•Mg to the E51Q mutant does not appear to to [Mg^{2+}] sensitive – meaning that it is likely that the second Mg does not contribute much to the stability of ADP•Mg binding to the mutant active site. This is consistent with the results from the crystal structures where there was little evidence of any Mg^{2+} binding to the MgI site. The structural and thermodynamic data of nucleotide binding suggest that nucleotide binding is no longer

stabilized by the second Mg^{2+} ion. In chapters 2 and 3, the essentiality of the second Mg^{2+} ion in catalyzing the phosphoryl transfer reaction was established. Thus, this leads to the question; does the E51Q reaction similarly require the second Mg^{2+}? Or is the role of Mg in the MgI site limited to stabilizing the nucleotide in the WT enzyme? If the latter is the case, it should be possible for the E51Q reaction to occur with no occupancy of the MgI site.

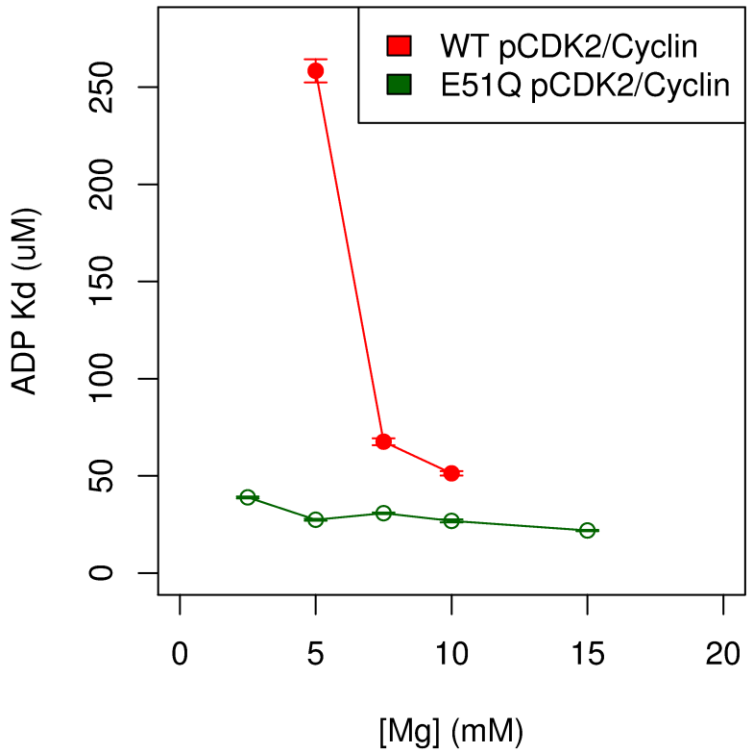

Figure 4-6. Binding affinity of pCDK2E51Q/Cyclin and pCDK2WT/Cyclin for ADP vs. $[Mg^{2+}]_{total}$.

Error bars represent estimated standard error from fitting of ITC data.

The ADP-binding data do support the hypothesis that the mutant kinase can bind di-phosphates more stably than WT. Unfortunately the ITC binding data cannot directly

determine if this increased binding specifically alters the rate of ADP release because the thermodynamics of ligand binding are described by the equation:

$$K_D = \frac{k_{off}}{k_{on}}, \quad where \quad ADP + Kinase \underset{k_{off}}{\overset{k_{on}}{\rightleftharpoons}} ADP/Kinase$$

An attractive corollary to the hypothesis is that Glu51 insertion increases the rate of ADP in the absence of MgI. Thus we would predict that ADP k_{off} for the mutant would be slower than k_{off} for wild type kinase under similar conditions. Since it is possible that both k_{on} and k_{off} for ADP•Mg are impacted by the mutation, it may be difficult to directly compare the dissociation constants of ADP for mutant and WT kinases, and thus inactive and active conformation kinases, without more information about the rates of nucleotide association/dissociation. A direct test would be to measure the rate of ADP release (or an ADP analogue, such as mant-ADP) using a fluorescence stop-flow. Our collaborator, Manju Hingorani, has attempted this experiment in a way similar to the methods described in (Brown et al., 1999b), and detected no usable signal using either mant-ADP or intrinsic (Trp) fluorescence.

Enzyme Kinetics of pCDK2^{E51Q}/Cyclin

ATP Titration

pCDK2^{WT}/Cyclin exhibits a strong dependence on MgI site occupancy to stabilize nucleotide binding to the active site. However, the structures and ITC results for pCDK2^{E51Q}/Cyclin suggest that the MgI site is not occupied under any of the tested conditions (up to ~38 mM $[Mg^{2+}]_{free}$ in the TS-mimic crystal soaks). If the role of occupancy of the MgI site in the wild type enzyme is limited to phosphate stabilization

then, there is a possibility that the mutant can catalyze the phosphoryl transfer reaction in the absence of MgI. To determine how many if a second Mg^{2+} ion was required for the mutant reaction, we used a similar approach as in chapter 3 to establish the essentiality of two divalents to the WT reaction.

Figure 4-7 shows an ATP titration at two different constant $[Mg^{2+}]_{total}$ concentrations. Briefly, because of the low micromolar range dissociation constant for the ATP•Mg complex ($ATP^{4-} + Mg^{2+} <-> ATPMg^{2-}$, $K_d \sim 28\ \mu M$), titrating ATP^{4-} into the reaction will progressively chelate free Mg^{2+}, so that at very high [ATP], $[Mg^{2+}]_{free}$ will be very low. For example, we predict that at the 10 mM [ATP] data point with 5 mM $[Mg^{2+}]_{total}$, that the effective $[Mg^{2+}]_{free}$ would be about 28 μM. Since the reaction is inhibited as $[Mg^{2+}]_{free}$ is constricted, this implies that a second Mg^{2+} ion is required for the reaction. Furthermore, the 8 mM $[Mg^{2+}]_{total}$ curve is shifted upward relative to the 5 mM $[Mg^{2+}]_{total}$, consistent with the additional $[Mg^{2+}]_{free}$ increasing that rate of the reaction.

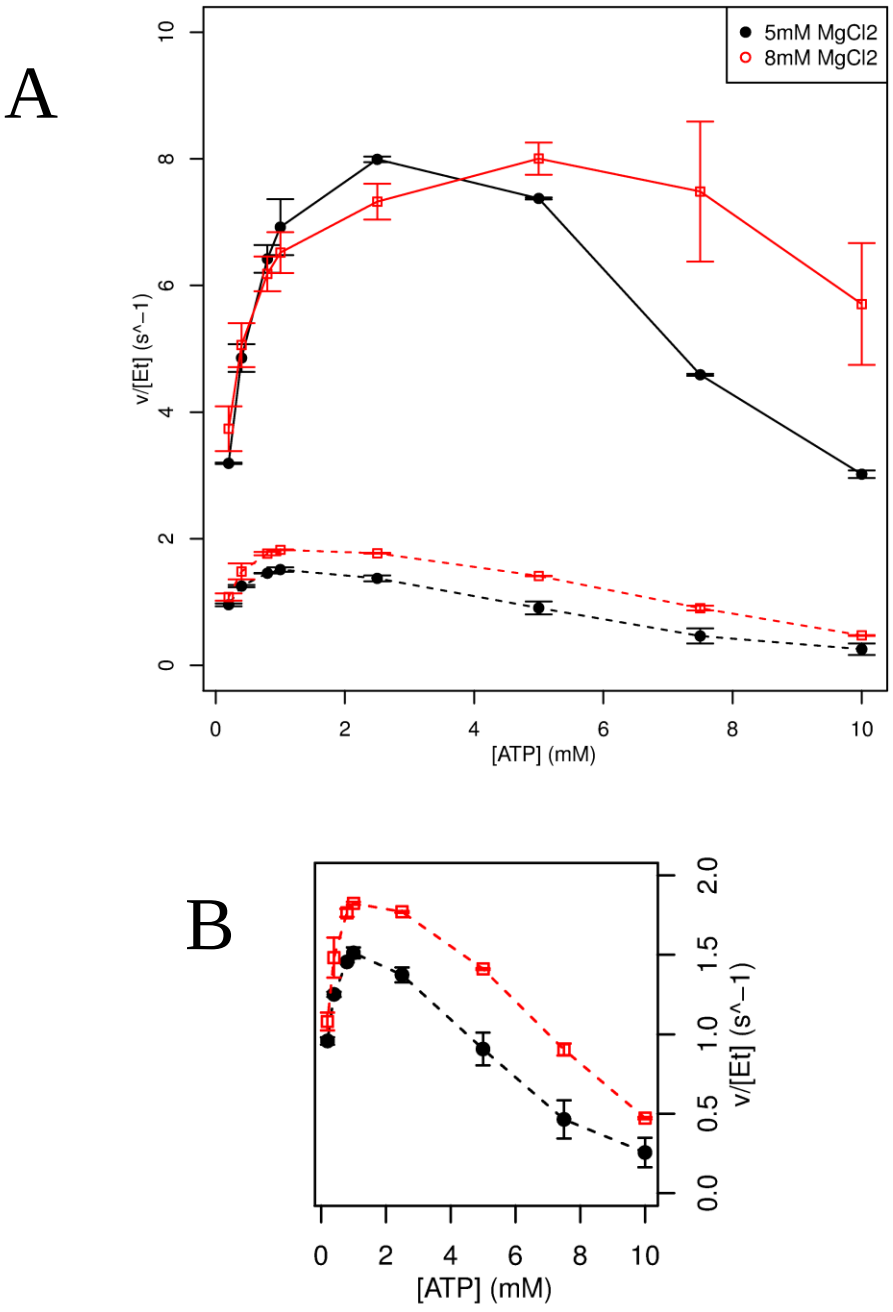

Figure 4-7. Enzyme kinetics: pCDK2WT/Cyclin and pCDK2^{E51Q}/Cyclin ATP Titration at constant $[Mg^{2+}]_{total}$

Constant 5 mM (black) or 8 mM (red) $[Mg^{2+}]_{total}$ is maintained in all experimental conditions while $[ATP^{4-}]$ is varied between 200 μM and 10 mM. Points plotted at mean position, error bars represent standard error. Panel A) pCDK2^{WT}/Cyclin (solid lines), pCDK2^{E51Q}/Cyclin (dashed lines), and Panel B) Just pCDK2^{E51Q}/Cyclin zoomed in to see the shape of the curve

Mg^{2+}_{free} Titration

Titrating free Mg^{2+} ions into the reaction should isolate the effects of stabilizing this catalytically essential Mg^{2+} ion in the active site – presumably in the MgI site based on our prior knowledge of pCDK2^{WT}/Cyclin structures and reaction cycle. Figure 4-8 shows how increasing concentrations of $[Mg^{2+}]_{free}$ activate the reaction. Unlike the pCDK2^{WT}/Cyclin Mg^{2+}_{Free} titration experiments, there is no apparent inhibition at high $[Mg^{2+}]_{free}$. In this case each [ATP] concentration curve resembles a single-site binding hyperbola, suggesting that the second Mg^{2+} ion is behaving like a normal activator of the reaction, rather than the more complex relationship the second Mg^{2+} played in the wild type reaction.

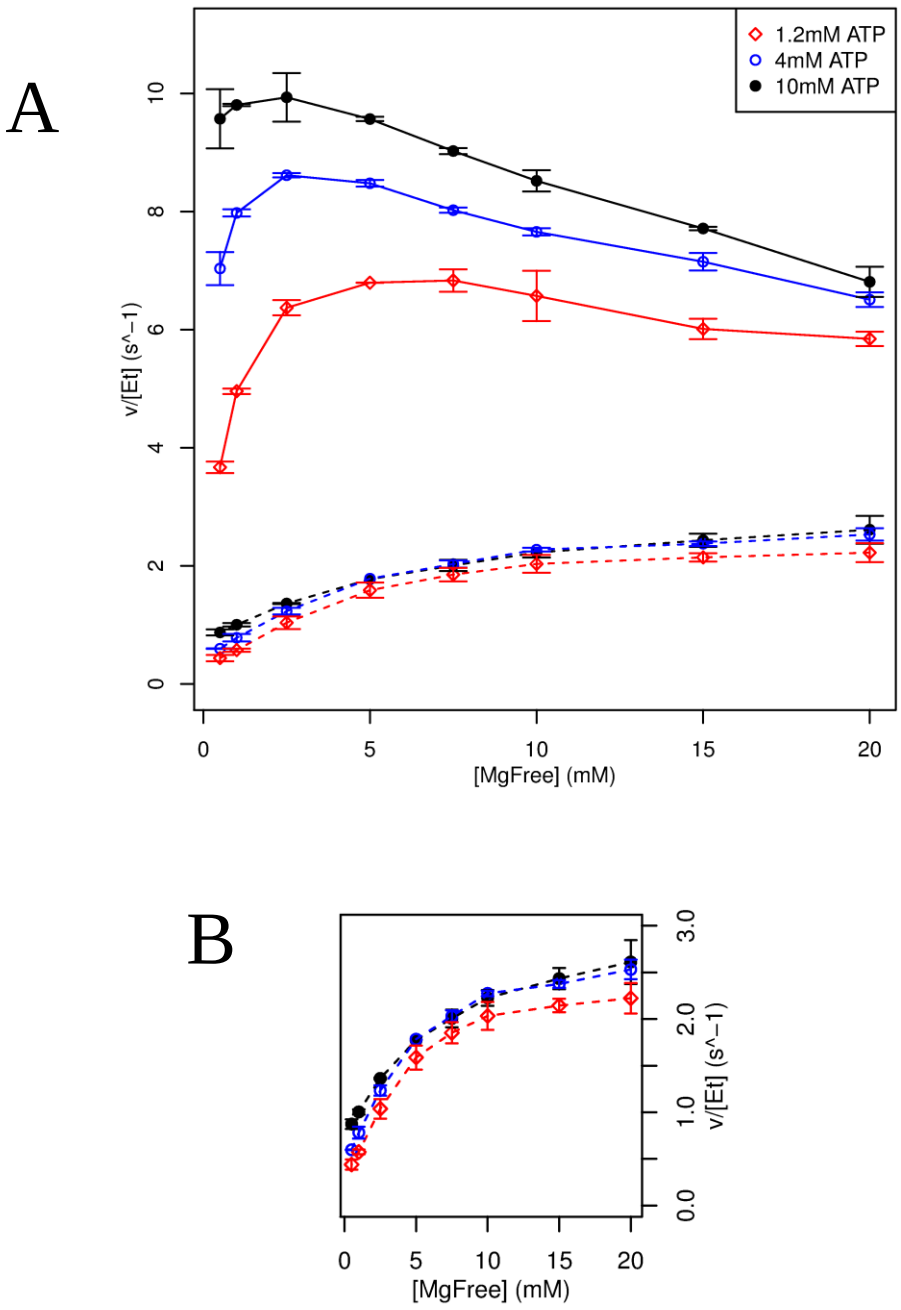

Figure 4-8. Enzyme kinetics: pCDK2^{WT}/Cyclin vs pCDK2^{E51Q}/Cyclin Mg^{2+}_{free} Titration at constant [ATP]

Constant 1.2 mM (black), 4 mM (blue), and 10 mM (red) ATP as $[Mg^{2+}]_{free}$ is titrated from 500 µM to 20 mM. Total $MgCl_2$ varied from 1.6 mM to 30 mM. Points plotted at mean velocity, error bars represent standard error. Panel A) WT in solid lines, E51Q in dashed lines. Panel B) pCDK2^{E51Q}/Cyclin activity zoomed in

$K_{M(ATP•Mg)}$ vs. $[Mg^{2+}]_{free}$

As discussed in chapter 3, pCDK2^{WT}/Cyclin exhibited a strong $[Mg^{2+}]_{free}$ effect on $K_{M(ATP•Mg)}$, which we interpreted as the increased occupancy of the second Mg^{2+} (to the MgI site) hyperbolically decreasing $K_{M(ATP•Mg)}$. In chapter 3, we concluded that the second Mg^{2+} had a strong stabilizing effect on the ATP phosphates as well as the ADP phosphates.

Figure 4-9 shows $K_{M(ATP•Mg)}$ for pCDK2^{E51Q}/Cyclin at 1 mM, 5 mM and 20 mM $[Mg^{2+}]_{free}$. The relationship between $K_{M(ATP•Mg}$) and $[Mg^{2+}]_{free}$ is less clear for the mutant. First, the mutant's $K_{M(ATP•Mg)}$ is lower at 1 mM and 5 mM $[Mg^{2+}]_{free}$ than it the WT $K_{M(ATP•Mg)}$, (E51Q: 313.86 μM and 89.16 μM vs WT: 787.45 μM and 341.93 μM respectively), which is consistent with ATP•Mg binding more stably to the E51Q active site than the WT active site. The increase in $K_{M(ATP•Mg)}$ at 20 mM $[Mg^{2+}]_{free}$ is more difficult to explain, but one possibility is that at such high $[Mg^{2+}]_{free}$, the ATP•2Mg species will begin to build up in solution (KD for ATP•1Mg binding a 2nd Mg is about 25 mM $[Mg^{2+}]_{free}$, (Storer and Cornish-Bowden, 1976)), and it is possible that the ATP•2Mg is an excellent substrate for pCDK2^{WT}/Cyclin, but a poor substrate for pCDK2^{E51Q}/Cyclin. This is borne out by the decrease in k_{cat}/K_M(ATP•Mg), or catalytic efficiency of ATP, at 20 mM $[Mg^{2+}]_{free}$ in Figure 4-9F, and is consistent with the relatively reduced binding affinity that pCDK2^{E51Q}/Cyclin has for the 2nd Mg^{2+} ion.

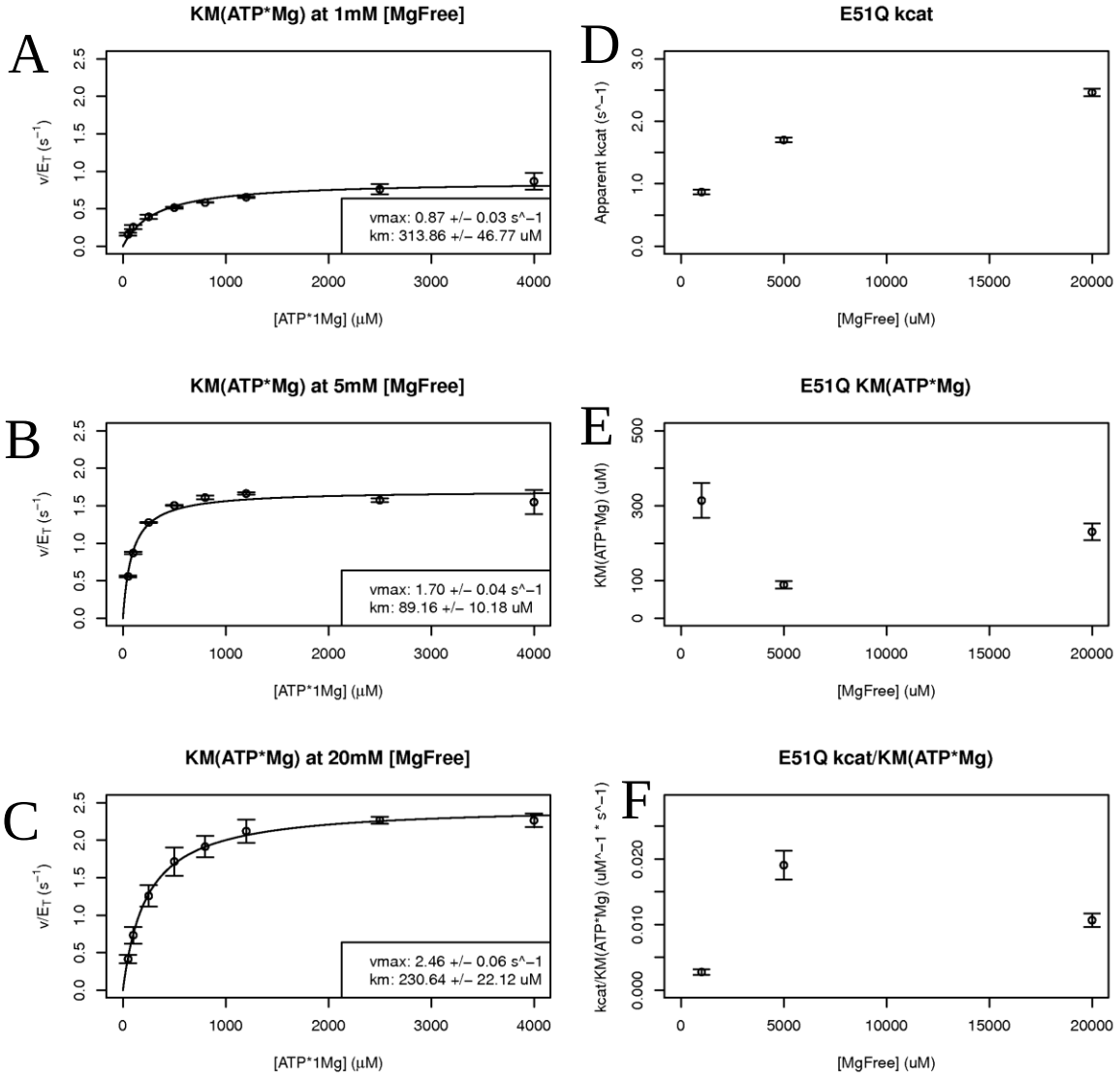

Figure 4-9. Enzyme kinetics: pCDK2^{E51Q}/Cyclin $K_{M(ATP•Mg)}$ vs $[Mg^{2+}]_{free}$ **(A-C)** $K_{M(ATP•Mg)}$ measured at 1 mM, 5 mM, and 20 mM $[Mg^{2+}]_{free}$. Kinetic data fit to model v=(vmax*[ATP•Mg])/(K_M + [ATP•Mg]) **D)** Computed k_{cat} (v/[E_T] at infinite ATP•Mg) vs $[Mg^{2+}]_{free}$, **E)** Computed $K_{M(ATP•Mg)}$ vs $[Mg^{2+}]_{free}$, **F)** $k_{cat}/K_{M(ATP•Mg)}$ – catalytic efficiency of ATP•Mg vs $[Mg^{2+}]_{free}$.

Solvent viscosity effect at saturating [ATP•Mg] and [H1] vs. $[Mg^{2+}]_{free}$ for pCDK2^{E51Q}/Cyclin

There appear to be two major effects of neutralizing the net charge on E51 (making the E51Q mutation): 1) nucleotide phosphates bind to the active site with higher affinity, and do not require MgI to provide stabilization, and 2) the apparent binding affinity of Mg^{2+} to the MgI site is diminished. Thus the reduced reaction rate of the mutant could have two explanations. One possibility is that the increased binding affinity of phosphates to the active site could slow ADP release, which is limiting the overall rate of the reaction. A second possibility is that the decreased Mg binding affinity for Mg^{2+} to the MgI site is dramatically decreasing the efficiency of the reaction. These explanations are not mutually exclusive, and the true explanation for the diminished reaction velocity may exist between these two limiting scenarios.

To determine which is the dominant effect – either on chemistry (MgI binding) or product release (phosphate affinity), we varied the solvent viscosity to determine the proportional dependence of the reaction rate on product release. See the Chapter 3 Appendix for the detailed justification for this. The higher the measured viscosity effect on k_{cat}^{App}, the more the rate of the reaction is dominated by product release. Figure 4-10 shows that the viscosity effect on k_{cat} is highest at 20 mM $[Mg^{2+}]_{free}$, and diminishes at lower $[Mg^{2+}]_{free}$. However, the highest observed viscosity effect of ~0.3 on k_{cat} for the mutant is significantly lower than the viscosity effect on k_{cat} of the pCDK2^{WT}/Cyclin – which is essentially constant and >0.7 at all test $[Mg^{2+}]_{free}$ (Figure 3-9B). Based on the 20 mM $[Mg^{2+}]_{free}$ viscosity effect, the rate of product release for the mutant is 8.06 s^{-1}, which is very similar to the modeled rate of ADP•1Mg release from the WT enzyme

(chapter 3) of 7.56 s^{-1}. The increasing viscosity effect as a function of $[Mg^{2+}]_{free}$ indicates that as the second Mg^{2+} ion is stabilized the rate of product formation increases, but similar to the sub-saturating ATP viscosity effect titrations for the WT (Figure 3-9A), it is likely the increase in the viscosity effect reflects sub-saturation of the MgI site more than a change in the catalytic mechanism. As a side note, this result reinforces the very tight binding affinity $pCDK2^{WT}$/Cyclin at the MgI site when ATP is bound – the viscosity effect vs. $[Mg^{2+}]_{free}$ was unchanging, which is interpretable as that at all conditions tested, all substrates (including MgI) were saturating the reaction. Thus, these data indicate that phosphoryl transfer is the rate limiting step for $pCDK2^{E51Q}$/Cyclin, and this appears to be due to inefficiency in binding Mg^{2+} to the MgI site.

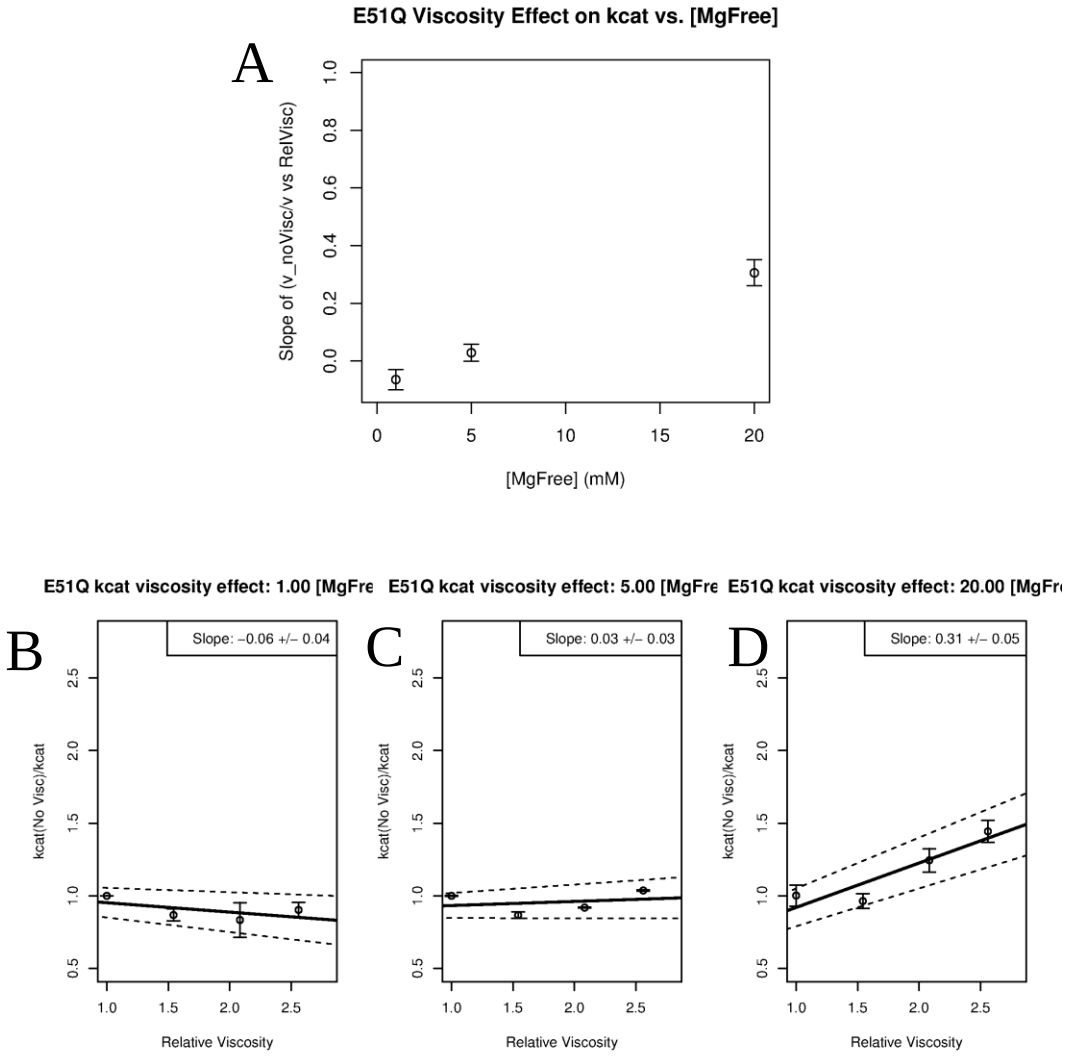

Figure 4-10. Enzyme kinetics: pCDK2^{E51Q}/Cyclin Viscosity effect on k_{cat}^{App}
Panel A) Viscosity effect on kcatApp vs $[Mg^{2+}]_{free}$**, Panels B-D):** Underlying fits for each viscosity effect experiment.

Enzyme Kinetics of Src^{WT} and Src^{E310Q} varying [ATP] and $[Mg^{2+}]_{free}$

To determine if the electrostatic role of the conserved glutamate is conserved in different families of protein kinases, we performed the same mutation at the homologous site (E310) in the catalytic domain of the protein kinase c-Src. Previously published crystal structures of c-Src in both the active and inactive conformations show that Src also rotates its c-α-helix as part of the activation (Xu et al., 1999; Azam et al., 2008).

Therefore, our model of kinase activity would predict that the E310Q mutation in c-Src would have similar effects as the E51Q mutation has in CDK2. Because of the significantly lower yield during protein expression and purification of c-Src^{WT} and c-Src^{E310Q}, we did not have a sufficient amount of protein to attempt crystallography or ITC experimentation. However to verify the number of Mg^{2+} ions for optimal activity and determine if $[Mg^{2+}]_{free}$ activates the reaction in both the c-Src^{WT} and c-Src^{E310Q} we performed the ATP titration and $Mg^{2+}{}_{Free}$ titration enzyme kinetic experiments.

Figure 4-11 shows ATP titration experiments at constant $MgCl_2$ for c-Src^{WT} and c-Src^{E310Q}. Similar to CDK2, the shape of the curve indicates a requirement for both ATP•Mg and a second Mg^{2+} ion in the active site to catalyze the reaction for both mutant and WT c-Src. This can be seen by the inhibition at high [ATP] where consequently $[Mg^{2+}]_{free}$ is diminished. Figure 4-12 shows the $Mg^{2+}{}_{Free}$ titration experiment showing that for both c-Src^{WT} and c-Src^{E310Q} the reaction is activated by $[Mg^{2+}]_{free}$. The hyperbolic shape of the curve as MgI is titrated into the c-Src^{WT} reaction shows that the second Mg^{2+} functions as a simple Michaelis-Menten style activator. The lack of an inhibition at high $[Mg^{2+}]_{free}$ of the WT curve could be due to 1) a different mode of release of ADP•Mg in Src than CDK2 – e.g. ADP•2Mg releases as efficiently as ADP•1Mg, or MgI re-binding to the ADP•1Mg complex is less favorable, or 2) because these experiments were performed at sub-saturating protein substrate. The use of sub-saturating substrate concentrations could obscure effects of product release in the enzyme kinetics. The nearly linear shape of the MgI activation ($Mg^{2+}{}_{Free}$ titration) of c-SrcE^{310Q} indicates that the $K_{MgActivation}$ of the second Mg^{2+} ion is significantly higher than the tested conditions and cannot be determined with accuracy.

These results suggest that 1) c-Src^{WT} and c-Src^{E310Q} require two Mg^{2+} ions for activity, and 2) that neutralizing the net charge on E310 dramatically alters the binding of the second Mg^{2+} in the active site, similar to pCDK2/Cyclin. One important difference is the magnitude of the change in overall activity. Neutralizing the charge on E51 in pCDK2/Cyclin diminishes its activity by at most 5x, whereas performing the homologous mutation in c-Src results in a 44x reduction of activity. The crystallography of pCDK2/Cyclin demonstrates that cyclin stabilizes the active conformation of pCDK2, whereas the c-Src has no analogous allosteric activator. Thus it is possible that by neutralizing the net charge on E310, a side-effect was a destabilization of the active conformation, which combined with the other effects of the mutation result in a much greater loss of activity in c-Src than in pCDK2/Cyclin.

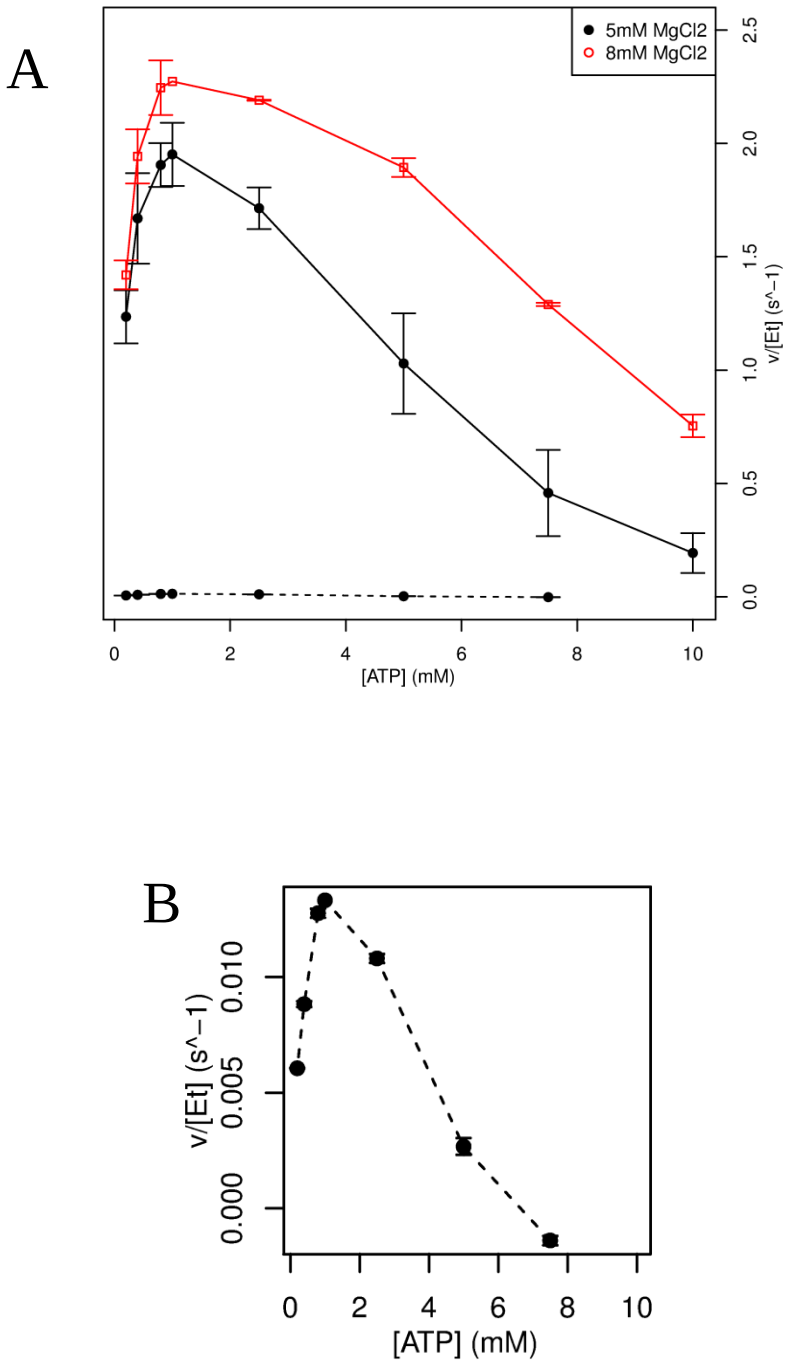

Figure 4-11. Enzyme kinetics: c-Src^{WT} and c-Src^{E310Q} ATP Titration at constant $[Mg^{2+}]_{total}$

Constant 5 mM (black) or 8 mM (red) $[Mg^{2+}]_{total}$ is maintained in all experimental conditions while $[ATP^{4-}]$ is varied between 200 μM and 10 mM. Points plotted at mean position, error bars represent standard error. Panel A) c-Src^{WT} (solid lines), c-Src^{E310Q} (dashed lines), and Panel B) Just c-Src^{E310Q}

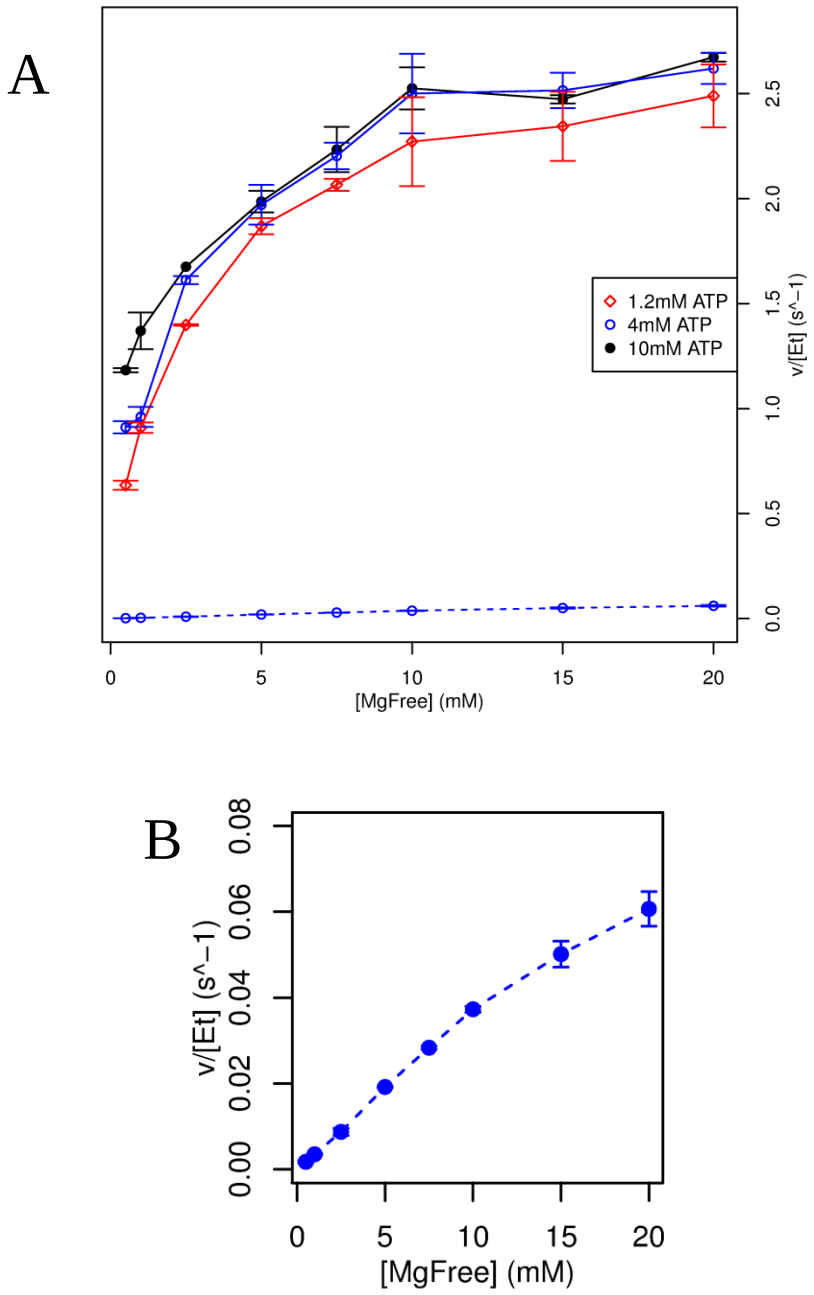

Figure 4-12. Enzyme kinetics: c-Src^{WT} vs c-Src^{E310Q} Mg^{2+}_{free} Titration at constant [ATP] Constant 1.2 mM (black), 4 mM (blue), and 10 mM (red) ATP as $[Mg^{2+}]_{free}$ is titrated from 500 μM to 20 mM. Total $MgCl_2$ varied from 1.6 mM to 30 mM. Points plotted at mean velocity, error bars represent standard error. Panel A) WT in solid lines, E310Q in dashed lines. Panel B) c-SrcE310Q activity

Relative free energy of binding MgI and ADP•Mg

The enzyme kinetics experiments provide excellent evidence that the E51Q mutation and therefore rotation of the c-α-helix specifically alters the observed $[Mg^{2+}]_{free}$ effect and maximal catalytic rate. Based on these experiments and crystal structures we suggest that these effects can be isolated to electrostatic modification of the second Mg^{2+} ion binding at the MgI site and to tighter binding of nucleotide phosphates. The enzyme kinetics experiments cannot specifically report on the MgI site because that experiment reports enzyme activity on a macro-scale, and it is possible that a variety of effects related to the mutation could give rise to the observed behavior. Therefore, we used a Free Energy Perturbation scheme to directly calculate the effects of MgI binding and ADP•1Mg binding between the WT and mutant enzymes, according to the thermodynamic cycles shown in Figure 4-13.

From chapter 3, the upper-bound $K_{MgActivation}$ of MgI to the ATP•Mg bound state of $pCDK2^{WT}$/Cyclin is ~400μM (-4.71 kcal/mol at 303 K), while the $K_{MgActivation}$ of MgI for $pCDK2^{E51Q}$/Cyclin is > 4mM (-3.3 kcal/mol at 303 K). Thus, the expected ΔΔG of binding MgI between the WT and mutant enzymes is -1.39 kcal/mol (mutant is the reference state, negative indicating that MgI binds more tightly to the wild type). The calculated ΔΔF of binding MgI to the ATP•Mg complex for pCDK2/Cyclin is -11.487 kcal/mol, and for c-Src is -5.386 kcal/mol.

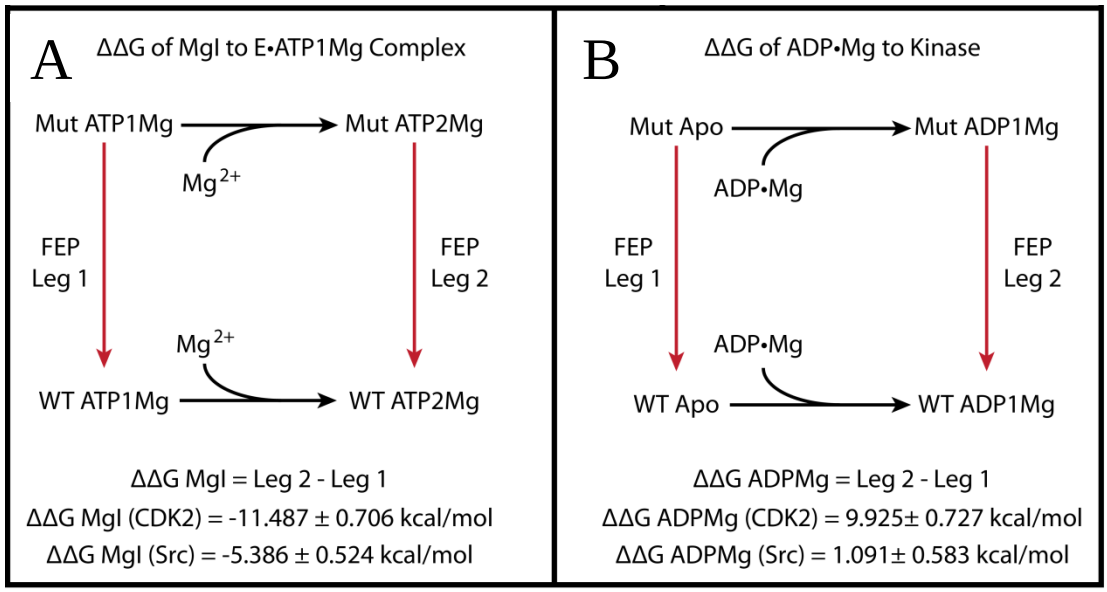

Figure 4-13. Free energy perturbation calculations of relative binding free energies.

Panel A) Relative free energy of binding MgI to the Enzyme•ATP•1Mg complex for pCDK2/Cyclin and c-Src. **Panel B)** Relative free energy of binding ADP•1Mg to apo enzyme for pCDK2/Cyclin and c-Src.

The ITC data for pCDK2/Cyclin suggest that ADP•1Mg binds significantly tighter to the mutant than WT, though we do not have an estimate of the binding affinity of ADP•1Mg to WT, and thus do not have an estimate of the relative change in binding affinity of ADP•1Mg between WT and mutant. Figure 4-13b shows the calculated ΔΔF of binding ADP•1Mg to the apo enzyme for pCDK2/Cyclin is 9.925 kcal/mol, and for c-Src is 1.091 kcal/mol. The underlying components of the ΔΔF for ADP•1Mg binding the apo kinase, shown in Table 4-5, suggest that the reason for the relative stabilization of nucleotide in c-Src differs from pCDK2/Cyclin. For pCDK2/Cyclin, the ΔF of making the mutation when bound to ADP•1Mg substantially favors the mutant, while the ΔF for apo pCDK2/Cyclin is relatively modest. In the case of c-Src, neither ADP•1Mg binding nor the apo state are stabilized in the mutant form, but the extent of apo mutant destabilization is greater than ADP•1Mg mutant destabilization, thus giving a net

stabilizing effect when nucleotide is bound. The underlying cause of this may be that E310 plays a stronger role in stabilizing the active conformation in c-Src than it does in pCDK2/Cyclin. This seems reasonable because c-Src does not have an analog to CDK's Cyclin to stabilize the active conformation, and may need to rely on things like the K495/E310 salt bridge to stabilize the active conformation.

Table 4-5. Q → E Free Energy Differences.

	pCDK2/Cyclin ΔF	**c-Src ΔF**
ATP•**2Mg**	-16.04 ± 0.52 kcal/mol	-7.90 ± 0.38 kcal/mol
ATP•**1Mg**	-4.55 ± 0.48 kcal/mol	-2.52 ± 0.36 kcal/mol
ATP•**1Mg Protonated D145**	-4.24 ± 0.45 kcal/mol	-1.54 ± 0.55 kcal/mol
ATP•**2Mg with Protein Substrate**	-17.79 ± 0.56 kcal/mol	Not determined
ATP•**1Mg with Protein Substrate**	+3.89 ± 0.62 kcal/mol	Not determined
ADP•1Mg	+7.33 ± 0.52 kcal/mol	-3.87 ± 0.47 kcal/mol
Apo	-2.59 ± 0.51 kcal/mol	-4.96 ± 0.34 kcal/mol

Helmholtz free energy difference (ΔF) of making Q → E modification in pCDK2/Cyclin and c-Src in a variety of ligand-bound states. Data from Figure 4-21 to Figure 4-31. Negative values indicate a preference for WT, positive values indicate a preference for mutant. Red lines are the components of ΔΔF of MgI binding, Green lines are the components of ΔΔF of ADP•1Mg binding.

The calculated ΔΔF of MgI binding to the pCDK2/Cyclin/ATP•Mg complex exceeds the experimentally observed -1.39 kcal/mol. The overestimation of the ΔΔF can likely be attributed to 1) limited sampling, especially in the ATP•1Mg state, where a variety of phosphate conformations may be accessible over much longer timescales; additionally protonation/monovalent binding effects were not considered – only the

limiting cases of ATP•1Mg and ATP•2Mg, and 2) the very strong interaction energies with the divalent Mg^{2+} in the non-polarizable Amber force field. To attempt to minimize the artifacts introduced by these effects the trajectories and analysis were performed with 16 Angstrom non-bonded cutoffs (as opposed to the more usual 12A cutoffs). Despite the over-estimation of the value of ΔΔF MgI, the trends in the data are likely to be correct, and agree with the experimental observations, which is 1) that MgI binding is significantly increased by the electronegative charge of the Glutamate (negative ΔΔF values) in both pCDK2/Cyclin and c-Src, and 2) that the ADP phosphates are destabilized in $pCDK2^{WT}$/Cyclin in the absence of MgI (positive ΔΔF values).

Electrostatic stabilization of MgI in the active kinase conformation

Figure 4-14 shows the calculated electrostatic potential of the active site for $pCDK2^{WT}$/Cyclin and $pCDK2^{E51Q}$/Cyclin. The introduction of the charged Glu sidechain in the active site upon kinase activation alters the interactions between the Lys and phosphates and also helps to stabilize the binding of MgI by generating, in combination with the nucleotide phosphates, a strong electrostatic deficit in the active site, which can be neutralized by MgI binding. Figure 4-14 panels B, C, and D show the widespread field effect that the Glutamate has relative to the neutral mutant or inactive conformation has. The -10 k_bT/e cutoff in the change in potential shown by the volumetric representation in the figure includes the MgI site, K33, and the phosphates, as well as other regions of the active site, indicating that the glutamate alters not just these interactions but adjusts the electrostatics of the entire active site to optimize kinetic activity.

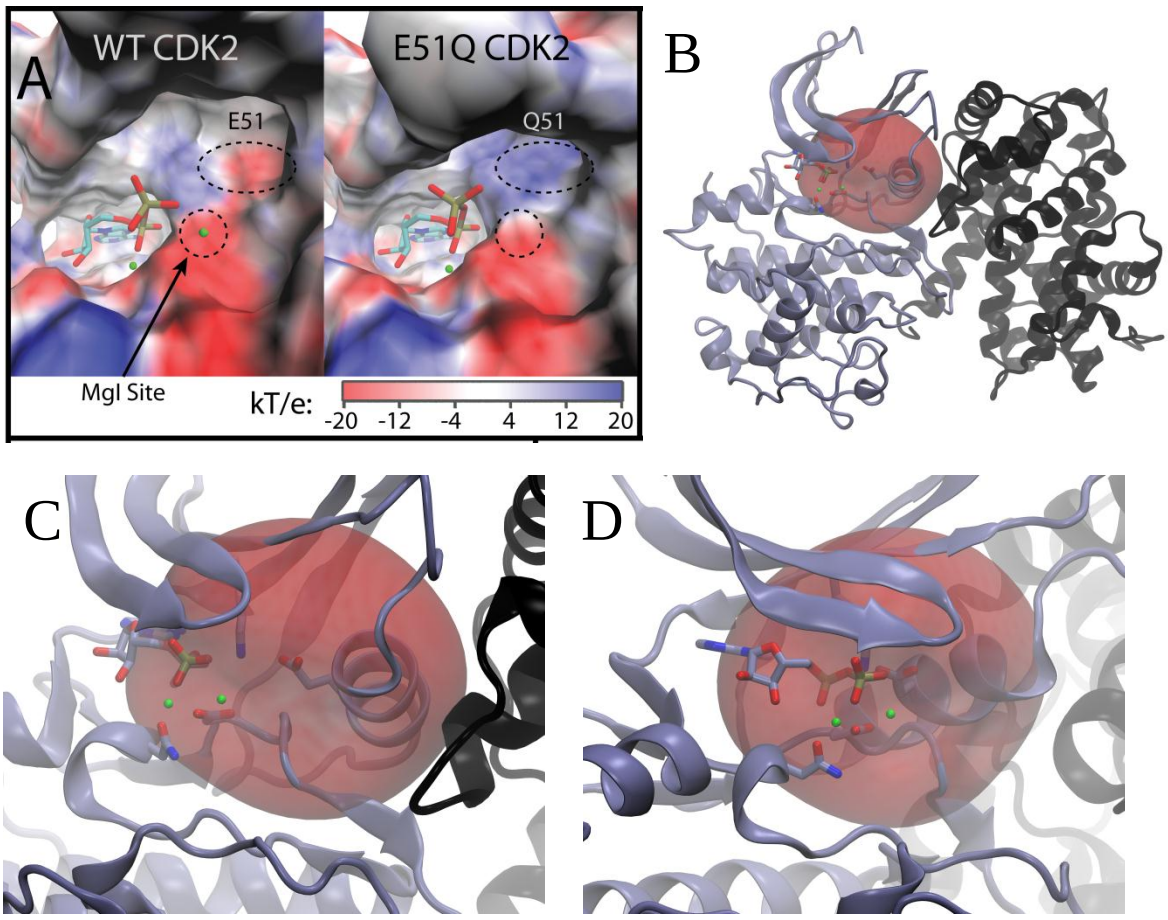

Figure 4-14. Electrostatics of E51Q mutation

Panel A) Solvent accessible surface colored by APBS electrostatic potential computed without ligands at 303 K with 0.15 M ionic strength scaled from -20 to +20 k_bT/e. Shows overall electronegative shift of active site upon Glu insertion. **Panels B, C, D)** Electrostatic potential difference (WT – E51Q), calculated using pCDK2^{E51Q}/Cyclin/ADP•1Mg structure and modified pCDK2$^{E51Q\rightarrow WT}$/Cyclin/ADP•1Mg. Surface potential shows electrostatic field effect where difference <= -10 k_bT/e.

Discussion

The rotation of the c-α-helix is a conserved mechanism of protein kinase regulation, observed by X-ray crystallography for representatives of three evolutionarily divergent families of protein kinases: CDK2, c-Src, and EGFR. The active conformation that is achieved by the kinase following c-α-helix rotation has been described for many different kinases. Though some of the conserved attributes of the active kinase have been determined, the relative contributions to activity are less well understood. For example,

one universally observed theme of protein kinase activation is the construction of the hydrophobic ("R") spine (Kornev et al., 2006). The exact contributions to kinetic activity by the hydrophobic spine are unclear, though it may make indirect contributions to "DFG" motif stabilization in some kinases and possibly have stabilizing effects on the overall protein conformation (Taylor and Kornev, 2011). Another important conserved component of the active protein kinase conformation mechanically dependent on c-α-helix rotation is the insertion of a negatively charged glutamate (CDK2:Glu51) into the active site of the kinase (Radzio-Andzelm et al., 1995). Because this is the only direct modification of the active site upon activation, it is very likely that the effects of the active site glutamate are strongly connected to activation of chemistry.

Structures and simulations of pCDK2^{WT}/Cyclin/ADP•1Mg from chapter 3 led us to describe an "electrostatic deficit" in the CDK2 active site. To stabilize ADP•Mg in the active site in equilibrium MD simulations, we found that some counter charge needed to be introduced into the active site such as second Mg^{2+} ion in the MgI site, protonation of D145 or the ADP β-phosphate, or an explicit Na^{+} ion. These simulations, combined with the pCDK^{WT}/Cyclin K_M(ATP•Mg) and ADP binding affinity experiments demonstrate the electrostatic character of the cooperativity between nucleotide phosphates and the second Mg^{2+}. In the present work we hypothesized that the removal of a negative charge from the active site could similarly stabilize phosphate binding while simultaneously weakening binding of the second Mg^{2+} ion.

Since the negatively charged glutamate (E51) is introduced into the CDK2 active site as an effect of the allosteric regulation by Cyclin, we therefore hypothesize that the glutamate electrostatically destabilizes nucleotide phosphate binding and activates the

kinase by stabilizing the essential second Mg^{2+} ion. Neutralizing the negative charge on E51 by creating the pCDK2^{E51Q}/Cyclin mutant tests this hypothesis by modeling the electrostatic effects of the regulatory removal of Glu charge from the active site while maintaining all other aspects of the active kinase domain. Crystal structures of this mutant demonstrate that it maintains all aspects of the active kinase conformation and is still competent to bind nucleotide in similar conformations as the wild type active conformation.

The TS-mimic and ADP-bound mutant structures show that occupancy of the MgI site is less favorable for pCDK2^{E51Q}/Cyclin than pCDK2^{WT}/Cyclin, since there is very little crystallographic evidence for the presence of a second Mg^{2+} in the mutant active site. Despite this, steady state kinetics of the pCDK2^{E51Q} and c-Src^{E310Q} mutants provide strong evidence that a second Mg^{2+} ion is utilized by the reaction (Figure 4-7 and Figure 4-11), and that the second Mg^{2+} ion is an activator (Figure 4-8 and Figure 4-12). The kinetics only report on the total rate of the reaction at a macro-scale and thus the observed $[Mg^{2+}]_{free}$ effects on the mutant reaction cannot be directly designated as effects owing to occupancy of the MgI site observed for the WT kinase.

The ITC ADP•Mg binding experiments show that $[Mg^{2+}]$ does not have a strong effect on pCDK2^{E51Q}/Cyclin affinity for ADP•Mg (Figure 4-5). pCDK2^{WT}/Cyclin, on the other hand, does demonstrate a strongly cooperative effect of $[Mg^{2+}]$ on affinity for ADP•Mg, which we did attribute to MgI site occupancy in chapter 3. The proximity of the E/Q51 sidechain to the MgI site (5A) combined with the loss of a $[Mg^{2+}]$ effect on $K_{d(ADP•Mg)}$ in the pCDK^{E51Q}/Cyclin mutant reinforces our earlier conclusion that the

cooperative binding of phosphates in the WT enzyme is due to the occupancy of the MgI site.

Two lines of evidence strongly suggest that the observed $[Mg^{2+}]_{free}$ effects in the enzyme kinetics experiments can be attributed to the MgI site in both WT and mutant kinetics experiments. First, the mutant crystal structures show that mutant still binds the MgII site without difficulty, but MgI occupancy is significantly reduced. The ITC experiments combined with the structural information strongly indicate that the site being modified by the mutation is the MgI site. Second, the calculations of both pCDK2/Cyclin and c-Src demonstrate that the binding affinity of MgI is strongly destabilized in the mutant. We therefore conclude that the $[Mg^{2+}]_{free}$ affect observed in the mutant steady-state kinetics can similarly be attributed to occupancy of the MgI site. The activation of mutant kinase kinetics by $[Mg^{2+}]_{free}$ combined with lack of cooperativity of $[Mg^{2+}]_{free}$ on ADP•Mg binding suggests that the mutant/ATP•Mg complex prior to chemistry has higher occupancy of the MgI site than the mutant/ADP•Mg complex following chemistry.

A simple model that can explain these effects is based on the electrostatic-deficit concept, such that MgI binding affinity is proportionally related to the net charge of the active site. Total active site net charges are shown in Table 4-6. The WT kinetics, ITC data and structures from chapter 3 have shown that cooperative binding of free Mg and nucleotide•Mg binding occurs in the ATP•Mg and ADP•Mg bound states. Furthermore ADP•1Mg can be stabilized in the WT active-site when a +1 charge is introduced by protonation or monovalent cation binding (net -1 charge – see chapter 3). We suggest that occupancy of the mutant's MgI site is possible only when ATP•Mg is bound to

completely neutralize the mutant's active site, and that ADP•1Mg is stable in the mutant active-site without MgI occupancy in much the same way that protonation stabilized ADP•1Mg in the WT active-site. While the charge distribution in the active-site is certain to play a role in the thermodynamics of nucleotide and Mg^{2+} binding, it can be seen in Figure 4-14 that the introduction of negative charge at the E51 site has strong and diffuse effects throughout the entire phosphate binding region of the active-site, lending some credibility to the simpler net charge model.

Table 4-6. Net charge on mutant/WT active sites

Activesite Net Charge	WT	E51Q
Apo	-1	0
Kinase/$(ATP•Mg)^{2-}$	-3	-2
Kinase/$(ADP•Mg)^{1-}$	-2	-1

The kinetic model of $pCDK2^{WT}$/Cyclin activity from chapter 3 estimates the $K_{MgActivation}$ of the MgI site at < 400 μM $[Mg^{2+}]_{free}$, whereas mutant $pCDK2^{E51Q}$/Cyclin appears to have a $K_{MgActivation}$ of the MgI site of > 4 mM $[Mg^{2+}]_{free}$ (Figure 4-8). Thus, the ten fold shift in $K_{MgActivation}$ translates to a ΔΔG relative stabilization of MgI of about -1.39 kcal/mol. This change in MgI binding is significant because normal physiological $[Mg^{2+}]_{free}$ is 1 mM (Grubbs, 2002). Thus, when the conserved Glu is inserted into the active-site, $K_{MgActivation}$ for MgI is adjusted such that MgI binding becomes favorable given physiological conditions. The solvent viscosity titration experiments show that the E51Q mutant is not rate-limited by product release, indicating that chemistry is rate limiting because of the inefficiency in binding MgI to the active-site. Therefore, the

much slower rate of pCDK2^{E51Q}/Cyclin mutant catalysis can be readily explained by defective MgI binding.

c-Src activity was particularly sensitive to this mutation (c-Src^{E310Q}), exhibiting a 44-fold reduction in maximal rate, compared to pCDK2/Cyclin's five fold reduction. One important difference between CDK2 and Src is the strong stabilization of the active conformation that Cyclin affords CDK2. The SH2 domain of c-Src binds to the catalytic domain in a similar fashion as Cyclin binds CDK2, but with the opposite effect – the SH2 inactivates c-Src. For this work, the SH2 domain was omitted from the c-Src construct to maximally stabilize the active conformation. Therefore, it is possible that c-α-helix positioning is partially stabilized by the E310/K295 (homologous to CDK2's E51/K33) salt bridge. By making the E310Q mutation, we may have destabilized the active conformation of c-Src resulting in much less activity. That said, the proportion of the c-Src population that was active at any given time during the monitored reaction gave exactly the same shape of the curves as pCDK2^{E51Q}/Cyclin. Therefore, we interpret the c-Src and c-Src^{E310Q} data as being consistent with our model derived from CDK2.

Conclusions

The regulatory interaction of Cyclins with CDKs, the SH2 domain with Src-family kinases, or asymmetric homo-dimerization of receptor tyrosine kinases like EGFR can regulate kinase activity by stabilizing alternative conformations of the c-α-helix. The active conformation of the c-α-helix introduces an electronegative charged glutamate into the active site. In this work we have demonstrated the mechanism of activation for this conserved glutamate is to optimize the electrostatics of the active site, which manipulates

nucleotide and Mg^{2+} co-factor binding propensities. Specifically, the conserved glutamate shifts the binding affinity at the CDK2 MgI site to within reach of physiological concentrations of $[Mg^{2+}]_{free}$ when ATP•Mg is bound. We tested pCDK2/Cyclin and c-Src, and found that the E → Q mutation model for the electrostatically inactivating the kinase had similar effects, suggesting that this mechanism of regulation is conserved. There are a variety of effects of the conformational differences observed between inactive and active kinases, including alteration of k_{cat} and $K_{M(Protein\ Substrate)}$. Thus, kinases are fantastically sensitive to regulatory manipulation because the several of the kinetic properties are altered simultaneously. Regulatory manipulation of Mg^{2+} is important because the occupancy of the MgI site is essential to catalytic progression, and under physiological conditions it is the last and potentially weakest binding substrate.

Appendix

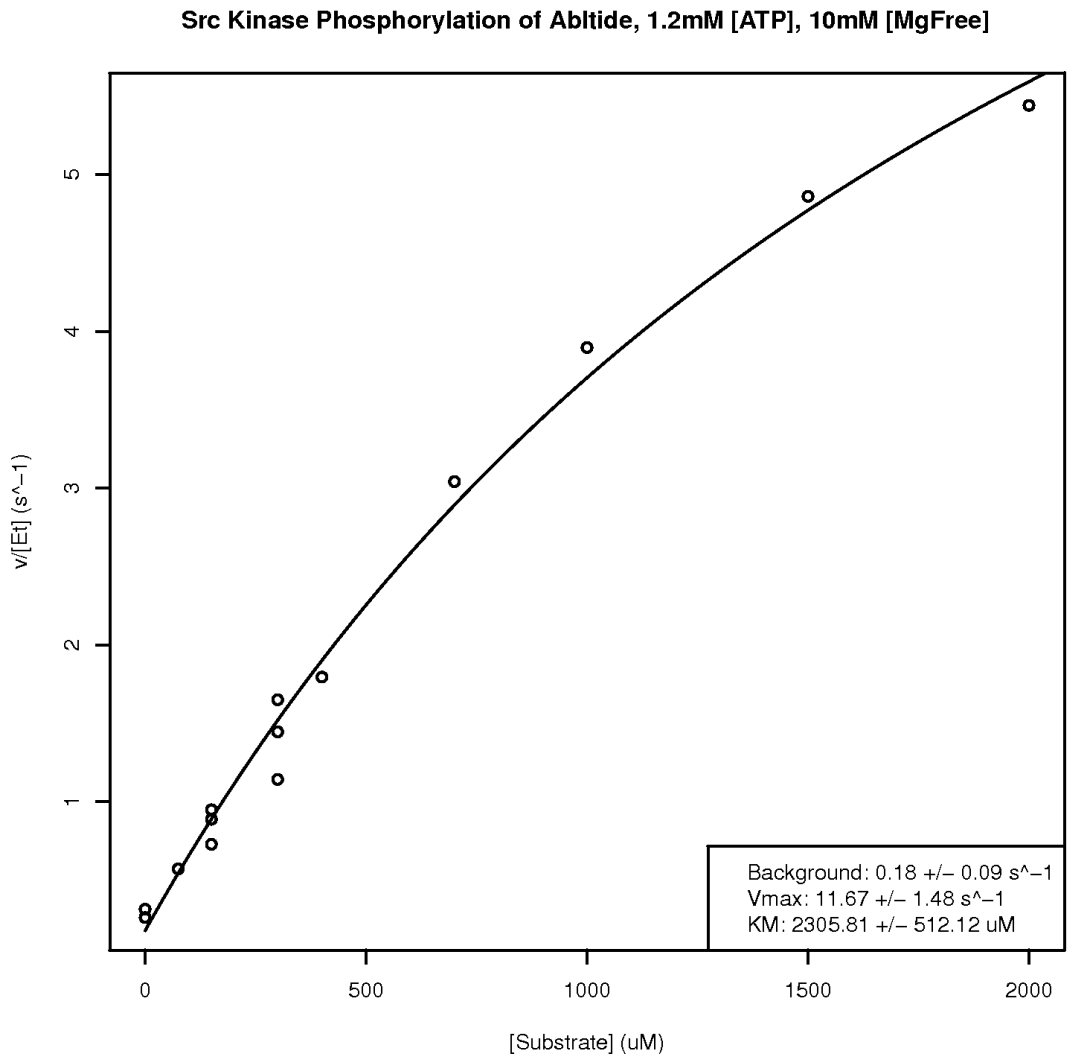

Figure 4-15. Enzyme kinetics: KM(Abltide) for c-Src^{WT} with 1.2 mM [ATP], 10 mM $[Mg^{2+}]_{free}$

Data fit to model v=background + (vmax*[abltide])/(K_M + [abltide])

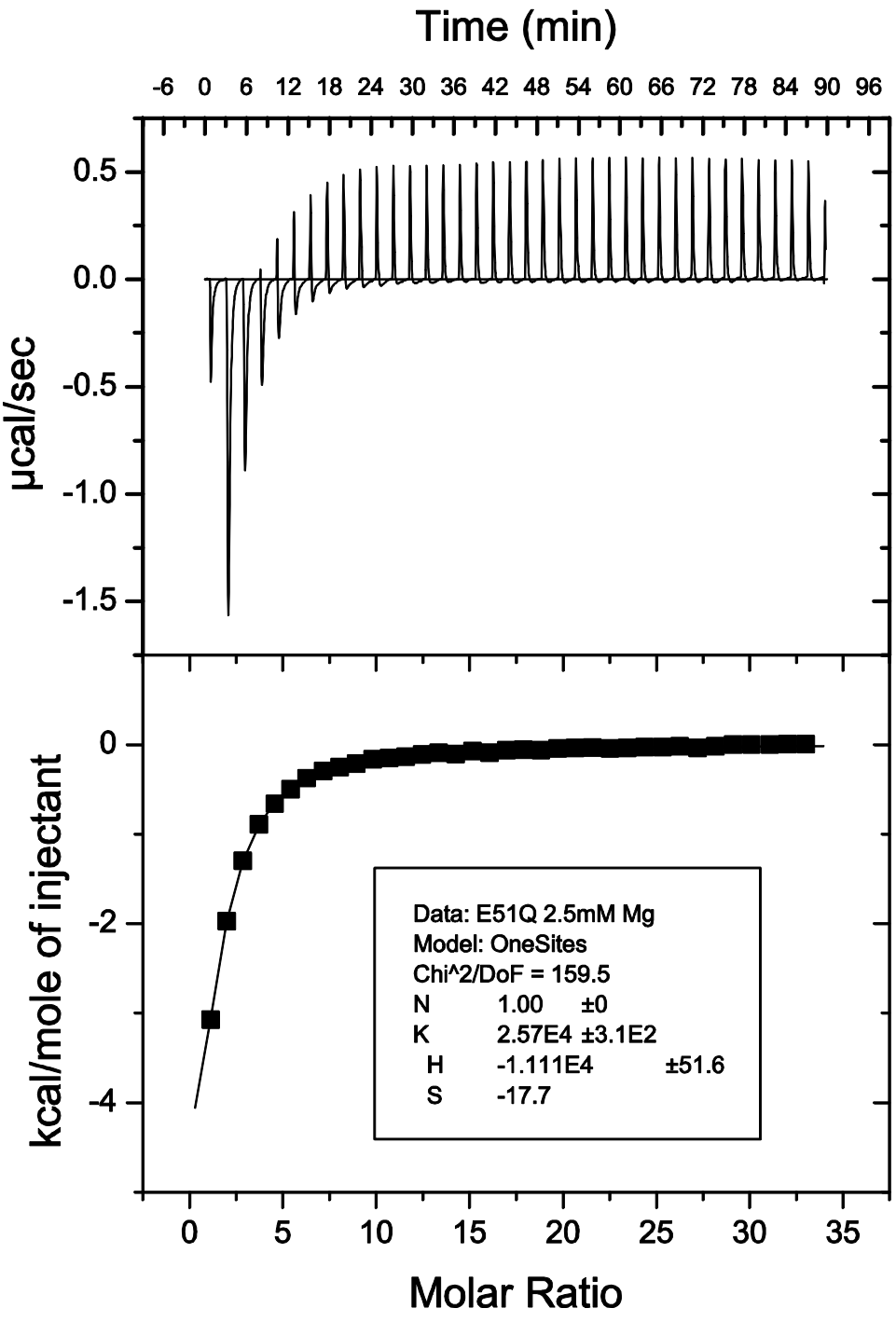

Figure 4-16. ITC of pCDK2^{E51Q}•CyclinA binding ADP with 2.5 mM $[Mg^{2+}]_{total.}$

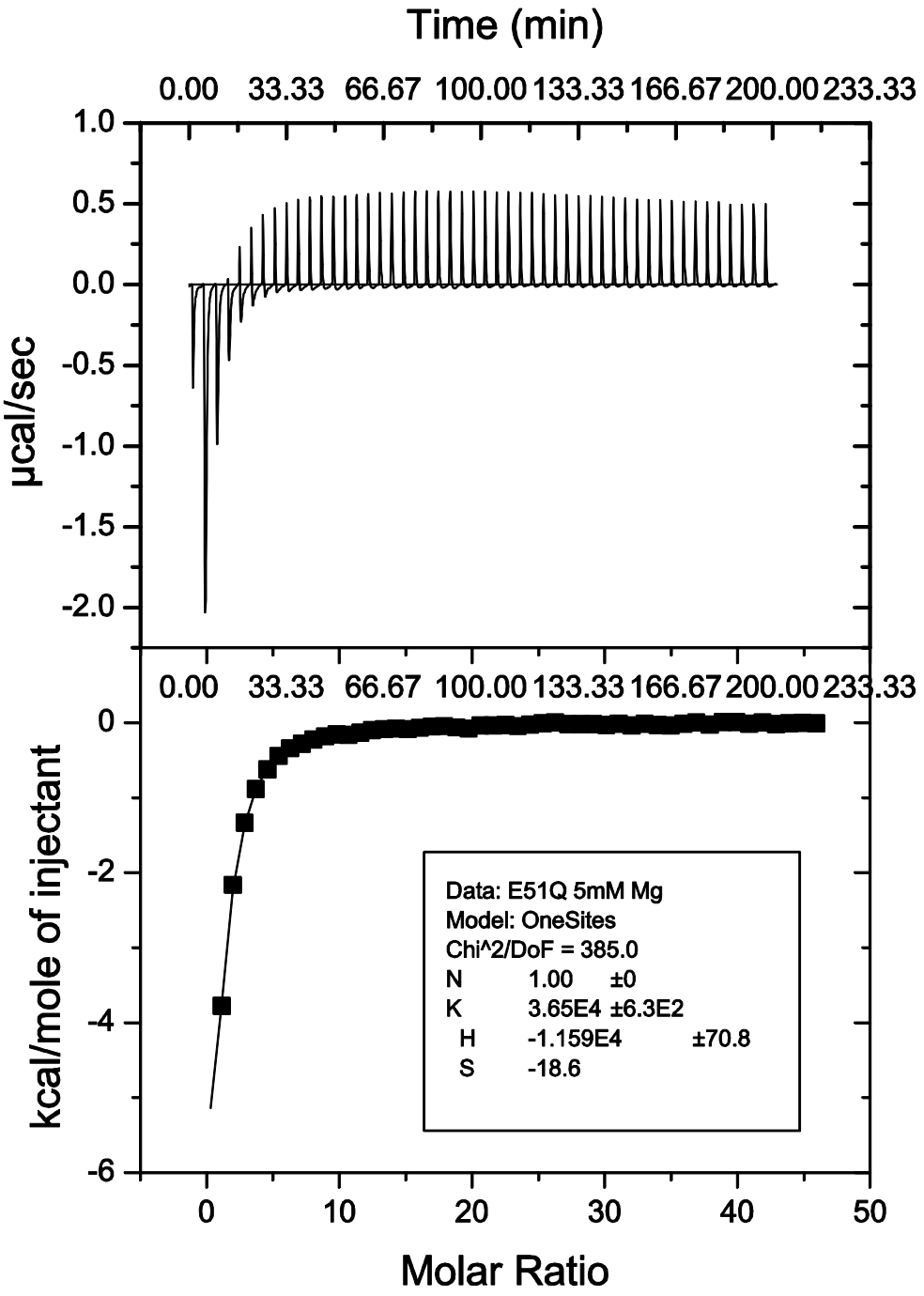

Figure 4-17. ITC of pCDK2^{E51Q}•CyclinA binding ADP with 5 mM $[Mg^{2+}]_{total.}$

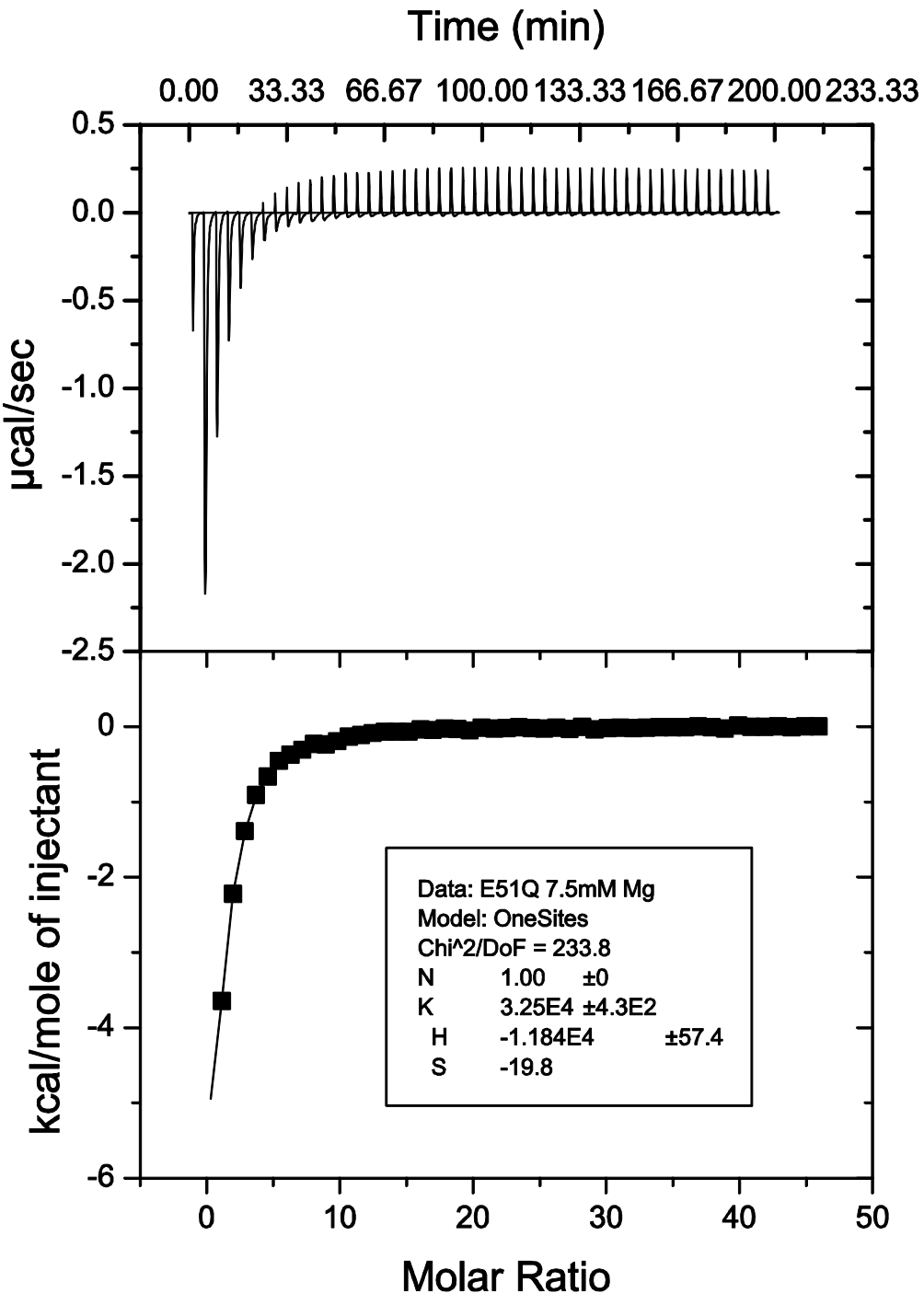

Figure 4-18. ITC of pCDK2^{E51Q}•CyclinA binding ADP with 7.5 mM $[Mg^{2+}]_{total.}$

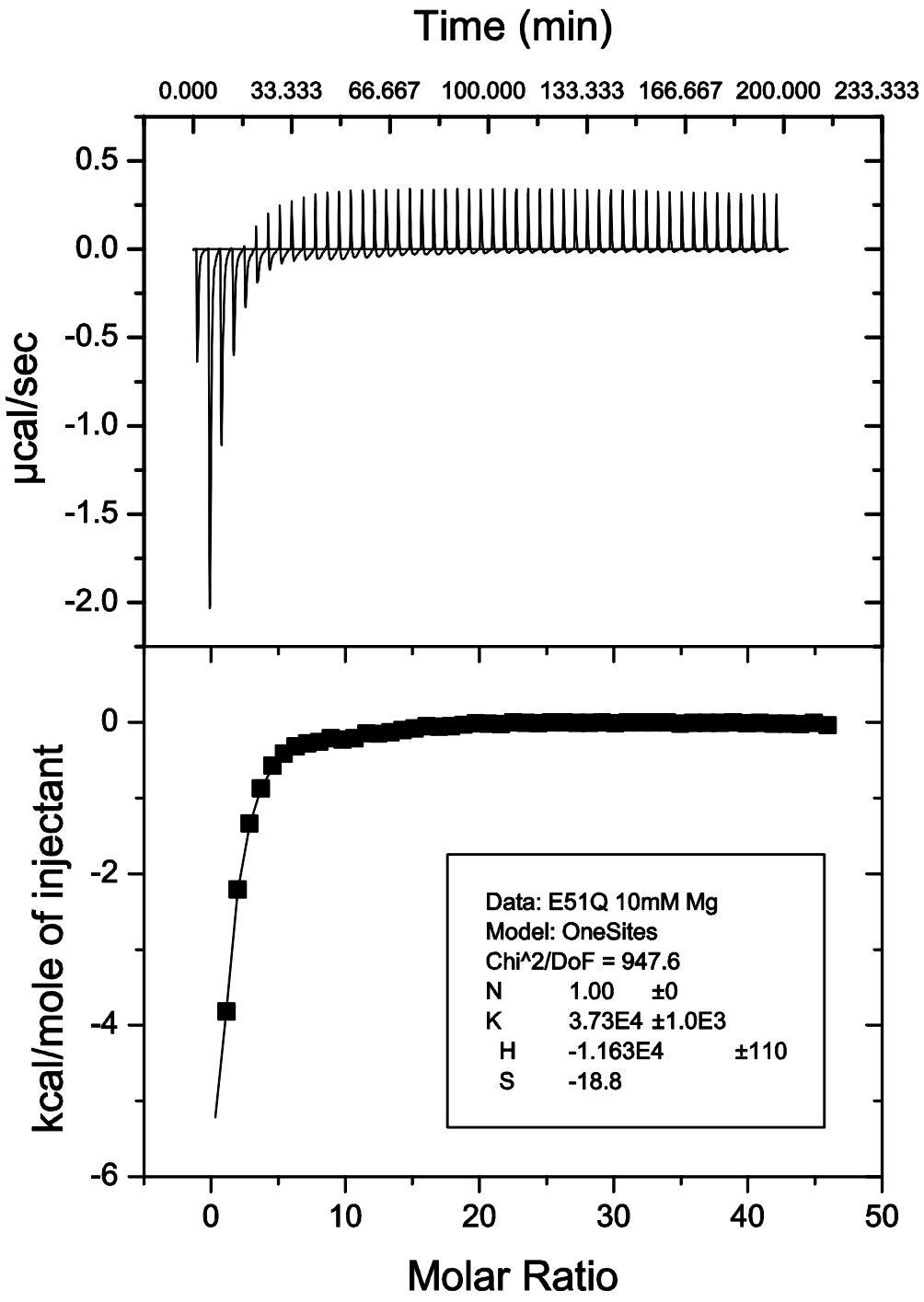

Figure 4-19. ITC of pCDK2^{E51Q}•CyclinA binding ADP with 10 mM $[Mg^{2+}]_{total.}$

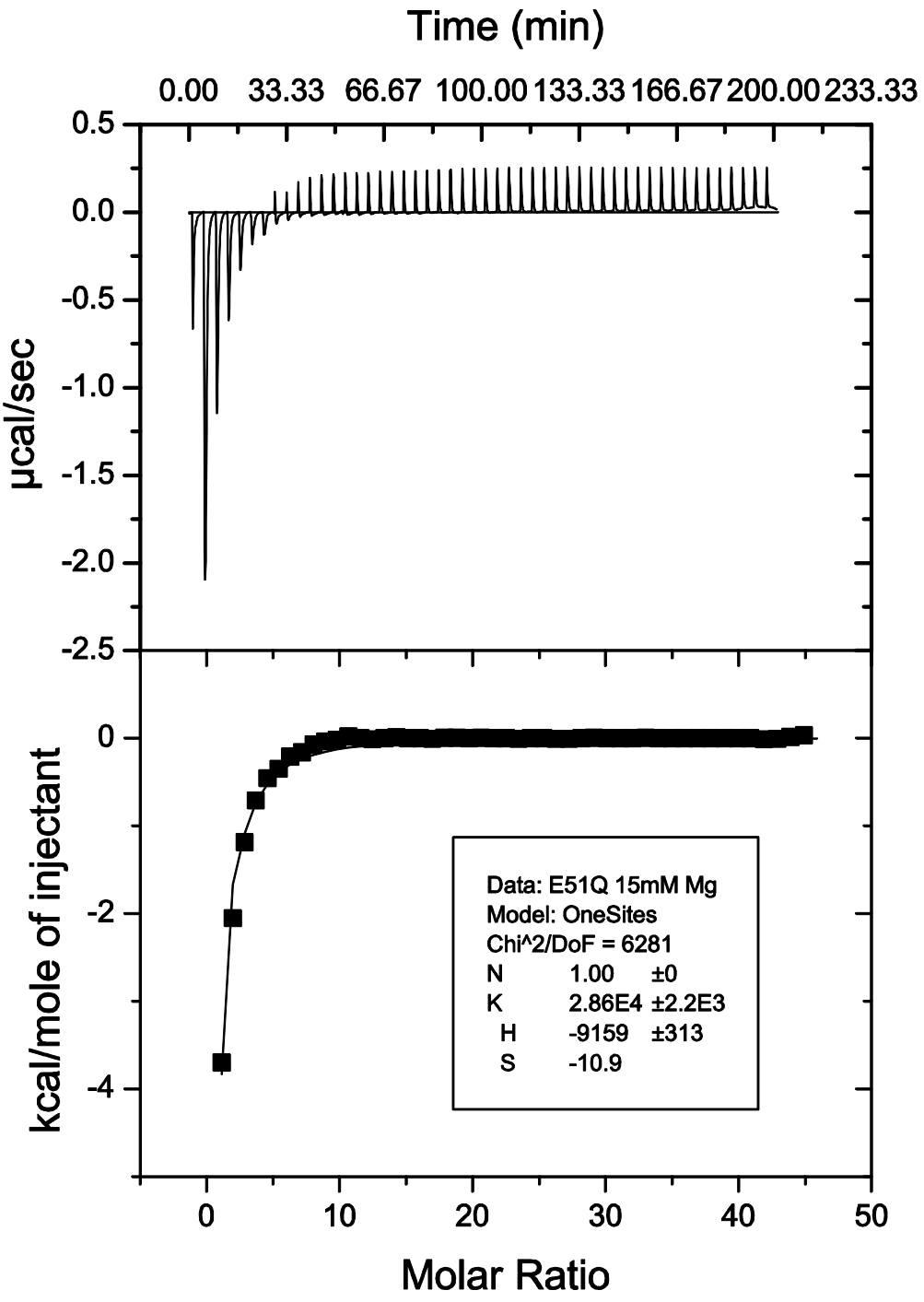

Figure 4-20. ITC of pCDK2^{E51Q}•CyclinA binding ADP with 15 mM $[Mg^{2+}]_{total.}$

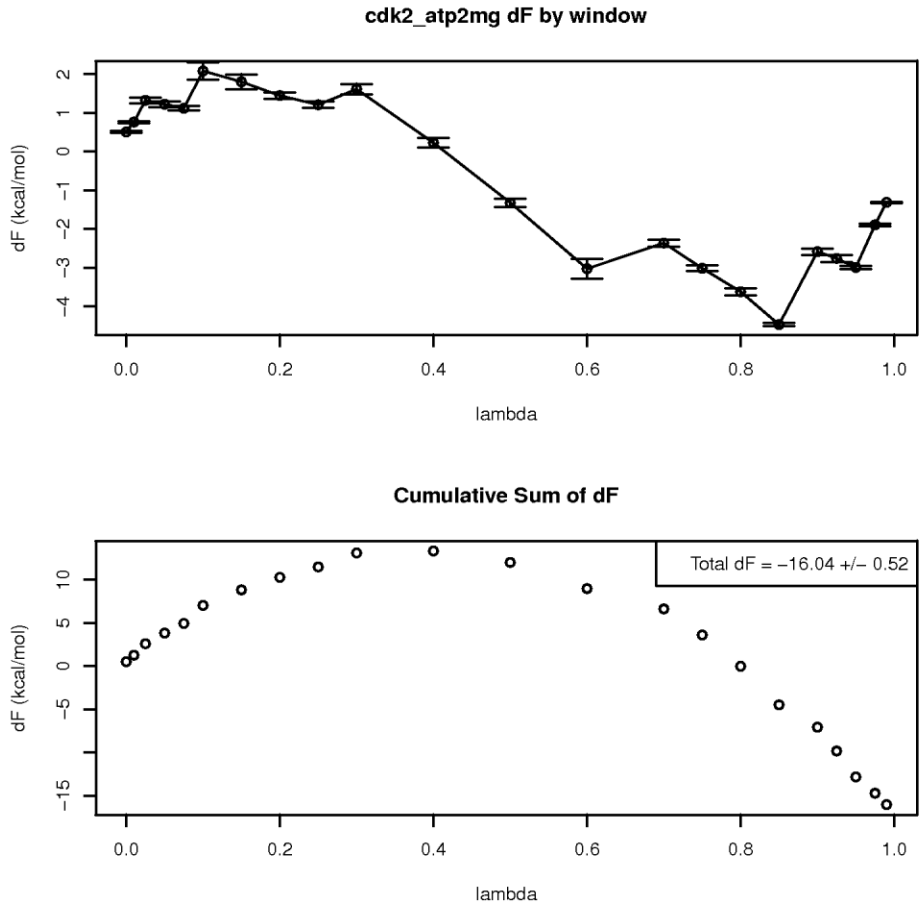

Figure 4-21. Free Energy Perturbation pCDK2/Cyclin ATP•2Mg

Top panel) Free energy difference contribution for $windowSet_{i,i+1}$, where lambda=i is the x-axis position. The plotted partial DF is the mean of three separate sets of trajectories, the error bars represent the standard error of the three trajectories. **Bottom panel)** the cumulative running sum of the values in the top panel. The final value gives the total DF of making the E → Q mutation in pCDK2/Cyclin with ATP and 2 Mg ions bound.

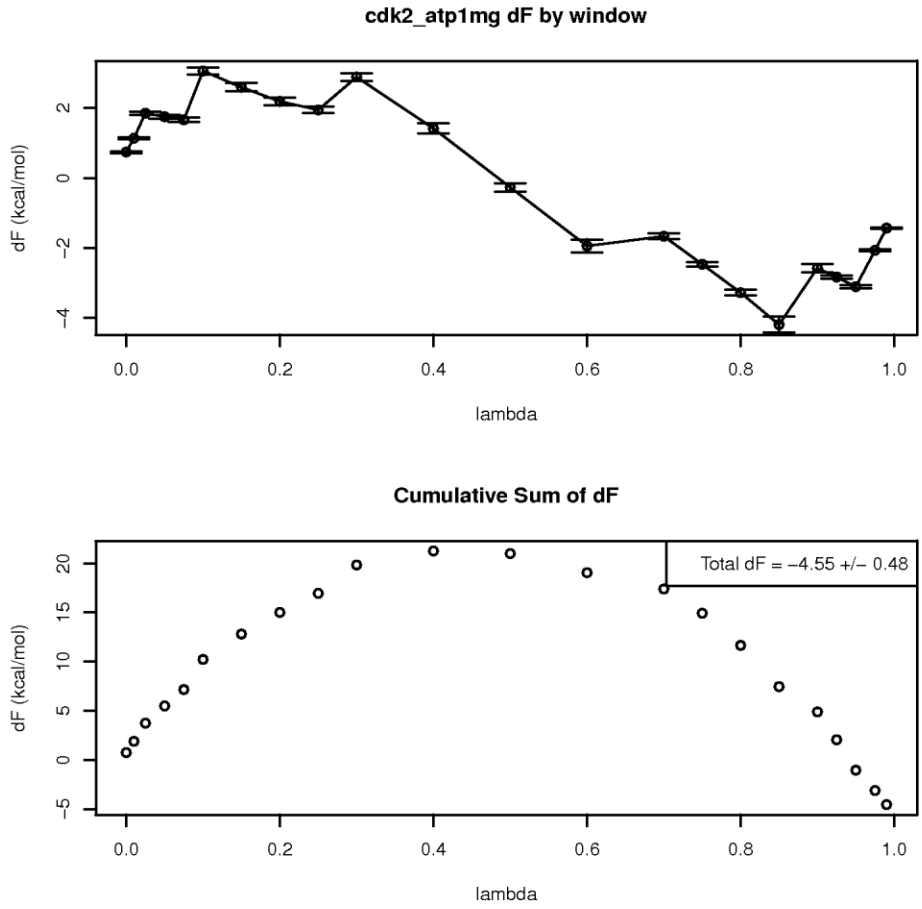

Figure 4-22. Free Energy Perturbation pCDK2/Cyclin ATP•1Mg

Top panel) Free energy difference contribution for $windowSet_{i,i+1}$, where lambda=i is the x-axis position. The plotted partial DF is the mean of three separate sets of trajectories, the error bars represent the standard error of the three trajectories. **Bottom panel)** the cumulative running sum of the values in the top panel. The final value gives the total DF of making the E → Q mutation in pCDK2/Cyclin with ATP and 1 Mg ion bound.

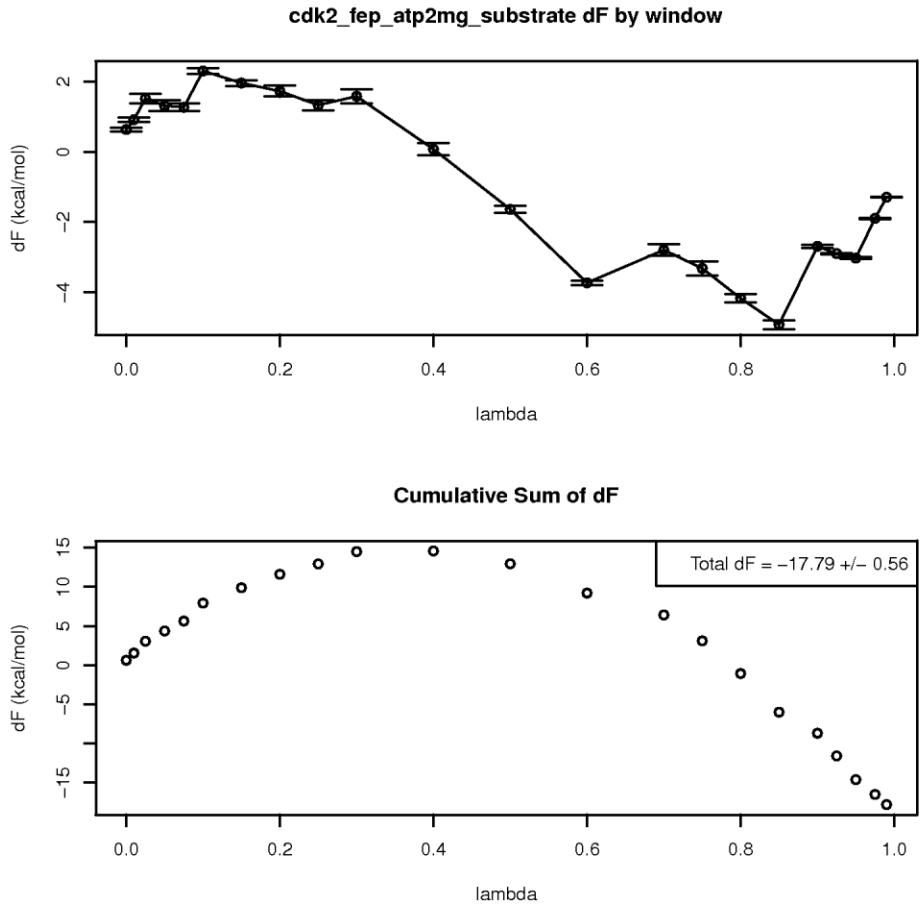

Figure 4-23. Free Energy Perturbation pCDK2/Cyclin ATP•2Mg and Protein Substrate

Top panel) Free energy difference contribution for $windowSet_{i,i+1}$, where lambda=i is the x-axis position. The plotted partial DF is the mean of three separate sets of trajectories, the error bars represent the standard error of the three trajectories. **Bottom panel)** the cumulative running sum of the values in the top panel. The final value gives the total DF of making the E → Q mutation in pCDK2/Cyclin with ATP, 2 Mg ions, and protein substrate peptide bound.

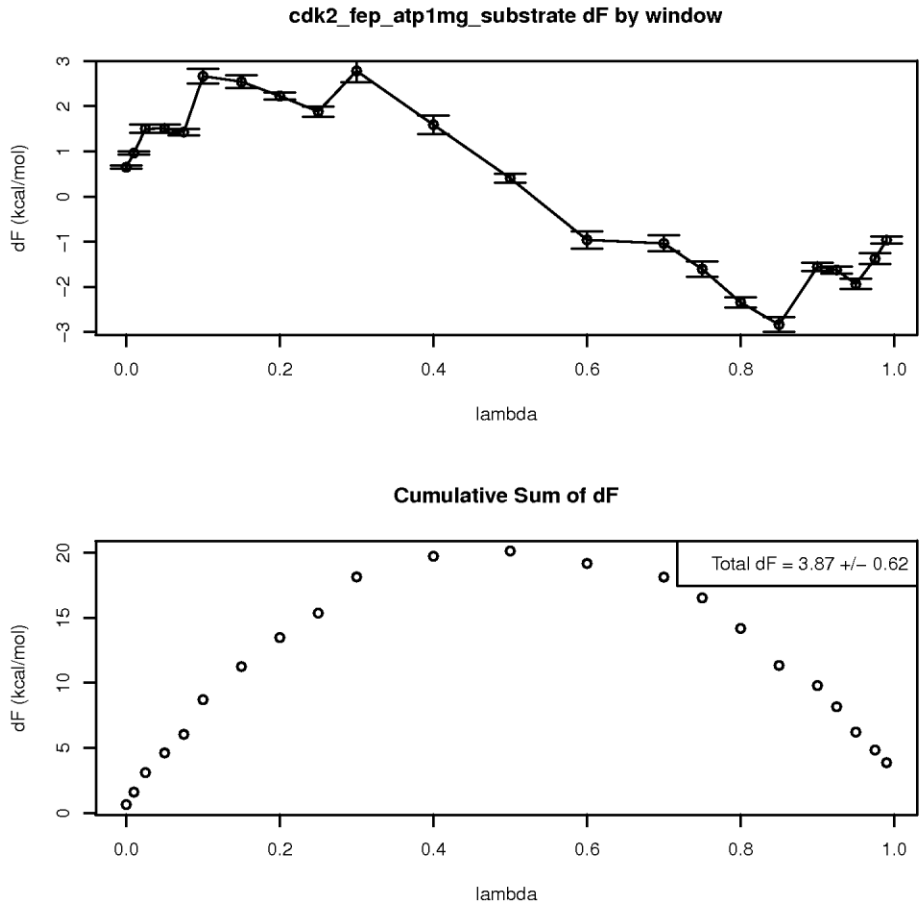

Figure 4-24. Free Energy Perturbation pCDK2/Cyclin ATP•1Mg and Protein Substrate

Top panel) Free energy difference contribution for $windowSet_{i,i+1}$, where lambda=i is the x-axis position. The plotted partial DF is the mean of three separate sets of trajectories, the error bars represent the standard error of the three trajectories. **Bottom panel)** the cumulative running sum of the values in the top panel. The final value gives the total DF of making the E → Q mutation in pCDK2/Cyclin with ATP, 1 Mg ion, and protein substrate peptide bound.

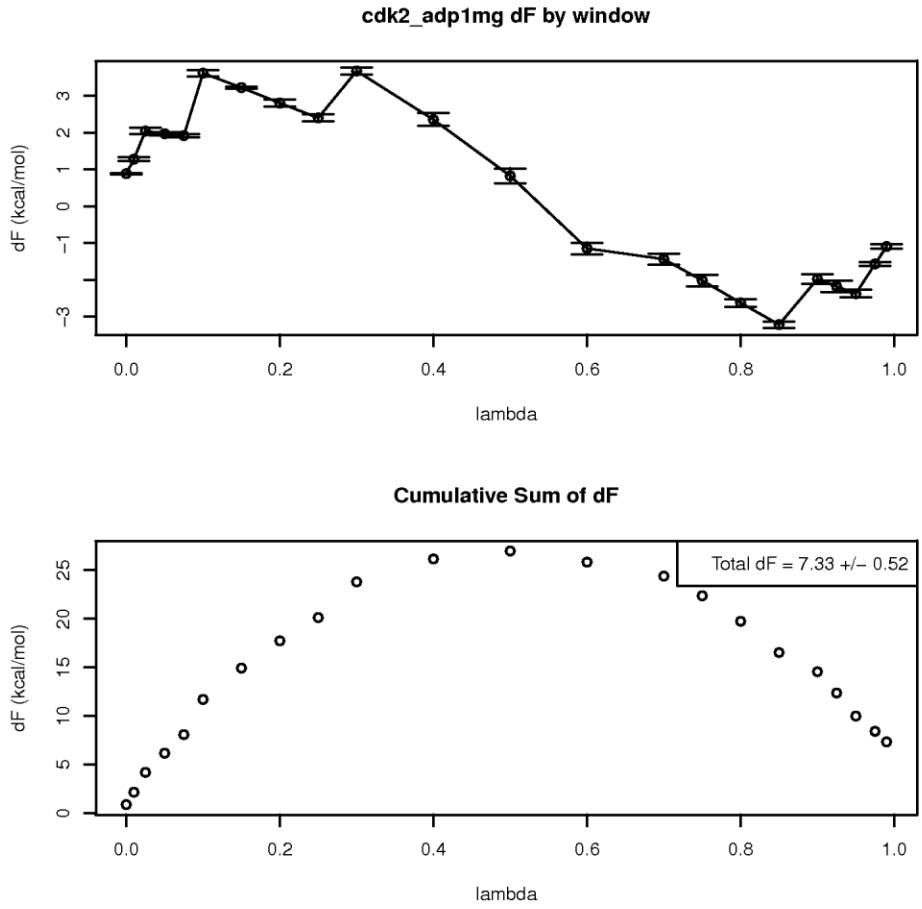

Figure 4-25. Free Energy Perturbation pCDK2/Cyclin ADP•1Mg

Top panel) Free energy difference contribution for $windowSet_{i,i+1}$, where lambda=i is the x-axis position. The plotted partial DF is the mean of three separate sets of trajectories, the error bars represent the standard error of the three trajectories. **Bottom panel)** the cumulative running sum of the values in the top panel. The final value gives the total DF of making the E → Q mutation in pCDK2/Cyclin with ADP and 1 Mg ion bound.

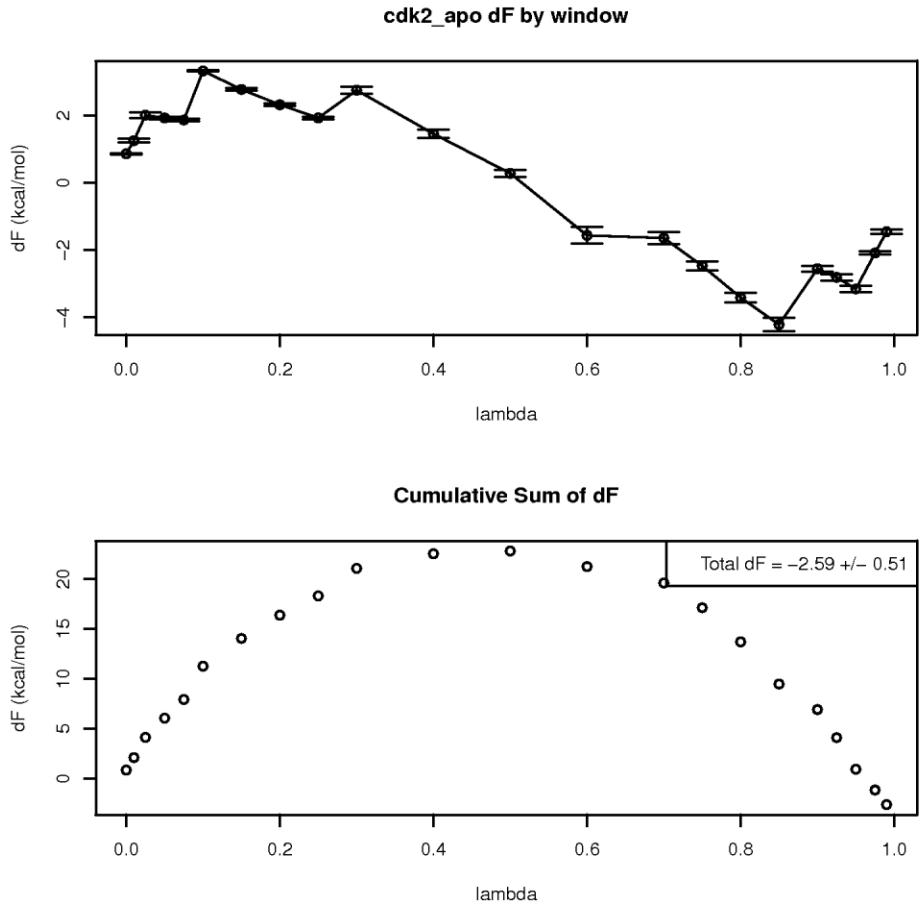

Figure 4-26. Free Energy Perturbation apo pCDK2/Cyclin

Top panel) Free energy difference contribution for $windowSet_{i,i+1}$, where lambda=i is the x-axis position. The plotted partial DF is the mean of three separate sets of trajectories, the error bars represent the standard error of the three trajectories. **Bottom panel)** the cumulative running sum of the values in the top panel. The final value gives the total DF of making the E → Q mutation in apo pCDK2/Cyclin.

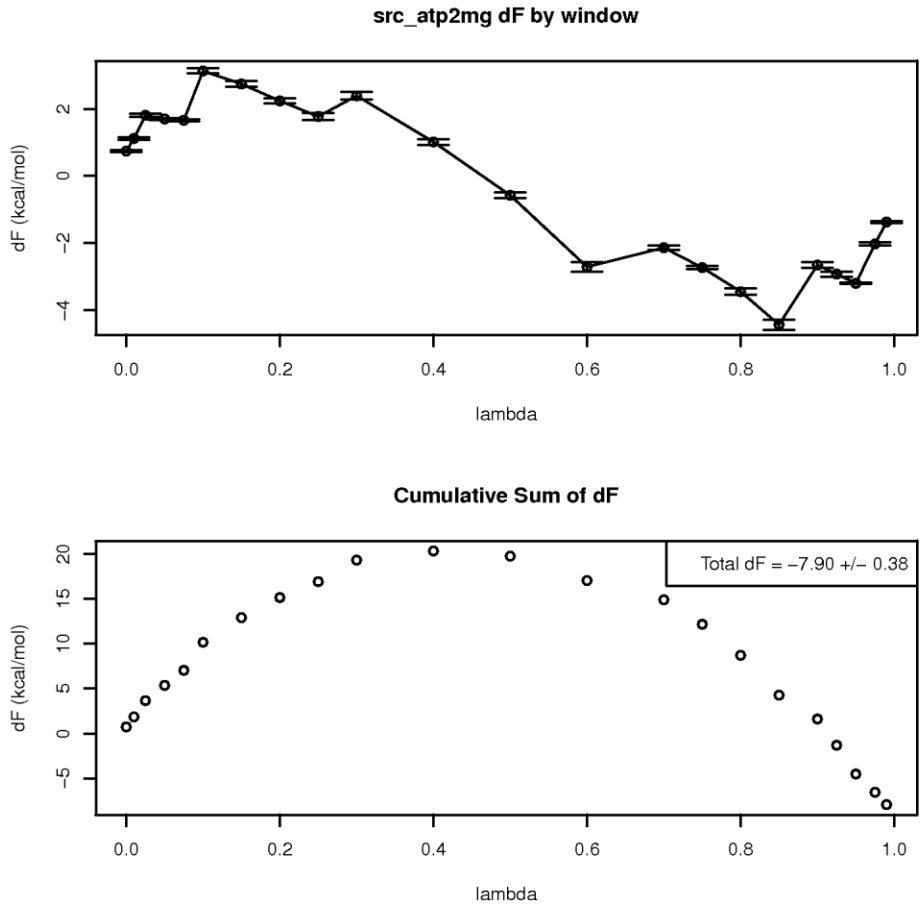

Figure 4-27. Free Energy Perturbation c-Src ATP•2Mg

Top panel) Free energy difference contribution for $windowSet_{i,i+1}$, where lambda=i is the x-axis position. The plotted partial DF is the mean of three separate sets of trajectories, the error bars represent the standard error of the three trajectories. **Bottom panel)** the cumulative running sum of the values in the top panel. The final value gives the total DF of making the E → Q mutation in c-Src with ATP and 2 Mg ions bound.

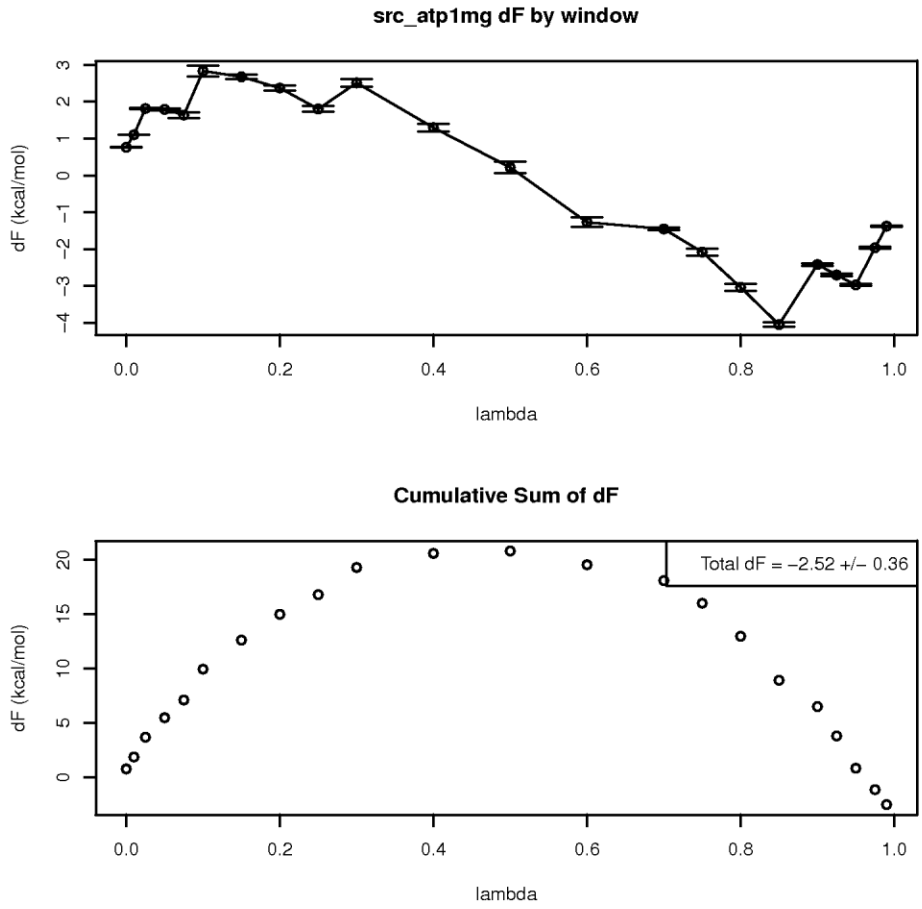

Figure 4-28. Free Energy Perturbation c-Src ATP•1Mg

Top panel) Free energy difference contribution for $windowSet_{i,i+1}$, where lambda=i is the x-axis position. The plotted partial DF is the mean of three separate sets of trajectories, the error bars represent the standard error of the three trajectories. **Bottom panel)** the cumulative running sum of the values in the top panel. The final value gives the total DF of making the E → Q mutation in c-Src with ATP and 1 Mg ion bound.

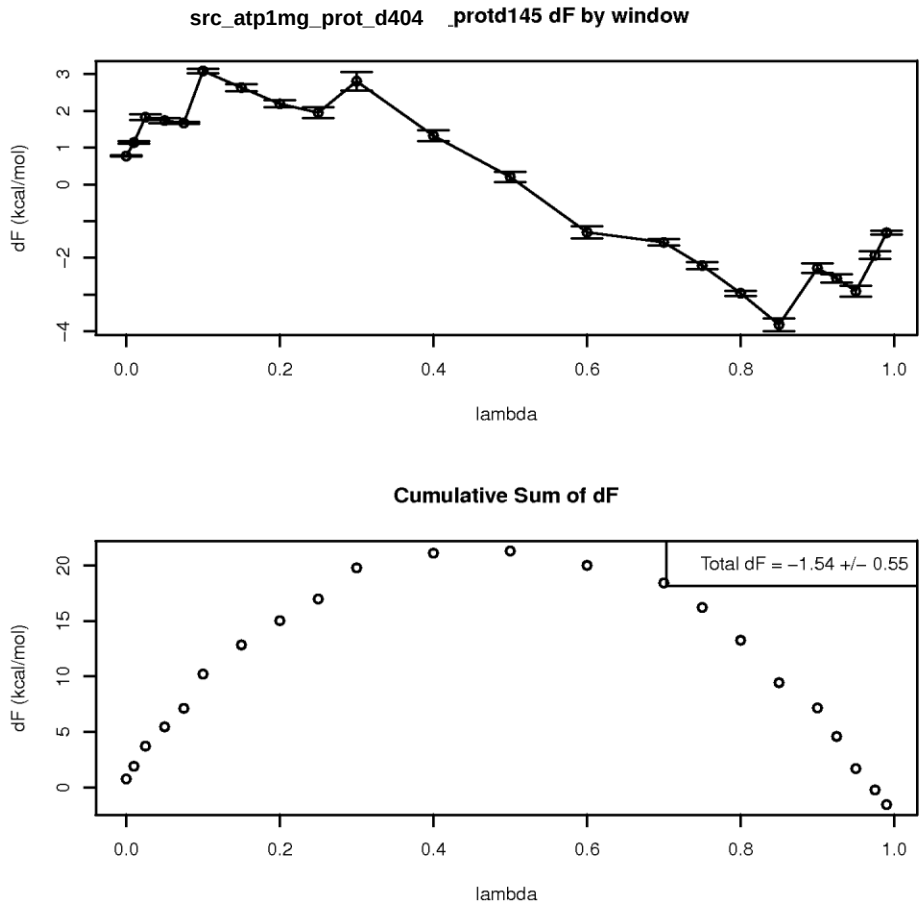

Figure 4-29. Free Energy Perturbation c-Src ATP•1Mg with Protonated DFG

Top panel) Free energy difference contribution for $windowSet_{i,i+1}$, where lambda=i is the x-axis position. The plotted partial DF is the mean of three separate sets of trajectories, the error bars represent the standard error of the three trajectories. **Bottom panel)** the cumulative running sum of the values in the top panel. The final value gives the total DF of making the E → Q mutation in c-Src with protonated DFG and ATP and 1 Mg ion bound.

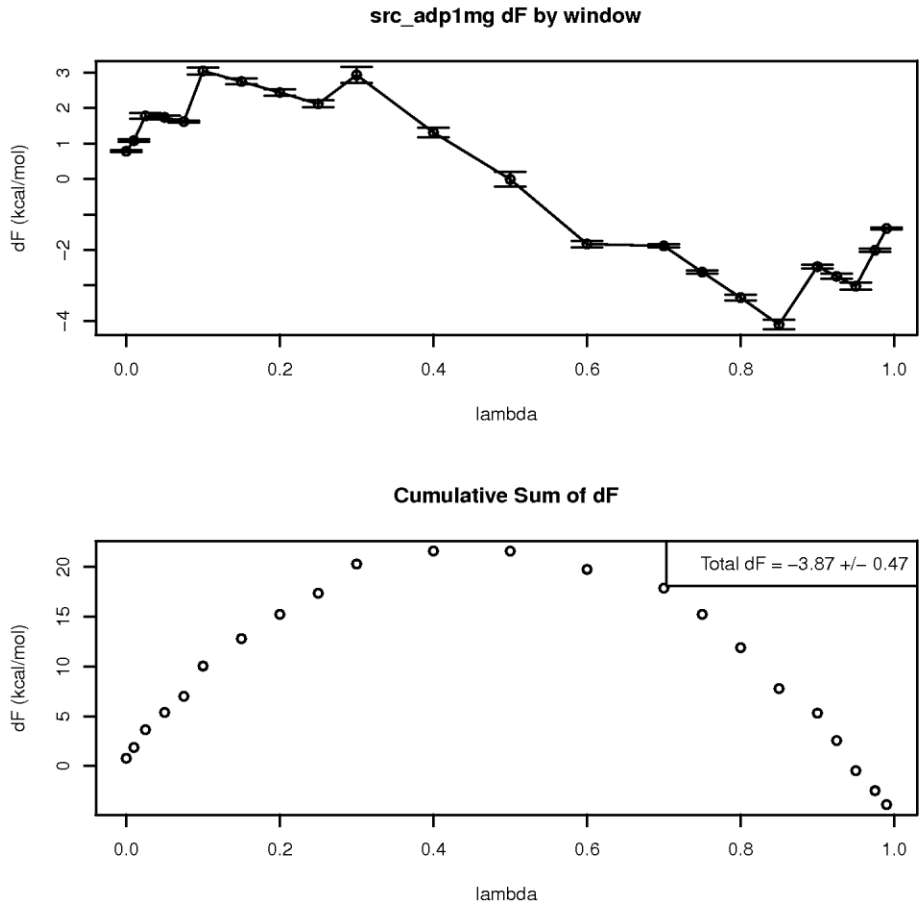

Figure 4-30. Free Energy Perturbation c-Src ADP•1Mg

Top panel) Free energy difference contribution for $windowSet_{i,i+1}$, where lambda=i is the x-axis position. The plotted partial DF is the mean of three separate sets of trajectories, the error bars represent the standard error of the three trajectories. **Bottom panel)** the cumulative running sum of the values in the top panel. The final value gives the total DF of making the E → Q mutation in c-Src with ADP and 1 Mg ions bound.

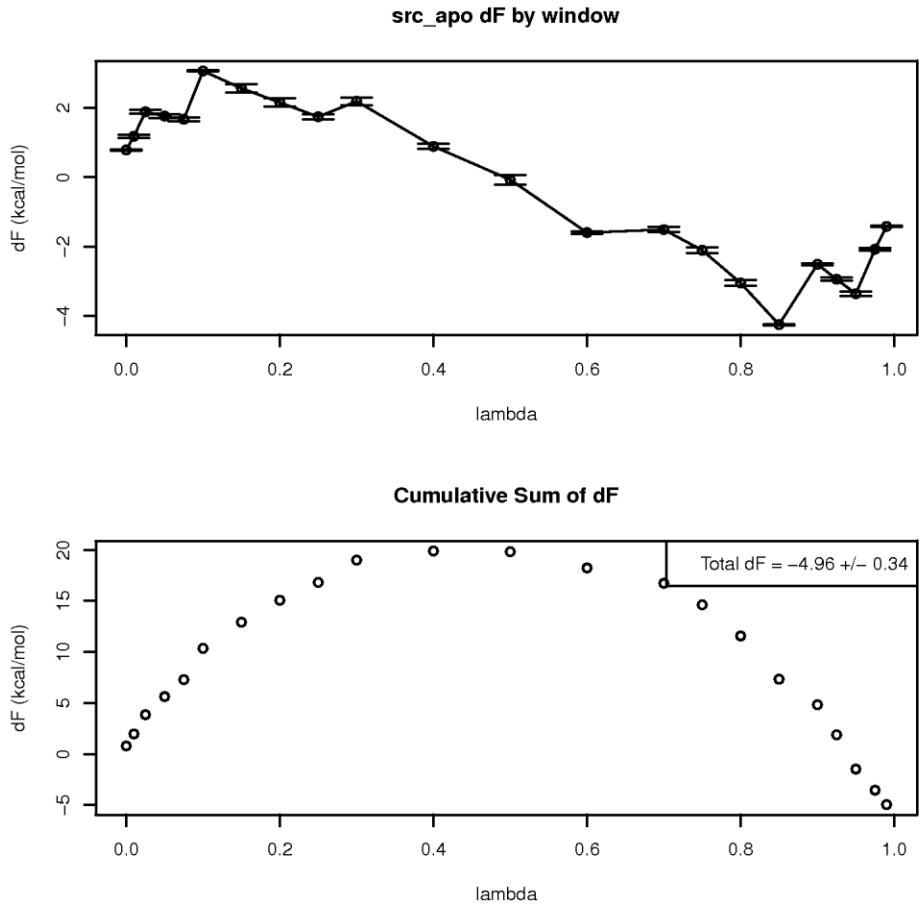

Figure 4-31. Free Energy Perturbation apo c-Src

Top panel) Free energy difference contribution for $windowSet_{i,i+1}$, where lambda=i is the x-axis position. The plotted partial DF is the mean of three separate sets of trajectories, the error bars represent the standard error of the three trajectories. **Bottom panel)** the cumulative running sum of the values in the top panel. The final value gives the total DF of making the E → Q mutation in apo c-Src.

CHAPTER 5

Conclusions

In this dissertation I have discussed my research of the catalytic mechanism of the protein kinase CDK2. This work has been a combination of computational and experimental investigation. I have solved a variety of crystal structures of CDK2, including a transition state mimic, ADP, and ATPγS structures for WT and E51Q mutant CDK2. Based on these structures, and structures solved by others and deposited in the Protein Data Bank, I have performed numerous molecular dynamics simulations of CDK2 in a variety of ligand-bound states. From these structures and simulations, I generated testable hypotheses – such as the requirement of the 2^{nd} Mg^{2+} ion in the catalytic cycle and the electrostatic deficit concept for stabilizing or destabilizing nucleotides in the protein kinase active site depending on the charge state of the overall active site. The steady-state enzyme kinetics experiments gave an excellent readout to both test hypotheses and interpret the functional requirements of the kinase. The fundamental purpose of this research is to explain the catalytic mechanism of Cyclin Dependent Kinase 2, and in particular to determine how the second, activating and essential Mg^{2+} ion interacts in the active site, and determine if CDK2 regulation manipulates the binding of the second Mg^{2+} ligand specifically.

This work resolves open questions in the protein kinase field about the essentiality of a second Mg^{2+} in the kinase phosphorylation reaction (chapters 2 and 3). Furthermore, based on this investigation I have dissected the functionality of the metals at each stage of

the catalytic cycle (chapter 3), and can propose and have derived a model which explains these data (chapter 3).

The detection of this essential co-factor of the protein kinase reaction has proved challenging, because it is weakly bound relative to the other substrates and products, and has a significant interaction with both ATP and ADP in solution, making its effects challenging to sort out. My model is that the second Mg^{2+} can bind/release with $K_{MgActivation}$ affinity to the ATP•E complex where MgI site occupancy promotes transition state formation, and can bind/release to the ADP•E complex (product complex) with $K_{MgInhibition}$ affinity where MgI site occupancy opposes product release. One excellent model to understand how different kinases give different kinetic responses to $[Mg^{2+}]$ is that the activated kinase conformation $K_{MgActivation}$ and $K_{MgInhibition}$ have evolved differently for different protein kinases.

The model, combined with our knowledge from chapters 2 and 3 that the second Mg^{2+} binding affinity is a function of active-site electrostatics, and the idea of evolutionary balancing of $K_{MgActivation}$ and $K_{MgInhibition}$ suggests that regulatory manipulation of active-site electrostatics could therefore also optimize $K_{MgActivation}$ and $K_{MgInhibition}$ for catalysis. Therefore, we determined in chapter 4 that the allosteric regulation of protein kinase activity can indeed alter the binding characteristics of Mg^{2+} to activate or inhibit kinase activity.

Results Summary

Chapter 2 relates our investigation of the transition state of pCDK2/Cyclin. In this chapter we solved a transition state mimic structure of pCDK2/Cyclin which shows a potential transition state coordination of the active site. The structure endeavors to mimic the chemically unstable transition state by using a MgF_3^- (using $MgCl_2$ and NaF to form the MgF_3^-) to replace the γ-phosphate in the transition state, taking advantage on the concept that the role of the enzyme is to stabilize the chemical TS (Figure 2-1). Significantly, NaF is shown to inhibit the reaction, suggesting that the MgF_3^- mimics the TS well (Figure 2-10), unlike a previous attempt at pCDK2/Cyclin TS-mimic with NO_3^- (Cook et al., 2002). Therefore this structure is the second TS-mimic structure for a protein kinase, the first was of PKA. Significantly, many of the structural features of the TS-mimic for PKA (Madhusudan et al., 2002) and CDK2 are similar (Figure 2-4). For the first time, we showed that a second Mg^{2+} ion binds to the active site of pCDK2/Cyclin, and that the Gly-rich loop closed conformation is specifically correlated to the pCDK2/Cyclin TS. Prior to this structure, CDK2 was thought to use only a single Mg^{2+} ion to catalyze the reaction.

The structural similarity of the protein kinase TS of CDK2 and PKA was not limited to protein kinases. Aligning the phosphates of the CDK2 TS and a TS-mimic of the small g-protein Rho bound to its GAP, we find that many of the structural requirements of the protein kinase TS are conserved in the small g-protein TS (Figure 2-12). The Rho p-loop coordinates the phosphates in a similar manner as the protein kinase Gly-loop; one of the Mg^{2+} positions is exactly conserved, and the other is replaced

with the GAP Arg finger. The data strongly suggest that both coordination geometry and charge complementarity is essential to hydrolyzing NTPs.

One of the principal results of the TS-mimic was discovery of the conserved binding of the 2nd Mg^{2+} ion. Looking more closely into the functionality of this 2nd Mg^{2+} ion, we found a variety of effects. First, simulations predict that binding the 2nd Mg^{2+} ion to the E•ATP•Mg complex stabilizes the Gly-loop conformational change to the closed position, and that removing the Mg^{2+} ion stabilizes Gly-loop opening (Figure 2-7). Second, titrating $MgCl_2$ into the reaction, we found complex effects on the reaction rate – at low Mg^{2+}, the reaction is activated, while at high [Mg^{2+}], the reaction becomes more inhibited (Figure 2-6).

In chapter 3, we hypothesized that the complex effects of $MgCl_2$ on the reaction may both be attributable to the second Mg^{2+} ion – that is, that the second Mg^{2+} ion (in the MgI site) both activates and inhibits the reaction. The mechanism to achieve this is that the 2nd Mg^{2+} ion has activating effects on one step of the catalytic cycle, while slowing another step. Extensive steady state kinetics showed that the origin of the activating effects of the second Mg^{2+} ion were by reducing $K_{M(ATP•Mg)}$ by over 30 fold (Figure 3-3). Furthermore, $k_{cat}/K_{M(ATP•Mg)}$, or catalytic efficiency of ATP•Mg, showed a monotonically increasing behavior, indicating that as the 2nd Mg^{2+} ion was stabilized in the active site the transition state was being formed ever more quickly. Combined with the essential nature of the 2nd Mg^{2+} in forming the TS, we concluded that the true activation effect of the 2nd Mg^{2+} is in cooperatively stabilizing catalytically productive binding of ATP•Mg into the active site of pCDK2/Cyclin. We found that the $K_{MgActivation}$ of the 2nd Mg^{2+} ion is <400μM $[Mg^{2+}]_{free}$, significantly lower than the 1mM physiological $[Mg^{2+}]_{free}$.

Since the stabilization of the 2nd Mg^{2+} activates chemistry and ATP•Mg binding, the inhibitory capacity of the 2nd Mg^{2+} must therefore occur in the product release step of the reaction. Thus, we investigated ADP release from pCDK2/Cyclin. We presented two new crystal structures of pCDK2/Cyclin bound to ADP•Mg, one with both Mg^{2+} ions, and the other with just one (Figure 3-4). ITC experiments show that the binding of ADP becomes tighter at high [Mg^{2+}] (Figure 3-3F). The combination of the result that the 2nd Mg^{2+} is in equilibrium with the E•ADP•Mg complex and the cooperative binding of ADP•Mg to pCDK2/Cyclin, suggests that the second Mg^{2+} is responsible for the cooperative binding of ADP•Mg to the active site, similar to the cooperative binding of ATP•Mg to the active site.

Since the inhibition of activity must be occurring in the product release step, and because ADP•2Mg binds more tightly, we suggest that the rate of ADP release decreases when the MgI site is occupied. The $K_{MgInhibition}$ of the 2nd Mg^{2+} is about 9mM $[Mg^{2+}]_{free}$, thus the inhibiting effects of the second Mg^{2+} are unlikely to play a strong role under physiological conditions. However, if the active site affinity for the 2nd Mg^{2+} was tightened to improve binding of ATP•Mg, it would be likely that ADP•Mg release would be similarly affected, resulting in a net reduction in activity.

Solvent viscosity titration experiments were performed to isolate the effects of the second Mg^{2+} on product release (Figure 3-9). In theory, when all the substrates are saturating, these experiments can discriminate between phosphoryl-transfer being slow, or product release being slow – based on the idea that solvent viscosity will slow the rate of bimolecular steps like product diffusion, but not unimolecular steps like phosphoryl-transfer. Under saturating substrate conditions, the rate limiting aspect of the CDK2

reaction is always product release, independent of $[Mg^{2+}]_{free}$. Therefore, the slowest step for the kinase is always release the products, and that the inhibition at high $[Mg^{2+}]_{free}$ only slows it further – possibly rebinding of the 2nd Mg^{2+} ion to the ADP•1Mg complex. Therefore, we concluded that the release of the ADP•2Mg product was likely an ordered event, such that the 2nd Mg^{2+} could release independently of ADP•1Mg, and usually prior to ADP•1Mg. Because extrapolating to infinite $[Mg^{2+}]_{free}$ doesn't reduce the reaction rate to 0, the 2nd Mg^{2+} isn't completely inhibitory, implying there must some slow rate of ADP•2Mg release (Figure 3-3).

Finally, we investigated the electrostatic effects of the ADP•1Mg structure by molecular dynamics simulation. We found that additional positive charge was required to stabilize the electronegative phosphates in the similarly electronegative active site (Figure 3-8). By protonating the phosphates or the Asp145 sidechain, or by including an explicit Na^{+} ion in the active site, the phosphates and active site retained the ADP•1Mg crystal structure conformation much more faithfully. The inclusion of a +1 charge allowed the phosphates to interact stably in the active site without the requirement for the 2nd Mg^{2+} ion. Thus, in the absence of the charge, the electrostatic deficit in the active site results in destabilizing repulsion of the phosphates and the active site.

In chapter 4, I demonstrated the functional relevance of the two-metal catalytic mechanism in the regulation of kinase activity. We investigated the allosteric activation of CDK2 by Cyclin. The binding of Cyclin stabilizes a conformational change which helps to create the aforementioned active site electrostatic deficit by inserting a negatively charge Glu sidechain into the active site. We hypothesized that the generation of this electrostatic deficit would simultaneously increase binding of the second Mg^{2+}

while destabilizing phosphates in the absence of the 2nd Mg^{2+}. We modeled the electrostatic effects of neutralizing this charge (similar to the monomeric, inactive CDK2) by making the E51Q mutation to CDK2. Because the c-α-helix conformational change is conserved across many kinases, we made the homologous E310Q mutation in the kinase catalytic domain of c-Src to determine the generality of our conclusions.

By neutralizing the charge on the conserved Glu51, nucleotide binding is stabilized (Figure 4-6, Figure 4-9) in pCDK2/Cyclin, while 2nd Mg^{2+} ion binding is destabilized (Figure 4-5, Figure 4-8, Figure 4-12). Crystal structures verify that all conformational aspects of the active pCDK2/Cyclin structure are maintained by the E51Q mutant. Thus, only the electrostatic effects of the pCDK2/Cyclin active site are altered by the mutation. Therefore, we conclude that the binding of the second Mg^{2+} is made favorable under physiological conditions by the insertion of the conserved Glutamate upon activation. Free energy perturbation calculations (i.e. making the mutation *in silico*), show that the effects of neutralizing charge at the Glutamate site significantly adjust the relative free energy of binding the second Mg^{2+} to the active site (Figure 4-13 and Figure 4-21 through Figure 4-31). Finally, reaction kinetics and calculations of c-Src^{WT} and c-Src^{E310Q} show that the electrostatic regulation of binding the 2nd Mg^{2+} ion is conserved in at least c-Src. Thus, not only is the 2nd Mg^{2+} ion a required component of the protein kinase reaction, but it is also represents a conserved site of allosteric regulation of protein kinase activity.

Final Conclusions & Future Directions

The data presented herein, principally for CDK2, suggest a model in which the protein and ATP•Mg substrates bind to the kinase active site, but as the final and weakest

binding component of the reaction, the second Mg^{2+} is finally required to organize the active site into the catalytically competent conformation (Figure 3-1B). Because of the high conservation of the protein kinase active site residues, we suggest that this mechanism is strongly conserved within the protein kinase family, and that a one-metal mechanism will be a higher energy pathway than the two-metal mechanism.

One clear future direction that could be taken would be to calculate potentials of mean force for both one-metal and two-metal reactions to determine the barrier heights of each reaction, and the relative contributions and roles of the active site residues under each scenario. A two-metal calculation was performed for PKA (Cheng et al., 2005), while one-metal calculations have been performed for pCDK2/Cyclin (De Vivo et al., 2007; Smith et al., 2011). One challenge with such a calculation will be to properly model and sample the pre-chemistry state as there are no known pCDK2/Cyclin/ATP/2Mg structures, and thus it may be challenging to model such a state accurately enough for meaningful PMF calculations using the QM/MM methodology.

Another important result of this research is that we have presented a coherent and well supported model for the functionality of the 2nd divalent binding site in protein kinases. Because of the diversity of responses observed for different protein kinases as the second Mg^{2+} is stabilized in the active site, the functional role of this metal has been debated for many years. By adjusting the $K_{MgActivation}$ and $K_{MgInhibition}$ properties of the 2nd Mg^{2+} binding site for the ATP•Mg and ADP•Mg bound states respectively, we can model the full diversity of observed Mg^{2+}-dependent responses. An important assumption of this model is the $K_{MgInhibition}$ is specifically related to a Magnesium dependent slowing of ADP release. Given the kinetic tools available, we have isolated this inhibitory effect of

[Mg^{2+}] to the product release step, and have demonstrated that Mg^{2+} dependent slowing of ADP release is likely correct. An excellent test of this aspect of our model would be to directly observe the rate of ADP release as Mg^{2+} is varied. This could be achieved via fluorescence stop-flow in a similar manner as described in (Brown et al., 1999b). Our collaborator, Prof. Manju Hingorani, attempted this measurement with both intrinsic Trp fluorescence and labeled ADP (mant-ADP), and observed no usable signal. In the future, further effort could be invested by fluorescently labeling other sites of the CDK2 catalytic domain to determine if a better signal can be obtained, similar to what was achieved for Protein Kinase A at a single Mg^{2+} concentration (Lew et al., 1997).

The revelation that the binding of the 2^{nd} Mg^{2+} is a conserved feature of the regulation of protein kinases (Chapter 4) may help to explain some mutational effects on kinase activity and provide possible new avenues of research for therapeutic inhibition. Combined regulatory effects of destabilization of Mg^{2+} binding, the hydrophobic spine deconstruction, reduction in protein substrate binding, and possible larger effects on conformational stability are employed to inactivate kinase activity. These multiple effects of kinase regulation to destabilize the fully active protein kinase conformation demonstrate the subtlety and sensitivity of kinase regulation.

REFERENCES

Adams, J.A. (2001). Kinetic and catalytic mechanisms of protein kinases. Chem Rev *101*, 2271–2290.

Adams, J.A., and Taylor, S.S. (1992). Energetic limits of phosphotransfer in the catalytic subunit of cAMP-dependent protein kinase as measured by viscosity experiments. Biochemistry *31*, 8516–8522.

Adams, J.A., and Taylor, S.S. (1993). Divalent metal ions influence catalysis and active-site accessibility in the camp-dependent protein kinase. Protein Science *2*, 2177–2186.

Adams, P.D., Afonine, P.V., Bunkóczi, G., Chen, V.B., Davis, I.W., Echols, N., Headd, J.J., Hung, L.-W., Kapral, G.J., Grosse-Kunstleve, R.W., et al. (2010). PHENIX : a comprehensive Python-based system for macromolecular structure solution. Acta Crystallographica Section D Biological Crystallography *66*, 213–221.

Azam, M., Seeliger, M.A., Gray, N.S., Kuriyan, J., and Daley, G.Q. (2008). Activation of tyrosine kinases by mutation of the gatekeeper threonine. Nat Struct Mol Biol *15*, 1109–1118.

Baker, N.A., Sept, D., Joseph, S., Holst, M.J., and McCammon, J.A. (2001). Electrostatics of nanosystems: Application to microtubules and the ribosome. Proceedings of the National Academy of Sciences of the United States of America *98*, 10037 –10041.

Bao, Z.Q., Jacobsen, D.M., and Young, M.A. (2011). Briefly bound to activate: transient binding of a second catalytic magnesium activates the structure and dynamics of CDK2 kinase for catalysis. Structure *19*, 675–690.

Barker, S., Kassel, D.B., Weigl, D., Huang, X., Luther, M., and Knight, W.B. (1995). Characterization of pp60c-src Tyrosine Kinase Activities Using a Continuous Assay: Autoactivation of the Enzyme Is an Intermolecular Autophosphorylation Process. Biochemistry *34*, 14843–14851.

Bas, D.C., Rogers, D.M., and Jensen, J.H. (2008). Very fast prediction and rationalization of pKa values for protein-ligand complexes. Proteins *73*, 765–783.

Baxter, N.J., Blackburn, G.M., Marston, J.P., Hounslow, A.M., Cliff, M.J., Bermel, W., Williams, N.H., Hollfelder, F., Wemmer, D.E., and Waltho, J.P. (2008). Anionic charge is prioritized over geometry in aluminum and magnesium fluoride transition state analogs of phosphoryl transfer enzymes. J. Am. Chem. Soc. *130*, 3952–3958.

Baxter, N.J., Olguin, L.F., Goličnik, M., Feng, G., Hounslow, A.M., Bermel, W., Blackburn, G.M., Hollfelder, F., Waltho, J.P., and Williams, N.H. (2006). A Trojan horse transition state analogue generated by MgF3− formation in an enzyme active site. Proceedings of the National Academy of Sciences *103*, 14732 –14737.

Berendsen, H.J.C., Postma, J.P.M., van Gunsteren, W.F., DiNola, A., and Haak, J.R. (1984). Molecular dynamics with coupling to an external bath. J. Chem. Phys. *81*, 3684.

Berman, H.M., Battistuz, T., Bhat, T.N., Bluhm, W.F., Bourne, P.E., Burkhardt, K., Feng, Z., Gilliland, G.L., Iype, L., Jain, S., et al. (2002). The Protein Data Bank. Acta Crystallographica Section D Biological Crystallography *58*, 899–907.

Brooks, B.R., Brooks III, C.L., Mackerell Jr., A.D., Nilsson, L., Petrella, R.J., Roux, B., Won, Y., Archontis, G., Bartels, C., Boresch, S., et al. (2009). CHARMM: The biomolecular simulation program. Journal of Computational Chemistry *30*, 1545–1614.

Brown, N.R., Noble, M.E.M., Endicott, J.A., and Johnson, L.N. (1999a). The structural basis for specificity of substrate and recruitment peptides for cyclin-dependent kinases. Nat Cell Biol *1*, 438–443.

Brown, N.R., Noble, M.E.M., Lawrie, A.M., Morris, M.C., Tunnah, P., Divita, G., Johnson, L.N., and Endicott, J.A. (1999b). Effects of Phosphorylation of Threonine 160 on Cyclin-dependent Kinase 2 Structure and Activity. Journal of Biological Chemistry *274*, 8746 –8756.

Camerini-Otero, R.D., Sollner-Webb, B., and Felsenfeld, G. (1976). The organization of histones and DNA in chromatin: Evidence for an arginine-rich histone kernel. Cell *8*, 333–347.

Case, D.A., Cheatham, T.E., Darden, T., Gohlke, H., Luo, R., Merz, K.M., Onufriev, A., Simmerling, C., Wang, B., and Woods, R.J. (2005). The Amber biomolecular simulation programs. Journal of Computational Chemistry *26*, 1668–1688.

Case, D.A., Darden, T.A., Cheatham III, T.E., Simmerling, C.L., Wang, J., Duke, R.E., Luo, R., Merz, K.M., Pearlman, D.A., Crowley, M., et al. (2006). AMBER 10. University of California, San Francisco.

Chen, X., Mitsutake, N., LaPerle, K., Akeno, N., Zanzonico, P., Longo, V.A., Mitsutake, S., Kimura, E.T., Geiger, H., Santos, E., et al. (2009). Endogenous expression of HrasG12V induces developmental defects and neoplasms with copy number imbalances of the oncogene. Proceedings of the National Academy of Sciences *106*, 7979 –7984.

Cheng, Y., Zhang, Y., and McCammon, J.A. (2005). How Does the cAMP-Dependent Protein Kinase Catalyze the Phosphorylation Reaction: An ab Initio QM/MM Study. Journal of the American Chemical Society *127*, 1553–1562.

Cieplak, P., Cornell, W.D., Bayly, C., and Kollman, P.A. (1995). Application of the multimolecule and multiconformational RESP methodology to biopolymers: Charge derivation for DNA, RNA, and proteins. J. Comput. Chem. *16*, 1357–1377.

Collett, M.S., and Erikson, R.L. (1978). Protein kinase activity associated with the avian sarcoma virus src gene product. Proc. Natl. Acad. Sci. U.S.A. *75*, 2021–2024.

Cook, A., Lowe, E.D., Chrysina, E.D., Skamnaki, V.T., Oikonomakos, N.G., and Johnson, L.N. (2002). Structural Studies on Phospho-CDK2/Cyclin A Bound to Nitrate, a Transition State Analogue: Implications for the Protein Kinase Mechanism†,‡. Biochemistry *41*, 7301–7311.

Cook, P.F., Neville, M.E., Jr, Vrana, K.E., Hartl, F.T., and Roskoski, R., Jr (1982). Adenosine cyclic 3',5'-monophosphate dependent protein kinase: kinetic mechanism for the bovine skeletal muscle catalytic subunit. Biochemistry *21*, 5794–5799.

Cornell, W.D., Cieplak, P., Bayly, C.I., Gould, I.R., Merz, K.M., Ferguson, D.M., Spellmeyer, D.C., Fox, T., Caldwell, J.W., and Kollman, P.A. (1995). A Second Generation Force Field for the Simulation of Proteins, Nucleic Acids, and Organic Molecules. Journal of the American Chemical Society *117*, 5179–5197.

Druker, B.J., Talpaz, M., Resta, D.J., Peng, B., Buchdunger, E., Ford, J.M., Lydon, N.B., Kantarjian, H., Capdeville, R., Ohno-Jones, S., et al. (2001). Efficacy and safety of a specific inhibitor of the BCR-ABL tyrosine kinase in chronic myeloid leukemia. N. Engl. J. Med. *344*, 1031–1037.

Dudev, T., and Lim, C. (2004). Monodentate versus Bidentate Carboxylate Binding in Magnesium and Calcium Proteins: What Are the Basic Principles? The Journal of Physical Chemistry B *108*, 4546–4557.

Emsley, P., Lohkamp, B., Scott, W.G., and Cowtan, K. (2010). Features and development of Coot.

Endicott, J.A., Nurse, P., and Johnson, L.N. (1994). Mutational analysis supports a structural model for the cell cycle protein kinase p34. Protein Engineering *7*, 243 –257.

Evans, P. (2006). Scaling and assessment of data quality.

Frick, D.N., Banik, S., and Rypma, R.S. (2007). Role of divalent metal cations in ATP hydrolysis catalyzed by the hepatitis C virus NS3 helicase: magnesium provides a bridge for ATP to fuel unwinding. J. Mol. Biol. *365*, 1017–1032.

Frisch, M.J., Trucks, G.W., Schlegel, H.B., Scuseria, G.E., Robb, M.A., Cheeseman, J.R., Montgomery, J., Vreven, T., Kudin, K.N., Burant, J.C., et al. Gaussian 03, C.02.

Grace, M.R., Walsh, C.T., and Cole, P.A. (1997). Divalent Ion Effects and Insights into the Catalytic Mechanism of Protein Tyrosine Kinase Csk†. Biochemistry *36*, 1874–1881.

Graham, D.L., Lowe, P.N., Grime, G.W., Marsh, M., Rittinger, K., Smerdon, S.J., Gamblin, S.J., and Eccleston, J.F. (2002). MgF3− as a Transition State Analog of Phosphoryl Transfer. Chemistry & Biology *9*, 375–381.

Greenman, C., Stephens, P., Smith, R., Dalgliesh, G.L., Hunter, C., Bignell, G., Davies, H., Teague, J., Butler, A., Stevens, C., et al. (2007). Patterns of somatic mutation in human cancer genomes. Nature *446*, 153–158.

Grubbs, R.D. (2002). Intracellular magnesium and magnesium buffering. BioMetals *15*, 251–259.

Hagopian, J.C., Kirtley, M.P., Stevenson, L.M., Gergis, R.M., Russo, A.A., Pavletich, N.P., Parsons, S.M., and Lew, J. (2001). Kinetic Basis for Activation of CDK2/Cyclin A by Phosphorylation. Journal of Biological Chemistry *276*, 275 –280.

Harding, M.M. (2001). Geometry of metal–ligand interactions in proteins. Acta Crystallographica Section D *57*, 401–411.

Harper, J.W., and Adams, P.D. (2001). Cyclin-dependent kinases. Chem Rev *101*, 2511–2526.

Henzler-Wildman, K.A., Thai, V., Lei, M., Ott, M., Wolf-Watz, M., Fenn, T., Pozharski, E., Wilson, M.A., Petsko, G.A., Karplus, M., et al. (2007). Intrinsic motions along an enzymatic reaction trajectory. Nature *450*, 838–844.

Homeyer, N., Horn, A.H.C., Lanig, H., and Sticht, H. (2005). AMBER force-field parameters for phosphorylated amino acids in different protonation states: phosphoserine, phosphothreonine, phosphotyrosine, and phosphohistidine. J Mol Model *12*, 281–289.

Hornak, V., Abel, R., Okur, A., Strockbine, B., Roitberg, A., and Simmerling, C. (2006). Comparison of multiple Amber force fields and development of improved protein backbone parameters. Proteins: Structure, Function, and Bioinformatics *65*, 712–725.

Huse, M., and Kuriyan, J. (2002). The Conformational Plasticity of Protein Kinases. Cell *109*, 275–282.

Jeffrey, P.D., Russo, A.A., Polyak, K., Gibbs, E., Hurwitz, J., Massague, J., and Pavletich, N.P. (1995). Mechanism of CDK activation revealed by the structure of a cyclinA-CDK2 complex. Nature *376*, 313–320.

Jorgensen, W.L., Chandrasekhar, J., Madura, J.D., Impey, R.W., and Klein, M.L. (1983). Comparison of simple potential functions for simulating liquid water. J. Chem. Phys. *79*, 926.

Jura, N., Zhang, X., Endres, N.F., Seeliger, M.A., Schindler, T., and Kuriyan, J. (2011). Catalytic control in the EGF Receptor and its connection to general kinase regulatory mechanisms. Mol Cell *42*, 9–22.

Kamerlin, S.C.L., and Warshel, A. (2010). At the dawn of the 21st century: Is dynamics the missing link for understanding enzyme catalysis? Proteins: Structure, Function, and Bioinformatics *78*, 1339–1375.

Kannan, N., and Neuwald, A.F. (2005). Did Protein Kinase Regulatory Mechanisms Evolve Through Elaboration of a Simple Structural Component? Journal of Molecular Biology *351*, 956–972.

Khavrutskii, I.V., Grant, B., Taylor, S.S., and McCammon, J.A. (2009). A transition path ensemble study reveals a linchpin role for Mg(2+) during rate-limiting ADP release from protein kinase A. Biochemistry *48*, 11532–11545.

Killilea, D.W., and Ames, B.N. (2008). Magnesium deficiency accelerates cellular senescence in cultured human fibroblasts. Proceedings of the National Academy of Sciences *105*, 5768 –5773.

Kornev, A.P., Haste, N.M., Taylor, S.S., and Ten Eyck, L.F. (2006). Surface comparison of active and inactive protein kinases identifies a conserved activation mechanism. Proceedings of the National Academy of Sciences *103*, 17783 –17788.

Leslie, A.G.W. (1992). Recent changes to the MOSFLM package for processing film and image plate data. Joint CCP4 + ESF-EAMCB Newsletter on Protein Crystallography *26*,.

Levinson, A.D., Oppermann, H., Levintow, L., Varmus, H.E., and Bishop, J.M. (1978). Evidence that the transforming gene of avian sarcoma virus encodes a protein kinase associated with a phosphoprotein. Cell *15*, 561–572.

Lew, J., Taylor, S.S., and Adams, J.A. (1997). Identification of a Partially Rate-Determining Step in the Catalytic Mechanism of cAMP-Dependent Protein Kinase: A Transient Kinetic Study Using Stopped-Flow Fluorescence Spectroscopy†. Biochemistry *36*, 6717–6724.

Li, F., Gangal, M., Juliano, C., Gorfain, E., Taylor, S.S., and Johnson, D.A. (2002). Evidence for an internal entropy contribution to phosphoryl transfer: a study of domain closure, backbone flexibility, and the catalytic cycle of cAMP-dependent protein kinase. Journal of Molecular Biology *315*, 459–469.

Liu, M., Girma, E., Glicksman, M.A., and Stein, R.L. (2010). Kinetic mechanistic studies of Cdk5/p25-catalyzed H1P phosphorylation: metal effect and solvent kinetic isotope effect. Biochemistry *49*, 4921–4929.

Liu, Y., and Gray, N.S. (2006). Rational design of inhibitors that bind to inactive kinase conformations. Nat Chem Biol *2*, 358–364.

London, W.P., and Steck, T.L. (1969). Kinetics of enzyme reactions with interaction between a substrate and a (metal) modifier. Biochemistry *8*, 1767–1779.

Lowe, E.D., Noble, M.E., Skamnaki, V.T., Oikonomakos, N.G., Owen, D.J., and Johnson, L.N. (1997). The crystal structure of a phosphorylase kinase peptide substrate complex: kinase substrate recognition. Embo J *16*, 6646–6658.

Madhusudan, Akamine, P., Xuong, N.-H., and Taylor, S.S. (2002). Crystal structure of a transition state mimic of the catalytic subunit of cAMP-dependent protein kinase. Nat Struct Mol Biol *9*, 273–277.

Maegley, K.A., Admiraal, S.J., and Herschlag, D. (1996). Ras-catalyzed hydrolysis of GTP: a new perspective from model studies. Proceedings of the National Academy of Sciences *93*, 8160 –8166.

Malumbres, M., and Barbacid, M. (2007). Cell cycle kinases in cancer. Curr. Opin. Genet. Dev. *17*, 60–65.

Malumbres, M., and Barbacid, M. (2009). Cell cycle, CDKs and cancer: a changing paradigm. Nat Rev Cancer *9*, 153–166.

Manning, G., Whyte, D.B., Martinez, R., Hunter, T., and Sudarsanam, S. (2002). The Protein Kinase Complement of the Human Genome. Science *298*, 1912 –1934.

Martin, G.S. (2004). The road to Src. Oncogene *23*, 7910–7917.

Masterson, L.R., Cheng, C., Yu, T., Tonelli, M., Kornev, A., Taylor, S.S., and Veglia, G. (2010). Dynamics connect substrate recognition to catalysis in protein kinase A. Nat Chem Biol *6*, 821–828.

McCoy, A.J., Grosse-Kunstleve, R.W., Adams, P.D., Winn, M.D., Storoni, L.C., and Read, R.J. (2007). Phaser crystallographic software. J Appl Crystallogr *40*, 658–674.

Meagher, K.L., Redman, L.T., and Carlson, H.A. (2003). Development of polyphosphate parameters for use with the AMBER force field. Journal of Computational Chemistry *24*, 1016–1025.

Milde-Langosch, K., Bamberger, A.-M., Goemann, C., Rössing, E., Rieck, G., Kelp, B., and Löning, T. (2001). Expression of cell-cycle regulatory proteins in endometrial carcinomas: correlations with hormone receptor status and clinicopathologic parameters. Journal of Cancer Research and Clinical Oncology *127*, 537–544.

Mildvan, A.S. (1997). Mechanisms of signaling and related enzymes. Proteins: Structure, Function, and Bioinformatics *29*, 401–416.

Mittnacht, S., and Boshoff, C. (2000). Viral cyclins. Rev. Med. Virol. *10*, 175–184.

Morgan, D.O. (1997). CYCLIN-DEPENDENT KINASES: Engines, Clocks, and Microprocessors. Annual Review of Cell and Developmental Biology *13*, 261–291.

Morris, M.C., Gondeau, C., Tainer, J.A., and Divita, G. (2002). Kinetic Mechanism of Activation of the Cdk2/Cyclin A Complex. Journal of Biological Chemistry *277*, 23847 – 23853.

Mukherjee, K., Sharma, M., Urlaub, H., Bourenkov, G.P., Jahn, R., Südhof, T.C., and Wahl, M.C. (2008). CASK Functions as a Mg2+-independent neurexin kinase. Cell *133*, 328–339.

Nagar, B., Bornmann, W.G., Pellicena, P., Schindler, T., Veach, D.R., Miller, W.T., Clarkson, B., and Kuriyan, J. (2002). Crystal Structures of the Kinase Domain of c-Abl in Complex with the Small Molecule Inhibitors PD173955 and Imatinib (STI-571). Cancer Research *62*, 4236 –4243.

Nagar, B., Hantschel, O., Young, M.A., Scheffzek, K., Veach, D., Bornmann, W., Clarkson, B., Superti-Furga, G., and Kuriyan, J. (2003). Structural Basis for the Autoinhibition of c-Abl Tyrosine Kinase. Cell *112*, 859–871.

O'Sullivan, W.J., and Smithers, G.W. (1979). Stability constants for biologically important metal-ligand complexes. Meth. Enzymol. *63*, 294–336.

Painter, J., and Merritt, E.A. (2006a). Optimal description of a protein structure in terms of multiple groups undergoing TLS motion. Acta Crystallogr D Biol Crystallogr *62*, 439–450.

Painter, J., and Merritt, E.A. (2006b). TLSMD web server for the generation of multi-group TLS models. J Appl Crystallogr *39*, 109–111.

Pavletich, N.P. (1999). Mechanisms of cyclin-dependent kinase regulation: structures of cdks, their cyclin activators, and cip and INK4 inhibitors. Journal of Molecular Biology *287*, 821–828.

Praznikar, J., Afonine, P.V., Gregor, G., Adams, P.D., and Turk, D. (2009). Averaged kick maps: less noise, more signal...and probably less bias. Acta Crystallographica Section D Biological Crystallography *65*, 921–931.

R Development Core Team (2010). R: A Language and Environment for Statistical Computing (Vienna, Austria).

Radzio-Andzelm, E., Lew, J., and Taylor, S. (1995). Bound to activate: conformational consequences of cyclin binding to CDK2. Structure *3*, 1135–1141.

Russo, A.A., Jeffrey, P.D., Patten, A.K., Massagué, J., and Pavletich, N.P. (1996a). Crystal structure of the p27Kip1 cyclin-dependent-kinase inhibitor bound to the cyclin A-Cdk2 complex. Nature *382*, 325–331.

Russo, A.A., Jeffrey, P.D., and Pavletich, N.P. (1996b). Structural basis of cyclin-dependent kinase activation by phosphorylation. Nat Struct Mol Biol *3*, 696–700.

Santamaria, D., Barriere, C., Cerqueira, A., Hunt, S., Tardy, C., Newton, K., Caceres, J.F., Dubus, P., Malumbres, M., and Barbacid, M. (2007). Cdk1 is sufficient to drive the mammalian cell cycle. Nature *448*, 811–815.

Saylor, P., Wang, C., Hirai, T.J., and Adams, J.A. (1998). A Second Magnesium Ion Is Critical for ATP Binding in the Kinase Domain of the Oncoprotein v-Fps†. Biochemistry *37*, 12624–12630.

Schrödinger, L. (2010). The PyMOL Molecular Graphics System, Version 1.3r1.

Schulze-Gahmen, U., De Bondt, H.L., and Kim, S.-H. (1996). High-Resolution Crystal Structures of Human Cyclin-Dependent Kinase 2 with and without ATP: Bound Waters and Natural Ligand as Guides for Inhibitor Design†. Journal of Medicinal Chemistry *39*, 4540–4546.

Sgambato, A., Wolf, F.I., Faraglia, B., and Cittadini, A. (1999). Magnesium depletion causes growth inhibition, reduced expression of cyclin D1, and increased expression of P27KIP1 in normal but not in transformed mammary epithelial cells. Journal of Cellular Physiology *180*, 245–254.

Shaffer, J., and Adams, J.A. (1999). Detection of Conformational Changes along the Kinetic Pathway of Protein Kinase A Using a Catalytic Trapping Technique†. Biochemistry *38*, 12072–12079.

Shirts, M.R., and Chodera, J.D. (2008). Statistically optimal analysis of samples from multiple equilibrium states. The Journal of Chemical Physics *129*, 124105.

Smart, J.E., Oppermann, H., Czernilofsky, A.P., Purchio, A.F., Erikson, R.L., and Bishop, J.M. (1981). Characterization of sites for tyrosine phosphorylation in the transforming protein of Rous sarcoma virus (pp60v-src) and its normal cellular homologue (pp60c-src). Proc. Natl. Acad. Sci. U.S.A. *78*, 6013–6017.

Smith, G.K., Ke, Z., Guo, H., and Hengge, A.C. (2011). Insights into the Phosphoryl Transfer Mechanism of Cyclin-Dependent Protein Kinases from ab Initio QM/MM Free-Energy Studies. J. Phys. Chem. B *115*, 13713–13722.

Stevenson, L.M., Deal, M.S., Hagopian, J.C., and Lew, J. (2002). Activation Mechanism of CDK2: Role of Cyclin Binding versus Phosphorylation†. Biochemistry *41*, 8528–8534.

Storer, A.C., and Cornish-Bowden, A. (1976). Concentration of MgATP2- and other ions in solution. Calculation of the true concentrations of species present in mixtures of associating ions. Biochem J *159*, 1–5.

Sun, G., and Budde, R.J.A. (1997). Requirement for an Additional Divalent Metal Cation To Activate Protein Tyrosine Kinases†. Biochemistry *36*, 2139–2146.

Taylor, S.S., and Kornev, A.P. (2011). Protein Kinases: Evolution of Dynamic Regulatory Proteins. Trends Biochem Sci *36*, 65–77.

Thomas, S.M., and Brugge, J.S. (1997). CELLULAR FUNCTIONS REGULATED BY SRC FAMILY KINASES. Annual Review of Cell and Developmental Biology *13*, 513–609.

Valiev, M., Kawai, R., Adams, J.A., and Weare, J.H. (2003). The role of the putative catalytic base in the phosphoryl transfer reaction in a protein kinase: first-principles calculations. J. Am. Chem. Soc. *125*, 9926–9927.

De Vivo, M., Cavalli, A., Carloni, P., and Recanatini, M. (2007). Computational study of the phosphoryl transfer catalyzed by a cyclin-dependent kinase. Chemistry *13*, 8437–8444.

Waas, W.F., and Dalby, K.N. (2003). Physiological Concentrations of Divalent Magnesium Ion Activate the Serine/Threonine Specific Protein Kinase ERK2†. Biochemistry *42*, 2960–2970.

Walker, G.M. (1986). Magnesium and cell cycle control: an update. Magnesium *5*, 9–23.

Weinstein, I.B. (2002). Cancer. Addiction to oncogenes--the Achilles heal of cancer. Science *297*, 63–64.

Westheimer, F. (1987). Why nature chose phosphates. Science *235*, 1173 –1178.

Williams, J.C., Weijland, A., Gonfloni, S., Thompson, A., Courtneidge, S.A., Superti-Furga, G., and Wierenga, R.K. (1997). The 2.35 å crystal structure of the inactivated form of chicken src: a dynamic molecule with multiple regulatory interactions. Journal of Molecular Biology *274*, 757–775.

Winn, M.D., Murshudov, G.N., and Papiz, M.Z. (2003). Macromolecular TLS Refinement in REFMAC at Moderate Resolutions. In Macromolecular Crystallography, Part D, (Academic Press), pp. 300–321.

Wolf, F.I., and Cittadini, A. (1999). Magnesium in cell proliferation and differentiation. Front. Biosci *4*, D607–617.

Xie, X., Gu, Y., Fox, T., Coll, J.T., Fleming, M.A., Markland, W., Caron, P.R., Wilson, K.P., and Su, M.S.-S. (1998). Crystal structure of JNK3: a kinase implicated in neuronal apoptosis. Structure *6*, 983–991.

Xu, W., Doshi, A., Lei, M., Eck, M.J., and Harrison, S.C. (1999). Crystal structures of c-Src reveal features of its autoinhibitory mechanism. Mol. Cell *3*, 629–638.

Yang, L., Arora, K., Beard, W.A., Wilson, S.H., and Schlick, T. (2004). Critical role of magnesium ions in DNA polymerase beta's closing and active site assembly. J. Am. Chem. Soc. *126*, 8441–8453.

Zetterberg, A., Larsson, O., and Wiman, K.G. (1995). What is the restriction point? Curr. Opin. Cell Biol. *7*, 835–842.

Zhang, B., Zhang, Y., Wang, Z., and Zheng, Y. (2000). The role of Mg2+ cofactor in the guanine nucleotide exchange and GTP hydrolysis reactions of Rho family GTP-binding proteins. J. Biol. Chem. *275*, 25299–25307.

Zhang, X., Gureasko, J., Shen, K., Cole, P.A., and Kuriyan, J. (2006). An Allosteric Mechanism for Activation of the Kinase Domain of Epidermal Growth Factor Receptor. Cell *125*, 1137–1149.

Zheng, J., Knighton, D.R., Ten Eyck, L.F., Karlsson, R., Xuong, N., Taylor, S.S., and Sowadski, J.M. (1993a). Crystal structure of the catalytic subunit of cAMP-dependent protein kinase complexed with magnesium-ATP and peptide inhibitor. Biochemistry *32*, 2154–2161.

Zheng, J., Trafny, E.A., Knighton, D.R., Xuong, N., Taylor, S.S., Ten Eyck, L.F., and Sowadski, J.M. (1993b). 2.2 Å refined crystal structure of the catalytic subunit of cAMP-dependent protein kinase complexed with MnATP and a peptide inhibitor. Acta Crystallogr D Biol Crystallogr *49*, 362–365.

Zhou, J., and Adams, J.A. (1997). Is there a catalytic base in the active site of cAMP-dependent protein kinase? Biochemistry *36*, 2977–2984.

Zimmermann, B., Schweinsberg, S., Drewianka, S., and Herberg, F.W. (2008). Effect of metal ions on high-affinity binding of pseudosubstrate inhibitors to PKA. Biochemical Journal *413*, 93.